

# **Modification of Polypropylene/Polystyrene blend using Nanoclay and Sisal Cellulose nano fiber**

*Thesis submitted to  
Cochin University of Science and Technology  
in partial fulfilment of the requirements  
for the award of the degree of  
Doctor of Philosophy  
under the  
Faculty of Technology*

*by*

**Asha Krishnan K**



**Department of Polymer Science and Rubber Technology**

**Cochin University of Science and Technology**

**Kochi- 682 022, Kerala, India**

**October 2014**

## **Modification of Polypropylene/Polystyrene blend using Nanoclay and Sisal Cellulose nano fiber**

*Ph. D Thesis*

*Author*

---

**Asha Krishnan K**

Department of Polymer Science and Rubber Technology  
Cochin University of Science and Technology  
Cochin- 682 022, Kerala, India  
E-mail: ashakris8@gmail.com

---

*Supervising teacher*

---

**Dr. K.E. George**

Retd. Professor  
Department of Polymer Science and Rubber  
Technology  
Cochin University of Science and Technology  
Cochin- 682 022, Kerala, India

Principal  
Albertian Institute of Science and  
Technology,  
Archbishop, Angel Mary Nagar,  
Kochi, Kerala, India 682022  
E-mail: principal@aisat.ac.in

---

Department of Polymer Science and Rubber Technology  
Cochin University of Science and Technology  
Cochin- 682 022, Kerala, India

October 2014



**Department of Polymer Science and Rubber Technology**  
**Cochin University of Science and Technology**

Cochin- 682 022, Kerala, India

---

**Dr. K.E. George**  
Retd. Professor

Phone: +91 9446447851  
E mail: principal@aisat.ac.in

*Date: October 2014*

## **Certificate**

This is to certify that the thesis entitled **“Modification of Polypropylene/Polystyrene blend using Nanoclay and Sisal Cellulose nano fiber”** is a report of the bonafide research work carried out by **Ms. Asha Krishnan K** under my supervision and guidance in the Department of Polymer Science and Rubber Technology, Cochin University of Science and Technology, Cochin-682 022, and no part of the work reported in the thesis has been presented for the award of any degree from any other institution. All the relevant corrections and modifications suggested by the audience during the pre-synopsis seminar and recommended by the Doctoral committee have been incorporated in the thesis.

**Dr. K.E George**  
(Supervising Teacher)

## *Declaration*

I hereby declare that the thesis entitled “**Modification of Polypropylene/Polystyrene blend using Nanoclay and Sisal Cellulose nano fiber**” is based on the original research work carried out by me under the guidance and supervision of **Dr. K.E. George**, Retd. Professor, Department of Polymer Science and Rubber Technology, Cochin University of Science and Technology, Cochin-682 022 and no part of the work reported in this thesis has been presented for the award of any degree from any other institution.

Cochin-22  
October 2014.

**Asha Krishnan K**



*Dedicated to  
My beloved Parents.....*

---

## *Acknowledgements*

*First, let me bow before the Almighty God for being with me in every moment and giving me the strength to overcome all the hurdles. Without His blessings, I would not have been able to complete this thesis.*

*It is great pleasure for me to put on record my deep sense of gratitude for my guide, Dr. K.E. George, Retired Professor, Department of Polymer Science and Rubber Technology, Cochin university of Science and Technology for his proper guidance, motivation and freedom throughout my research work,*

*Prof. Dr. Sunil Narayanan Kutty, Head of the Department, Polymer Science & Rubber Technology and former head Prof. Eby Thomas Thachil for giving necessary facilities and support during the research.*

*I cherish the valuable advice and suggestions given by Prof. Dr. Rani Joseph, Prof. Philip Kurian, Prof. Thomas Kurian, Jaya Teacher and Jyothish Kumar Sir for the whole hearted cooperation throughout my research work. I express my gratitude to all the teaching and non-teaching staff of Department of Polymer Science & Rubber Technology for their support during these years.*

*I am very thankful to my dear friends Remya, Radhika and Sooraj for being with me to share my pains. There are no words to express my gratitude to Ayslu for her sincere friendship, timely help and caring. I owe special thanks to Dr. Ajalesh for his technical assistance and whole hearted cooperation for which I am very much obliged. I would like to express my sincere thanks to Preetha miss and Nishad for their help, cooperation and support during my thesis work. I am also grateful to Bibin sir, Jebin miss and Bindu miss, for their valuable advice and suggestions. I would like to express my deep sense of gratitude to Dr. Vidya G & Dr. Cimi for their support motivation, love and caring during the days in Athulya hostel. I gratefully acknowledge the valuable help extended to me by Rohit, Sunitha and Anjana miss during the initial stages of my research.*

*My sincere thanks to Cintil chechi & Jithin School of Chemical Sciences, M. G. University, for their support to overcome all hurdles during the isolation of cellulose nano fiber.*

*I am grateful to all my seniors especially Dr. Anna Dilfi, Dr. Saisy, Abilashattan, , Dr. Pramela, Mrs. Dennyamol, Dr. Zeena for inspiring and encouraging me. I would like to express my thanks to Newly miss, Bhavya, Shadiya, Neena, Jolly Sir, Renju chechi, Neena chechi, Sona chechi, Sreejesh, Bhagyesh, Dhanya chechi, Murali cheattan , Vidhya Francis, Teena Thomas, Resmi V C, Vineetha Varkey, Manoj Sir, Jayesh, July Chechi, Midhun , Sreedevi miss, Sinto chettan, Suma miss for the help rendered to me. I am thankful to Remya, Neethu, Anju, Sherin, Jisha, Sona stanly, Nisha, Jenisheattan, Sobha teacher, Divya, Abitha chechi, Renjitha miss, and Jasmine miss. I would like to express my heartfelt thanks to Shinu, Anil, Sreerenjani, Anakha, Nayana & Tinu.*

*I express my gratitude to STIC, CUSAT for characterization of the samples.*

*I would like to thank my parents and my brother for their love, prayers, care, patience and support, without which this thesis would not be a reality. I am thankful to aati for her love and encouragement.*

*Finally, I would like to thank all those who inspired, guided and accompanied me during the course of my life.....*

***Asha Krishnan K***

## *Preface*

Polymer blends have attracted great attention both industrially and academically because of their flexibility and versatility to create new materials with desired properties from existing virgin polymers. Polypropylene (PP) and polystyrene (PS) are two of the widely used plastics and their blends have also received considerable attention. This blend has been selected for this study because of the recent interest in these materials for automotive applications. However, PP and PS are widely regarded as immiscible due to lack of interfacial adhesion between the components. Properties of such blends can be improved by using compatibilizers such as homopolymers, graft, block or star copolymers. In recent years, a new concept of compatibilization by using nanoparticles has been introduced. In this study nanoclay and cellulose nano fibers are proposed to be used as modifiers. Nanocomposites based on polymer blends are particularly attractive due to the myriad types of polymer nanocomposites that can be generated. Traditionally nanoclays have been used as fillers in polymer systems due to the improved physical and mechanical properties of the resulting polymer nanocomposite. A large quantity of polymer-clay nanocomposites has been successfully prepared through the integration of clay in a wide variety of polymer matrices. Much of the work in this area has focused on montmorillonite clays. Hence, in this study low cost kaolin nanoclay with a 1: 1 type layered structure with chemical composition  $\text{Al}_2\text{Si}_2\text{O}_5(\text{OH})_4$  is proposed to be used.

Cellulose nano fiber based nanocomposites are very attractive because of their low density, nonabrasive, nontoxic, low cost and interesting specific properties. Nowadays, cellulose nano fibers has been greatly discussed and researched in a wide variety of applications. The high strength and stiffness

coupled with the small dimensions of cellulose nano fiber may impart useful properties to composite materials which can be used in a wide range of applications. The main reason for using cellulose nano fibers in polymer composites is its high stiffness making it an ideal material for reinforcement. In this study it is proposed to isolate cellulose nano fiber from sisal and use it as reinforcement in PP/PS blend.

Short fiber reinforced composites have several attractive characteristics that make them suitable for engineering and consumer applications. Since the inorganic filler has higher density compared to the polymer matrix, the filled polymer density may also increase and lead to greater moulded part weight. To overcome this drawback a composite with lower particle size filler is proposed to be used. Recently, it has been observed that incorporating filler particles into the matrix of fiber reinforced composites would give the desired performance for the hybrid composites at low to intermediate filler loadings. Micro/nano hybrid composites may result in synergism and find applications in a variety of engineering applications. A systematic study is proposed to be undertaken to understand the mechanical, thermal and morphological properties of various composites.

The investigations are presented in eight chapters as follows:

#### Chapter 1: INTRODUCTION

A concise prologue to the topic of study is presented in Chapter 1. Review on nanocomposites based on polymer blends with special reference to these properties and applications are briefly discussed. Scope and objectives of the present work are also discussed in this chapter.

## Chapter 2: MATERIALS AND METHODS

The details of the materials used and the experimental procedures for the preparation of nanocomposites and nano-micro hybrid composites adopted in the present study are outlined in Chapter 2. A brief description about the various techniques used for evaluating the mechanical, thermal and morphological properties of the composites is also presented in this chapter.

## Chapter 3: POLYPROPYLENE/ POLYSTYRENE/ CLAY NANOCOMPOSITES: EFFECT OF DIFFERENT MODIFICATIONS OF KAOLIN CLAY

The effect of Nanocaliber 100 (unmodified kaolin nanoclay) and modified kaolin nanoclays [Nanocaliber 100 V (Vinyl silane modified nanoclay), Nanocaliber 100Z (Dialkyl silane modified nanoclay, Nanocaliber 100A (Amino silane modified nanoclay), Nanocaliber 100M (Mercapto modified nanoclay)] on the properties of Polypropylene/Polystyrene blend is presented in Chapter 3. A comparison between experimental results (tensile modulus) and various models [Halpin-Tsai model, Takayanagi model, Hui-Shia, Voigt upper bound model and Reuss lower-bound] of PP/PS/clay nanocomposites has been presented.

## Chapter 4: POLYPROPYLENE/POLYSTYRENE BLENDS REINFORCED WITH HYBRID INORGANIC FILLERS: EFFECT OF MODIFIED KAOLIN NANOCLAYS AND SHORT GLASS FIBERS

This Chapter is divided into two sections.

4A. The effect of E- glass fiber and modified kaolin nanoclays (Nanocaliber 100 V and Nanocaliber 100Z) on the properties of PP/PS blend is described in this section. The fiber length and fiber loading is optimized. TGA, DSC, DMA and SEM analysis of hybrid composites are also presented. A

comparison between experimental results (tensile modulus) and various models [Parallel and Series model, Hirsch, Halpin-Tsai model, Modified Halpin –Tsai, Halpi – Pagano and Hui-Shia model] of PP/PS/EGF composites has been presented. A comparison between experimental results (tensile modulus) and various models [Parallel and series model, Guth model, Paul model, Counto model, Hirsch model, Halpin – Tsai] of hybrid composites has been presented.

- 4B. The effect of Alkali resistant glass fiber and modified kaolin nanoclays (Nanocaliber 100 V and Nanocaliber 100Z) on the properties of PP/PS blends is described in this part. These hybrid composites are also characterized using TGA, DSC, DMA and SEM

#### Chapter 5: POLYPROPYLENE/POLYSTYRENE/CLAY NANOCOMPOSITES: EFFECT OF VINYLTRIETHOXYSILANE MODIFICATION

This chapter comprises of two sections.

- 5A. The modification and characterization of kaolin nanoclay using vinyltriethoxysilane is described in this part. Nanoclay is modified by guest displacement method [Dimethylsulphoxide (DMSO) as precursor]. The modified clay is characterized by using FTIR, XRD, TGA and SEM.
- 5B. The effect of vinyltriethoxysilane modified nanoclay on the properties of polypropylene / polystyrene blend is discussed in this section. The characterization of PP/PS/clay nanocomposites is made by DMA, XRD and SEM. The thermal stability is determined by using TGA. Three kinetic methods namely Horowitz-Metzger, Broido's and Coats-Redfern methods are used to study the thermal degradation kinetics of PP/PS/clay nanocomposites.

Chapter 6: POLYPROPYLENE/ POLYSTYRENE/ CLAY NANOCOMPOSITES:  
EFFECT OF COMPATIBILIZERS

This chapter has two sections.

- 6A. The effect of itaconic acid (IA), a nonoil- based dicarboxylic acid as a compatibilizer on the properties of PP/PS/clay nanocomposites is discussed in this part. The degree of dispersion and morphology of nanocomposites are evaluated from X-ray diffraction and Transmission electron microscopy. The prepared nanocomposites are characterized using SEM, DSC and TGA.
- 6B. This part of the study deals with the effect of dimethyl itaconate as a compatibilizer on the properties of PP/PS/clay nanocomposites. These composites are also characterized using DMA, TGA, SEM, TEM and XRD.

Chapter 7: POLYPROPYLENE/ POLYSTYRENE/ SISAL CELLULOSE NANO  
FIBER COMPOSITES

This chapter comprises of two sections.

- 7A. This section deals with the isolation of cellulose nano fiber from sisal. The chemical composition, morphology and thermal properties of the nano fibers and their intermediate products is characterized using FTIR, Chemical analysis, SEM, TEM and TGA.
- 7B. The effect of cellulose nano fiber (CNF) on the properties of PP/PS blend is analyzed in this section. The characterization of CNF based composites is done using DMA, TGA, SEM and TEM.

The summary and conclusions of the study are presented in Chapter8.



## Contents

### Chapter -1

#### Introduction ..... 01 - 58

1.1	Polymer blends .....	03
1.1.1	Types of polymer blends .....	03
1.1.2	Evolution of Polymer Alloys and Blends .....	05
1.1.2.1	Commodity resins and their blends .....	05
1.1.2.2	Elastomer Blends .....	05
1.1.2.3	Engineering Polymer Blends .....	06
1.1.2.4	Recyclable blends .....	06
1.1.2.5	Polyolefin Blends .....	06
1.1.3	Review on Polymer blends .....	07
1.2	Role of compatibilizers in blending processes .....	11
1.2.1	Types of compatibilizers .....	12
1.2.1.1	Block or graft copolymers .....	12
1.2.1.2	Nonreactive polymers containing polar groups .....	13
1.2.1.3	Reactive functional polymer for compatibilization .....	13
1.2.1.4	Addition of low molecular weight chemicals .....	13
1.2.1.5	Interchange reactions .....	14
1.2.1.6	Addition of selective crosslinking agents .....	14
1.2.1.7	Compatibilization by ionomers .....	15
1.2.1.8	Compatibilization by fillers .....	15
1.2.1.8.1	Types of nano fillers .....	16
1.3	Polymer nanocomposites .....	17
1.4	Nanoclay .....	18
1.4.1	Kaolin clay .....	21
1.5	Polymer clay nanocomposites .....	23
1.5.1	Preparative methods and structure of polymer clay nanocomposites .....	24
1.5.1.1	Intercalation of Polymer or Prepolymer from Solution .....	24
1.5.1.2	In-situ Intercalative Polymerization Method .....	25
1.5.1.3	Melt Intercalation Method .....	25
1.5.2	Properties of Nanocomposites .....	26
1.5.2.1	Mechanical Properties .....	27
1.5.2.2	Barrier properties .....	27
1.5.2.3	Biodegradable polymer clay nanocomposites .....	28
1.5.2.4	Flammability reduction .....	28
1.5.3	Applications of Polymer clay nanocomposites .....	29
1.5.4	Polymer blend clay nanocomposites .....	30
1.5.5	Hybrid composites based on nanoclay .....	32

1.6	Cellulose .....	33
1.6.1	Preparative methods of nano cellulose.....	36
1.6.2	Classification of nanocellulose .....	38
1.6.2.1	Cellulose nanocrystals (CNC) .....	38
1.6.2.2	Cellulose nano fiber (Nanofibrillated cellulose- NFC).....	39
1.6.2.3	Bacterial nanocellulose .....	39
1.7	Nanocomposites of cellulose nano fibers .....	40
1.7.1	Preparative methods of nanocellulose based composites.....	40
1.7.1.1	Casting-evaporation Method .....	41
1.7.1.2	Sol- Gel Processing.....	41
1.7.1.3	Electrospinning.....	42
1.7.1.4	The layer-by-layer electrostatic assembly (LBL).....	42
1.7.1.5	Bottom – Up manufacture of bacterial cellulose nanocomposites.....	42
1.7.1.6	Melt compounding .....	43
1.7.2	Applications of cellulose based nanocomposites.....	43
1.8	Scope and Objectives of the work .....	45
	References .....	47

## ***Chapter -2***

### **Materials and Experimental techniques..... 59 - 76**

2.1	Materials.....	60
2.1.1	Polypropylene (PP).....	60
2.1.2	Polystyrene (PS) .....	60
2.1.3	Modified kaolin nanoclays .....	60
2.1.4	Glass fibers.....	60
2.1.5	Vinyltriethoxysilane (VTES).....	61
2.1.6	Itaconic acid .....	61
2.1.7	Dimethyl itaconate.....	61
2.1.8	Other chemicals .....	62
2.2	Methodology.....	62
2.2.1	Composite preparation .....	62
2.2.2	Preparation of test specimen.....	63
2.2.3	Characterization Techniques .....	64
2.2.3.1	X-ray Diffraction (XRD).....	64
2.2.3.2	Scanning Electron Microscopy (SEM).....	65
2.2.3.3	Thermogravimetric analysis (TGA).....	65
2.2.3.3.1	Kinetic analysis of thermal decomposition.....	66
2.2.3.4	Dynamic mechanical analysis (DMA) .....	69
2.2.3.5	Mechanical properties .....	71
(a)	Tensile properties.....	71

(b) Flexural properties .....	71
(c) Impact strength .....	72
(d) Hardness .....	73
2.2.3.6 Melt Flow Index (MFI) .....	73
2.2.3.7 Differential scanning Calorimetry (DSC).....	73
References .....	75

### *Chapter 3*

#### **Polypropylene/Polystyrene/clay nanocomposites:**

#### **Effect of different modifications of kaolin clay ..... 77 - 127**

3.1 Introduction .....	78
3.2 Methodology.....	81
3.2.1 Materials.....	81
3.2.2 Methodology .....	81
3.2.2.1 Nanocomposite preparation.....	81
3.2.2.2 Characterization.....	81
3.2.3 Theoretical modeling of tensile modulus .....	82
3.2.3.1 Effect of aspect ratio on the modulus ratio of PP/PS/clay nanocomposites.....	85
3.3 Results and Discussion.....	86
3.3.1 X-ray Diffraction .....	86
3.3.1.1 Relative Interaction of Nanocomposites .....	90
3.3.1.2 Number of Crystallites of PP/PS Nanocomposites .....	90
3.3.2 Transmission electron microscopy (TEM).....	91
3.3.2.1 Determination of aspect ratio of clay platelets.....	95
3.3.3 Scanning electron microscopy .....	97
3.3.4 Thermogravimetric analysis .....	98
3.3.4.1 Kinetic analysis of thermal decomposition.....	101
3.3.5 Dynamic mechanical analysis .....	103
3.3.5.1 Calculation of the activation energy.....	107
3.3.6 Differential scanning calorimetry .....	110
3.3.7 Mechanical Analysis.....	112
(a) Tensile properties .....	112
(b) Flexural properties .....	113
(c) Impact strength.....	115
(d) Hardness .....	115
3.3.8 Theoretical modeling of tensile modulus .....	116
3.3.9 Effect of UV aging on the tensile properties .....	119
3.3.10 Melt Flow Index .....	121
3.4. Conclusions .....	122
References .....	123

## *Chapter 4*

### **Polypropylene/Polystyrene blends reinforced with hybrid Inorganic fillers: Effect of modified kaolin nanoclays and short glass fibers..... 129 - 215**

#### **Part – A**

#### **Polypropylene/Polystyrene/E-glass fiber/ modified kaolin nanoclays hybrid composites**

4.A.1 Introduction.....	130
4.A.2 Methodology .....	133
4.A.2.1 Materials.....	133
4.A.2.2 Methodology .....	133
4.A.2.2.1 Composite preparation.....	133
4.A.2.2.2 Characterization .....	134
4.A.2.3 Theoretical background .....	134
4.A.2.3.1 Single fiber models.....	134
4.A.2.3.2 Multiple filler model.....	139
4.A.2.4 Determination of fiber aspect ratio .....	142
4.A.3 Results and Discussion .....	143
4.A.3.1 Polypropylene/Polystyrene/E- glass fiber composite.....	143
4.A.3.1.1 Effect of fiber length on mechanical properties of PP/PS /E- glass fiber composites.....	143
(a) Tensile properties.....	143
(b) Flexural properties .....	144
4.A.3.1.2 Effect of fiber loading on mechanical properties of E- glass fiber composites .....	144
(a) Tensile properties.....	144
(b) Flexural properties .....	145
(c) Impact strength .....	146
4.A.3.2 Hybrid effect of E- glass fiber and modified kaolin nanoclays on Polypropylene/Polystyrene blend .....	147
4.A.3.2.1 Effect of nanoclays on the mechanical properties of PP/PS/EGF composites .....	147
(a) Tensile properties.....	147
(b) Flexural properties .....	150
(c) Impact strength .....	151
(d) Hardness.....	152
4.A.3.3 Theoretical modeling of tensile modulus .....	153
(a) Single fiber model.....	153
(b) Multiple filler model .....	155
4.A.3.4 Effect of UV aging on the tensile properties .....	157
4.A.3.5 Density .....	158

4.A.3.6 Melt Flow Index .....	159
4.A.3.7 X-ray Diffraction .....	160
4.A.3.8 Scanning electron microscopy .....	161
4.A.3.9 Thermogravimetric analysis .....	162
4.A.3.9.1 Kinetic analysis of thermal decomposition .....	165
4.A.3.10 Dynamic mechanical analysis.....	169
4.A.3.10.1 Cole-Cole Plot analysis.....	172
4.A.3.11 Differential scanning calorimetry .....	173
4.A.4 Conclusions.....	175
References .....	176

## Part – B

### **Polypropylene/Polystyrene/alkali resistant glass fiber/modified kaolin nanoclays hybrid composites**

4.B.1 Introduction .....	181
4.B.2 Methodology .....	183
4.B.2.1 Materials.....	183
4.B.2.2 Methodology .....	183
4.B.2.3 Determination of aspect ratio of glass fiber.....	184
4.B.3 Results and Discussion .....	185
4.B.3.1 Polypropylene/Polystyrene/alkali-resistant glass fiber composite.....	185
4.B.3.1.1 Effect of fiber length on mechanical properties of PP/PS /AR glass fiber composites.....	185
(a) Tensile properties.....	185
(b) Flexural properties .....	186
4.B.3.1.2 Effect of fiber loading on mechanical properties of PP/PS /AR glass fiber composites .....	187
(a) Tensile properties.....	187
(b) Flexural properties .....	188
(c) Impact strength .....	189
4.B.3.2 Hybrid effect of alkali-resistant glass fiber and modified kaolin nanoclays on Polypropylene/Polystyrene blend.....	190
4.B.3.2.1 Effect of nanoclays on the mechanical properties of PP/PS/ARGF composites .....	190
(a) Tensile properties.....	190
(b) Flexural properties .....	192
(c) Impact strength .....	193
(d) Hardness.....	194
4.B.3.3 Theoretical modeling of elastic modulus .....	195
(a) Single fiber model.....	195
(b) Multiple filler model .....	196

4.B.3.4	Effect of UV aging on the tensile properties .....	198
4.B.3.5	Density .....	198
4.B.3.6	Melt Flow Index .....	199
4.B.3.7	X-ray Diffraction .....	200
4.B.3.8	Scanning electron microscopy .....	201
4.B.3.9	Thermogravimetric analysis .....	202
4.B.3.9.1	Kinetic analysis of thermal decomposition .....	204
4.B.3.10	Dynamic mechanical analysis .....	206
4.B.3.10.1	Cole-Cole Plot analysis .....	209
4.B.3.11	Differential scanning calorimetry .....	210
4.B.4	Conclusions .....	212
	References .....	213

## **Chapter 5**

### **Polypropylene/Polystyrene/clay nanocomposites:**

#### **Effect of vinyltriethoxysilane modification ..... 217 - 259**

##### **Part -A**

##### **Modification and characterization of kaolin nanoclay using vinyltriethoxysilane**

5.A.1	Introduction .....	218
5.A.2	Methodology.....	220
5.A.2.1	Modification of kaolin nanoclay.....	220
5.A.2.1.1	Intercalation of kaolin nanoclay by dimethylsulfoxide (DMSO) as precursor.....	221
5.A.2.1.2	Modification by vinyltriethoxysilane.....	222
5.A.2.2	Characterization.....	224
5.A.3	Results and Discussion .....	225
5.A.3.1	Fourier transform infrared spectroscopy .....	225
5.A.3.2	X-ray Diffraction .....	228
5.A.3.3	Scanning electron microscopy.....	230
5.A.3.4	BET Surface area.....	231
5.A.3.5	Bulk density.....	231
5.A.3.6	Particle size analysis .....	232
5.A.3.7	Thermogravimetric analysis .....	233
5.A.4	Conclusions .....	234
	References .....	234

**Part -B**  
**Polypropylene/Polystyrene/Vinyltriethoxysilane modified clay  
nanocomposites**

5.B.1 Introduction .....	237
5.B.2 Methodology .....	239
5.B.2.1 Materials.....	239
5.B.2.2 Nanocomposite preparation.....	239
5.B.3 Results and Discussion .....	240
5.B.3.1 X-ray diffraction .....	240
5.B.3.2 Scanning electron microscopy.....	241
5.B.3.3 Thermogravimetric analysis .....	242
5.B.3.3.1 Kinetic analysis of thermal decomposition .....	244
5.B.3.4 Dynamic mechanical analysis .....	245
5.B.3.5 Differential scanning calorimetry .....	248
5.B.3.6 Mechanical properties .....	250
(a) Tensile properties.....	250
(b) Flexural properties .....	251
(c) Impact strength .....	251
(d) Hardness.....	252
5.B.3.7 Effect of UV aging on the tensile properties of PP/PS/clay nanocomposites .....	253
5.B.3.8 Melt Flow Index .....	255
5.B.4 Conclusions .....	256
References .....	256

**Chapter 6**

**Polypropylene/ Polystyrene/clay nanocomposites:**

**Effect of compatibilizers ..... 261 - 317**

**Part-A**  
**Polypropylene/ Polystyrene/Itaconic acid /modified kaolin clay  
nanocomposites**

6.A.1 Introduction.....	262
6.A.2 Methodology .....	265
6.A.2.1 Materials.....	265
6.A.2.2 Preparation of the compatibilized blend and its characterization .....	265
6.A.2.3 Nanocomposite preparation.....	265
6.A.3 Results and Discussion .....	266
6.A.3.1 Effect of initiator (DCP) concentration on the mechanical properties of PP/PS/blend.....	266

(a) Tensile properties.....	266
(b) Flexural properties .....	268
6.A.3.2 Evidence of grafting IA onto PP/PS blend.....	269
6.A.3.2.1 Fourier Transform Infrared Spectroscopy .....	269
6.A.3.3 Effect of itaconic acid concentration on the mechanical properties of PP/PS blend .....	270
(a) Tensile properties.....	270
(b) Flexural properties .....	271
(c) Impact strength .....	272
6.A.3.3.1 Melt Flow Index (MFI) .....	273
6.A.3.4 Effect of itaconic acid (IA) grafting on the properties of PP/PS/clay nanocomposites .....	274
(a) Tensile properties .....	274
(b) Flexural properties .....	275
(c) Impact strength .....	277
(d) Hardness.....	278
6.A.3.5 Melt Flow Index .....	279
6.A.3.6 X-ray Diffraction .....	279
6.A.3.7 Transmission electron microscopy.....	281
6.A.3.8 Scanning electron microscopy .....	282
6.A.3.9 Thermogravimetric Analysis .....	282
6.A.3.9.1 Kinetic analysis of thermal decomposition.....	284
6.A.3.10 Dynamic mechanical analysis.....	286
6.A.3.11 Differential scanning calorimetry.....	288
6.A.4 Conclusions.....	289
References .....	289

## **Part B**

### **Polypropylene/ Polystyrene/ Dimethyl itaconate /modified kaolin clays nanocomposites**

6.B.1 Introduction.....	292
6.B.2 Methodology .....	293
6.B.2.1 Materials.....	293
6.B.2.2 Preparation of the compatibilized blend and its characterization .....	293
6.B.2.3 Nanocomposite preparation .....	294
6.B.3 Results and Discussion .....	294
6.B.3.1 Effect of initiator (DCP) concentration on the mechanical properties of PP/PS/blend .....	294
(a) Tensile properties.....	294
(b) Flexural properties .....	296



6.B.3.2	Evidence of grafting DMI onto PP/PS blend.....	297
6.B.3.2.1	Fourier Transform Infrared Spectroscopy .....	297
6.B.3.3	Effect of Dimethyl itaconate (DMI) concentration on the mechanical properties of PP/PS blend.....	297
(a)	Tensile properties.....	297
(b)	Flexural properties .....	299
(c)	Impact strength .....	300
6.B.3.3.1	Melt Flow Index.....	300
6.B.3.4	Effect of dimethyl itaconate (DMI) grafting on the properties of PP/PS/ clay nanocomposites .....	301
(a)	Tensile properties.....	301
(b)	Flexural strength .....	303
(c)	Impact strength .....	304
(d)	Hardness.....	305
6.B.3.5	Melt Flow Index .....	305
6.B.3.6	X-ray Diffraction .....	306
6.B.3.7	Transmission electron microscopy .....	307
6.B.3.8	Scanning electron microscopy .....	308
6.B.3.9	Thermogravimetric Analysis.....	309
6.B.3.9.1	Kinetic analysis of thermal decomposition .....	311
6.B.3.10	Dynamic mechanical analysis .....	312
6.B.3.11	Differential scanning Calorimetry .....	314
6.B.4	Conclusions .....	316
	References .....	316

## *Chapter 7*

### **Polypropylene/ Polystyrene / Sisal cellulose nano fiber composites ..... 319 - 364**

#### **Part-A**

##### **Isolation of cellulose nano fibers from Sisal**

7.A.1	Introduction.....	320
7.A.2	Methodology .....	322
7. A.2.1	Isolation of cellulose nano fibers (CNF).....	322
7.A.3	Results and Discussion .....	324
7.A.3.1	Chemical Analysis .....	324
7.A.3.2	Fourier transform infrared spectroscopy .....	325
7.A.3.3	X-ray Diffraction .....	327
7.A.3.4	Scanning electron microscopy.....	329
7.A.3.5	Transmission electron microscopy .....	330
7.A.3.6	Thermogravimetric analysis .....	331

7.A.4 Conclusions.....	333
References .....	334

**Part- B**

**Polypropylene/Polystyrene / Cellulose nano fiber composites**

7.B.1 Introduction .....	337
7.B.2 Methodology .....	339
7.B.2.1 Materials.....	339
7.B.2.2 Nanocomposite preparation.....	339
7.B.3 Results and Discussion.....	340
7.B.3.1 Mechanical properties .....	340
(a) Tensile properties.....	340
(b) Flexural properties .....	341
(c) Impact properties .....	342
(d) Hardness.....	343
7.B.3.2 Melt Flow Index .....	344
7.B.3.3 Scanning electron microscopy.....	344
7.B.3.4 Transmission electron microscopy .....	346
7.B.3.5 Thermogravimetric analysis .....	348
7.B.3.5.1 Kinetic analysis of thermal decomposition .....	350
7.B.3.6 Dynamic mechanical analysis .....	351
7.B.3.7 Differential scanning calorimetry .....	354
7.B.3.8 Water vapor transmission rate (WVTR) .....	355
7.B.4 Conclusions .....	361
References .....	362

**Chapter 8**

**Summary and Conclusions ..... 365 - 371**

**List of Publications**

**Curriculum Vitae**



# Chapter 1

## Introduction

- C o n t e n t s*
- 1.1 *Polymer blends*
  - 1.2 *Role of compatibilizers in blending processes*
  - 1.3 *Polymer nanocomposites*
  - 1.4 *Nanoclay*
  - 1.5 *Polymer clay nanocomposites*
  - 1.6 *Cellulose*
  - 1.7 *Nanocomposites of cellulose nano fibers*
  - 1.8 *Scope and Objectives of the work*

### *Abstract*

*This chapter gives an introduction on the general aspects of polymer blends and role of nanofillers as modifiers. A brief literature review on the recent developments in polymer nanocomposites is also included. The potential applications of the nanocomposites are mentioned. The scope and objectives of the present work are also mentioned.*

## **Introduction**

Nanotechnology is attracting worldwide attention due to its wide range of applications in traditional industry and advanced materials. Over the past two decades, scientists and engineers have been dominating the intricacies of working with nanoscale materials. Nanofillers have emerged as ultimate reinforcing agents for polymers. Due to its high surface area to volume size ratio, exhibition of novel and improved physical, chemical and biological properties; nanofillers are used in various fields such as optical devices, cosmetics, clothing and numerous consumer products. Among various nanoparticles, nanoclays and cellulose nano fibers are attracting attention due to their wide range of applications.

Polymer blends often present properties superior to individual polymers and is a more cost effective means of achieving a desired set of properties than synthesizing a new polymer. Most of the polymer blends are immiscible from the thermodynamic point of view due to the negligibly small entropy of mixing. In order to improve the immiscible polymer blend, the interfacial adhesion must be improved. Modification of polymer blends with nanofillers can generate a myriad of possibilities and a variety of engineering materials. Nanocomposites based on polymer blends have attracted increasing attention as the compounding may add versatility to the novel class of polymer nanocomposites. Modification of polymer blends with nanofillers is the topic of this thesis.

The present study aims to investigate the effect of nanoclay and cellulose nano fiber as modifiers for polypropylene /polystyrene blend to widen the spectrum of its applications. A brief introduction to the subject is

presented in this chapter. An outline of the objective of work is given at the end of the chapter.

## **1.1 Polymer blends**

Polymer blends have gained an increasing popularity in industrial and scientific area for last thirty years. This is mainly due to the ability of these materials to combine the properties of their components in a unique product. Mixing of two or more different polymers together to produce blends or alloys and makes it possible to make a final product with various property combinations. Polymer blends are physical mixtures of two or more structurally different polymers with no covalent bond between them and the components in the blends are adhering together through Van der Waals forces, dipole interactions or hydrogen bonding. For securing a set of specific properties required for an application, blending can be used and can also be used as a cost saving device. Therefore, a costly polymer can be combined with a less expensive polymer to produce adequate performance at a significantly reduced price to the customer [1, 2]. The first polymer blend was made by Thomas Hancock, based on a simple mechanical mixture of natural rubber with Gutta-percha. The first patented polymer blend was a mixture of natural rubber with gutta percha and it was patented by Alexander Parkes in 1846. The first patent on blends of two synthetic polymers was granted in 1928 for poly (vinyl chloride)/poly (vinyl acetate) blend prepared by latex blending.

### **1.1.1 Types of polymer blends**

According to the thermodynamic point of view there are three basic types of polymer blends. They are miscible, partially miscible and immiscible blend.

The miscibility of two polymers is determined by free energy of mixing. If the free energy is negative, the polymers mix at a microscopic level and can develop a single phase.

$$\Delta G_{\text{mix}} = \Delta H_{\text{mix}} - T\Delta S \dots\dots\dots (1.1)$$

In completely miscible blends,  $\Delta H_{\text{mix}} < 0$  due to specific interactions and the homogeneity is observed at least on a nanometer scale. One of the examples for miscible blend over a wide temperature range and in all compositions is PS/PPO, which combines the heat resistance, the inflammability and the toughness of PPO with the good processability and the low cost of PS. This type of blend exhibits only one glass transition temperature ( $T_g$ ), and is in between the  $T_g$ s of both blend components.

In the case of partially miscible blends a part of one blend component is dissolved in the other. This type of blend exhibits fine phase morphology and better properties and is referred to as compatible. Both blend phases are homogeneous and have their own  $T_g$  and both the  $T_g$ s are shifted from the values for the pure blend components towards the  $T_g$  of the other blend component. An example for partially miscible blend is PC/ABS blends, which combine the heat resistance and toughness of PC with the low temperature impact, processability, stress cracking resistance and low cost of ABS.

Most of the polymer blends are immiscible due to the negligibly small entropy of mixing. Polymers have a high degree of disorder and adding a different polymer causes no significant change in entropy. Therefore, the mixing enthalpy has to be negative, to make polymer spontaneously mix.

Many polymers are miscible when a small amount of the other component is added, but immiscible for high loading content [3-5].

### **1.1.2 Evolution of Polymer Alloys and Blends**

The historical evolution of the polymer blend technology is in the following order:

- 1) Commodity resins (Styrenics, Acrylics, PP etc.)
- 2) Engineering resins (PA, PC, PPE etc.)
- 3) Specialty resins (PSF, PAE, PPS, LCP, PEI, PEA, etc)

#### **1.1.2.1 Commodity resins and their blends**

The commodity resins represent 71% of all consumed plastics in the world market. Specific film formulations were commonly based on polyolefin blends in order to achieve the proper balance of processing, environmental stress crack resistance, modulus, toughness, transparency, filler acceptance, printability, tear resistance, shrinkage characteristics and permeability. In blends of PE or PP with PS, polystyrene offers higher modulus and lower shrinkage during molding while the polyolefin's offer improved toughness and chemical resistance. Blend of PS and PE have been commercial as biaxially oriented, filled films for printable water resistance.

#### **1.1.2.2 Elastomer Blends**

The blending of different types of rubbers and then curing into the final product such as automotive tires has been known in the rubber industry. Blending has been an alternative and lower cost approach to making thermoplastic elastomers compared to the block copolymer. An important need for developing the commercial blends containing a high

volume fraction of a rubbery polymer and minor amounts of a rigid, amorphous or crystalline thermoplastic is to combine the elastomeric character of the rubber component with the melt processability of the thermoplastic. For example in the case of NBR/EPDM blend EPDM is saturated non polar rubber with poor solvent resistance and poor adhesion. Blending of EPDM with NBR with excellent solvent resistance and adhesion properties can improve the disadvantage of EPDM.

### **1.1.2.3 Engineering Polymer Blends**

Emerging applications of engineering polymer blends include automotive panel and food packaging. Blends, which could offer an interesting combination of properties with proper compatibilization, include PPS/PSF, PEI/PPS, PA/PEI, and PC/PPS.

### **1.1.2.4 Recyclable blends**

Syndiotactic polystyrene (sPS), are prepared by blending sPS with a copolymer of styrene and with an elastomer, *e.g.*, SEBS, SBS, SBR. The compositions are reported to maintain good impact resistance, elongation and retention of physical properties upon recycling. Another example is the recycling of automobile panels made up of PC-ABS blends. Several studies have revealed that the effective recycling of compatible PC-ABS mixtures, which were found to be independent of either the blend composition or the chemical constituent of SAN in the ABS [6].

### **1.1.2.5 Polyolefin Blends**

Polyolefin (PO) constitutes the largest group among all the commercial thermoplastics. Recently the usages of polyolefin blends have



increased due to the increased applications in medicine and packaging. HDPE, LDPE, LLDPE and polypropylene are the four most widely used polyolefins. D. Curto *et al.* studied the rheological behavior of HDPE/LDPE blends and they observed synergetic properties of the both [7].

### 1.1.3 Review on Polymer blends

#### (a) *Polystyrene (PS) / Poly (methyl methacrylate) (PMMA)*

Polystyrene (PS) and Poly (methyl methacrylate) (PMMA) are immiscible and combination of PS and PMMA can be used to prepare an antireflection coating for glass. Xue Li *et al.* studied the effect of molecular weight of PS on the surface morphologies and thermal stabilities of PS/PMMA blend and they reported that the surface morphology of PS/PMMA blend was controlled by the annealing conditions and polymer molecular weight [8]. The surface properties of PS/PMMA blends nanostructured polymeric layers were reported by Prosycevas *et al.*. According to them the formation of blend morphology could be explained by two factors: difference in the solubility of the two polymers in the solvent and rewetting of PMMA-rich domains from the PS-rich phase [9].

#### (b) *Polycarbonate (PC) / Poly (methyl methacrylate)(PMMA)*

Bisphenol A polycarbonates (PC)/poly (methyl methacrylate) (PMMA) have received attention because of their potential application as gas separation membrane, pearl material, substrate of the optical data storage discs, packaging material, etc. Specific interactions in polycarbonate (PC)/poly (methyl methacrylate) (PMMA) blends were studied by A.K. Singh *et al.* and they reported that there were specific interactions between PC and PMMA [10]. The morphology, miscibility and mechanical properties

for polymethyl methacrylate/polycarbonate (PMMA/PC) polymer blends prepared by solution casting method were reported by Manasvi Dixit *et al.* and they concluded that the increase in the PC content in PMMA matrix reduced the mobility of main chain movements and enhanced the toughness of PMMA/PC blends [11].

(c) *High density polyethylene / Polystyrene blend*

Polystyrene (PS) and high density polyethylene (HDPE) are two of the most widely used plastics in the world. PS is an example for high modulus material that has limited impact resistance, whereas polyethylene is an example for tough material that has poor stiffness. An increase in impact strength of PS can be achieved by adding HDPE. PS/HDPE blends exhibit more balanced properties, which are advantageous for a number of applications, e.g., in packaging where different barrier properties of HDPE and PS can be beneficially combined [12]. Kyonsuku Min *et al.* reported the phase morphology, rheological properties, and processing behavior of mechanical blends of polystyrene (PS) and a high density polyethylene (PE) blend and they studied the melt spinning and extrudate behavior of blends. They reported that additional small amounts of PE to PS greatly increased its shrinkage [13].

(d) *Polypropylene/Polystyrene blend*

*Polypropylene*

PP is the third-largest volume polyolefin and one of the major plastics used worldwide. In 1954, G. Natta of Milan following the work of K. Ziegler in Germany found that Ziegler-Natta catalyst were capable of producing high molecular weight polymers from propylene and the

commercial PP was first introduced by Montecatini as Moplen in 1957. PP is a linear hydrocarbon polymer containing little or no unsaturation. Semi crystalline PP (Figure 1.1) is a thermoplastic material containing both crystalline and amorphous phase and the amount of each phase depends on structural and stereochemical characteristics of the polymer chain. Polypropylene has excellent physical, mechanical and thermal properties when used in room temperature.

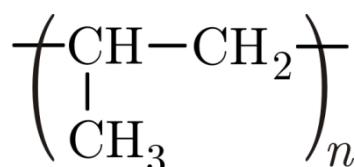


**Figure 1.1 Structure of Polypropylene**

PP has excellent electrical and insulating properties, chemical inertness, and moisture resistance and it is resistant to a variety of chemicals at relatively high temperatures and insoluble in all organic solvents at room temperature. PP is free from environmental stress cracking. PP is used in applications ranging from injection-molded and blow-molded products, fibers and filaments to films and extrusion coatings. It is relatively stiff and has high melting point, low density and impact resistant [14, 15].

### *Polystyrene*

Polystyrene (Figure 1.2) is a clear, colorless commodity polymer widely used in automobiles, consumer electronics, insulation and packaging. Polystyrene consists of a carbon backbone saturated with hydrogen, with one hydrogen in each mer unit replaced by an aromatic ring. PS is clear, hard, easily processed and low cost. Because of the excellent properties, PS

is now used in electrical/electronic, automotive and industrial films applications. The major problem with polystyrene is low impact strength and poor chemical resistance [16, 17].

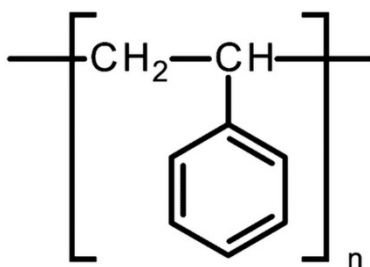


**Figure 1.2 Structure of Polystyrene**

#### *Polypropylene/ Polystyrene (PP/PS) blend*

An important characteristic of PP/PS blend is the impact strength/stiffness that reportedly exceeds the performance of conventional PP and with those of other engineering resins such as acetals, PC/ABS, PC/PBT. The reinforced grades reportedly exhibit improved stiffness and creep resistance compared to PP alone and may compete against reinforced polyamides and polyesters, in applications that do not require high temperature performance. Typical applications in development with PP/PS blends include automotive bumper beams, pillars, sporting and recreational equipment, sledge hammer handles and other consumer tools & appliance components. Blending amorphous and semi crystalline polymers give higher  $T_g$  of the amorphous PS, reinforce the PP matrix yields higher strength and heat distortion temperature, while the high  $T_m$ , high melt flow characteristics of PP are maintained. The semi crystalline polymer offers solvent and chemical resistance and the amorphous polymer yields the rigidity, melt strength & dimensional stability. The PP/PS blend is used for the manufacture of

molded parts of vehicle interior parts and trims because of its high scratch resistance and matte surface, tactile properties. In such applications they can substitute painted parts from ABS [2, 18].

Kazuhiro Yoshida *et al.* reported the effects of bulk morphology on the mechanical properties of PP/ PS blend and they found out that the crystallinity of PP influenced the mechanical properties of PP/PS blend and also they reported that the adhesion between the PP matrix and PS droplets was poor [19]. Wantinee Viratyaporn *et al.* investigated the impact resistance of PP/PS blend in their study and they reported that PS/PP blend appeared to be an excellent engineering material from the perspective of tensile modulus and impact resistance [20]. Mitsuyoshi Fujiyama *et al.* studied the structure and properties of injection molded PP/PS blend and they found out that flexural properties are increased and crystallization temperature decreased by PS content [21]. Especially PP/PS blends exhibit low impact strength, low wear resistance and high friction. Several problems of these blends may be due to the poor compatibility of the blend components and these problems can be improved by using compatibilizers.

## 1.2 Role of compatibilizers in blending processes

Compatibilizers are macromolecular species, which exhibit interfacial activities in heterogeneous polymer blends. The role of compatibilizers in the polymer blending is to decrease interfacial tension. Good interfacial adhesion is required for stress transfer from one phase to the other and for cracks initiated at the interface has to be prevented from growth until catastrophic failure occurs. Refinement and stabilization of the phase morphology and the enhancement of the interfacial adhesion improve an inferior immiscible

polymer blend to a new material in which the beneficial properties of both blend components are united. Compatibilizers reduce particle size by lowering the interfacial tension, preventing particles from coalescing, and results in an increase of adhesion at the interface, which results in improved properties [22].

Most of the commercially used compatibilizers are random copolymers, block copolymers consisting of dissimilar blocks. The design of nanostructured blends creates opportunities to develop new materials which can be used for specific applications. The three major classes of compatibilizers can be distinguished from each other in terms of the mechanism by which they reduce the interfacial tension between incompatible polymers [23, 24].

### **1.2.1 Types of compatibilizers**

#### **1.2.1.1 Block or graft copolymers**

A heterogeneous blend of polymers I and II can be compatibilized by a diblock copolymer poly (C-b-D), in which block C is miscible with polymer I and that block D is miscible with polymer II. Each block of a poly (I-b-II) compatibilizer penetrates into the parent phase to be entangled with the constitutive chains and thus the interfacial adhesion is enhanced. Good interfacial adhesion is important for the effective stress transfer from one phase to the other and the cracks initiated at the interface to be prevented from growth until catastrophic failure occurs. For example,  $\omega$ -dihydroxy PS has been synthesized as a macro monomer for the synthesis of poly (PBT-g-styrene) [25].

#### **1.2.1.2 Nonreactive polymers containing polar groups**

In this type of compatibilization specific interactions are introduced into the blend by chemical modification of the blend components using suitable functional groups. In this type of compatibilization, a drop in the interfacial tension and an increase in the interphase thickness can also be observed. For polymer combinations with very large differences in polarity, a certain degree of compatibility between the two phases can be induced. e.g. Styrene has been copolymerized with sulphonated styrene [2].

#### **1.2.1.3 Reactive functional polymer for compatibilization**

A reactive polymer which is miscible with one blend component and reactive towards functional groups attached to the second blend component results in the formation of block or grafted copolymers. Reactive polymers can be generated by free radical copolymerization or by melt grafting of reactive groups on to chemically inert polymer chains at the interface of an immiscible polymer blend. Maleic anhydride is the most commonly used type of reactive group in such polymers. Some of these types of polymers are often effective as coupling agents between polymers and inorganic fillers in composites [26].

#### **1.2.1.4 Addition of low molecular weight chemicals**

A different strategy for blend compatibilization relies upon the addition of low molecular weight chemicals. Various procedures may be described, depending on the added chemical:

- a peroxide, that activates inert polyolefin and results in the formation of branched copolymer
- a bifunctional chemical that forms block copolymer

- a mixture of a peroxide and a bifunctional chemical, which leads to the formation of branch or graft copolymer

One of the recent techniques for the compatibilization of polymer blend involves the addition of just one chemical, i.e. peroxide, to an incompatible blend. Maleic anhydride (MA) and citric acid are examples of chemicals with two different functionalities used to compatibilize PPO/PA (rubber) blends. MA is reactive with the phenolic end groups of the PPO chains and with the amine end groups of the PA chains [4].

#### **1.2.1.5 Interchange reactions**

When two or more polycondensates are blended in the melt, several interchange reactions can occur and it depends up on the type of polymers, nature and concentration of the reactive, blending temperature, moisture content, residence time in the melt and the presence and concentration of an interchange catalyst. PC, PET, PBT, and PA have attracted the most attention by interchange reactions compatibilization including ester interchange, amide interchange, amide ester exchange, transesterification, aminolysis, and acidolysis [27].

#### **1.2.1.6 Addition of selective crosslinking agents**

Compatibilization of polymer blends by the addition of low molecular weight chemicals requires that both blend components to participate in chemical reactions which results in the formation of grafted or block copolymers, further affecting the development of the blend morphology. Dynamic vulcanization, i.e. the selective crosslinking of the dispersed phase, prevents it from undergoing coalescence. For example sulphur/ accelerator



combinations are used as a crosslinking agent for the vulcanization of PP/EPDM blend.

#### **1.2.1.7 Compatibilization by ionomers**

Ionomers are polymeric species carrying low number of pendant ionic groups per molecule. Mostly, the ionic groups result from neutralization of sulphonic acid or carboxylic acid groups. These groups are inserted into the polymer chains by copolymerization or chemical modification of existing polymers and at elevated temperatures, these ionic crosslinks become reversible. If two different ionomers which based on immiscible polymers are mixed in the melt, the ionic domains may reorganize and the newly formed clusters may contain ionic species of both immiscible polymers. As a result a branched copolymer is generated at the interface result in the formation of stable compatibilized multiphase blend. e.g.: compatibilization of PC/PVDF by zinc carboxylate containing poly (methylmethacrylate) ionomers [28].

#### **1.2.1.8 Compatibilization by fillers**

Several groups have reported that when nanoscale fillers are added to polymer blend, both the dynamics as well as the morphology of the blend can change. Recently, an original concept of compatibilization by using nano-particles like silica nano-particles, carbon nanotube has been proposed [29-31]. A Karim *et al.* [32] first reported that transient surface directed lateral concentration gradients were formed around particle inclusions and it is similar to those observed at planar interfaces. Ginzburg *et al.* [33] reported that strong interactions between the fillers and one of the phases hinder the coarsening of the interfaces. Yan ZHU [34] *et al.* reported a novel

compatibilization mechanism, “cutting” to compatibilize the immiscible PP/PS blends. The organoclay platelets tend to form a “knife-like structure” in the PS domain under the shear stress of the continuous PP phase during compounding. The “clay knife” can split the dispersed PS domain and results in reduction of PS domain size and enhanced dispersion. W. Zhang *et al.* reported that functionalized nanoparticles can be used as a compatibilizer for polymer blend and it can improve the properties of blend such as flammability and mechanical properties [35].

#### 1.2.1.8.1 Types of nano fillers

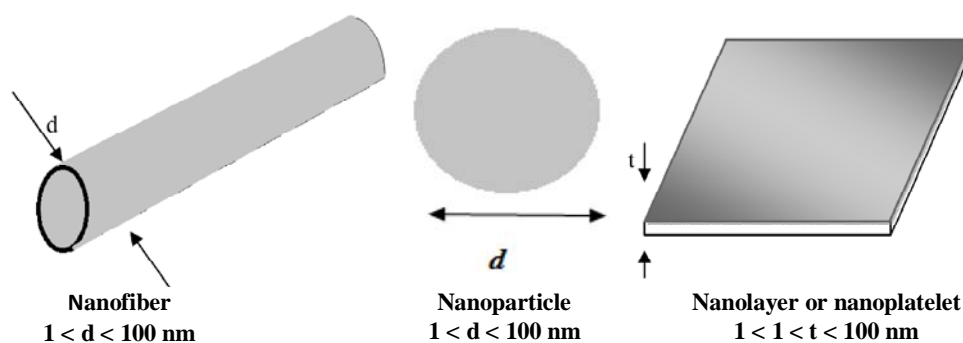


**Figure 1.3** Various types of nanofillers

The particles in the range of nanometer from 1nm to 1 $\mu$ m could be called as nanoparticles but most frequently nanoparticles are in the size range of 1–100 nm. Their chemical and physical properties differ from those of the bulk solids. Nanoscale fillers are grouped into three categories. Fiber or tube fillers have a diameter <100 nm and an aspect ratio of at least 100. Plate-like nanofillers are layered materials with a thickness on the order of 1nm, but with an aspect ratio in the other two dimensions of at least 25. Three dimensional (3D) nanofillers are equi-axed particles <100 nm in their largest dimension [36, 37].

### **1.3 Polymer nanocomposites**

Polymer nanocomposites have attracted great attention academically and industrially due to the superior properties such as modulus, strength, toughness and barrier far from those of conventional micro composites and with those of metals. In polymer nanocomposites, the filler has at least one dimension in the nanometer scale and its nanoscale dispersion within the polymer matrix leads to the improved interfacial interaction between the polymer and inorganic filler which causes to the superior properties than that of pure polymer. The nanoscale is counted where the dimensions of filler particles (diameter), platelets (thickness) or fibers (diameter) are in the size range of 1-100nm (Figure 1.3). Properties such as mechanical, thermal, barrier, durability, chemical stability, flame retardancy, scratch/ wear resistance, biodegradability as well as optical, magnetic and electrical properties can be improved by nanocomposite technology. The end properties of a nanocomposite are determined by the component properties, composition, micro-structure and interfacial interactions. Clays are one group of nano-fillers which have been widely used for the preparation of polymer nanocomposites. Recently there has been a growing interest for the development of polymer/clay nanocomposites due to their improved properties compared to the conventional filled polymers in very low filler. Clay minerals are belonging to a main group of silicates with layered structure known as layered silicates [38, 39]. Organoclays are qualified as “inorganic” compatibilizers for two reasons. Surface modified organoclays, can form in-situ grafts by absorbing many matrix polymer chains of both polymers. This will lower the interfacial tension between the immiscible polymers and also the plate-like organoclays, in a stacked structure, have narrow gaps between each plate. The absorption

of polymer chains on plate decreases the chain mobility, which retards phase growth by coalescence.

Cellulose is considered to be one of the abundant natural biopolymer in the world. Recently a number of high-performance materials are developed using the high-strength micro and nanocellulosic fibers for industrial applications. Nanocellulose is biosynthesized from a number of living organisms ranging from higher to lower plants, some amoebae, sea animals, bacteria and fungi.

#### **1.4 Nanoclay**

Clay is a naturally occurring material composed of fine-grained minerals, which show plasticity through a varying range of water content, and which can be hardened when dried or fired. Clay deposits are mostly composed of clay minerals (phyllosilicate minerals) and water is trapped in the mineral structure by polar attraction. Figure 1.4 illustrates the images for the comparison of various types of clays.

Clay minerals include the following groups:

- Kaolin group which includes the minerals kaolinite, dickite, halloysite and nacrite. Some sources include the serpentine group due to structural similarities.
- Smectite group which includes dioctahedral smectites such as montmorillonite and nontronite and trioctahedral smectites for example saponite.
- Illite group which includes the clay-micas. Illite is the only common mineral.

- Chlorite group includes a wide variety of similar minerals with considerable chemical variation.

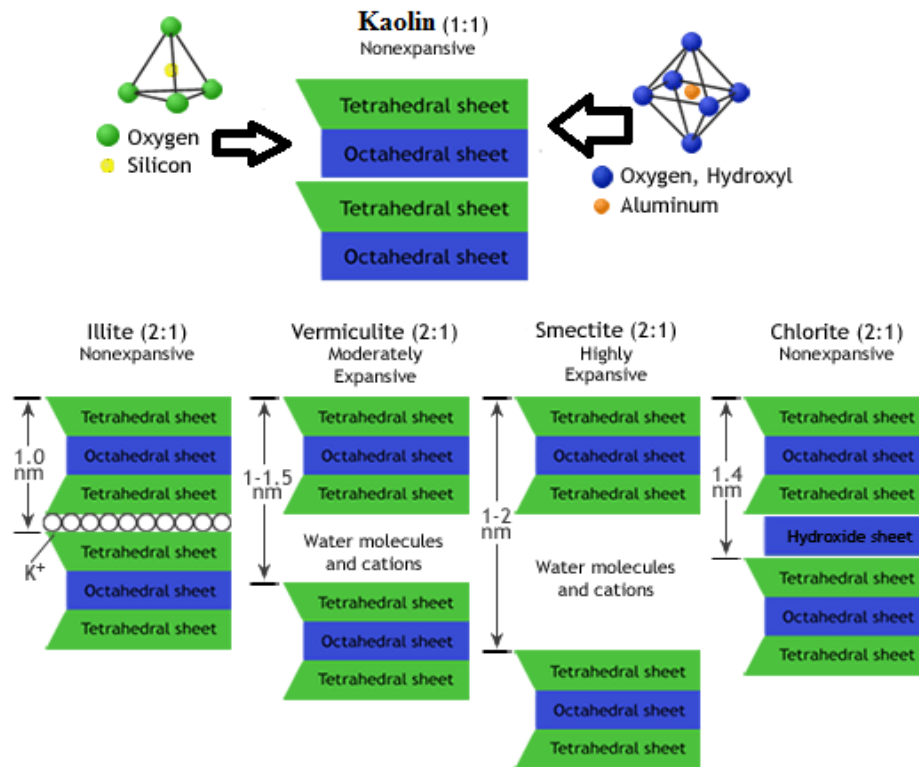


**Figure 1.4 Comparison of various types of clays**

Clay minerals are characterized by

- Two-dimensional sheets of corner sharing  $SiO_4$  and  $AlO_4$  tetrahedra and these tetrahedral sheets have the chemical composition of  $(AlSi)_3O_4$ , and each tetrahedron shares 3 of its vertex oxygen atoms with other tetrahedra forming a hexagonal array in two-dimensions as given in Figure 1.5. The fourth vertex is not shared with another tetrahedron and all of the tetrahedra "point" in the same direction.

- 2) In clays the tetrahedral sheets are always bonded to octahedral sheets formed from small cations, such as aluminum or magnesium, coordinated by six oxygen atoms as shown.
- 3) The unshared vertex from the tetrahedral sheet also form part from one side of the octahedral sheet but an additional oxygen atom is located above the gap in the tetrahedral sheet at the center of the six tetrahedra and this oxygen atom is bonded to a hydrogen atom forming an -OH group in the clay structure.

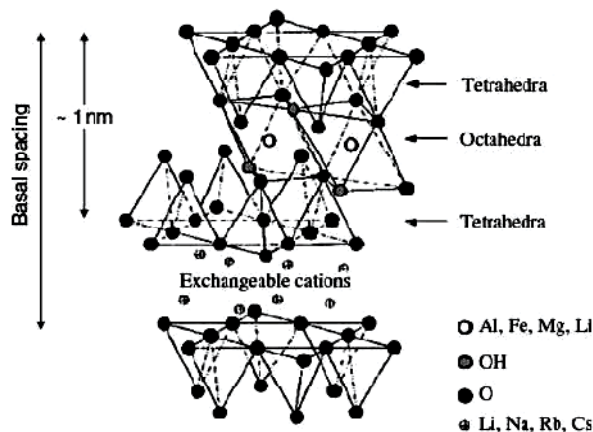


**Figure 1.5 Structure of a layered silicate [40]**

- 4) Clays can be categorized depending upon the way that tetrahedral and octahedral sheets are packaged into layers. If there is only one tetrahedral and one octahedral group in each layer; the clay is known as 1:1 clay. The two tetrahedral sheets with the unshared vertex of each sheet pointing towards each other and forming each side of the octahedral sheet is 2:1 clay.
- 5) Depending upon the composition of the tetrahedral and octahedral sheets, the layer will have no charge, or will have a net negative

charge. If the layers are charged, then this charge is balanced by interlayer cations such as  $\text{Na}^+$  or  $\text{K}^+$  and in each case the interlayer can also contain water. The crystal structure is formed from the stack of layers interspaced with the interlayer [41].

### 1.4.1 Kaolin clay

Kaolin [Figure 1.6] is the common name comprised totally or substantially of the aluminum silicate clay mineral kaolinite. Kaolin is a clay mineral with the chemical composition  $\text{Al}_2\text{Si}_2\text{O}_5(\text{OH})_4$ . Milled and air-classified grades of raw kaolin contain small amounts of related sheet silicates like mica, illite, chlorite, smectite and quartz. Kaolin has a platy structure; its value in coatings derives more from its contribution to optical properties than to physical properties.

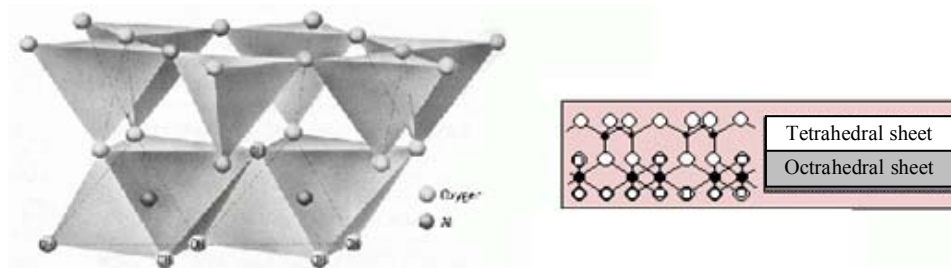


**Figure 1.6 Structure of Kaolin clay**

Kaolin ( $\text{Al}_2\text{Si}_2\text{O}_5(\text{OH})_4$ ) is a 1:1 phyllosilicate containing a gibbsite octahedral layer and a silicon oxide tetrahedral sheet and there is a certain degree of Van der Waals attraction and hydrogen bonding between the hydroxyl groups of the gibbsite layer and the oxygen atoms of the adjoining silica layer, providing a large cohesive energy. The ability to modify clay by insertion of an organic guest species into the layers opens up a range of uses

for these materials. Smectite clays possess exchangeable cations within their interlayer that facilitate the encapsulation of polar organic molecules and kaolin has no exchangeable cations within their layers [42]. The insertion of organic molecules into kaolin is obtained by guest displacement method. Displacement involves the replacement of a directly intercalated species (e.g., NMF, urea etc.) by a second organic molecule and the kind of guest species intercalated between the layers of kaolin is limited due to the hydrogen bonding between the octahedral side and tetrahedral side. The interlayer bonding between kaolin develops from the hydrogen bonding between the inner surface hydroxyl groups of the octahedral gibbsite-like sheet and the oxygen of the adjacent tetrahedral siloxane sheet. Because of the hydrogen-bonding between its layers, kaolin has often been classified as non-expandable. Limited number of polar guest species such as N-methylformamide (NMF), Urea, Dimethylsulfoxide (DMSO) can be directly intercalated. Six requirements need to be satisfied for guest molecules to be intercalated successfully into kaolin: (1) the hydrogen bonds should be broken; (2) the d- spacing of the clay has to be expanded; (3) the organophilicity of kaolin has to be modified; (4) the intercalation guest must have strong polarity; (5) the intercalation guest monomer must be of an appropriate size and (6) the intercalated organic molecule should be bound with some functional group in the clay such as an hydroxyl of  $\text{Al}_2(\text{OH})_4$  octahedral sheets, an oxygen atom of a  $\text{SiO}_4$  tetrahedron, or both [43].

The reactive guest molecules are classified into three types by Weiss et al. is as follows:



- Compounds like urea, formamide (Figure 1.7), hydrazine etc. which can form strong hydrogen bond with silicate layers and it contains suitable hydrogen bond with silicate layers.

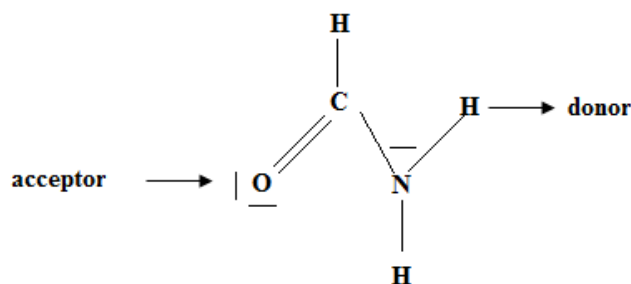


**Figure 1.7 Structure of formamide**

- Compounds with the possibility of strong dipole interactions with silicate layers like dimethyl sulphoxide (DMSO) (Figure 1.8).

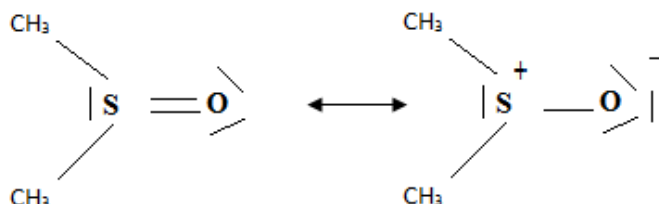


**Figure 1.8 Structure of DMSO**

- Alkali salts ( $\text{K}^+$ ,  $\text{NH}_4^+$ ) of short chain fatty acids [44, 45].

## 1.5 Polymer clay nanocomposites

Polymer/clay nanocomposites (PCN) have received intense attention and research interest because of the unique properties which can never be obtained by micro size fillers. The concept of PCN was developed in the late 1980s and Toyota was the first company to commercialize these

nanocomposites. PCN is a class of hybrid materials made from nanoscale particles such as layered silicates with layer thickness in nanometer dimension. Several applications have been identified in various industrial sectors, for example automobiles (gasoline tanks, bumpers, interior and exterior panels etc.), construction (building sections, structural panels), aerospace (flame retardant panels, high performance components), electronics and electrical (printed circuit boards, electric components), food packaging (containers, wrapping films), and coatings and pigments. Since the improvements in the material properties in a nylon-6/clay nanocomposite demonstrated by the Toyota research group, numerous other polymers have been investigated by many researchers around the world. These include, but are not limited to, Polypropylene[46-48], Polyethylene,[49-51] Polystyrene[52,53], Poly(ethylene oxide)[54,55], Polycaprolactone[56,57], Polyimides[58] Polyamides[59], Poly(ethyleneterephthalate) [60], Polycarbonate [61], Polyurethane[62] and epoxy resins[63].

### **1.5.1 Preparative methods and structure of polymer clay nanocomposites**

#### **1.5.1.1 Intercalation of Polymer or Prepolymer from Solution**

This method is based on a solvent system in which polymer or prepolymer is soluble and the silicate layers are swellable. The layered silicate is first swollen in a solvent, such as water, chloroform etc. when the polymer and clay solutions are mixed and the polymer chains intercalate and displace the solvent within the interlayer of the clay particles. Upon solvent removal, the intercalated structure remains, resulting in polymer clay nanocomposites. For example G. Jeon *et al.* [64] applied this technique for the preparation of nanocomposites of nitrile-based copolymer and

polyethylene-based polymer with organically modified MMT. Sur *et al.* [65] applied this technique for the preparation of polysulfone (PSF)-organoclay nanocomposites.

#### **1.5.1.2 *In-situ Intercalative Polymerization Method***

In this type of polymerization method, organoclay is swollen within the liquid monomer or a monomer solution so that the polymer formation can occur in between the intercalated sheets. Polymerization can be initiated either by heat or radiation or by the diffusion of a suitable initiator, or by an organic initiator or catalyst fixed through cation exchange inside the interlayer before the swelling step by the monomer.

#### **1.5.1.3 *Melt Intercalation Method***

Melt intercalation method involves annealing, statically or under shear, a mixture of the polymer and organoclay above the softening point of the polymer. This method has great advantages over either in-situ intercalative polymerization or polymer solution intercalation. First, this method is environmentally benign due to the absence of organic solvents and second is compatible with current industrial process, such as extrusion and injection molding. The melt intercalation method allows the use of polymers which were previously not suitable for other two methods [66, 67].

There are three possible arrangements of layered silicate clays, which can be obtained when they are dispersed in a polymer matrix:

Conventional micro composite is formed if the polymer cannot intercalate between the silicate sheets. Beyond this traditional class of

polymer-filler composites, two other types of composites can be obtained. An Intercalated structure is the separation of clay layers by increasing the interlayer spacing and exfoliated or delaminated structure is the complete separation of clay platelets into random arrangements. This is the ideal nanocomposite arrangement but is harder to achieve during synthesis and or processing. Figure 1.9 depicts the schematic representation for the possible arrangements of clay layers in polymer matrix.

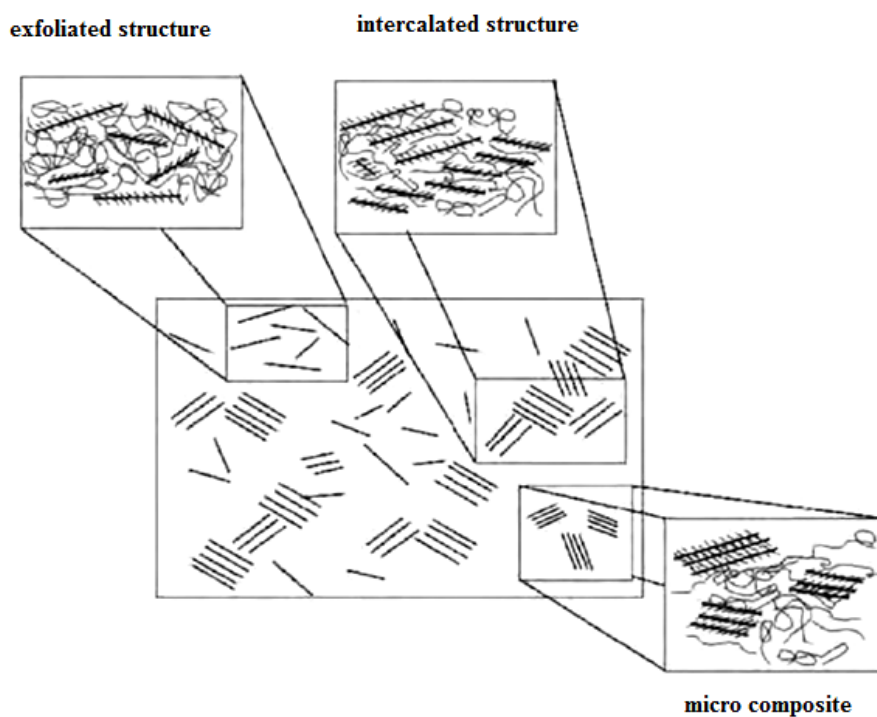


**Figure 1.9 Schematic representation for the possible arrangements of clay layers in polymer matrix**

### 1.5.2 Properties of Nanocomposites

Several properties like mechanical strength, thermal properties, flammability and barrier properties of polymer nanocomposites are improved

when compared to neat polymer counterparts. The extent of the enhancement is dependent on the type of polymer and nanoclay used as well as the extent of dispersion of the nano-particle within the polymer matrix.

#### **1.5.2.1 Mechanical Properties**

The modified organoclays improved the mechanical properties of the polymer even with a low level of filler loading, 1-5 wt%. At a low filler loading, polymers such as Nylon-6 show significant improvement in mechanical properties like increase in Young's modulus of 103%, and in tensile strength of 49%. For composites with good interaction between filler and matrix, the mechanical properties tend to increase with increasing volume fraction and decreasing particle size.

#### **1.5.2.2 Barrier properties**

Barrier properties against oxygen, carbon dioxide, ultraviolet, moisture and volatiles are the most important properties that a nanocomposite food packaging can offer. The improvement in the barrier properties by incorporation of nanoclays in the polymer matrix can be explained by the layered clay sheets as impermeable obstacles in the path of the diffusion process. In a well exfoliated and dispersed state, individual clay platelets are believed to increase the barrier properties by creating a maze or 'tortuous path' that retards the progress of gas and vapor molecules through the polymer matrix. It has been found that moisture absorption and diffusion is dependent on the type of organoclay used [68]. Examples include packaging for processed meat, cereals, cheese etc. The use of nanocomposites in packaging application expected to enhance the shelf life of many types of

foods. Figure 1.10 gives the schematic presentation for the formation of 'tortuous path' in a polymer clay nanocomposite

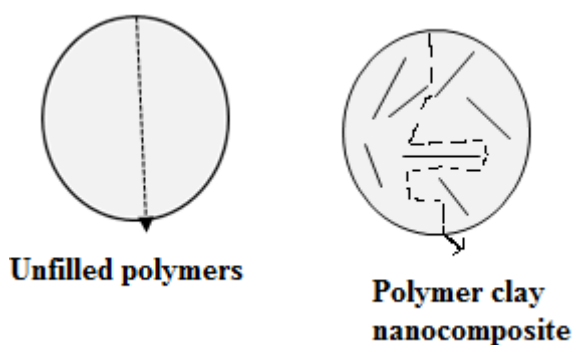


**Figure 1.10** Schematic presentation for the formation of 'tortuous path' in a polymer clay nanocomposite

### **1.5.2.3 Biodegradable polymer clay nanocomposites**

In recent years lot of research has been carried out on biodegradable polymers as packaging materials in order to reduce the environmental pollution caused by plastic wastes. This special class of polymer follows microbially induced chain scission leading to mineralization, called biodegradation, under a few conditions such as pH, humidity, oxygenation and the presence of some metals. Biodegradability of the biodegradable polymers is significantly improved by the addition of nanoclay. Toyota Technological Institute commercialized PLA/layered silicate nanocomposites for packaging and short term disposable applications. Biodegradable polymers such as starch, polylactic acid (PLA) and polycaprolactone (PCL) have attracted attention in the packaging industry [69].

### **1.5.2.4 Flammability reduction**

The improvement in flammability is due to the char formation during the nanocomposite combustion. The char formed on the surface during

burning insulates the underlying material and reduces volatile products escape into the flame area. This property can determine by measuring the heat release rate (HRR) of the nanocomposites.

As a result of the platelet orientation in polymer clay nanocomposites; it shows dimensional stability in two dimensions instead of one for isotropic fillers. R.A.Vaia *et al.* [70] reported that an intercalated PEO/ clay nanocomposites showed higher ionic conductivity at lower temperature when compared to conventional PEO/LiBF<sub>4</sub> mixture and this increase was due to the fact that the PEO was not able to crystallize when intercalated hence nonconductive in nature. The intercalation of clay particles within the polymer matrix found to increase the solvent resistance of clay nanocomposite and as a result the potential usage of these materials in fuel tank and fuel line components for car was also increased. The other properties that are strongly affected by the addition of clay particles are optical transparency and scratch resistance. The presence of nanoclay is found to enhance the transparency and reduce haze. Both intercalated and exfoliated structure show higher thermal stability when compared to conventional microcomposites and this may be due to the decreased permeability of volatile products due to the homogeneous dispersion of clay particles [71].

### **1.5.3 Applications of Polymer clay nanocomposites**

The most common use of polymer-clay nanocomposites is in mechanical reinforcement of thermoplastics. Polyamide-6 clay nanocomposite produced by Ube/Toyota was used to replace a metal component near the engine block that yielded some weight savings. The clay in this application improved the heat distortion temperature of the material. Polymer clay nanocomposites

are used in various fields of injection molding; engine cover, timing belt cover, oil reservoir tank and fuel house. The timing belt covers made from Nylon-6 clay hybrid nanocomposite by injection molding was the first example of polymer clay nanocomposites. Another use of polymer-clay nanocomposites is in flame retardant applications; especially the clay nanocomposite can replace part of the flame retardant package while maintaining fire safety ratings at a lower flame retardant loading. Clay nanocomposites can also be used for gas-barrier materials. Nano clays create a complex network in the polymer matrix, such that various gases either diffuse very slowly or not at all through polymer chains and pinholes in thin films or thicker polymer parts. It is used in food packaging applications. Polymer clay nanocomposites are used in the manufacture of automotive parts and also in wire and cable applications. Due to its stability against aggressive chemicals, they are used in corrosive protective coating [72, 73]. Nanocomposites can also be used in the improvement of ablative properties in aeronautics.

#### **1.5.4 Polymer blend clay nanocomposites**

Nanocomposites based on polymer blends have attracted increasing attention among the scientists because the compounding may lead to a new kind of high performance material, which may combine the advantages of the polymer blends and the merits of polymer nanocomposites together. Sangah Gam *et al.* investigated the phase separation of poly (methyl methacrylate) (PMMA) / poly (styrene-ran-acrylonitrile) (SAN) films with thickness from 140 nm to 2500 nm and silica NP concentrations from 1 to 10 wt%. Directed interfacial segregation of nanoparticles (NPs) at the interphase of phase-separated polymer blend film stabilizes the film in either bicontinuous



(3D) or discrete (2D) structures [74]. M. Hemmati *et al.* studied the effects of the nanoclay concentration and the mixing rate on nanoclay dispersion and the properties of the polyethylene/polyamide (PE/PA). Enhanced mechanical properties (including elasticity modulus and yielding stress) were obtained due to the presence of PA6 and the higher nanoclay content [75]. Hee B. Kim *et al.* studied the polymer blend/ organoclay nanocomposite at a fixed blending ratio was prepared using equal ratio of poly (ethylene oxide) (PEO) and poly (methyl methacrylate) (PMMA) via solvent casting method. Results showed that the increase of elasticity at a low frequency region had originated from the nanoscopic interaction between polymers and OMMT [76]. Anup K. Dhibar *et al.* [77] studied the cocontinuous phase morphology of asymmetric compositions of polypropylene/high-density polyethylene blend by the addition of clay and it was observed that the barrier effect of the clay platelets in the HDPE phase that restricted the phase inversion into the domain/matrix morphology. Y. Deyrail *et al.* reported the compatibilization of Polyamide/ Polystyrene blend by montmorillonite nanoclay and its effect on macroporosity of gas diffusion layers for proton exchange membrane fuel cells. They reported that MMT clay addition resulted in a modification of pore size distribution, which might be interesting to produce highly conductive GDLs with controlled porosity for the anode and the cathode [78]. Joung Sook Hong *et al* investigated the migration of clay and its localization in multiphase blend nanocomposite systems during the evolution of PBT/PS blend morphology and they found out that the blend morphology depended on the location of clay and its dispersion [79].

### 1.5.5 Hybrid composites based on nanoclay

Hybrid composites are materials made by combining two or more different types of fillers in a single matrix which leads to a great diversity of material properties. The reinforcement may be different types of fibers, particulate fillers or both. Hybridization results in fabricating products with reduced cost, high specific modulus, strength, corrosion resistance and thermal stability. Studies have revealed that the behavior of hybrid composites appears to be the weigh sum of the individual components in which there is more favorable balance between the advantages and disadvantages inherent in any composite material. The properties of hybrid composites are controlled by factors like nature of matrix, length and relative composition of the reinforcements, fiber- matrix interface and hybrid design [80]. Maries Idicula *et al.* studied the short randomly oriented banana and sisal hybrid fiber reinforced polyester composite and they reported that the mechanical properties of the hybrid composites showed a positive hybrid effect when the volume ratio of the fiber was varied in the hybrid composites at each fiber loading [81]. Maya Jacob *et al.* reinforced natural rubber with oil palm fiber and untreated sisal fiber and they found out that increasing the concentration of fibers resulted in reduction of tensile strength and tear strength, but improved modulus of the composites [82]. Al-Mosawi Ali evaluated the mechanical properties of epoxy composites reinforced with hybrid Palms - Kevlar fibers and they reported that there was an increase in mechanical properties with increasing reinforcement [83].

Recently, works based on nanoclay and glass fibers have also been studied. Due to the superior properties of glass fibers, the modulus of the

composites increases with increase in the volume fraction of glass fibers but results in decrease of strength and toughness. This decrease in properties may be due to the stress concentration, poor fiber-matrix adhesion and confinement of the matrix molecular mobility around the filler phase. The glass fiber composites at higher loading have certain drawbacks like increased molded part weight, brittleness and processing difficulty. To overcome these, hybrid composite with low filler concentration is desirable. Recently, it has been observed that by incorporating nanoclay particles into the fiber reinforced polymer composites would give the high performance for the hybrid composites at low filler loadings. The addition of nanoclay particles into the polymer fiber composites have been shown to give significant improvements in mechanical, barrier, and thermal properties. Normasmira A. Rahman *et al.* reported the similar results in their work [84]. Kusmono *et al.* [85] studied the effect of nanoclay on the properties of polyester resin and they found that the combination of clay and glass fiber had given a synergistic effect on the improvement in strength, stiffness, and toughness of unsaturated polyester (UP) matrix. Liu *et al.* reported that the addition of clay particles to the glass fiber reinforced vinyl ester composites results in the increase of thermal properties and durability [86].

## 1.6 Cellulose

Cellulose (Figure 1.11) is a renewable, biodegradable and the most abundant polymer in the world. Cellulose is an isotactic  $\beta$ -1, 4-polyacetal of cellobiose (4-O- $\beta$ -D-glucopyranosyl-D-glucose). The actual base unit, the cellobiose, consists of two molecules of glucose. The linear polymeric chains form sheets that are held together with hydrogen bonds and then,

these sheets are connected by Van der Waals bonds generating microfibril crystalline structures. The final structure of cellulose consists on crystalline and amorphous regions.

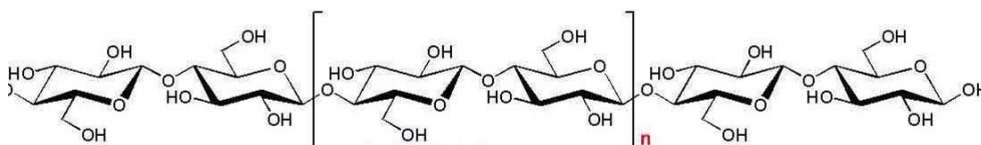


**Figure 1.11 Structure of cellulose**

Natural cellulosic fibers are synthesized mainly in plants and cellulose constitutes 40 to 50% of wood, 80% of flax and 90% of cotton fiber, green algae, some bacteria and animals have cellulose chains in their cell walls. Micro/nanofibrils isolated from natural fibers have much higher mechanical properties. Microfibers are defined as fibers of cellulose of 0.1-1 $\mu\text{m}$  in diameter, with a corresponding minimum length of 5-50 $\mu\text{m}$  while nanofibrils are at least one-dimensional at the nanometer scale (1-100nm). The small fibrils isolated from natural fibers normally have a wide range of diameters, most are below 100nm and some are above 0.1 $\mu\text{m}$  [87, 88]. Sisal leaves are used in this study. Sisal fiber is a hard fiber extracted from the leaves of sisal (Figure 1.12).



**Figure 1.12 Picture of sisal plant**

Sisal fibers are composed of cellulose (50–74%), lignin (8–11%), hemicellulose (10–14%), pectin (1%) and wax (2%) and because of its content; cellulose extraction from these fibers could lead to high quantity of nano fibers [89]. The raw sisal fiber bundles were composed of individual fibers linked together by massive cementing material like lignin, hemicellulose, wax and oils. Hemicelluloses are polysaccharides structurally different from cellulose in terms of several sugar moieties, extensive branching, and having lower molecular mass with a degree of polymerization (DP) of 50 – 200. Lignin is the most abundant natural organic polymer. Lignin is a randomly branched polyphenol, made up of phenyl propane (C<sub>9</sub>) units. Due to the lipophilic character, lignin decreases the permeation of water across the cell walls, which consist of cellulose fibers and amorphous hemicelluloses. Lignin gives rigidity to the cell walls and, in woody parts, together with hemicelluloses, functions as a binder between the cells generating a composite structure with outstanding strength and elasticity [90]. Figure 1.13 depicts a simplified representation in which the plant cell wall can be visualized as a collection of crystalline cellulose microfibrils sheathed by hemicellulose and lignin.

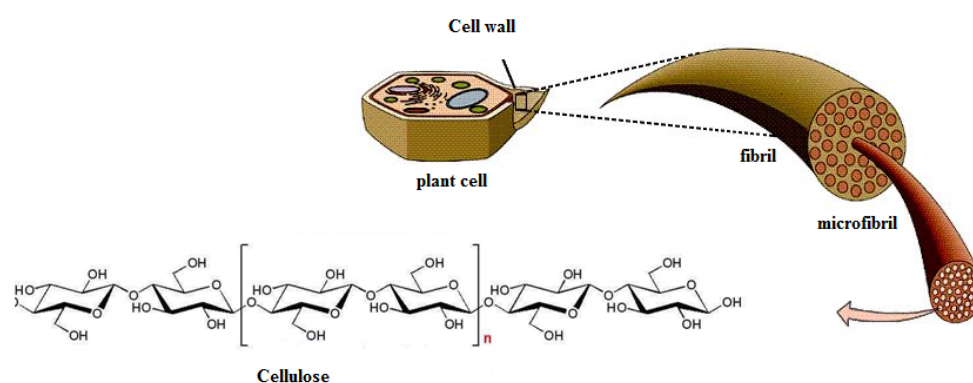


**Figure 1.13. Cellulose microfibril structure**

There is currently a significant interest in the processing of polymeric composites reinforced with nanosized particles. Due to nanoscale effect these nanocomposites display prominent properties when compared to conventional composites prepared from the same source. As a result, many efforts have been focused in recent years on obtaining and using nano fibers obtained from cellulose.

### **1.6.1 Preparative methods of nano cellulose**

Methods for producing microfibrillated cellulose were first reported by Herrick *et al.* [91] and Turbak *et al.* [92]. The principle was to pass dilute cellulosic wood pulp-water suspensions through a mechanical homogenizer [90]. High pressure homogenization is one of the methods used for the isolation of nano fibers. High pressure homogenization process includes passing the cellulose slurry at high pressure into a vessel through very small nozzle and due to the high velocity and pressure as well as impact and shear forces on fluid generates shear rates in the stream and decrease the size of fibers to nanoscale. Another method to break up cellulose into nanosize fibers is grinding. In grinding equipment, there is static and rotating grindstone and pulp slurry passes between these two stones and the mechanism of fibrillation in grinder is to break down of hydrogen bond, cell wall structure by shear forces and individualization of pulp to nanoscale fibers [93]. Cryocrushing is another method for the isolation of nanocellulose which demands the immersion of the water-swollen cellulose material in liquid nitrogen followed by the crushing of the material using a mortar and pestle. This method has been successfully used in the case of kraft fibers after refining [94]. High intensity ultrasonication is a mechanical process where oscillating power is used to isolate cellulose fibrils by hydrodynamic forces

of ultrasound [95]. B.M Cherian *et al.* used steam explosion process for the extraction of cellulose nanofibrils from pineapple leaf fibers [96]. Employing microwave is another way to obtain cellulose fibers disintegration to nano-scale. By gamma ray irradiation of cellulose fibers, a separation of a gas mixture was noticed due to the dehydrogenation, depolymerisation and glucoside chains destruction effects [97]. Nanocrystalline cellulose can be prepared by acid hydrolysis. Hydrolysis was carried out using sulphuric acid with constant stirring and immediately after the acid hydrolysis; the suspension was diluted 10 times with deionized water to stop the reaction. The suspension was centrifuged at 6000 rpm for 10 min in order to concentrate the cellulose and to remove excess aqueous acid. Then the resultant precipitate was rinsed, re-centrifuged, and dialyzed against water for 5 days until constant neutral pH [98]. Alkaline hydrolysis determines the partial separation of the cellulose fibers from the cell wall and an improvement of the physical and chemical characteristics of cellulose and these treatments are usually made using diluted solutions of NaOH (1-10%) at low or high temperatures and concentrated NaOH solutions over 10% only at low temperature. Yan Li *et al.* [99] reported that removal of non-cellulose components from cellulose fibers by enzyme treatment could increase the crystallinity, thermal stability and the amount of -OH groups of the treated fibers. Researchers from Toronto University were the first group that combined chemical treatment, mechanical refining, homogenization, and crushing of the water-soaked material in the presence of liquid nitrogen in order to get cellulose fibers [100]. Saito *et al.* proposed a process to obtain MFC based on TEMPO reaction and strong mixing. In their study individualized MFC was obtained by TEMPO-mediated oxidation at room temperature and stirring at 500 rpm [101, 102].

## 1.6.2 Classification of nanocellulose

Nanocellulose can be classified into three main categories on the basis of their dimensions, functions, and preparation methods. They are cellulose nanocrystals and nanofibrillated cellulose. Another type of nanocellulose is the bacterial nanocellulose (BNC) which is synthesized with a bottom-up method from glucose by a family of bacteria, *Gluconoacetobacter xylinus*.

### 1.6.2.1 Cellulose nanocrystals (CNC)

CNC exhibits elongated crystalline rod like shapes, and has very limited flexibility compared to NFC as it doesn't contain amorphous regions. Cellulose nanocrystal (CNC) [nanowhiskers, nanorods and rod-like cellulose crystals] is isolated from cellulose fibers by acid hydrolysis. Figure 1.14 shows the schematic representation of cellulose nano crystals. It has relatively lower aspect ratio and having a typical diameter of 2–20nm and the length varies between 100nm to several micrometers. CNC s have high aspect ratio and are highly crystalline and containing a high fraction of I $\beta$  structure. CNCs are needle shaped cellulose particles and the main features are their usage as reinforcement agents due to their large specific surface area. They have very high modulus of approximately 150GPa, have an ability to reinforce at lower loading, low density of about 1.566g/cm<sup>3</sup>, non-aggressive nature, nontoxic, biocompatibility and biodegradability. The degree of crystallinity and morphology depends on the source of cellulosic material, preparation conditions and experimental techniques [103,104].



Figure 1.14 Schematic representation of cellulose nanocrystals



### 1.6.2.2 Cellulose nano fiber (Nanofibrillated cellulose- NFC)

Nanofibrillar cellulose, cellulose nanofiber, cellulose nanofibril are the terms used for microfibrillated cellulose and is commercially available. Figure 1.15 shows the schematic representation of cellulose nano fiber. NFC consists of a bundle of stretched cellulose chain molecules with long, flexible and entangled cellulose nano fibers of 1–100nm size. Cellulose nano fibers are defined as long flexible particles consisting of elementary assemblies of distinct polymer units that have diameters in the order of tens of nanometers. They consist of crystalline and amorphous domains. NFC can be produced by delamination of wood pulp through mechanical pressure before and/or after chemical or enzymatic treatment [93]. NFCs are reminiscent of elementary fibrils in the wood and plant biosynthesis process and considered to consist of 36 cellulose chains arranged in I $\beta$  crystal structure. They can be produced through mechanical pressure before or after chemical treatment.

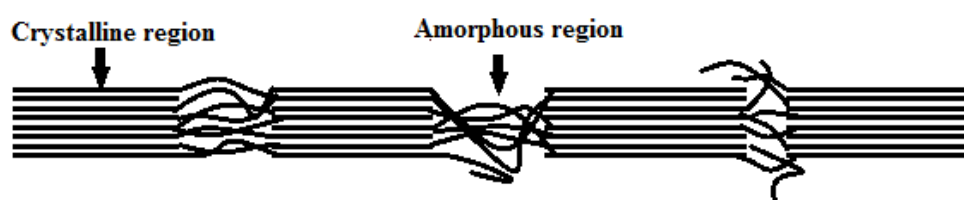


Figure 1.15 Schematic representation of cellulose nano fiber

### 1.6.2.3 Bacterial nanocellulose

Nanocellulose produced by the bacteria *Gluconacetobacter xylinus* is an emerging biomaterial with great potential in flexible radar absorbing materials, in scaffolds for tissue regeneration, water treatment, and medical applications. Bacterial cellulose nanofibril bundles have excellent intrinsic

properties due to their high crystallinity is of the same order as the elastic modulus of glass fibers. Compared with cellulose from plants, BC also have higher water holding capacity, higher degree of polymerization (up to 8000), and a finer web like network. BC is produced as a highly hydrated and relatively pure cellulose membrane and no chemical treatments are needed to remove lignin and hemicelluloses. Because of these characteristics, biomedical devices have gained a significant amount of attention owing to an increased interest in tissue-engineered products for both wound care and the regeneration of damaged or diseased organs. BC is pure cellulose made by bacterial fabrication by biochemical steps and by self-assembling of the secreted cellulose fibrils in the medium [105,106].

## **1.7 Nanocomposites of cellulose nano fibers**

Cellulose, a biopolymer, is the main component of all plant fibers. Cellulose nano fiber reinforced polymer composites have received much attention because of their low density, low cost, non-abrasiveness, fire resistance, lack of toxicity and biodegradable properties. A great deal of research has been done to study the effect of using cellulose nano fibers as the reinforcing agent for different polymer composites. Besides biodegradability and renewability, the productions of cellulosic fibers in nano dimensions add properties such as better mechanical characteristics and low density.

### **1.7.1 Preparative methods of nanocellulose based composites**

When processing cellulose nanocomposite, properties of CNs, nature of polymer matrix, and the interfacial interaction between the fillers and matrix should be considered.

### 1.7.1.1 Casting-evaporation Method

Casting-evaporation method involves casting a mixture of CN suspension and polymer solution on Teflon or into polypropylene dishes and allowing the solvent to evaporate at an appropriate temperature. These techniques are divided into three systems on the types of polymers used. Hydrosoluble or Hydrodispersible polymer in which, water is a preferred processing medium because of the good dispersion and high stability of the hydrophilic CNs in water. For example the preparations of CN reinforced starch [107].

Polymer emulsion is the stable dispersion of polymer microparticles into an aqueous medium and when polymer emulsion is mixed with CN suspension; both polymer particles and CNs stably disperse in water. For example the preparation of waterborne epoxies [108]. Non aqueous systems in which CNs may disperse in polar solvent and dispersion is better in solvent with higher polarity. Azizi Samir *et al.* dispersed freeze-dried tunicin CNs in N, N-dimethylformamide (DMF) without any coating surfactants or surface chemical modifications [109].

### 1.7.1.2 Sol- Gel Processing

This method is based on formation of template of CN and filling the template into a polymeric matrix. The individualized CNs are first formed in a three-dimensional template by self-assembly through a sol-gel method and this is achieved by a solvent exchange process with a water miscible solvent (e.g. acetone) in which the CN can form a well dispersed homogenous gel. The filler template is then immersed into a polymer solution, which must be miscible with the template solvent and cannot re-disperse the CN. Okonkwo

*et al.* used this technique to produce a nano Silica/cellulose/ PE composite material without the experienced particle agglomeration of the nano silica filler in the composite matrix [110].

### **1.7.1.3 Electrospinning**

This method is used to prepare fibers with diameters ranging from several microns down to 100 nm from a liquid, through the action of electrostatic forces. Electrospinning is suitable to produce fibers using large and complex molecules. In this method an electrical charge is used to draw a positively charged polymer solution from an orifice to a collector. This method is used to prepare nanocomposite fiber mats.

### **1.7.1.4 The layer-by-layer electrostatic assembly (LBL)**

In this method thin films of oppositely charged layers are deposited and this technique can also be utilized for nanoparticles. In LBL assembly sequential adsorption of positive or negative charged species by alternatively dipping into the solutions. The excess solution after each adsorption step is rinsed with solvent and after which a thin layer of charged species on the surface ready for next adsorption step is obtained. The advantages of the LBL assembly technique include simplicity, universality, and thickness control at nanoscale level and do not require highly pure components and sophisticated hardware [111]. P. Podsiadlo *et al.* studied the preparation of cellulose whiskers multilayer composites with a polycation, poly-(dimethyldiallylammonium chloride) (PDDA) by using the LBL technique [112].

### **1.7.1.5 Bottom – Up manufacture of bacterial cellulose nanocomposites**

This technique is developed by Grande *et al.* for the preparation of self assembled bacterial cellulose nanocomposite. This technique is based

on bottom up process [113]. Grande *et al.* produced BC- starch nanocomposites by this technique and these nanocomposites showed a high volume fraction of a strong phase of BC fibers covered by a starch phase [114].

#### **1.7.1.6 Melt compounding**

Melt compounding is the most commonly used process to produce composite in industrial scale. Very few studies have been reported concerning the processing of nanocellulose reinforced composites. The hydrophilic nature of nanocellulose results in agglomeration during drying and also when incorporated along with nonpolar matrices. This can be avoided by first mixing them, which is then fed into the extruder, or first dried and then extruded. Mehdi Jonoobi *et al.* prepared cellulose nano fiber (CNF) reinforced polylactic acid (PLA) by twin screw extrusion and they reported that the melt compounding process using the master batch is a very promising method to get better processability of cellulose nanocomposites and achieve improved mechanical and thermal properties for PLA [115]. An attempt to use PVA as a compatibilizer to promote the dispersion of cellulose whiskers within the PLA by compounding extrusion was reported by Daniel Bondeson *et al.* [116]. Han-Seung Yang *et al.* prepared the nanofibrilled filled polypropylene composites by melt blending in order to study the impact strength of the composites [117]. Mohammad L Hassan *et al.* prepared cellulose/polypropylene (PP) nanocomposites by twin-screw extrusion [118].

#### **1.7.2 Applications of cellulose based nanocomposites**

The potential applicability of nanocellulose is widely extended and the applications of nanocellulose are mainly considered to be in paper, packaging

products construction, automotive, furniture, electronics, pharmacy and cosmetics. For electro acoustic devices, nanocellulose is used as a membrane for high quality sound. It is also applied in membrane for combustible cells, additives for high quality electronic paper, ultrafiltrating membranes for water purification, membranes used to retrieve mineral and oils. The high strength and stiffness as well as the small dimensions of nanocellulose impart useful properties to composite materials reinforced with these fibers, which can be used in wide range of applications. Susheel Kalia *et al.* have reported that nanocellulose is used for producing acoustic diaphragms [119]. Crystalline nanocellulose offers potential advantages as a drug delivery excipient. Nanocellulose is used in biomedical industry which includes skins replacements for burnings and wounds, drugs releasing system; blood vessel growth; nerves, gum and bone reconstruction [120]. Nakayama *et al.* for the first time reported that the cellulose-polymer nanocomposite hydrogels composed of bacterial cellulose (BC) and gelatin [121].

Cellulose nanocrystals have been used as highly effective reinforcing nanofillers for improving mechanical properties of various electrospun polymer matrices. The application of electrospun polymer matrices includes optoelectronics, sensors, catalysis, filtration, energy-related materials and medicine [122]. Another application of nanocellulose is the preparation of very dense nano papers with excellent mechanical properties [123]. Cellulose based aerogels were developed by Stamm and co-workers during 1950's. Areogels are highly porous materials that have low density, high surface area, have the potential to be used for a wide variety of applications [124]. Wei Li *et al.* prepared nanocellulose aerogels from poplar alkaline

peroxide mechanical pulp using ultrasonication method and they reported that these aerogels acted as matrices which can prevent the growth and agglomeration of ferromagnetic  $\text{CoFe}_2\text{O}_4$  nanoparticles [125]. Mohammad Tajul Islam *et al.* used surface modified nanofibrils as a reinforcement for petrochemical based thermoset and thermoplastic polymers [126]. Ligia Maria Manzine Costa *et al.* prepared bionanocomposites with homogeneous porous distribution and prospective natural antimicrobial properties from electrospun PVA/pineapple nanofibers/ *Stryphno Dendron adstringens* bark extract for medical applications as cell scaffolds, *in vitro* tissue reconstructions [127]. Bacterial cellulose mats are very effective in promoting autolytic debridement, reducing pain, and accelerating granulation and are important for proper wound healing [128]. Cellulose nano fibers have showed remarkable characteristics as reinforcement materials for optically transparent composites [129].

## **1.8 Scope and Objectives of the work**

Polypropylene (PP) and polystyrene (PS) are two of the widely used plastics utilized for a wide range of applications due to their mechanical properties, ease of processing and low cost. A detailed study of the modification of Polypropylene (semi crystalline) / Polystyrene (amorphous) blend with kaolin nanoclay is proposed in this work. This blend has been selected for the study because of its recent interest in automotive applications. Blending an amorphous polymer and a semi crystalline polymer will offer a balance of impact strength/ stiffness. Depending upon the PS content in the blend, flexural modulus increases over that of PP while maintaining high levels of ductility and ultimate elongation. PP offers solvent and chemical

resistance while PS yields the rigidity, melt strength & dimensional stability. Higher  $T_g$  of the amorphous PS reinforces the PP matrix and yields higher strength and heat distortion temperature, while the high  $T_m$ , high melt flow characteristics of PP are maintained [130]. These two polymers have some complementary properties such as shrinkage (PP is high, PS is low), scratch resistance (PP is poor, PS is high), and barrier properties (PP is good, PS is poor). Because of these reasons, blending these two polymers is of significant commercial interest. But PP and PS used in this study are immiscible, which leads to the formation of multiphase systems with different morphology. So nanoclays and cellulose nano fibers are used as modifiers. Much of the work in this area has been focused on montmorillonite clays [131-133]. Hence, in this study low cost kaolin nanoclay with a 1: 1 type layered structure with chemical composition  $Al_2Si_2O_5(OH)_4$  is proposed to be used [134,135]. A systematic study is proposed to be undertaken to understand the mechanical, thermal and morphological properties of the modified nanocomposites.

For improving the stiffness and strength, glass fibers are added to plastics. Short fiber reinforced composites have several attractive characteristics that makes them suitable for domestic, electrical, and automotive applications. But the glass fiber composites at higher loading develop processing difficulties. To overcome these difficulties, hybrid composites with low nanoclay loadings are proposed to be investigated. Hence in this study it is proposed to reinforce PP/PS blend with nano / micro fillers to generate a new class of hybrid materials. The performance of the hybrid composites can be evaluated by studying their mechanical, thermal and morphological properties.



The main objectives of this work are:

- To study the effect of different modifications of kaolin nanoclay on the mechanical, thermal and morphological properties of Polypropylene/ Polystyrene blend.
- To investigate the beneficial effect of hybrid fillers on the properties of Polypropylene/ Polystyrene blend.
- To modify kaolin nanoclay using vinyltriethoxysilane and study its effect on the mechanical, thermal and morphological properties of PP/PS blend.
- To study the effect of compatibilizers on the properties of filled PP/PS blend.
- To isolate cellulose nanofiber from sisal and investigate the effect of cellulose nanofiber on the properties of PP/PS blend.

## **References**

- [1]. Polymer Blends: A Comprehensive Review Hard cover Lloyd Robeson (Author), L.M Robeson (Editor), ISBN-13: 978-156990408, 2007.
- [2]. Polymer Blends Handbook, L. A. Utracki, Vol.1, Kluwer Academic Pub, 2002, 1442.
- [3]. Mixing Rules for Complex Polymer Systems A. Franck, Ta Instruments Germany.
- [4]. Cor Koning, Martin Van Duin, Christophe Pagnouille, Robert Jerome, Pmg. P&M. Sri., 1998, 23, 707-757.

- [5]. Oluranti Sadiku-Agboola, Emmanuel Rotimi Sadiku, Adesola Taoreed Adegbola, Olusesan Frank Biotidara, *Materials Sciences And Applications*, 2011, 2, 30-41.
- [6]. H Larson, H Bertilson, *Polymer Recycling*, 1995, 1, 243-248.
- [7]. D. Curto, F. P. La Mantia, D. Acierno, *Rheologica Acta*, 1983, 22, 197-208.
- [8]. Xue Li, Yanchun Han, Lijia An, *Polymer*, 2003, 44, 8155–8165.
- [9]. I. Prosycevas, S. Tamulevicius, A. Guobiene, *Thin Solid Films*, 2004, 453–454, 304–311.
- [10]. A.K. Singh R.K. Mishra, Rajiv Prakash, Pralay Maiti, Akhilesh Kumar Singh, Dhananjai Pandey, *Chemical Physics Letters*, 2010, 486 (1–3), 32–36.
- [11]. Manasvi Dixit, Vishal Mathura, Sandhya Gupta, Mahesh Baboo, Kananbala Sharma, N. S. Saxena, 2009, 82( 12), 866–878.
- [12]. Tresa Sunitha George, Asha Krishnan, Newly Joseph, R. Anjana, K.E. George, *Polymer Composites*, 2012, 33(9), 1465–1472.
- [13]. Kyonsuku Min, James L. White, John F. Fellers, *Journal of Applied Polymer Science*, 2003, 29(6), 2117-2142.
- [14]. Effects of Clay Modification and Compatibilizers On The Mechanical, Morphological, And Thermal Properties Of Polyamide 6/ Polypropylene Nanocomposites, Kusmono, Phd Thesis, 2008.
- [15]. Cheung, Tjong, Sc, R.K Li, Mechanical Properties Of Calcium Carbonate Filled Beta –Crystalline Form Polypropylene Composite, Conference Proceeding-Society Of Plastic Engineers, Antec 1996.
- [16]. Texture Evolution in Processing Of Polystyrene-Clay Nanocomposites, David Richard Steinmetz, M.Tech Thesis 2007.

- [17]. Sani Amril Samsudin, Azman Hassan, Munirah Mokhtar, Syed Mustafa Syed Jamaluddin, *Malaysian Polymer Journal* , 2006, 1(1) , 11-24.
- [18]. High Performance Plastics, Nanoscale –Additives For PP/PS Blends, International Newsletter Ltd, 2005.
- [19]. Kazuhiro Yoshida, Takanobu Kawamura, Minoru Terano, Koh-Hei Nitta, *Journal Of Applied Polymer Science*,2008, 109, 211–217 .
- [20]. Impact Resistance of Selected Immiscible Polymer Blends, Wantinee Viratyaporn, Richard L. Lehman, Jayant Joshi, Society of Plastics Engineers [Spe] Annual Technical Conference Proceedings Cincinnati, 2007.
- [21]. Mitsuyoshi Fujiyama, *Journal of Applied Polymer Science*, 1997, 63(8), 1015–1027.
- [22]. Seahan Cho, Joung Sook Hong, Seung Jong Lee, Kyung Hyun Ahn, Jose Antonio Covas, Joao Manuel Maia, *Macromolecular Materials and Engineering*, 2011, 296, 341–348.
- [23]. *Polymer Blends*, S. Newman, D.R. Paul, Vol. I & II, Academic Press, New York, 1978.
- [24]. M. Xanthos, *Polymer Engineering & Science*, 1988,28(21) 1392–1400.
- [25]. *Concise Polymeric Materials Encyclopedia*, Joseph C. Salamone, CRC Press. Content: 1760, 1998.
- [26]. Leszek A. Utracki, *The Canadian Journal of Chemical Engineering*, 2002, 80.
- [27]. Types of Reactive Polymers Used in Blending, N.C. Liu , H. Huang, 2001, Publisher: Carl Hanser Verlag GmbH & Co. KG , 2001,13-42.
- [28]. N. Moussaif, C. Pagnouille, R. Jérôme, *Polymer*, 2000, 41(15), 5551–5562.

- [29]. L. Elias, F. Fenouillot, J.C. Majesté and Ph. Cassagnau, Marseille, août 2009, 24-28.
- [30]. Zhong-Ming Li, Sha-Ni Li, Xiang-Bin Xu, *Polymer-Plastics Technology and Engineering*, 2007, 46, 129–134.
- [31]. B. Baghaei, S. H. Jafari, H. A. Khonakdar, I. Rezaeian, L. As'habi, S. Ahmadian, *Polymer Bulletin*, 2009, 62, 255–270.
- [32]. A. Karim, T. M. Slawacki, S. K. Kumar, J. F. Douglas, S. K. Satija, C. C. Han, T. P. Russell, Y. Liu, R. Overney, J. Sokolov, M. H. Rafailovich; *Macromolecules*, 1998, 31, 857-862.
- [33]. [33] V. V. Ginzburg, F. Qiu, M. Paniconi, G. W. Peng, D. Jasnow, A. C. Balazs, *Physical Review Letters*, 1999, 82, 4026.
- [34]. Yan Zhu, Hai-Yun Ma, Li-Fang Tong, Zheng-Ping Fang, *J Zhejiang Univ Sci A*, 2008 9(11), 1614-1620.
- [35]. W. Zhang, M. Lin, A. Winesett, O. Dhez, A. LD. Kilcoyne, H. Ade, M. Rubinstein, K. V. P. M. Shafi, A. Ulman, D. Gersappe, R. Tenne, M. Rafailovich, J. Sokolov, H. L. Frisch, *Polymers for Advanced Technology*, 2011, 22 65–71.
- [36]. Monika Šupová, Gražyna Simha Martynková, Karla Barabaszová, *Science of Advanced Materials*, 2011, 3, 1–25.
- [37]. L.M. Manocha, Jignesh Valand, Nikesh Patel, Ashish warrier, S Manocha, *Indian journal of pure and Applied Physics*, 2006, 44, 135-142.
- [38]. R.V. Kurahatti, A.O. Surendranathan, S. A. Kori, Nirbhay Singh., A.V. Ramesh Kumar, Saurabh Srivastava, *Defence Science Journal*, 2010, 60( 5), 551-563.
- [39]. *Nanotechnology and Nanomaterials "Advances in Diverse Industrial Applications of Nanocomposites"*, book edited by Boreddy Reddy, ISBN 978-953-307-202-9, 2011.

- [40]. Masami Okamoto, *Rapra review reports*, 14(7), 2003.
- [41]. *Clay-Containing Polymeric Nanocomposites, Volume 1*, L.A. Utracki, rapra ,2004.
- [42]. *Kaolin Clay: Functional Optical Additives*, Peter A. Ciullo, Sara Robinson ,Norwalk, CT, 2003.
- [43]. Yanfeng Li, Dewen Sun, Xiaobing Pan, Bo Zhang, *Clays and Clay Minerals*, 2009, 57(6), 779–786, 2009.
- [44]. G. Lagaly, R. M. Barrer, K. Goulding, *Phil.TransR. Soc.Lond.A*, 1984, 311, 315-332.
- [45]. A. Weiss,W Thieleppe, H Orth, *Proc.int.clay conf. Jerusalem, Jerusalem : Israel University Press*, 1966, 1,277-293.
- [46]. Do Hoon Kim,Jun Uk Park, Kwang Soo Cho, Kyung Hyun Ahn, Seung Jong Lee, *Macromolecular Materials and Engineering*, 2006, 291, 1127–1135.
- [47]. Chae Hwan Hong, Young Bum Lee, Jin Woo Bae, Jae Young Jho, Byeong Uk Nam, Tae Won Hwang; *Journal of Applied Polymer Science*, 2005, 98, 427–433.
- [48]. S. Sánchez-Valdes,J. Méndez-Nonell,L. F. Ramos de Valle,T. Lozano-Ramírez,E. Ramírez-Vargas,M. L. López-Quintanilla, J. M. Gutiérrez-Rodríguez,*e-Polymers*,2009,126.
- [49]. V. P. Privalko, D.I. Balta Calleja, D. I. Sukhorukov, E. G. Privalko, R. Walter, K. Friedrich , *Journal of Thermal Analysis and Calorimetry*, 2000, 59 , 509-516 .
- [50]. Chungui Zhao, Huaili Qin, Fangling Gong, Meng Feng, Shimin Zhang, Mingshu Yang, *Polymer Degradation and Stability*, 2005, 87(1), 183–189.
- [51]. AGaboune,SS. Ray,A Ait-Kadi ,B Riedl, M J Bousmina, 2006, 6(2),530.

- [52]. Canan Esma Yeniova, Ulku Yilmazer; *Polymer Composites*, 2010, 31(11), 1853-1861.
- [53]. Shuichi Tanoue, Leszek A. Utracki, Andrés Garcia-Rejon, Pierre Sammut, Minh-Tan Ton That, Isabelle Pesneau, Musa R. Kamal, Jørgen Lyngaae-Jørgensen, *Polymer Engineering and Science*, 2004, 44( 6).
- [54]. Antonios Kellarakis, Emmanuel P. Giannelis; *Polymer*, 2011, 52(10) 2221-2227.
- [55]. T.N. Abraham, D. Ratna, S. Siengchin, J. Karger-Kocsis; *Polymer Engineering & Science*, 2009, 49( 2) , 379–390.
- [56]. M S Monteiro, CL Rodrigues, RP Neto, MI Tavares, *Journal of Nanoscience and Nanotechnology.*, 2012, 12(9), 7307- 13.
- [57]. Leandro N. Ludueña, Analía Vazquez, Vera A. Alvarez, *Journal of Applied Polymer Science*, 2008, 109(5), 3148–3156.
- [58]. Hong-Wen Wang, Rui-Xuan Dong, Ching-Lin Liu, Hsin-Yu Chang, *Journal of Applied Polymer Science*, 2007, 104(1), 318-324.
- [59]. K.P Pramoda; Tianxi Liu, Zhehui Liu, Chaobin He, Hung-Jue Sue, *Polymer Degradation and Stability*, 2003, 81(1), 47-56.
- [60]. Anne Ammala , Carmen Bell, Katherine Dean, *Composites Science and Technology*, 2008, 68(6), 1328–1337.
- [61]. Supratim Suin, Sandip Maiti, Nilesh K. Shrivastava, B.B. Khatua, *Materials & Design*, 2014, 54, 553–563.
- [62]. Xia Cao; L. James Lee , Tomy Widya, Christopher Macosko, *Polymer*, 2005, 46( 3), 775–783.
- [63]. Asif Abdul Azeez; Kyong Yop Rhee; Soo Jin Park , David Hui, *Composites Part B: Engineering*, 2013, 45( 1), 308–320.

- [64]. G. Jeon, T. Jung, W. Lee, D. Hudson, *Polymer Bulletin*, 1998, 41, 107.
- [65]. G.S. Sur, H.L. Sun, S.G. Lyu, J.E. Mark, *Polymer*, 2001, 42, 9783.
- [66]. *Polymer/Clay Nanocomposites*, Masami Okamoto, Toyota Technological Institute, Tempaku, Nagoya, Japan, *Encyclopedia of Nanoscience and Nanotechnology*.
- [67]. Quang T. Nguyen, Donald G. Baird, *Advances in Polymer Technology*, 2006, 25(4), 270–285.
- [68]. Jeffrey Jordan, Karl I. Jacob, Rina Tannenbaum, Mohammed A. Sharaf, Iwona Jasiuk, *Materials Science and Engineering A*, 2005, 393, 1–11.
- [69]. Sudip Ray, Siew Young Quek, Allan Easteal, Xiao Dong Chen, 2006, 2(4).
- [70]. R.A. Vaia, S. Vasudevan, W. Krawiec, L.G. Scanlon, E.P. Giannelis, *Advanced Materials*, 1995, 7, 154.
- [71]. Masami Okamoto, *Encyclopedia of Nanoscience and Nanotechnology*, H.S. Nalwa Editor, 2004, 8, 791-843.
- [72]. Alexander B. Morgan, *Material Matters*, 2011, 2(1), 1-6.
- [73]. Amirhossein Esfandiari, Hossein nazokdast, Abo-Saeed Rashidi, Mohamad- Esmaeel Yazdanshenas, *Journal of Applied Polymer Sciences*, 2008, 8(3), 545-561.
- [74]. Sangah Gam, Aysenur Corlu, Hyun-Joong Chung, Kohji Ohno, Michael J. A. Hore and Russell J. Composto, *Soft Matter*, 2011, 7, 7262-7268.
- [75]. M. Hemmati H. Shariatpanahi A. Fereidoon, J. Aalaie, M. Ghorbanzadeh Ahangari, *Polymer-Plastics Technology and Engineering* 2012, 51(1).
- [76]. Hee B. Kim, Joon S. Choi, Chung H. Lee, Sung T. Lim, Myung S. Jhon, Hyoung Jin Choi, *European Polymer Journal*, 2005, 41(4), 679–685.
- [77]. Anup K. Dhibar, Jin Kon Kim, Bhanu B. Khatua, *Journal of Applied Polymer Science*, 2011, 119, 3080–3092.

- [78]. Y. Deyrail, F.Mighri, M. Bousmina , S.Kaliaguine, *Fuel Cells*, 2007, 6, 447–452.
- [79]. Joung Sook Hong, Yong Kyoung Kim, Kyung Hyun Ahn, Seung Jong Lee, *Journal of Applied Polymer Science*, 2008, 108(1), 565–575.
- [80]. G Kalaprasad, Sabu Thomas, *International Plastics Engineering and Technology*, 1995, 1, 87-98.
- [81]. Maries Idicula, Kuruvila Joseph, Sabu Thomas, *Journal of Reinforced Plastics and Composites*, 2010, 29, 112-29.
- [82]. Maya Jacob, Sabu Thomas, K.T. Varughese, 2004,64(7-8),955-965.
- [83]. Al-MosawiAli, *Research Journal of Engineering Sciences*, 2012, 1(3), 22-25.
- [84]. Normasmira A. Rahman, Aziz Hassan, R. Yahya, R.A. Lafia-Araga, *SainsMalaysiana* 2013, 42(4), 537–546.
- [85]. Kusmono, ZainalArifinMohdIshak, *International Journal of Polymer Science*, 2013, 2013, Article ID 797109,7.
- [86]. Improved durability and thermal stability of glass fiber reinforced composites using clay-polymer nanocomposites, Liu, Mingyang, M. Phil Thesis, 2009.
- [87]. Sreekumar janardhanan, Mohini M Sain, *Bioresources*, 2006, 1(2), 176-188.
- [88]. Strategies for improving mechanical properties of polypropylene/cellulose composites, Espert, Ana, PhD thesis, 2005.
- [89]. Juan I. Moran Al Vera A. Alvarez, Viviana P. Cyras Analia Vazquez, *Cellulose*, 2008 15, 149–159
- [90]. Cintil Jose Chirayil, Lovely Mathew and Sabu Thomas, *Reviews on Advanced Material Science*, 2014, 37, 20-28.



- [91]. F.W. Herrick, R.L Casebier, J.K. Hamilton, *Journal of Applied polymer Science, Applied polymer Symposium*,1983, 37, 797.
- [92]. A.F. Turbak, F.W. Snyder, K.R Sandberg, *Journal of Applied Polymer Science*, 1983, 37, 815.
- [93]. H.P.S. Abdul Khalil, Y. Davoudpour, Md. Nazrul Islam, Asniza Mustapha, K. Sudesh, Rudi Dungani, M. Jawaid, *Carbohydrate Polymers*, 2014, 99 , 649–665.
- [94]. T Wang, L T Drzal, *ACS Applied Materials and Interfaces*, 2012, 4, 5079–5085.
- [95]. Adriana N. Frone, Denis M. Panaitescu, Dan Donescu; *U.P.B. Scientific Bulletin, Series B*, 2011, 73(2).
- [96]. B.M. Cherian, A.L. Leao, S.F. Souza, S. Thomas, L.A. Pothan and M. Kotaisamy, *Carbohydrate Polymers*, (2010), 81.
- [97]. Mohd Harfiz Salehudin, Dr Eraricar Saleh, Prof. Madya Dr. Ida Idayu Muhamad & Siti Nur Hana Mamat; *International Conference on Agricultural and Food Engineering for Life* , 2012, 26-28 .
- [98]. B. Wang, M. Sain, *Composites Science and Technology*, 2007, 67 (11–12), 2517–2521.
- [99]. Y. Li, K.L. Pickering, *Composites Science and Technology*,2008, 68(15-16), 3293–3298.
- [100]. A. Bhatnagar, M. Sain, *Journal of Reinforced Plastics Composites*, 2005, 24(12), 1259-1268.
- [101]. T Saito, Y Nishiyama, J L Putaux, Vignon, M.,Isogai, *Biomacromolecules*, 2006, 7, 1687-1691.
- [102]. T Saito, S Kimura, Y Nishiyama, A Isogai, *Biomacromolecules* 2007, 8, 2485-2491.

- [103]. Hudson AlvesSilverio, Wilson PiresFlauzinoNeto, Noelio Oliveira Dantas, Daniel Pasquini, *Industrial Crops and Products*, 2013, 44, 427– 436]
- [104]. WilsonPiresFlauzinoNeto, Hudson AlvesSilverio, NoelioOliveriaDantas, Daniel Pasquini, *Industrial Crops and Products*, 2013, 42, 480-488
- [105]. Gabriel Molina de Olyveria, Ligia Maria Manzine Costa, Pierre Basmaji, Lauro Xavier Filho, *Journal of Nnotechnology in Engineering and Medicine*, 2012, 2(3), 8.
- [106]. Nimeskern L, Martínez Ávila H, Sundberg J, Gatenholm P, Müller R, Stok KS, *J MechBehav Biomededical Materials.*, 2013, 12-21.
- [107]. M N Angles, A Dufresne, *Macromolecules*, 2000, 33(22), 8344-8353.
- [108]. M M Ruiz, J Y Cavaille, A Dufresne, C Craillat, J F Gerard, *Macromolecular Symposia*, 2001, 169, 211-222.
- [109]. M. A. S Azizi Samir, F Alloin, M Paillet, A Dufresne, , *Macromolecules*, 2004, 37(11), 3413-3416.
- [110]. E. M. Okonkwo, O, Ofoegbu, J.U Mmereole, *Journal of Nanotechnology Progress in International*, 2010, 3,26-39.
- [111]. Alain Dufresne, *Molecules*, 2010, 15, 4111-4128.
- [112]. P Podsiadlo, S Y Choi, B Shim, J Lee, M Cuddihy, N A Kotov, 2005, 6, 2914–2918.
- [113]. *Advances in Natural Polymers: Composites and Nanocomposites*, Sabu Thomas, P. M. Visakh, Aji. P Mathew, Springer Science & Business Media, 2012, 432.
- [114]. C J Grande, F G Torres, C M Gomez, O P Troncoso, J Canet-Ferrer, J Martinez- Pastor, *Polymers & Polymer Composites*, 2008, 16, 181-185.
- [115]. Mehdi Jonoobi, Jalaluddin Harun, Aji P. Mathew, Kristiina Oksman, *Composites Science and Technology*, 2010, 70 , 1742–1747.
- [116]. D Bondeson, K Oksman, *Composites Part A*, 200, 38, 2486–92.

- [117]. Han-Seung Yang, Douglas J. Gardner, Jacques W. Nader, *Composites: Part A*, 2011, 42, 2028–2035.
- [118]. Mohammad L Hassan, Aji P Mathew, Enas A Hassan, Shiamaa M Fadel, Kristiina Oksman, *Journal of Reinforced Plastics and Composites* 2014, 33(1), 26–36.
- [119]. Susheel Kalia, Alain Dufresne, Bibin Mathew Cherian, B. S. Kaith, Luc Avérous, James Njuguna, Elias Nassiopoulos, *International Journal of Polymer Science*, 2011, 2011, 35.
- [120]. D. Klemm, D. Schumann, U. Udhardt, S. Marsch, *Progress in Polymer Science*, 2001, 26(9), 1561–1603.
- [121]. Nakayama, A, Kakugo, A., Gong, J. P., Osada, Y, Takai, M., Erata, T, Kawano, S, 2004, 14(11), 1124-1128.
- [122]. Nanotechnology and Nanomaterials- Recent Development in Applications of Cellulose Nanocrystals for Advanced Polymer-Based Nanocomposites by Novel Fabrication Strategies, chapter 6 Chengjun Zhou , Qinglin Wu, 2006, 103-120.
- [123]. M. Henriksson, L.A. Berglund, T. Nishino, *Biomacromolecules*, 2008, 9, 1579.
- [124]. Robert J. Moon, Ashlie Martini, John Nairn, John Simonsen, Jeff Youngblood, *Chem, Soc, Rev*, 2011, 40, 3941-3994.
- [125]. Wei Li, Xin Zhao, Shouxin Liu, *carbohydrate polymers*, 2013, 94, 278-285.
- [126]. Mohammad Tajul Islam, Mohammad Mahbubul Alam, Marina Zoccola, *International Journal of Innovative Research in Science, Engineering and Technology*, ISSN: 2319-8753, 2013, 2(10), 5444-5451.
- [127]. Ligia Maria Manzine Costa, Gabriel Molina de Olyveira, Bibin Mathew Cherian, Alcides Lopes Leao, Sivoney Ferreira de Souza, Mariselma Ferreira, *Industrial Crops and Products* , 2013,41 , 198– 202.

- [128]. Advances in Natural Polymers, Edition: 18, Chapter: CHAPTER 10, Publisher: Springer Berlin Heidelberg, Editors: Sabu Thomas, P. M. Visakh, Aji. P. Mathew, 337-359.
- [129]. S Iwamoto, A N Nakagaito, H Yano, M Nogi, Applied Physics A, 2005, 81, 1109-1112.
- [130]. Evaluation of the effects of Nanofil® Nanoclays in the blending of Polypropylene and Polystyrene, Robert J. Opalko; Ph.D Thesis, 2008.
- [131]. Yun Zhu, Hai-yun Ma, Li-fang Tong, Zheng-ping Fang, Journal of Zhejiang University Science A, 2008, 9(11),1614-1620.
- [132]. Kyun yl Kim, Dong Uk Ju, Gi Joon Nam, Jae Wook Lee, Macromolecular symposia,2007,249-250,283-288.
- [133]. Suprakas Sinha Ray, Steve Pouliot, Mosto Bousmina, Leszek A. Utracki, Polymer, 2004, 45, 8403-8413.
- [134]. Tamer A.Elbokl, Christian Detellier; Journal of Physics and Chemistry of Solids, 2006, 67, 950-955.
- [135]. Qian Zhang, Qinfu Liu, James E. Mark, Isao Noda, Applied clay Science 2009,46, 51-56.

.....✂.....

## Chapter 2

# Materials and Experimental Techniques

---

<b>Contents</b>	2.1 <i>Materials</i>
	2.2 <i>Methodology</i>

---

### *Abstract*

*This chapter gives a detailed description about the materials and experimental techniques used for the preparation of nanocomposites. The different characterization techniques employed are also described.*

## **2.1 Materials**

### **2.1.1 Polypropylene (PP)**

Polypropylene homopolymer (REPOL H200MA) with a melt flow index of 25g/10 min (230<sup>0</sup>C/2.16Kg) was purchased from Reliance Industries limited, Mumbai, India.

### **2.1.2 Polystyrene (PS)**

General purpose Polystyrene (MFI (200<sup>0</sup>C/5Kg) is 12g/10 min) was obtained from Supreme Petrochem Ltd India

### **2.1.3 Modified kaolin nanoclays**

Modified kaolin nanoclays were obtained from English India Clays Limited Veli, Thiruvananthapuram, Kerala, India. The clays had a bulk density of 0.2-0.03g/cc and a BET specific surface area of 28-30m<sup>2</sup>/g. The samples used were unmodified kaolin nanoclay (Nanocaliber 100), vinyl silane modified nanoclay (Nanocaliber 100V - N100V), dialkyl silane modified nanoclay (Nanocaliber 100 Z- N100Z), mercapto silane modified kaolin nanoclay (Nanocaliber 100 M denoted as N100M) and amino silane modified kaolin nanoclay (Nanocaliber 100 A- N100A)

### **2.1.4 Glass fibers**

E- Glass fiber: E-Glass fiber with a diameter of 13 μm, Specific Gravity-2.6g/c, tensile strength-3.5GPa, tensile modulus-72Gpa was obtained from Sharon Industries Ltd, Kochi, India.

AR glass fiber (Alkali resistant glass fiber): Cem-FIL® 54 with a diameter of 10μm, specific gravity: 2.68 g/cm<sup>3</sup>, tensile Strength: 1,700 MPa

and modulus of elasticity: 72 G Pa was obtained from Sharon Industries Ltd, Kochi, India.

### 2.1.5 Vinyltriethoxysilane (VTES)

Vinyltriethoxysilane (98%) was supplied by Lancaster synthesis, East gate, England.

### 2.1.6 Itaconic acid

Itaconic acid (Figure 2.1) pure AR with molecular weight of 130.10, melting range of 165-167°C was supplied by Spectrochem Pvt. Ltd. India

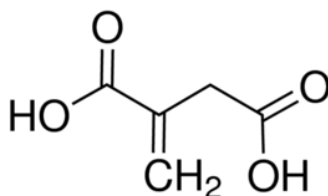


**Figure 2.1 Structure of itaconic acid**

### 2.1.7 Dimethyl itaconate

Dimethyl itaconate (Figure 2.2) (97%) with molecular weight of 158.16, boiling point of 207-208°C was supplied by Alfa Aesar.

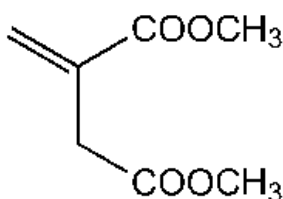


**Figure 2.2 Structure of dimethyl itaconate**

### 2.1.8 Other chemicals

Glacial acetic acid was obtained from Spectrochem Pvt. LTD Mumbai. Sodium hydroxide (NaOH) pellets purified obtained from SDFCL, Sd fine – chem limited. Sodium hypochlorite solution about 4%w/v available chlorine was supplied by Merck specialties private limited.

## 2.2 Methodology

### 2.2.1 Composite preparation

A thermo Haake Rheomix 600 (Figure 2.3) mixing chamber with a volumetric capacity of 69cm<sup>3</sup> fitted with roller rotors was used for melt mixing of polymers with fillers. In the chamber, the roller rotors rotate in opposite directions in order to affect a shearing force on the material mostly by shearing the material against the walls of the mixing chamber. The granules in the desired proportion were fed to the chamber through a vertical chute with a ram. There is a small clearance between the rotors which rotate at different speeds at the chamber wall. In these clearances dispersive mixing takes place. The shape and motion of the rotors ensure that all particles undergo high intensive shearing flow in the clearances. The mixer consists of three sections and each section is heated and controlled by its own heater and temperature controller. It is designed to maintain very accurate and uniform temperature profiles throughout the mixer.





**Figure 2.3 Thermo Haake Polylab System**

Since mechanical dissipation heat is developed in the small gap between rotors and chamber, the heat conducts to the center bowl and raises the set temperature. In this case, the heater at the center bowl is automatically shut off and circulation of cooling air is activated [1].

Three types of composites (nanoclay composites, short glass fiber/nanoclay hybrid composites and cellulose nano fiber composites) were prepared by this method. A mixing time of 8 minutes at a counter rotating rotor speed of 50 rpm was used for the mixing of the samples.

### **2.2.2 Preparation of test specimen**

The hot mix from the mixing chamber was immediately pressed using a hydraulic press at a pressure of  $100\text{kg}/\text{cm}^3$  and the resulting sheets were cut to small pieces. The test specimen were prepared using injection DSM Micro 10cc Injection Molding Machine (Figure 2.4), with a barrel temperature of  $190^\circ\text{C}$ . The specimens were molded at identical conditions and the properties were taken as the average property of six samples.



**Figure 2.4 DSM Micro 10cc Injection Molding Machine**

## **2.2.3 Characterization Techniques**

### **2.2.3.1 X-ray Diffraction (XRD)**

The samples were analyzed in a Bruker AXS D8 Advance X-Ray Powder Diffractometer (Cu K $\alpha$  radiation) in order to find the change in basal spacing of composites. The samples were scanned in the range of 3-80° at increment step of scanning 0.020° at a wave length of 1.5406 Å and Ni filter open at 30kV and 20mA. The particle size was calculated by the Scherer's Equation  $t = K\lambda/B\cos\theta$  where  $t$  = crystallite thickness,  $\lambda$  = X-ray wavelength,  $B$  = Full width half max (FWHM) of the diffraction peak,  $\theta$  = diffraction angle and  $K$  = Scherer's constant. It provides information on the changes of the inter-layer spacing of the clay upon the formation of clay nanocomposites. The formation of an intercalated structure should result in a decrease in  $2\theta$ , indicating an increase in  $d$ - spacing and if the complete exfoliation takes place, no peak is shown in the XRD pattern and the broadening of the peak is considered to be result of partial exfoliation [2].

### **2.2.3.2 Scanning Electron Microscopy (SEM)**

SEM is a very useful tool to investigate the morphology of fractured surfaces. In SEM, the electron beam incident is scanned across the specimen surface causes various phenomena of which the emission of secondary electrons is used for the surface analysis. Emitted electron strikes the collector and the resulting current is amplified and used to modulate the brightness of the cathode ray tube. There is a one- to- one correspondence between the number of secondary electrons collected from any particular point on the specimen surface and the brightness of the analogous point on the screen and thus an image of the surface is progressively built up on the screen. The SEM observations reported in the present study were made on the fracture surface of the tensile specimens. Morphology of the tensile fractured surfaces of the specimens was investigated by using JEOL Model JSM 6390LV scanning electron microscope (SEM). The samples were subjected to gold sputtering prior to electron microscopy to give the necessary conductivity [3].

### **2.2.3.3 Thermogravimetric analysis (TGA)**

TGA is a method of thermal analysis in which changes in physical and chemical properties of materials are measured as a function of increasing temperature or as a function of time while the substance is subjected to a controlled temperature programme. The sample was placed in a temperature programmed furnace. Thermal stability was analyzed using TGA Q-50 of TA instruments under N<sub>2</sub> atmosphere. The samples weight of about 5–7 mg was heated at a rate of 20°C/min from ambient temperature to 600°C. The corresponding weight changes were noted with the help of an ultra-sensitive microbalance. The data of weight loss versus temperature and time was

recorded online in the TA Instrument's Q series Explorer software. The analysis of the thermogravimetric (TG) and derivative thermogravimetric (DTG) curves were done using TA Instrument's Universal Analysis 2000 software version 3.38.

The oxidation index (OI) was calculated based on the weight of carbonaceous char as related by the empirical equation:

$$\text{OI} \times 100 = 17.4 \times 0.4\text{CR} \dots\dots\dots (2.1)$$

#### 2.2.3.3.1 Kinetic analysis of thermal decomposition

To evaluate the thermal stability and kinetic parameters of the sample, non-isothermal thermal degradation kinetics was used. The reaction rate can be described in terms of reaction mechanism,  $f(\alpha)$ ; where  $\alpha$  is the degree of conversion;  $\alpha = (W_0 - W_t) / (W_0 - W)$  [ $W_0$  is the initial weight of the sample,  $W_t$  is the weight remaining at a given temperature  $T$ ,  $W$  is the final weight] and a temperature –dependent function,  $k(T)$ :

$$\frac{d\alpha}{dt} = k(T)f(\alpha) \dots\dots\dots (2.2)$$

By substituting the Arrhenius equation in the temperature dependent term  $k(T) = A \exp(-E_a/RT)$ ,

$$\frac{d\alpha}{dt} = A \exp\left(-\frac{E_a}{RT}\right) f(\alpha) \dots\dots\dots (2.3)$$

Where  $\alpha$  is the conversion degree or fractional weight loss,  $t$  is the reaction time,  $A$  is the pre-exponential factor,  $R$  is the gas constant,  $T$  is the absolute temperature,  $E_a$  is the apparent activation energy and  $f(\alpha)$  is the reaction model.

If the constant heating rate of TGA process is set as  $\beta = dT/dt$ , the conversion degree  $\alpha$  can be expressed as the function of the temperature. The temperature is dependent on the heating time. Therefore,

$$\frac{d\alpha}{dt} = \frac{d\alpha}{dT} \frac{dT}{dt} = \beta \frac{d\alpha}{dT} \dots\dots\dots (2.4)$$

$\beta$  is the heating rate in TGA. The combination of equation (2.3) & (2.4) gives the following relationship

$$\frac{d\alpha}{dT} = A/\beta \exp\left(-\frac{E_a}{RT}\right) f(\alpha) \dots\dots\dots (2.5)$$

Rearranging the equation (2.5)

$$\frac{d\alpha}{f(\alpha)} = \frac{A}{\beta} \exp\left(-\frac{E_a}{RT}\right) dT \dots\dots\dots (2.6)$$

Eq.2.6 is the basic relation to determine the kinetic parameters on the basis of TG data.

After the integration of previous equation,  $g(\alpha)$  can be obtained,

$$g(\alpha) = \int_{\alpha}^0 d\alpha / f(\alpha) = A/\beta \int_{T_0}^T \exp\left(-\frac{E_a}{RT}\right) dT \dots\dots\dots (2.7)$$

where  $g(\alpha)$  is the integral conversion function. The left hand side of the equation can be resolved in terms of the reaction mechanism that better fits the decomposition process. The Table 2.1 shows the expressions of  $g(\alpha)$  corresponding to each one of the mechanism functions  $f(\alpha)$  and “n” is the reaction order [4,5].

**Table 2.1 Algebraic expressions of functions  $f(\alpha)$  and  $g(\alpha)$  and its corresponding mechanisms**

Symbol	$f(\alpha)$ function	$g(\alpha)$ function	Mechanism model
	$(1-\alpha)^n$	$[1-(1-\alpha)]$	Phase boundary-controlled reaction(plane symmetry)
R2		$2[1-(1-\alpha)^{1/2}]$	Phase boundary-controlled reaction (contracting area)
R3		$3[1-(1-\alpha)^{1/3}]$	Phase boundary-controlled reaction(contracting volume)
F <sub>n</sub>	$(1-\alpha)$	$-\ln(1-\alpha)$	Reaction order with $n=1$
	$1/n(1-\alpha)^{1-n}$	$1-1-(1-\alpha)^{1/2} \quad 1-(1-\alpha)^{1/3}$	$n$ th Reaction order with $n=1/2, 1/3$
A <sub>n</sub>	$[-\ln(1-\alpha)]^{(1-n)}(1-\alpha)$	$[-\ln(1-\alpha)^n]$	Random nucleation and growth of nuclei(Avrami-Erofeev equation) $n=2/3, 1/2, 1/3, 1/4$
P <sub>n</sub>	$1/n(\alpha)^{1-n}$	$\alpha^n$	Power law $n=1/4, 1/3, 1/2, 3/2$

The integral in the right hand side has no analytical solution and several kinds of approximation are generally used. Flynn–Wall–Ozawa [6], Friedman [7], Kissinger [8], Freeman-Carroll [9] and other researchers have used several differential and integral methodologies, involving either a single thermogram or multiple thermograms with different heating rates have been developed. In the present investigation, three different non isothermal methods are used for the computation of the kinetic parameters. The three well-known kinetic methods such as Broido (BR), Horowitz-Metzger (H-M) and Coats-Redfern (C-R) methods are applied in this study and their main equations are given below [10].

I. Horowitz-Metzger (HW) method

$$\ln \left[ \ln \left( \frac{1}{1-\alpha} \right) \right] = E_a \theta / RT_s^2 \dots\dots\dots (2.8)$$

where  $E_a$  the activation energy,  $\theta=T-T_s$ ,  $T_s$  the DTG peak temperature and  $T$  the temperature corresponding to weight loss. Plot of  $\ln [-\ln (1-\alpha)]$  verses  $\theta$  should give a straight line whose slope is  $E_a/RT_s^2$ .

II. Coats – Redfern(C R) method

$$\ln \left( \frac{g(\alpha)}{T^2} \right) = \ln \left[ \frac{AR}{\beta E_a} \left( 1 - \frac{2RT}{E_a} \right) \right] - \frac{E_a}{RT} \dots\dots\dots (2.9)$$

where  $\alpha$  is the fraction of the sample decomposed at temperature  $T$ ,  $A$  is the frequency factor,  $\beta$  is the heating rate ,  $E_a$  is the activation energy and  $R$  is the gas constant. A plot of  $\ln [g(\alpha)/T^2]$  {where  $g(\alpha)$  is the integrated from of various kinetic model equation as given in Table 2.1} against the reciprocal of absolute temperature ( $1/T$ ) gives the slope for evaluation of activation energy.

III. Broido’s method (BM)

$$\log(-\log(1-\alpha)) = - \left( \frac{E_a}{2.303R} \right) \left( \left( \frac{1}{T} \right) + C \right) \dots\dots\dots (2.10)$$

where  $(1-\alpha)$  is the fraction of initial molecules not yet decomposed,  $T$  the peak temperature of the derivative curve of TG,  $R$  the universal gas constant and  $E_a$  is the activation energy which can be calculated from the plot of  $\log(-\log(1-\alpha))$  verses  $1/T$ .

**2.2.3.4 Dynamic mechanical analysis (DMA)**

DMA is used for studying the viscoelastic behavior of polymers. A sinusoidal stress is applied and the strain in the material is measured,

allowing one to determine the complex modulus [11]. Dynamic mechanical analysis measures the mechanical properties of materials as a function of time, temperature and frequency. Dynamic mechanical analysis was carried out using a dynamic mechanical analyzer (DMA Q-800, TA instruments). Rectangular shaped specimens of dimension 35 X 4 X 3 mm<sup>3</sup> were used. DMA tests were conducted at a frequency of 1 Hz. A temperature ramp was run from 38 to 125°C at a heating rate of 3°C/min. Storage modulus, loss modulus and  $\tan \delta$  are used to generate the information about crystalline as well as amorphous nature in polymers. The variation of these components as a function of temperature is used to study the molecular motion in the polymers.

The storage modulus measures the stored energy, representing the elastic portion, and the loss modulus measures the energy dissipated as heat, representing the viscous portion. For viscoelastic materials, the modulus is a complex quantity.

$$E^* = E' + i E'' \dots\dots\dots (2.11)$$

$E'$  = storage modulus corresponding to the elastic response to the deformation and it is a measure of stiffness.

$E''$  = loss modulus corresponding to the plastic response to the deformation and it is associated with the dissipation of energy as heat when material is deformed.

$E''/E' = \tan \delta$ , useful for determining the occurrence of molecular transition such as glass transition temperature.



### 2.2.3.5 Mechanical properties

#### (a) Tensile properties

Tensile properties were evaluated using Shimadzu Autograph AG-I series universal testing machine at a crosshead speed of 50 mm/min with a load cell capacity of 10KN, according to ASTM D 638. The length between the jaws at the start of each test was fixed to 50 mm. A minimum of five samples were tested in each composite and the average results were recorded.

#### (b) Flexural properties

The flexural test measures the force required to bend a beam under three point loading conditions. Flexural modulus is used as an indication of material's stiffness when flexed. The data is used to select materials for parts that will support loads without flexing. Flexural strength was measured by three point loading system using UTM (Shimadzu AG-1) with a load cell capacity according to ASTM D 790. The flexural properties were determined using rectangular shaped samples at a crosshead speed of 5mm/min. A minimum of five samples were tested in each sample and the average results were recorded.

The flexural strength is given by

$$S = 3PL/2bd^2 \dots\dots\dots (2.12)$$

Where S = flexural strength, P = maximum load at the moment of break, b = width of the specimen, L= length of the span and d = the thickness of the specimen.

The maximum strain ( $r$ ) in the outer fibers is given by

$$r = 6Dd / L^2 \dots\dots\dots (2.13)$$

where,  $D$  is the deflection.

The flexural modulus is calculated from the slope of initial portion of the flexural stress strain curve

**(c) Impact strength**

The impact strength describes the ability of a material to absorb shock and impact energy without breaking. The impact strength is calculated as the ratio of impact absorption to test specimen cross-section. Toughness is dependent upon temperature and the shape of the test specimen. The area under the stress-strain curve is directly proportional to the toughness of the material. Higher the impact strength of the material, higher will be the toughness and vice versa.

The Izod impact strength of the injection molded samples was determined as per ASTM D 256. The test was carried out using REIL IMPACTOR JUNIOR (CEAST) machine with a pendulum of 4kJ and striking velocity of 3.4m/s. Sample is clamped vertically in the base of the machine. A pendulum swings on its track and strikes the sample. The energy lost as the pendulum continuous on its path is measured from the distance of follow through. The impact energy is directly read from the machine.

$$\text{Impact strength} = \text{Impact energy (J)} / \text{Thickness (m)} \dots\dots (2.14)$$

**(d) Hardness**

Durometer hardness test measures the penetration of a specified indenter into the material under specified conditions of force and time. Hardness of the test samples were determined using Durometer hardness Shore D according to the ASTM D 2240. The specimen is first placed on a hard flat surface. The indenter for the instrument is then presses into the specimen making sure that it is parallel to the surface.

**2.2.3.6 Melt Flow Index (MFI)**

Melt flow index is a measure of the ease of flow of the melt of a thermoplastic polymer. It is defined as the mass of polymer, in grams, flowing in 10 minutes through a capillary of a specific diameter and length by a pressure applied via prescribed alternative gravimetric weights for alternative prescribed temperatures. Melt Flow Index (MFI) is a measure of the plastic's ability to flow and it is inversely related to melt viscosity. The melt flow index of the test samples was determined using a CEAST Modular Line Melt Flow Indexer, according to ASTM D1238 (230°C/2.16kg). MFI is used to determine how a polymer will process. The apparatus is reheated to a specified temperature and the material loaded into the cylinder from the top and a specified weight is applied on a piston. The weight exerts a force on the molten polymer and it immediately starts flowing through the die. A sample of the melt is taken after desired period of time and is weighed accurately. MFI is expressed as grams of polymer/10 minutes of total time of the test [12].

**2.2.3.7 Differential scanning calorimetry (DSC)**

DSC is a thermoanalytical technique in which the difference in the amount of heat required to increase the temperature of a sample and

reference is measured as a function of temperature. It is used to investigate thermal transitions, such as phase changes, crystallization, melting, glass transitions of a material as a function of temperature [13]. When the sample undergoes a physical transformation such as phase transitions, more or less heat will need to flow to it than the reference to maintain both at the same temperature. Whether less or more heat must flow to the sample depends on whether the process is exothermic or endothermic. Heat flow i.e. heat absorption (endothermic) or heat emission (exothermic), is measured as a function of time or temperature of the sample and the result is compared with that of a thermally inert reference. The materials, as they undergo changes in chemical and physical properties, which are detected by transducers, which changes into electrical signals that are collected and analyzed to give thermograms. The melting and crystallization parameter, such as melting point ( $T_m$ ), Heat of fusion ( $\Delta H_f$ ), temperature of crystallization ( $T_c$ ), and Heat of crystallization ( $\Delta H_c$ ) were used for the comparison of composites.

DSC measurements were made on a DSC Q 100 (TA instruments). The samples were heated from 30°C to 250°C at the rate of 50°C/min and kept at isothermal for 3 minutes in order to remove the thermal history, cooled from 250°C to room temperature then reheated from room temperature to 250°C at heating rate of 10°C/min under nitrogen atmosphere

Based on the mechanism of operation, DSCs can be classified into two types: heat-flux DSC and power-compensated DSC. In a heat flux DSC, the sample material, enclosed in a pan and an empty reference pan are placed on a thermoelectric disk surrounded by a furnace. The furnace is heated at a linear heating rate, and the heat is transferred to the sample and reference

pan through the thermoelectric disk. In a power-compensated DSC, the sample and reference pans are placed in separate furnaces heated by separate heaters. The sample and reference are maintained at the same temperature, and the difference in thermal power required to maintain them at the same temperature is measured and plotted as a function of temperature or time [14].

## **References**

- [1]. Sinto Jacob, Modification of Short fiber reinforced PP and HDPE using nanosilica, Phd. Thesis, 2009.
- [2]. J.G.Ryu, H.Kim, J.W.Lee, Polymer Engineering and science, 2004, 44 (7).
- [3]. Electron microscopy of polymers, G H Michler, H Goerge, Springer, 2008.
- [4]. J. Palacios, R. Perera, C. Rosales, C. Albano, J. M. Pastor, Polymer Degradation and Stability, 2012, 7, 729–737.
- [5]. C. Zhao, H. Qin, F. Gong, M. Feng, S. Zhang, M. Yang, Polymer Degradation and Stability, 2005, 87, 183–189.
- [6]. T. Ozawa, Thermochim. Acta, 1992, 203, 159–165.
- [7]. H. L. Friedman, Journal of Polymer Science: Polymer Symposia, 1964, 6, 183–195.
- [8]. H. E. Kissinger, Analytical Chemistry, 1957, 29, 1702–1706.
- [9]. E. S. Freeman, B. Carrol, Journal of Physical Chemistry, 1958, 62, 394–397.
- [10]. Asha K. Krishnan, K. E. George, Polymers for Advanced Technologies, 2014, 25(9), 955–962.

- [11]. H Wang, D.G Thompson, J.R Schoonover, R Steven, S Aubuchon, RAP Richard, *Macromolecules*, 2001, 34, 7084
- [12]. *Handbook of plastic testing and failure analysis 3<sup>rd</sup> edition*, John Wiley & sons, V Shah, Hoboken, NJ, 2007
- [13]. P W Zhu, G P Zhang, J Y Yu, G Dai, *Journal of Applied Polymer Science*, 2004, 91,431
- [14]. Pooria Gill Tahereh, Tohidi Mogha dam, Bijan Ranjbar, *Journal of Biomolecular Techniques*, 2010, 21(4), 167–193

.....❧.....

## Chapter 3

# Polypropylene/Polystyrene/clay nanocomposites: Effect of different modifications of kaolin clay

Contents	3.1 Introduction
	3.2 Methodology
	3.3 Results and Discussion
	3.4 Conclusions

### Abstract

Nanoclay composites based on polypropylene (PP)/polystyrene (PS) blends were prepared by melt mixing in a Thermo Haake Rheocord mixer. The effect of modified clays on the properties of nanocomposites has been studied. The degree of dispersion and morphology of nanocomposites were evaluated from X-ray diffraction (XRD), Transmission Electron Microscopy (TEM) and Scanning electron microscopy (SEM). Nanocomposites prepared from modified clays show improved tensile strength and modulus as compared to those prepared from unmodified clay. Vinyl silane and dialkyl silane modified nanocomposites show considerable improvement in mechanical properties. Thermogravimetric analysis (TGA) shows improved thermal stability of PP/PS/clay nanocomposites. The dynamic mechanical analysis reveals higher storage moduli over a temperature range of 40–125°C for nanocomposites and the extent of increase in the storage modulus is dependent on the type of clay. Transmission electron microscopic (TEM) observations show that vinyl silane modified nanoclay layers are intercalated on the polymer matrix and are located at the interface between the two polymers and dialkyl silane modified nanoclay layers are partially exfoliated on the polymer matrix and were located at the interface and also on the PP phase.

1. Effect of Modified Kaolin Clays on the Mechanical Properties of Polypropylene/Polystyrene Blends; Asha K. Krishnan, Tresa Sunitha George, R. Anjana, Newly Joseph, K. E. George; Journal of Applied Polymer Science; Vol. 127, Issue 2, p 1409–1415, 2013.
2. Polymer blend nanocomposites: Effect of mercapto silane modified kaolin clay on the thermal properties of Polypropylene/Polystyrene blend; Asha Krishnan. K and K. E. George; Polymers for Advanced Technologies, Vol. 25, Issue 9, p 955–962, 2014.

### 3.1 Introduction

Nanotechnology promises revolutionary technological changes for a wide range of applications in traditional industry and advanced materials. Nanostructured materials have the potential to significantly impact on the growth at every level of the world economy in the 21<sup>st</sup> century. Polymer-clay nanocomposites are a class of hybrid materials composed of organic polymer matrix in which layered inorganic particles with nanoscale dimension is distributed. As a result of the nanometer-scale dispersion, nanocomposites exhibit markedly improved mechanical, thermal, and physicochemical properties, gas and water vapor impermeability, resistance to flammability and thermal degradation as compared with the conventional composites [1–3]. These nanocomposites synergistically integrate the advantages of organic polymers and those of the inorganic filler.

Polypropylene (PP) and Polystyrene (PS) are two of the most widely used commercial polymers and hence the hybridization of PP/PS blends with nanostructured fillers may be useful in generating a variety of useful materials [3]. PP and PS used in this study are immiscible, which leads to the formation of multiphase system with different morphology that depends on the composition of the blend, viscosity ratio of the components, interfacial tension between the two phases and processing condition of the blends. Especially PP/PS blends exhibit low impact strength, low wear resistance and high friction [4]. Several problems of these blends may be caused by poor compatibility of the components. These features can be improved by using compatibilizers. As PP and PS are immiscible, a considerable amount of work on compatibilizing PP and PS has been done



by using compatibilizers such as Styrene Butadiene block copolymer (SBS), Styrene Ethylene Butylene styrene copolymer (SEBS), Styrene- Ethylene/ Propylene Diblock Copolymer (SEP) and PP-g-PS [5]. Sani Amril Sasudin *et al.* studied the effect of SEBS on the impact strength and flexural modulus of PS/ PP blends and they found that the addition of SEBS increased the impact strength of the blends but reduced the flexural strength and flexural modulus [6]. Chang –jiang You *et al.* studied the effect of Styrene- Ethylene/ Propylene Diblock Copolymer (SEP) on the compatibilization of PP/PS blend. The results showed that SEP diblock copolymer could act as compatibilizer in PP/PS immiscible blends which increased the mechanical properties [5]. Studies on the reactive compatibilization of PP/PS blend have been reported because of the lack of functional groups in both PP and PS. Dicumyl peroxide (DCP) was employed by Xie and Zheng in order to generate in- situ PP-g-PS graft copolymer in one step extrusion process and the dispersed particle size was greatly reduced [7].

In recent years, the possible application of relatively cheap organoclays as modifiers is getting significant attention. Organoclays are being widely used as an attractive alternative to conventional fillers. The first demonstration of polymer clay nanocomposites was reported by Kojima and co-workers [8, 9]. Since the early 1990 polymer blends have been used as the matrices of polymer nanocomposites. Much of the work in this area has focused on montmorillonite. Yun Zhu *et al.* found out that MMT clay can play a significant role in reducing the dispersed domain sizes in PP/PS blend. The results showed that the organoclay platelets tend to form knife like structure in the PS domain under the shear stress of the continuous PP phase during compounding [10]. Kyunyl Kim *et al.* successfully prepared PP/PS clay

nanocomposites by continuous compounding with high intensity ultrasonic waves during extrusion process which enhanced the interfacial interaction between the immiscible polymer blend [11]. Suprakas Sinha Ray *et al.* studied the role of Closite 20 A (C20A) as an interfacial modifier in PS/PP or PS /PP-g-MA blends. The results clearly indicated that C20A simultaneously acts as nanofiller and modifier [12].

Hence, in this study kaolin nanoclay with a 1: 1 type layered structure with chemical composition  $\text{Al}_2\text{Si}_2\text{O}_5(\text{OH})_4$  is proposed to be used. It is a layered silicate mineral with one tetrahedral sheet linked through oxygen atoms to one octahedral sheet of alumina octahedral. The layers are held together via hydrogen bonds, dipolar interactions and Van der Waals forces, which result in a low intrinsic inner surface reactivity. Because of the hydrophilic character of kaolin and hydrophobic properties of polymer the modification of kaolin is necessary [13, 14]. Modification was done by coupling of organosilane compounds, with two kinds of reactive groups (inorganic and organic) in a single molecule. A chemical reaction between the functional groups (such as -OH) of filler and the alkoxy groups of silane is expected to occur, creating a silane-functionalized surface [15]. The silane grafting of clay has received much attention in recent years, both in the industry and academy. Silane modified kaolin nanoclay has many applications; it is used in paper, paint, rubber, plastics, and ceramic industries.

A comparative study of Nanocaliber 100 (unmodified kaolin nanoclay) along with four types of commercially available modified nanoclays viz. Nanocaliber 100 V (vinyl silane modified kaolin nanoclay) Nanocaliber100 A (amino silane modified kaolin nanoclay), Nanocaliber 100 M (mercapto

silane modified kaolin nanoclay) and Nanocaliber 100 Z (dialkyl silane modified kaolin nanoclay), on the static and dynamic mechanical properties of Polypropylene/ Polystyrene blends has proposed to be investigated. The morphological and thermal properties of PP/PS blend have also been explored.

## **3.2 Methodology**

### **3.2.1 Materials**

The details of the polymers and nanoclay types used for the study are discussed in Chapter 2 (sections 2.1.1, 2.1.2& 2.1.3).

### **3.2.2 Methodology**

#### **3.2.2.1 Nanocomposite preparation**

PP/PS (80/20) and the nanoclays Nanocaliber 100 V, Nanocaliber 100, Nanocaliber 100M, Nanocaliber 100Z and Nanocaliber 100 A in varying amounts (1-5wt %) were prepared by melt mixing using an internal mixer (Haake Rheomix 600) at 180°C with a rotor speed of 50 rpm, and the mixing time is 8 min for each sample. After mixing the melt was pressed in a hydraulic press, cut into pieces and injection molded in a DSM Micro 10cc Injection Molding Machine, with barrel temperature of 190°C.

#### **3.2.2.2 Characterization**

The details of the characterization techniques used for the study are given in the section 2.2.3. Transmission electronic microscopy (TEM) was performed on a JEM2100 at an acceleration voltage of 200 KV. In order to assess resistance of the tensile samples to aging, samples were UV –irradiated

using a low pressure mercury vapor discharge lamp (TUV 30 W,  $\lambda=253.7$  nm) in air atmosphere at room temperature for 360 hours. Samples were mounted on racks positioned 5 cm from the lamps and the temperature in the cabinet was maintained at  $30 \pm 2^\circ\text{C}$ . The UV irradiated samples were then subjected to tensile test.

### 3.2.3 Theoretical modeling of tensile modulus

In the present study Halpin-Tsai model, Takayanagi model, Hui-Shia, Voigt upper bound model and Reuss lower-bound prediction models for elastic moduli of filled polymers are used to predict the elastic- mechanical response.

Halpin and Tsai developed a well-known composite theory for predicting the stiffness of unidirectional composites as a function of aspect ratio. The Halpin–Tsai model is chosen in this work because of its effectiveness in predicting the stiffness of glass fiber reinforced composites, their adaptability for different filler geometries, particularly disks and for their prevalence in the literature [16]. Halpin-Tsai equations are widely used to estimate the reinforcing effect of filler in the composites. The elastic modulus of composite materials reinforced by fibers or flake like fillers can be predicted by Halpin- Tsai equation [17, 18]. The equation theoretically predicts Young’s modulus of a composite material. The Halpin-Tsai model may be expressed as:

$$E_c/E_m = (1 + \zeta \eta \phi_f) / (1 - \eta \phi_f) \dots\dots\dots(3.1)$$

where  $\eta = (E_f / E_m - 1) / (E_f / E_m + \zeta)$

where  $E_c$ ,  $E_f$  and  $E_m$  are Young's moduli of composites, filler and polymer matrix respectively,  $\Phi_f$  is the filler volume fraction and  $\zeta$  is the shape parameter dependent on filler geometry, orientation and loading direction. In a particular direction,  $\zeta = 2(l/d)$  for fibers or  $2(l/t)$  for disk-like platelets where  $l$ ,  $d$  and  $t$  are the length, diameter and thickness of the dispersed fillers. A 2-D disc-like clay platelets contribute less to modulus than 1-D fiber-like fillers. So a modulus reduction factor (MRF) is introduced to modify the Halpin-Tsai model and the corresponding equation is represented as [19]:

$$E/E_m = 1 + \{ \zeta (MRF) \eta \phi_f / (1 - \eta \phi_f) \} \dots\dots\dots(3.2)$$

MRF might lie in the range between 0.167 and 1 for randomly disposed short fibers and in a special case of platelet fillers, MRF = 0.66 has been shown to well predict the tensile moduli of rubber/clay nanocomposites over a wide range of clay volume fractions [20].

By assuming fibers as aligned and both the fibers and matrix are under the uniform strain in the fiber direction,  $\zeta \rightarrow \infty$  the Halpin-Tsai model predictions concerning the elastic modulus reach the upper-bound. Then the theory is referred as Voigt rule of mixtures (ROM) [21, 22] and the equation may be stated as:

$$E_c = \phi_f E_f + (1 - \phi_f) E_m \dots\dots\dots(3.3)$$

Reuss [23] applied the same uniform stress on the fiber and matrix in the transverse direction (normal to the fiber direction) and got the effective modulus in the transverse direction. In such case  $\zeta \rightarrow 0$ , the Halpin-Tsai

model equation reaches at the lower bound elastic modulus value corresponding to the elastic response. Then the theory is referred to as Reuss inverse rule of mixtures (IROM) [24] and the equation may be stated as:

$$1/E_c = \phi_f/E_f + (1 - \phi_f)/E_m \dots\dots\dots(3.4)$$

If the effects of interface are neglected ( $t=0$ ), the well-known Ji's model for tensile modulus prediction reduces to the two-phase model of Takayanagi [25, 26]. The Takayanagi model prediction underestimates the Young's modulus as the effect of interfacial contribution which plays a functional role in stress-transfer mechanism is neglected.

$$E = E_0 [(1-\beta) + \beta / \{(1-\beta) + \beta E_1/E_0\}]^{-1} \dots\dots\dots(3.5)$$

where  $\beta = \sqrt{\phi_f}$ ,  $\phi_f$  is the volume fraction of the platelets.

Hui-Shia model (H-S model) [27, 28] was developed to predict the tensile modulus of composites with the simple assumption of perfect interfacial bonding between the polymer matrix and clay is given by:

$$E_c/E_m = 1 / \{1 - \phi_f/4(1/\zeta + 3/\zeta + \square)\} \dots\dots\dots(3.6)$$

Where  $\zeta = \phi_f + E_m/E_f - E_m + 3(1 - \phi_f) [\{(1-g) \alpha^2 - g/2\} / \alpha^2 - 1]$

$$g = \pi/2\alpha$$

$$\square = (1 - \phi_f) [\{3(\alpha^2 + 0.25) g - 2 \alpha^2 / (\alpha^2 - 1)\}]$$

where  $\alpha$  is the inverse aspect ratio of dispersed fillers and  $\alpha = t/l$  for disk-like platelets ( $\alpha \leq 0.1$ ).

### 3.2.3.1 Effect of aspect ratio on the modulus ratio of PP/PS/clay nanocomposites

Figures 3.1 and 3.2 depict the effect of aspect ratio on the modulus in Equations (3.1) and (3.6) respectively. The figures show that the modulus ratio increases with increasing aspect ratio. Thus at high aspect ratios, the level of reinforcement is predicted to be higher for the nanocomposites. In general, both theories emphasize the strong effects of filler modulus and aspect ratio. Dispersion of nanoclay layers of high aspect ratios into the matrix is considered as the major contributor to the enhancement of stiffness in clay nanocomposites.

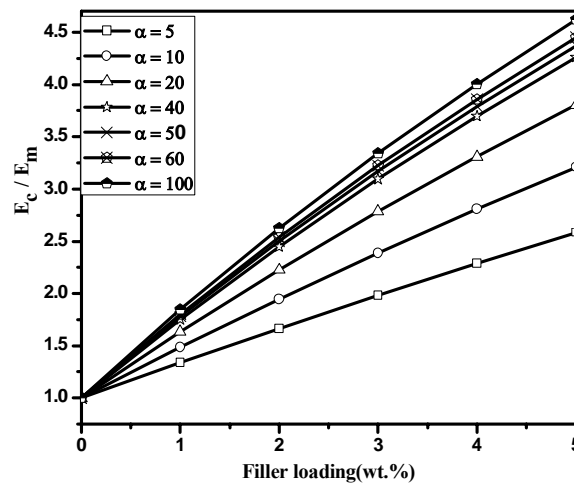


**Figure 3.1 Effect of aspect ratio on the modulus ratio of PP/PS/clay nanocomposite (Halpin-Tsai)**

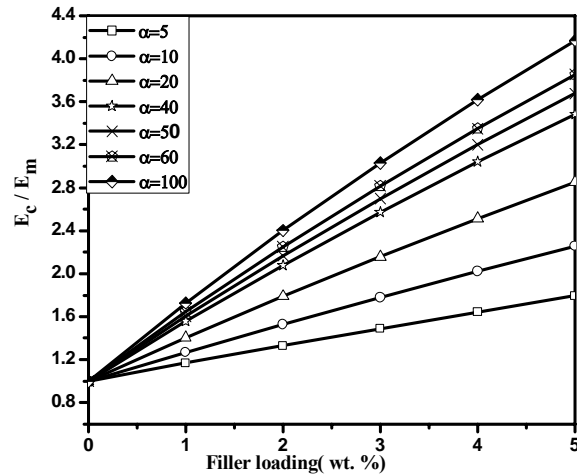


Figure 3.2 Effect of aspect ratio on the modulus ratio of PP/PS/clay nanocomposite (Hui-Shia)

### 3.3 Results and Discussion

#### 3.3.1 X-ray Diffraction (XRD)

X-ray diffraction is extremely useful to analyze the structure and morphology of polymer nanocomposites. The change in interlayer spacing of clay gives more information about the formation of nanocomposites. The formation of an intercalated structure should result in a decrease in  $2\theta$ , indicating an increase in the d-spacing. The interlayer d-spacing observed by XRD for polymer-clay nanocomposites has been used to describe the nanoscale dispersion of clay in the polymer matrix [29].



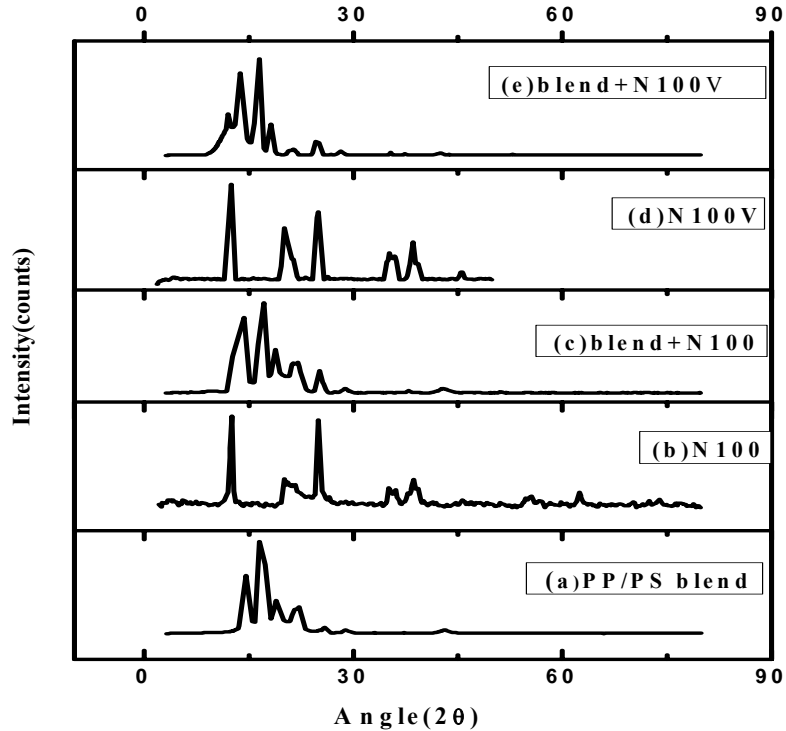


**Figure 3.3 XRD patterns of (a) PP/PS blend, (b) N100, (c) blend+N100, (d) N100V and (e) blend+N100V**

Figures 3.3 & 3.4 depict the XRD patterns of N100, N100V, N100Z, N100M, N100 A, PP/PS pure blend and its nanocomposites reinforced with the five types of modified nanoclays at 3wt %. Diffraction peaks that appear at  $2\theta = 15^\circ - 20^\circ$  corresponds to the monoclinic  $\alpha$  form of the PP (Figure 3.3(a)) [30, 31]. The PP/PS/clay nanocomposites have slightly different intensity of reflections than PP/PS blend and this indicates the modification of the crystalline nature of PP in the PP/PS/clay nanocomposites. The original basal reflection peak for N100 is  $12.54^\circ$  having an intergallery spacing of 7.05 nm and the peaks for N100V and N100A are at  $12.44^\circ$  and at  $12.28^\circ$ , respectively, and have an intergallery spacing of 7.11 and 7.20 nm.

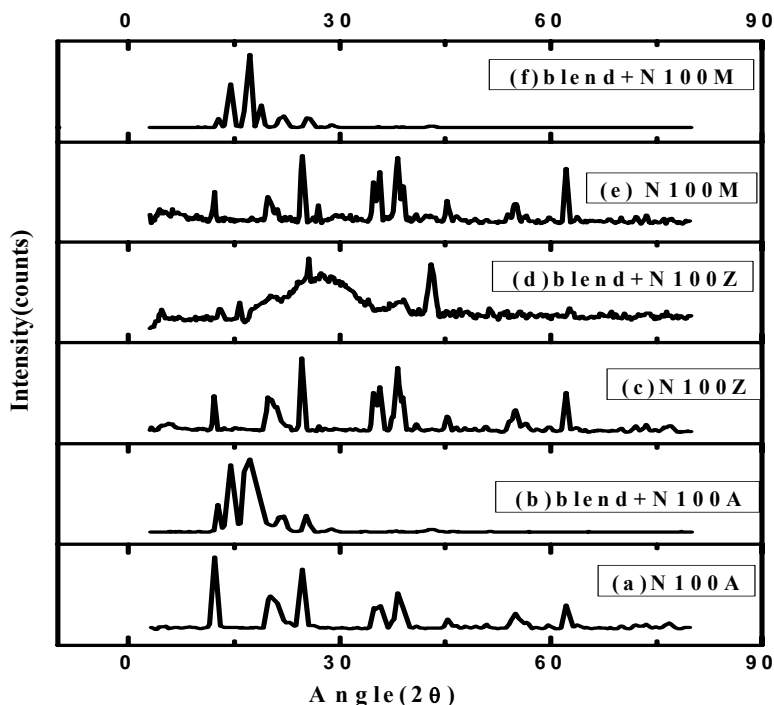


**Figure 3.4** XRD patterns of (a) N100A (b) blend+N100A (c) N100Z (d) blend+N100Z (e) N100M and (f) blend+N100M

For the PP/PS/N100V nanocomposite, the characteristic peak of N100V is shifted to  $2\theta = 12.08^\circ$ , corresponding to a d-spacing of 7.32 nm, which indicates that some PP/PS molecular chains are intercalated between the nanoclay galleries, forming an intercalated structure. Characteristic peak for PP/PS/N100A nanocomposite is at  $12.74^\circ$ , has a d-spacing of 6.99 nm and peak for PP/PS/N100 is at  $12.67^\circ$  having a d-spacing of 6.99 nm. The XRD does not show any shift in the diffraction peak for the PP/PS/N100A and PP/PS/N100 nanocomposites. The characteristic peak for N100M is at  $12.19^\circ$  having an intergallery spacing of 7.25 nm. PP/PS/N100M nanocomposite shows the characteristic peak at  $12.76^\circ$  and has a d-spacing of 6.93 nm. This shows that these blends can be considered as conventional micro composites. The

basal reflection peak for N100Z is  $12.18^\circ$  having an intergallery spacing of 7.26 nm. There is a broadening of peak and reduction of intensity is observed in the case of PP/PS/N100Z modified clay nanocomposite. This shows an improved dispersion of nanoclay layers in the polymer matrix and it confirms partial exfoliation of nanoclay in the nanocomposite. When nanoclay exfoliates, there will be a decrease in the intensity of the diffraction peaks due to a reduction in the degree of crystallinity of the silicate sheets.

The extent of nanoclay intercalation in a polymer nanocomposite depends on three important factors: clay–clay interaction, polymer–surfactant interaction and polymer–clay interaction. Surfactants can weaken clay–clay interaction so as to allow polymer interaction between clay layers; these same surfactants can also sterically hinder the access of polymer chains to the nanoclay surface. Hence, the selection of an appropriate surfactant for the polymer of interest is of utmost important in melt processing [32]. By incorporating surfactant with hydrophobic tails on the nanoclay surface will efficiently reduce clay–clay interaction. During melt blending, the presence of vinyl silane groups and dialkyl silane groups enhances the ability of the PP/PS chains to intercalate between the nanoclay galleries. This is due to the increased nanoclay gallery distance and favorable interactions between the surfactant and the polymer molecule. Vinyl silane and dialkyl silane modified nanoclays are found to be more suitable for PP/PS blend [33]. N100V and N100Z modified nanoclays exhibits a maximum basal spacing which is probably due to the difference in structure of the surfactants used in the modification of unmodified kaolin nanoclay.

### 3.3.1.1 Relative Interaction of Nanocomposites

Relative interaction (RI) of the nanocomposites has been computed as a percentage increase in d-spacing according to the following equation [34]:

$$RI = (d-d_0)/d_0 \times 100 \dots\dots\dots (3.7)$$

where  $d_0$  and  $d$  are the d-spacing of the nanoclay and corresponding nanocomposites respectively.

As the nanocomposite with N100Z is showing a broad peak due to partial exfoliation, it is impossible to calculate RI in accordance with the above equation. The nanocomposite with N100V only shows intercalated structure and its RI (%) value is 3.017 %.

### 3.3.1.2 Number of Crystallites of PP/PS/clay nanocomposites

When the polymer molecules exist in a nanoclay gallery, the d-spacing value is usually high and when the molecules do not exist in a gallery, the d-spacing value is expected to be lower. The d-spacing of nanocomposites is the average value of the different d-spacing between the platelets of a clay crystallite. According to the Daumas–Herold model, [35] the stage structure of clay nanocomposites were determined as follows.

Crystallite thickness can be calculated by using the Scherrer equation:

$$t = (K \times \lambda)/B \cos \theta \dots\dots\dots (3.8)$$

where  $t$  = crystallite thickness

$K$  = a constant (0.91 for clay)

$\lambda$  = X-ray wavelength

$B$  = Full width half max (FWHM) of the diffraction peak

$\theta$  = diffraction angle

The number of platelets in a clay crystallite can be calculated by the following formula:

$$N = t/d_{001} + 1 \dots\dots\dots(3.9)$$

where N= no. of clay platelets (stacks) in a clay crystallite and d<sub>001</sub>: d-spacing of corresponding nanocomposites

**Table 3.1 Number of crystallites of PP/PS/clay nanocomposites**

Samples	Crystallite thickness(nm)	No of clay platelets
Blend +3wt % N100	24.57	4.52
Blend +3wt % N100A	24.58	4.54
Blend +3wt % N100M	18.16	3.62
Blend +3wt % N100V	18.13	3.42
Blend +3wt % N100Z	—	—

Crystalline thickness and the number of clay platelets of PP/PS nanocomposites containing five clays (N100, N100A, N100M, N100Z and N100V) measured using equations 3.8 and 3.9 are listed in Table 3.1. From the table it can be observed that the nanocomposites with N100 and N100A shows crystallite thickness of 25 nm but in the case of N100V modified nanocomposite it reduced to 18nm. This decrease in the crystallite thickness or number of stacks in the N100V based nanocomposites can be due to the possible exfoliation of a few layers from the end of the stacks into the melt.

### **3.3.2 Transmission electron microscopy (TEM)**

The dispersion and location of organoclay in the polymer blends has a significant influence on the morphological development of the blends as well as on the effect of organoclay as a modifier. Transmission electron

microscopy is an effective method to find out the location of nanoclay particles in polymer.

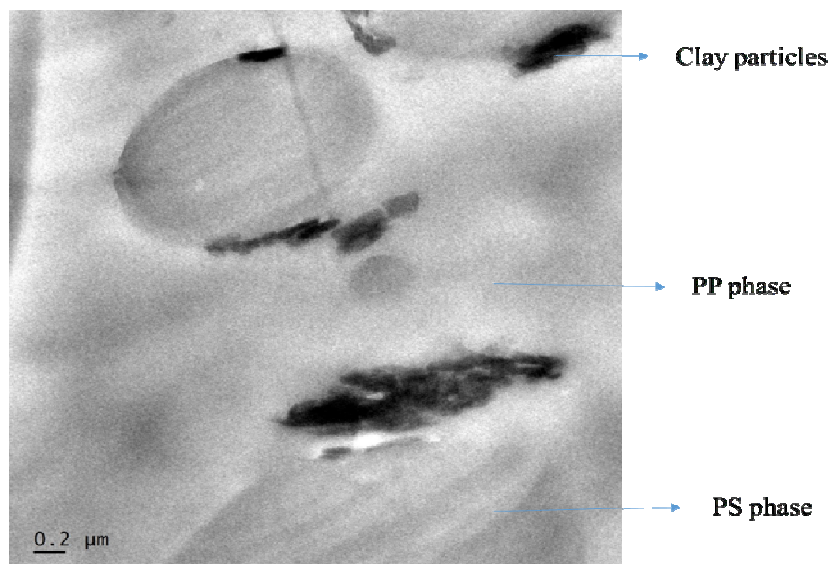


**Figure 3.5 Low magnification transmission electron microscopic image of PP/PS/3wt% N100V**

The low magnification TEM image of PP/PS/3wt%N100V and PP/PS/3wt%N100Z nanocomposites are illustrated in the Figures 3.5 & 3.6 respectively. The figure shows a bright field TEM image of nanoclay-filled PP/PS blend that gives a general view of the dispersed PS domains (ellipsoid) in the PP matrix. Besides, the nanoclay particles (dark lines) are easily visualized in the TEM photographs. In PP/PS/3wt%N100V nanocomposite, the nanoclay particles are located in the PP/PS interface; thereby it acts as a modifier. But in the case of PP/PS/3wt%N100Z nanocomposite the nanoclay particles are present both in PP/PS interface and also in PP phase. Therefore the nanoclay particles act as modifier and also as reinforcing filler.

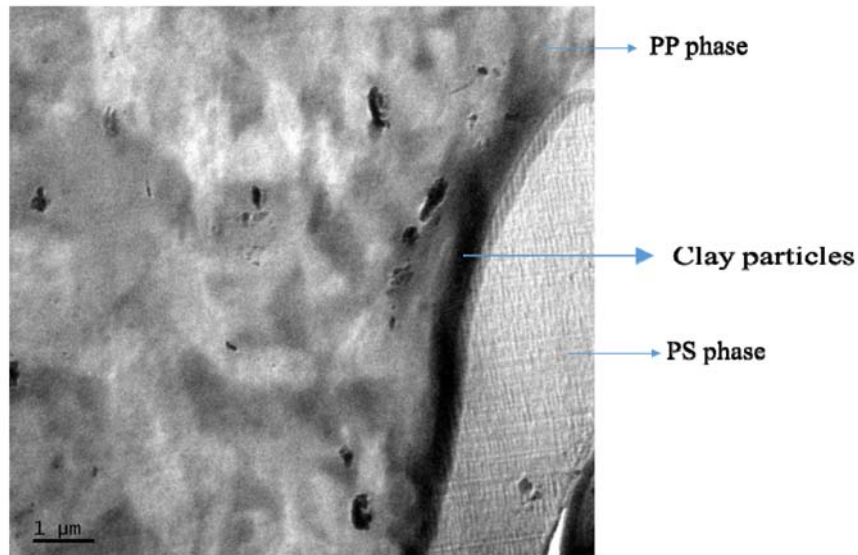


**Figure 3.6** Low magnification transmission electron microscopic image of PP/PS/3wt% N100Z

TEM analysis was carried out to localize the nanoclay particles in the blend and to have more insight into nanoclay interfacial activity. TEM bright field images of PP/PS/N100Z nanocomposites with 3 and 5wt% loadings are displayed in Figures 3.7(a) and 3.7 (b). The bright phase of the picture is the matrix phase and the dark phase the particle phase. In the TEM photographs (Figure 3.7(a)) most of platelets appear to be well-dispersed and are in a random distribution. There are few locations in which the nanoclay platelets are appeared to be agglomerated in the matrix [36]. The nanoclay particles are found to be agglomerated in PP/PS blend having 5 wt% of nanoclay loading.

TEM bright field images of PP/PS/N100V nanocomposites with 3 and 5wt% loadings are shown in the Figures 3.8(a) and 3.8(b). The bright phase of the picture is the matrix phase, and the dark phase is the particle

phase. The dark entities are the cross section of intercalated nanoclay layers. The intercalation of the modified kaolin nanoclay by the polymer blend is further evidenced in Figure 3.8(a). The polymer molecules separate the clay particles into individual layers of nanometer thickness.

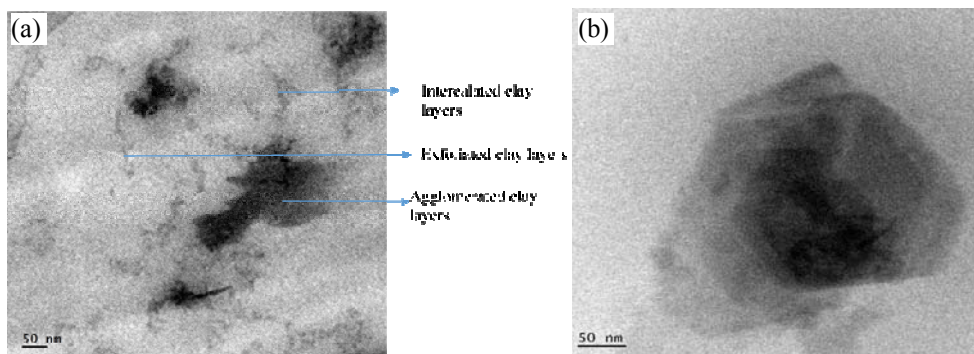


**Figure 3.7** Transmission electron microscopic bright field images of (a) PP/PS/3 wt% N100Z nanocomposite and (b) PP/PS/5 wt% N100Z nanocomposite

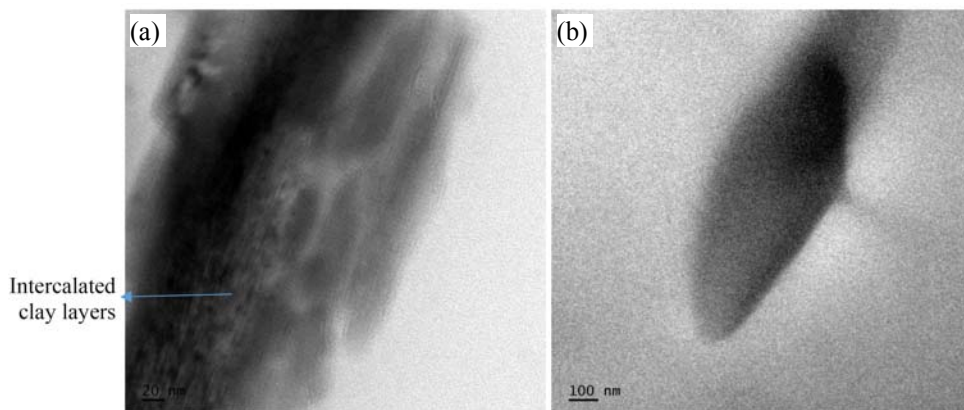


**Figure 3.8** Transmission electron microscopic bright field images of (a) PP/PS/3 wt% N100V nanocomposite and (b) PP/PS/5 wt% N100V nanocomposites



The intercalation of the modified kaolin nanoclay by the polymer blend is further evidenced by the TEM analysis and it supports the results obtained from XRD. TEM image of PP/PS/N100V nanocomposite with 5 wt% clay loading is shown in Figure 3.8(b). Nanoclay particles are found to be agglomerated in PP/PS blend at higher filler loadings which is in good agreement with the mechanical properties discussed in section 3.3.7.

### **3.3.2.1 Determination of aspect ratio of clay platelets**

In order to model the modulus of nanocomposites, the aspect ratio of nanoclay platelets must be determined. TEM photographs are used to analyze the length and thickness of the clay platelets for the determination of aspect ratio. The silicate layers have good plane orientation. Therefore, the aspect ratio of nanoclay platelets should be directly calculated by measuring the length and thickness of the dark lines in TEM photographs at different magnifications. The statistical data of the aspect ratio for the clay nanocomposites are shown in the Figures 3.9(a) & 3.9(b). These data were obtained by measuring TEM photographs of nanocomposites at different magnifications [17]. The average aspect ratio for PP/PS/N100Z (Figure 3.9(a)) nanocomposite is found to be 36 and for PP/PS/N100V (Figure 3.9(b)) nanocomposite is 30.

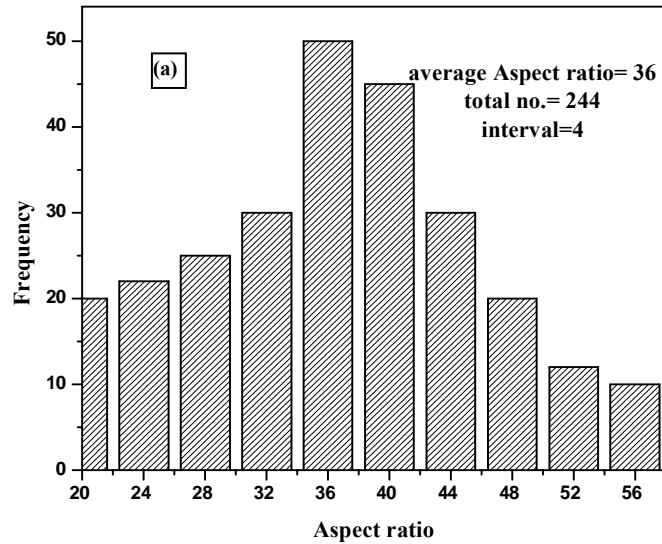


Figure 3.9(a) Histogram of the aspect ratio of clay platelets in PP/PS/N100Z nanocomposites

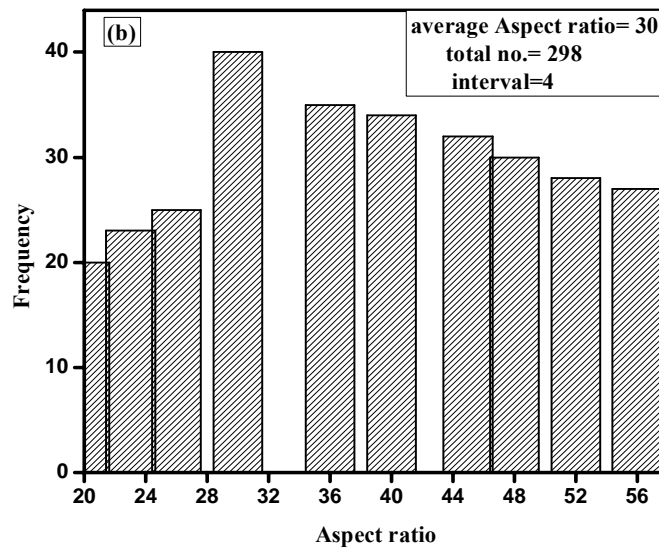
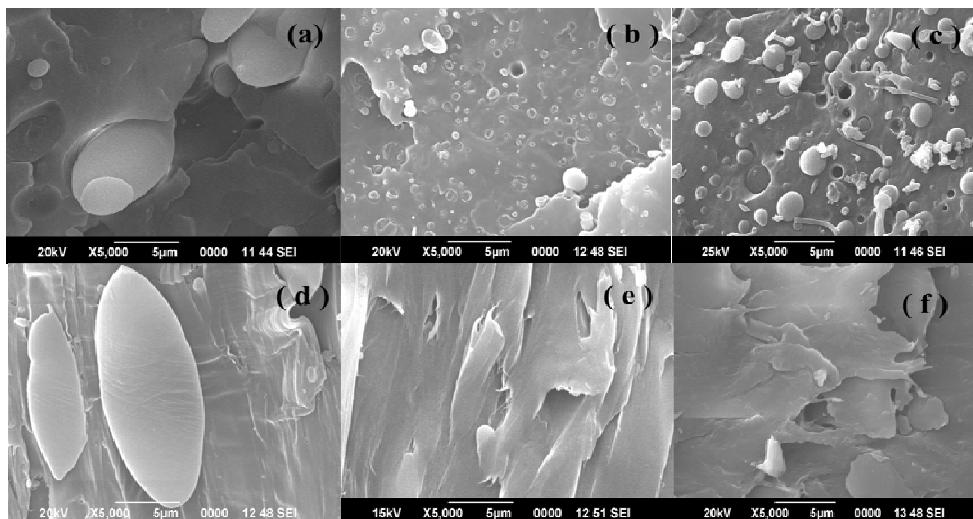


Figure 3.9 (b) Histogram of the aspect ratio of clay platelets in PP/PS/N100V nanocomposite

### **3.3.3 Scanning electron microscopy (SEM)**

The changes in the phase morphology of PP/PS blend with different types of nanoclay modifications at 3wt% are shown in the Figure 3.10. On the basis of the morphology of organoclay, we can explain how the silane modification of the nanoclay edges affects the dispersion process of clay nanoparticles in a polymer matrix. The morphology of the fractured cross sections of the tensile samples is illustrated in Figure 3.10. PP/PS blend (Figure 3.10 (a)) exhibits a morphology in which spherical domains of PS phase are surrounded by the continuous PP phase. The interface between the spherical domains and the PP matrix shows weak interfacial adhesion between two phases.

The PP/PS/N100 nanocomposite (Figure 3.10(b)) contains aggregates of micro sized particles, which shows weak interfacial interaction. SEM analysis shows that the nanoclays are dispersed in the polymer matrix in the form of large and small aggregates in PP/PS/N100A nanocomposites (Figure 3.10(c)). The weak interface between the dispersed phase (PS) and the continuous phase (PP) results in reduction of properties in PP/PS/N100A nanocomposite. A similar result obtained for PP/PS/N100M nanocomposite also explains the reduction in mechanical properties (Figure 3.10 (d)).



**Figure 3.10 SEM images of (a) PP/PS blend, (b) PP/PS/N100, (c) PP/PS/ N100A, (d) PP/PS/N100M (e) PP/PS/N100V and (f) PP/PS/N100Z**

SEM photograph of a typical homogeneous dispersion is observed in the N100V modified clay nanocomposite and in N100Z modified clay nanocomposite (Figures 3.10(e) & 3.10(f)). Addition of N100V and N100Z clays improve adhesion between two components giving a homogeneous morphology. Thus the improved homogeneity increases the tensile and flexural properties. This result is in complete agreement with the observed mechanical properties (section 3.3.7) and corroborates the XRD results (section 3.3.1). The nanocomposites prepared using vinyl silane and dialkyl silane modification exhibits better dispersion of nanoclay layers within the polymer matrix than the unmodified as well as amino silane modified kaolin nanoclay and mercapto silane modified kaolin nanoclay.

### 3.3.4 Thermogravimetric analysis (TGA)

In most cases the incorporation of nanoclay into the polymer matrix is found to enhance the thermal stability. The thermal stability of

nanocomposites has been investigated using TGA; Table 3.2 presents the results of TGA of PP/PS nanocomposites. The temperature at which 50% degradation occurs ( $T_{50}$ ), a measure of the onset of degradation ( $T_0$ ), maximum degradation temperature ( $T_{max}$ ) and the fraction of material that remains at  $600^\circ\text{C}$  (denoted as residues) are recorded. It is also observed that all five types of clay nanocomposites (3wt %) show higher degradation temperature than pure PP/PS. Figures 3.11 & 3.12 show the TG and DTG curves of neat PP/PS (80/20) and nanocomposites with different modified kaolin nanoclays at 3wt %.

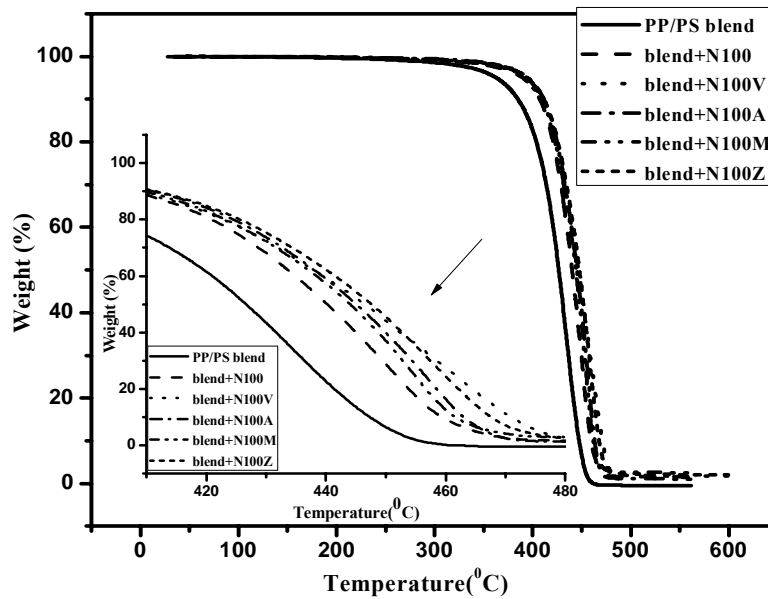


**Figure 3.11** TG curves of PP/PS blend, PP/PS/N100, PP/PS/N100V, PP/PS/N100A, PP/PS/N100M and PP/PS/N100Z. The inset shows their TG curves in temperature range  $410\text{-}480^\circ\text{C}$

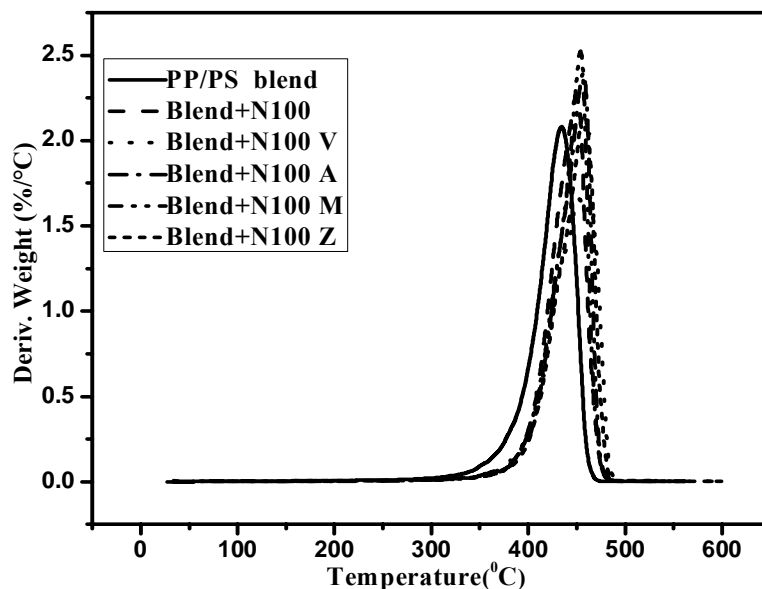


**Figure 3.12** DTG curves of PP/PS blend, PP/PS/N100, PP/PS/N100V, PP/PS/N100A, PP/PS/N100M and PP/PS/N100Z

The maximum decomposition temperature of the clay nanocomposites increases in the order N100, N100M, N100A, N100Z and N100V. Pure blend shows an onset degradation temperature of 370.5°C. For the unmodified clay this temperature shifts to 390.8°C, the corresponding value for vinyl, dialkyl, mercapto and amino modified clay nanocomposites are 397.3°C, 393.2°C, 394.6°C and 395.1°C, respectively. Improved thermal stability of nanocomposites may be due to the formation of highly charred carbonaceous silicate cumulating on the nanocomposites surface. The charred surface layer formed during decomposition shields the thermal shock due to heat penetration to the underlying material; on the other hand such cumulative char layer tends to retard diffusion of volatile products

through nanocomposites [37-39]. The temperature at which weight loss reaches 50% shifts to higher temperatures on the addition of nanoclay.

The oxidation index values for PP/PS/clay nanocomposites can be observed from the Table 3.2. Higher the values of oxidation index (OI), higher will be the thermal stability [40, 41].

**Table 3.2 Results from DTG curve of PP/PS/clay nanocomposites**

Samples	50% mass loss (°C)	Tonset (°C)	Tmax (°C)	Residue at 600 °C (%)	OI
PP/PS blend	426.6	370.5	434.4	0.46	0.032
Blend +3wt % N100	440.1	390.8	450.1	1.5	0.104
Blend +3wt % N100A	445.0	395.1	456.8	1.09	0.076
Blend +3wt % N100M	444.0	394.6	453.7	1.76	0.122
Blend +3wt % N100V	446.4	397.3	460.7	1.77	0.124
Blend +3wt % N100Z	446.4	393.3	458.8	2.10	0.146

### 3.3.4.1 Kinetic analysis of thermal decomposition

Kinetic parameters were evaluated from TGA curves using the plots of Horowitz-Metzger (HM) method, Broido's method (BR) and Coats Redfern (CR) methods.

**Table 3.3 Activation energy (J/mol) calculated by Horowitz-Metzger, Broido's and Coats-Redfern methods of PP/PS/clay nanocomposites**

Samples	Coats –Redfern	Broido's	Horowitz- Metzger
PP/PS blend	174	181	175
Blend +3wt % N100	185	212	184
Blend +3wt % N100A	193	213	187
Blend +3wt % N100M	190	221	195
Blend +3wt % N100V	196	228	196
Blend +3wt % N100Z	194	223	196

The CR, BR and HM plots for the thermal degradation of PP/PS/ clay nanocomposites with different modified kaolin nanoclays at 3wt % from the onset degradation temperature to the maximum degradation temperature are shown in the Figures 3.13(a), 3.13(b) & 3.13 (c) respectively. The activation energy ( $E_a$ ) calculated using each method is given in Table 3.3. The respective concurrency value ( $R^2$ ) close to unity is chosen. BR, HW and CR methods gave comparable values of  $E_a$ .

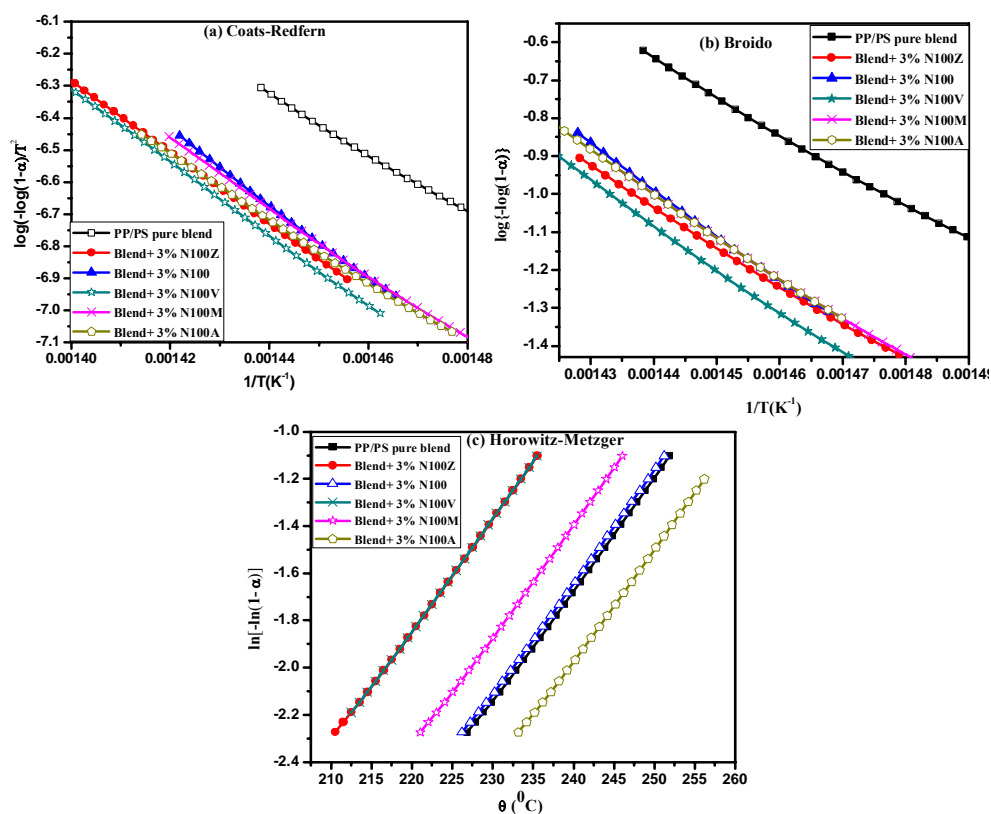


**Figure 3.13** Kinetic plots for the determination of activation energy of PP/PS blend, PP/PS/N100, PP/PS/N100V, PP/PS/N100A, PP/PS/N100M, and PP/PS/N100Z using (a) Coats-Redfern equation (b) Broido's method (c) Horowitz-Metzger equation



From Table 3.3 it is clear that  $E_a$  values are higher for nanocomposites compared to pure blend. The improvement in thermal stability and  $E_a$  values of the nanocomposites are attributed to the dispersion of nanoclay particles in the polymer matrix which restricts the easy diffusion of volatiles from the bulk [42].

Lower  $E_a$  of pure blend may be due to the presence of different kinds of polymer di-radicals produced due to the bond scission and unzipping during degradation process. In the nanocomposites the nanoclay platelets confine the radicals and prevent the decomposition reaction [40, 42]. In nanocomposites the nanoclay layers delay the volatilization of the products originated by carbon-carbon bond scission in the polymer matrix [43]. The influence of modified kaolin nanoclays is higher than that of unmodified clay. The modified kaolin nanoclays can make layered silicates disperse more homogeneously in the polymer matrix. As can be seen from the Table 3.3, the nanocomposites with N100V and N100Z clays show higher  $E_a$  values.

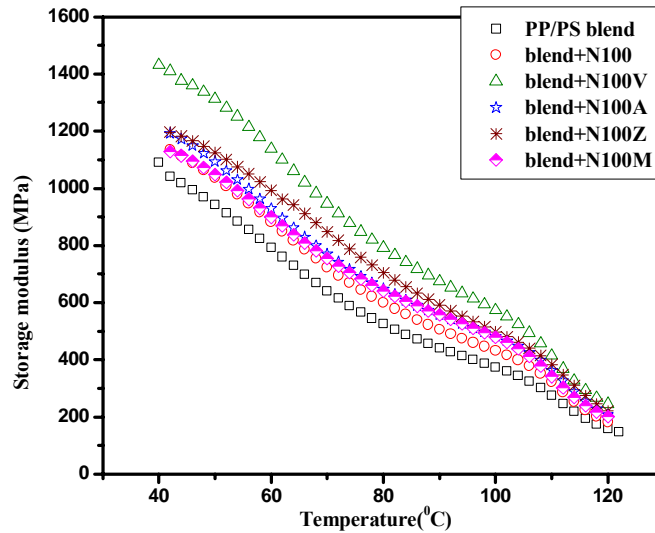
### **3.3.5 Dynamic mechanical analysis (DMA)**

DMA is used to study the relaxation in polymers. DMA measurement consists of the observation of time-dependent deformation behavior of a sample under periodic mostly sinusoidal deformation force with very small amplitudes. Thus, it is possible to calculate storage modulus  $E'$  and loss factor  $\tan \delta$  as a function of temperature and deformation frequency. The analysis of storage modulus and  $\tan \delta$  curves is very useful in ascertaining the performance of the sample under cyclic stress and temperature

**Table 3.4 Storage moduli and  $T_g$  values of PP/PS blend, PP/PS/N100, PP/PS/N100V, PP/PS/N100A, PP/PS/N100M, and PP/PS/N100Z**

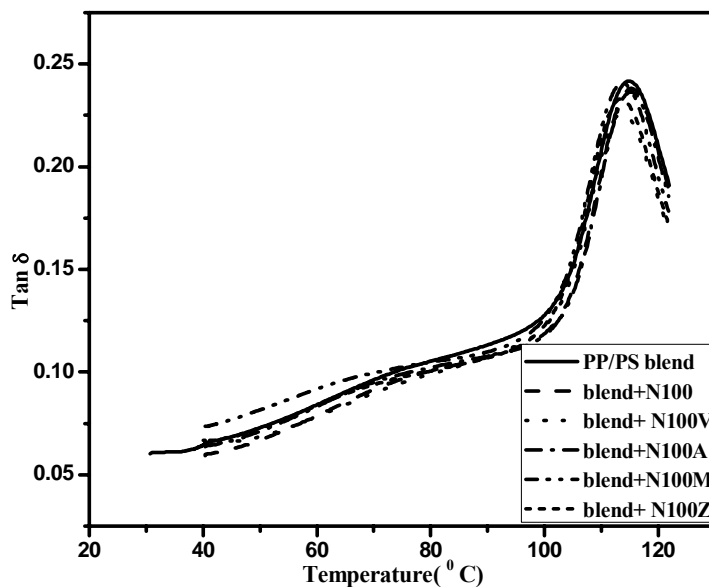
Samples	Storage modulus				$T_g$ (°C) from $\tan \delta$
	45°C	80°C	100°C	120°C	
PP/PS blend	1007	525.3	374.1	159.0	114.95
Blend +3wt % N100	1101	599.7	431.8	182.8	114.67
Blend +3wt % N100A	1162	647.5	481.7	207.6	114.35
Blend +3wt % N100M	1005	590.3	447.0	187.0	114.49
Blend +3wt % N100 V	1369	792.7	573.6	245.6	114.35
Blend +3wt % N100 Z	1175	709.1	503.2	217.8	113.46

Figure 3.14 compares dynamic storage modulus curves of nanocomposites with different modified kaolin nanoclays at 3 wt % and PP/PS pure blend. PP/PS/clay nanocomposites exhibit higher storage moduli over the entire temperature range of the study (40–125°C). It is evident from the Figure 3.14, the nanocomposites with vinyl silane modified nanoclay and dialkyl silane modified nanoclay shows noticeably higher values of storage modulus over the range of temperature. This further show the overall superiority of the vinyl silane modified and dialkyl silane modified kaolin nanoclays in improving the mechanical behavior of the blend. This observation clearly illustrates the effect of intercalation of the polymer in clay layers, leading to the dispersion of nanoclay platelets in the polymer matrix. The enhancement of storage modulus strongly depends on the aspect ratio of the dispersed nanoclay particles and the intercalation of the polymer chains inside the nanoclay galleries [44-46]. When a polymer matrix is reinforced with rigid filler particles, the polymer interface adjacent to the nanoclay particle is highly restrained mechanically. Active surface area of the filler increases because of the intercalation of the polymer chains inside the nanoclay galleries.



**Figure 3.14 Storage modulus curves of PP/PS blend, PP/PS/N100, PP/PS/N100V, PP/PS/N100M, PP/PS/N100Z and PP/PS/N100A**

Polymer chains inside the nanoclay galleries are immobilized and the effective immobilization of these chains is responsible for the enhancement of the hydrodynamic storage modulus. The variation of  $\tan \delta$  [ratio of loss and storage modulus ( $E''/E'$ )] plotted as a function of temperature is shown in Figure 3.15. The  $\tan \delta$  curves represent the ratio of dissipated energy to stored energy and relates to the  $T_g$  of the polymer.  $\tan \delta$  is useful in determining the occurrence of molecular mobility transitions such as  $T_g$ . From the figure it can be noticed that there is a slight decrease in  $T_g$  with the addition of nanoclays. The reduction is attributed to the plasticizing action of the various surfactants of organically modified clays. Such plasticizing action may be responsible for the improved mobility of polymer chains which cause reduction in  $T_g$  [47]. Table 3.4 shows the  $T_g$  values obtained for the pure PP/PS blend and the modified nanocomposites from the  $\tan \delta$  curves.



**Figure 3.15** Tan  $\delta$  curves of PP/PS blend, PP/PS/N100, PP/PS/N100V, PP/PS/N100M, PP/PS/N100Z and PP/PS/N100A

In order to clarify the effect of nanoclay addition in enhancing the blend properties, the relative storage moduli of PP/PS /nanoclay composites to those of PP/PS blend is plotted in Figure 3.16. The relative storage moduli of PP/PS/clay nanocomposites were higher than those of the respective PP /PS matrix at all temperature range. In Figure 3.16, “hump like curves” are observed which may be attributed to the hindrance of polymer chain movement due to the presence of nanoclay particles [48-50]. This “hump like curves” could be attributed to the resistance of the applied stress as a result of development of polymer-nanoclay network.

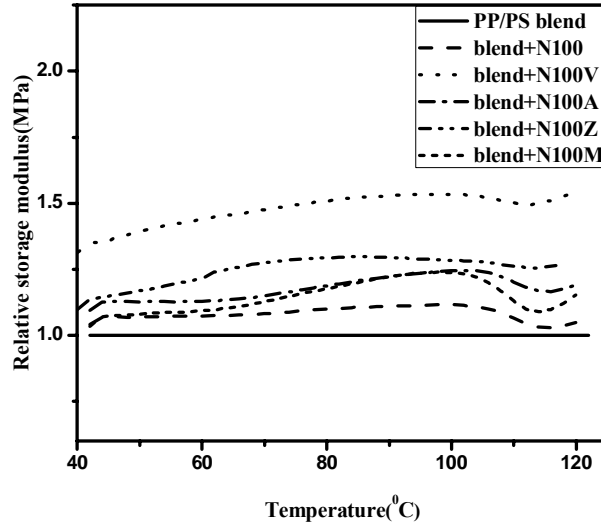


**Figure 3.16** Relative storage modulus curves of PP/PS blend, PP/PS/N100, PP/PS/N100V, PP/PS/N100M, PP/PS/N100Z and PP/PS/N100A

### 3.3.5.1 Calculation of the activation energy

The nanocomposites with N100 V and N100 Z show higher storage modulus over the range of temperature. So the nanocomposites with N100V and N100Z are used to study the effect of frequency on the dynamical mechanical properties. In order to investigate the effect of frequency on the dynamical mechanical properties of PP/PS clay nanocomposites, DMA tests were performed over a temperature range of 40 to 125°C and at five different frequencies (0.1, 1, 3, 5 and 10 Hz). The temperature dependence of  $\tan \delta$  for PP/PS/5wt%N100Z nanocomposite and PP/PS/5wt%N100V nanocomposite at the five frequencies studied is shown in the Figures 3.17(a) and 3.17(b). From the figure it can be seen that the relaxation peak shifts to higher temperature as the frequency increases from 0.1Hz to 10 Hz. Weixia Zhong *et al.* obtained similar observation in their studies. They reported that the relaxing unit of PP chain segments shift to higher temperature as the

frequency increases [51]. From the relaxation peaks; obtained from  $\tan \delta$  curves at different measuring frequencies, the activation energy of the PP/PS/clay nanocomposites was calculated using the Arrhenius equation [52]:

$$f = f_0 \exp - \frac{E_a}{RT} \dots\dots\dots(3.10)$$

where  $f_0$  is a constant and  $f$  the frequency of the test, R is the gas constant,  $E_a$  is the activation energy and T is the temperature corresponding to the maximum of the  $\tan \delta$  curve in Kelvin scale.

**Table 3.5 Activation energies of PP/PS/ clay nanocomposites**

Samples	Activation energy ( $E_a$ ) (J/mol)
PP/PS blend	533
Blend +1wt % N100Z	622
Blend +3wt % N100Z	638
Blend +5wt % N100Z	657
Blend +1wt % N100V	645
Blend +3wt % N100V	700
Blend +5wt % N100V	716

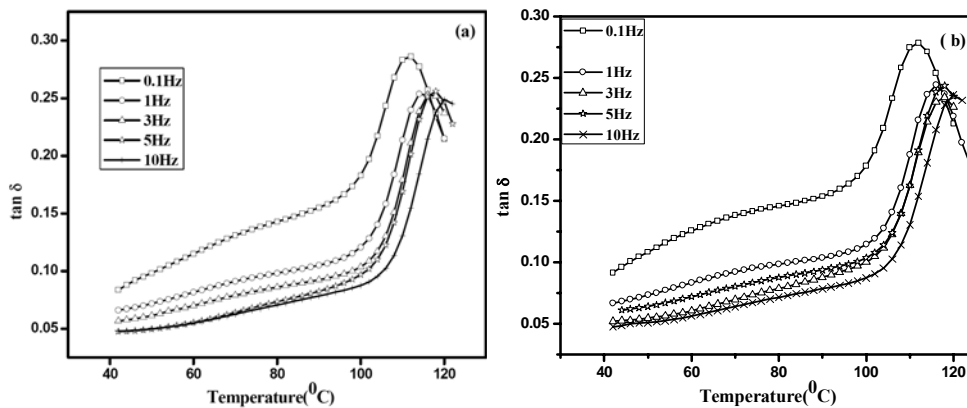


**Figure 3.17 Effect of frequency on DMA curves of (a) PP/PS/5wt%N100Z clay nanocomposite (b) PP/PS/5wt%N100V clay nanocomposite**

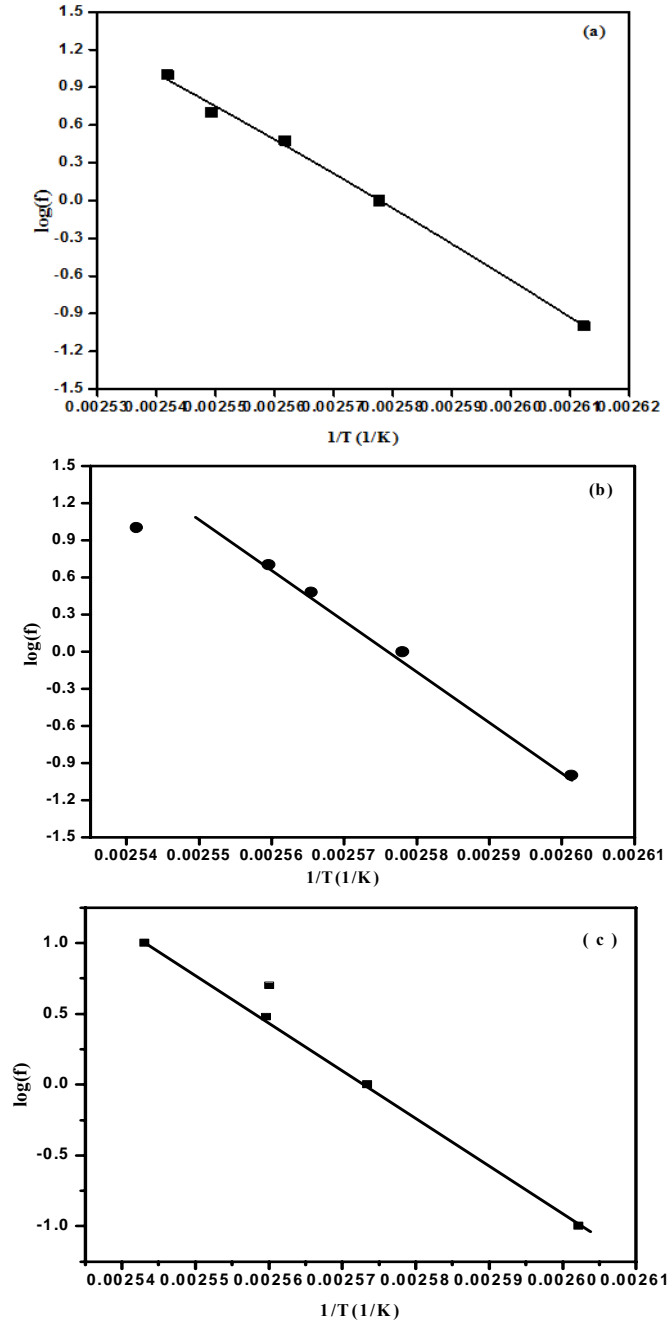


**Figure 3.18 Representative Arrhenius plots for the activation energy of (a) PP/PS blend (b) PP/PS/5wt%N100Z nanocomposite(c) PP/PS/5wt%N100V nanocomposite**

A plot of  $\log f$  versus  $1/T$  gives a straight line and the activation energies for the nanocomposites are calculated from the slope of this line (Figure 3.18). Activation energies calculated according to equation 3.10 are given in Table 3.5. From the table it can be observed that the activation energy of the nanocomposites is higher than that of the PP/PS blend. The restricted flow and the enhanced temperature sensitivity of the nanocomposites may be attributed to the increased interfacial adhesion between modified kaolin clays and the polymer matrix [53]. This result is also attributed to the better dispersion of clay platelets in polymer matrix [54].

### 3.3.6 Differential scanning calorimetry (DSC)

DSC measures the amount of energy absorbed or released by a sample as it is heated cooled or held at a constant temperature. The crystallization temperature ( $T_c$ ), the apparent melting temperature ( $T_m$ ) and the corresponding enthalpies ( $\Delta H$ ) are shown in the Table 3.6. The DSC melting and cooling curves for PP/PS blend and nanocomposites with different modified kaolin clays at 3 wt % are shown in the Figure 3.19.

**Table 3.6 DSC parameters of PP/PS blend, PP/PS/N100, PP/PS/N100V, PP/PS/N100M, PP/PS/N100Z and PP/PS/N100A**

Samples	$T_c$ (°C)	$\Delta H_c$ (J/g)	$T_m$ (°C)	$\Delta H_m$ (J/g)
PP/PS blend	111.9	61.1	158.4	32.4
Blend+3wt%N100	114.1	45.0	159.2	21.0
Blend+3wt%N100V	114.4	63.3	160.2	40.0
Blend+3wt%N100A	112.8	56.7	160.7	27.9
Blend+3wt%N100M	113.7	62.1	159.0	39.9
Blend+3wt%N100Z	113.9	63.7	161.1	40.5



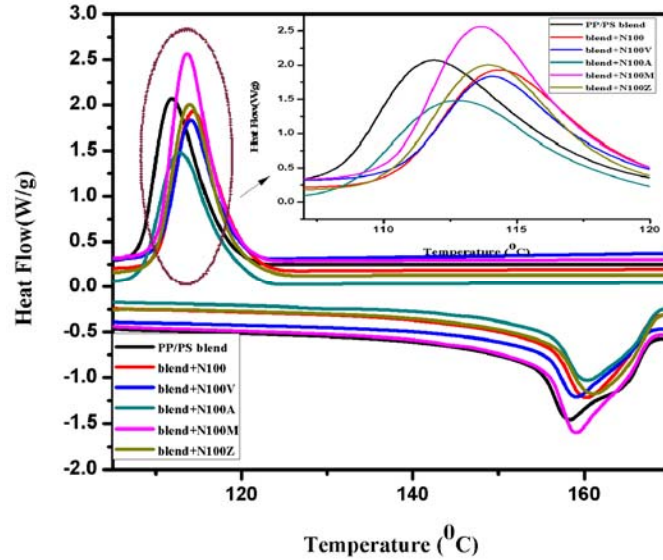


**Figure 3.19 DSC curves melting and crystallization curves of PP/PS blend, PP/PS/N100, PP/PS/N100V, PP/PS/N100M, PP/PS/N100Z and PP/PS/N100A.**

Crystallization temperature of all nanocomposites is increased with increase in nanoclay loading as given in the Table 3.6. The crystallization temperature of PP/PS blend is 111.8°C and the presence of nanoclay increases  $T_c$  up to 114°C. This increase in  $T_c$  indicates the nucleating effect of nanoclays in the polymer matrix [55]. The extent of increase in crystallization temperature varies slightly with the type of nanoclays. The order of magnitude of  $T_c$  for the different nanoclays is as shown: Blend/N100V  $\approx$  Blend/N100  $\square$  Blend/N100Z  $\approx$  Blend/N100M  $\square$  Blend/N100A  $\square$  PP/PS Blend. The melting temperatures of the studied samples of the nanocomposites were increased, in comparison to pure polymer matrix. This increase in  $T_m$  values signifies that the crystal structure in nanocomposites is more perfect than in polymer matrix. The increase in  $\Delta H_m$  values of the nanocomposites [Blend/N100Z & Blend/N100V] than that of the neat polymer matrix indicates a higher thermal stability of the nanocomposites [56].

### 3.3.7 Mechanical Analysis

#### (a) Tensile properties

The tensile strength and tensile modulus as a function of increasing filler loading of unmodified and modified nanocomposites are depicted in Figures 3.20 and 3.21, respectively. Tensile properties increase initially with increasing filler loading reaches an optimum and then decreases. The insertion of the polymer chains inside the silicate layers leads to an increase in the surface area of interaction between the nanoclay and polymer matrix thereby resulting in an increase in strength and modulus. The increment in tensile strength and modulus is also attributed to the reinforcing characteristics of dispersed nanoclay layers. Nanoclay platelets present in the polymer matrix act as an efficient stress transfer agent in nanocomposite, inducing plastic deformation into the base polymer [57]. The mechanical properties of the compatibilized polymer blends are likely to be improved compared to corresponding uncompatibilized ones because of the lower interfacial tension and enhanced interfacial adhesion, which results in more efficient stress transfer between the phases during fracture [7]. Sanjay K Nayak *et al.* reported that the increase in tensile modulus was due to the resistance exerted by the nanoclay layers against the plastic deformation of the polymer and the stretching resistances of polymer chains with an extended conformation in the gallery [34]. The decrease in tensile properties at higher loadings may be due to the agglomeration of nanoclay particles. The stress acting on a small part of the material surface would be much greater than the average stress applied to the test specimen in the presence of nanoclay agglomerates.

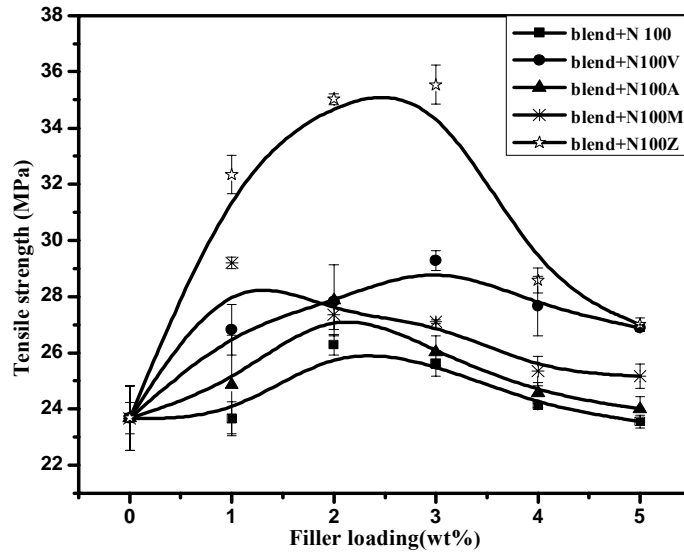


**Figure 3.20** Variation of tensile strength with clay loadings

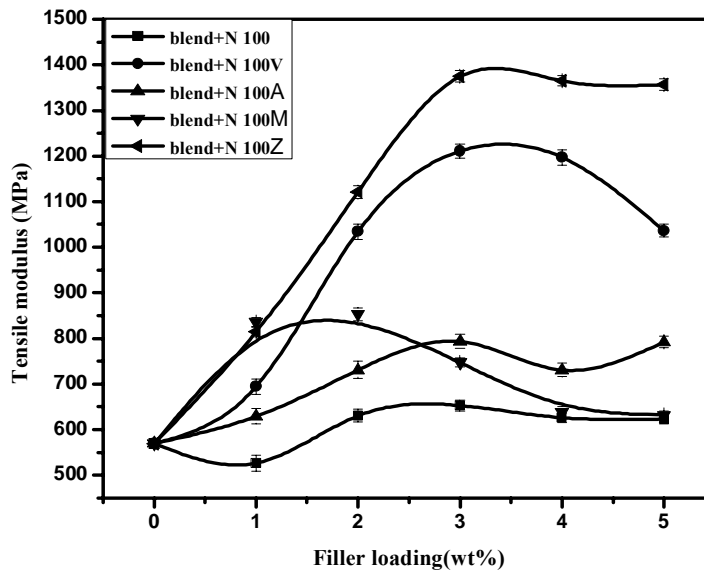


**Figure 3.21** Variation of tensile modulus with nanoclay loadings

**(b) Flexural properties**

Effect of organoclay type on flexural properties of nanocomposites is presented in Figures 3.22 and 3.23, respectively. The increase in flexural

strength and modulus indicates that the nanocomposites have become more rigid and less flexible. The enhancement in the mechanical properties is more pronounced in PP/PS blend with N100V and N100Z loadings. From the result it can be concluded that vinyl silane modified kaolin nanoclay (N100V) and dialkyl silane modified kaolin nanoclay (N100Z) have better interaction with the matrix.

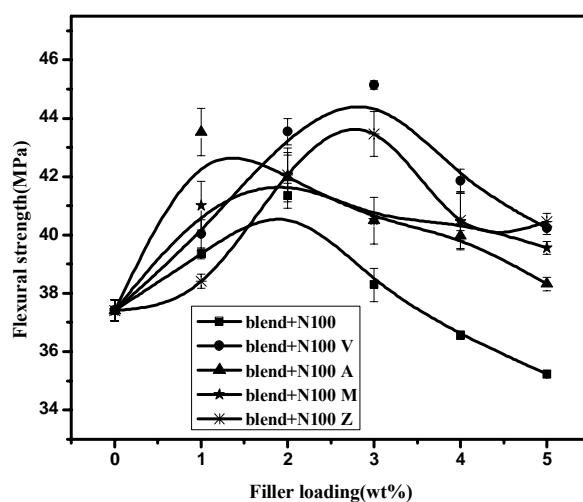


Figure 3.22 Variation of flexural strength with nanoclay loadings

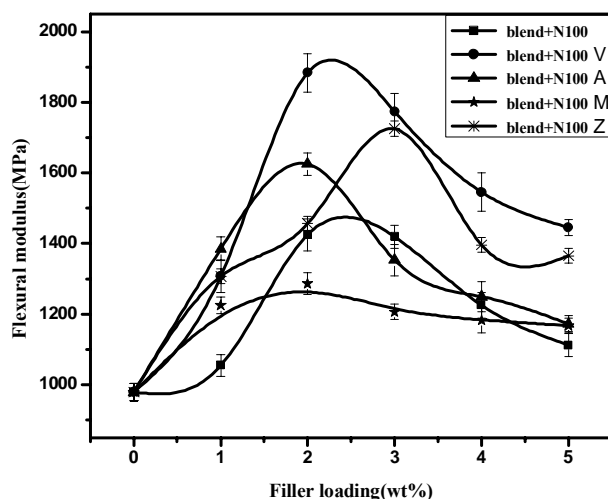
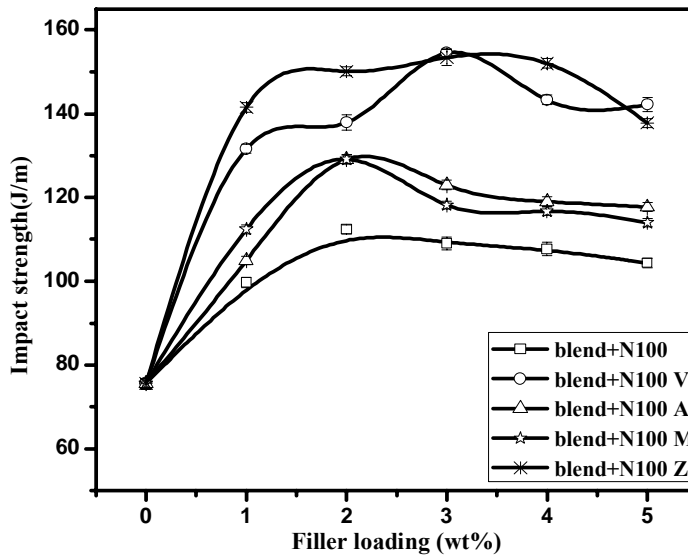


Figure 3.23 Variation of flexural modulus with nanoclay loadings

**(c) Impact strength**

The effect of nanoclay modification on the impact strength with increasing clay loadings is given in the Figure 3.24.



**Figure 3.24** Variation of impact strength with nanoclay loadings

The impact strength increases with clay loading after reaches a maximum value thereafter decreases. The enhancement of impact strength is due to the dispersion of stress by intercalated nanoclay layers. Thus the intercalated clay layers in the nanocomposite play a role in hindering the crack path caused by impact. When the interaction between the polymer and the clay layers increases the stress transfer is more prominent [58]. The stress distribution is dominant in the nanocomposites with the addition of vinyl silane and dialkyl silane modified nanoclays.

**(d) Hardness**

Hardness is a measure of resistance to indentation. Surface hardness indicates the degree of compatibility and crosslink density [59]. Figure 3.25

gives the variation of hardness with increasing clay loading. The surface hardness of the nanocomposites increases with increase in nanoclay content and reaches a maximum and thereafter shows a reverse trend. The improvement in hardness is due to the presence of intercalated and exfoliated nanoclay platelets in polymer matrix. The intercalated or exfoliated nanoclay platelets restrict indentation and increase the hardness of the nanocomposites. At higher nanoclay loading, the reinforcing effect of clay gets decreased due to agglomeration [60].

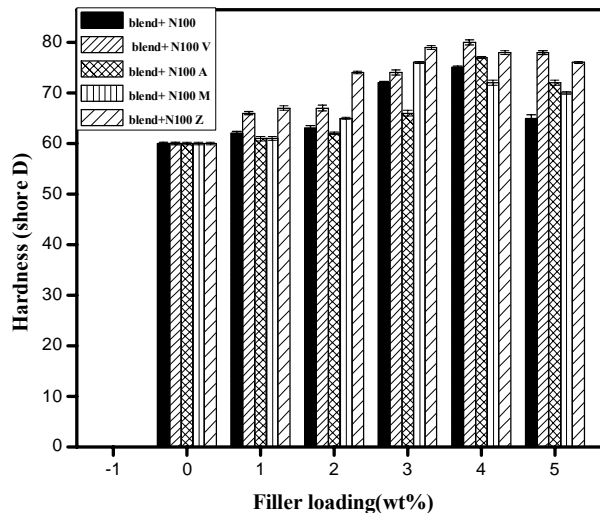


Figure 3.25 Variation of hardness with clay loadings

### 3.3.8 Theoretical modeling of tensile modulus

Figures 3.26 and 3.27 exhibit the comparison between the experimental data and the results provided by various theoretical models fit tensile moduli for PP/PS/ modified kaolin nanoclay nanocomposites with N100Z and N100V respectively. By considering that  $E_0 = 569.38\text{MPa}$  (Figure.3.21) and  $E_1 = 12\text{GPa}$  [61], the tensile modulus prediction tends to follow a trend with the experimentally determined values.

Among all the model fits the predicted moduli based on modified Halpin-Tsai (with a modulus reduction factor) and Hui - Shia model shows the closest proximity to the experimentally determined tensile modulus values at lower nanoclay loading up to 3 wt%. But at higher loadings the magnitude of the tensile modulus is converged to Takayanagi model in the case of PP/PS/N100Z nanocomposites (Figure.3.26). Lower bound and upper bound model stay largely deviated from the predicted moduli. The predicted moduli by Halpin-Tsai equation are higher than the experimental data. This could be attributed to the contribution of plate-like clay to the tensile modulus which is less than a fiber like dispersed phase. The morphology differences between the plate-like filler (two dimension) and fiber like filler (one dimension) which is neglected in the composite theories are taken into account in the modified Halpin-Tsai model. MRF is related to the morphology and aspect ratio of the filler [17]. The experimental results also shows close proximity to the Hui- Shia model which indicates a perfect interfacial bonding between nanoclay and the polymer matrix as per the assumptions of the model. An imperfect interface reduces the reinforcing efficiency of the nanoclay platelets as it is implied that the interface in nanocomposites plays an important role in the effective load transfer from the matrix to the fillers. At higher nanoclay loadings, the clay clusters act as a stress concentrates which results in deviation of the experimental result from the Hui-Shia model. In Takayanagi model the effect of interfacial contribution which plays a functional role in stress-transfer mechanism is neglected.

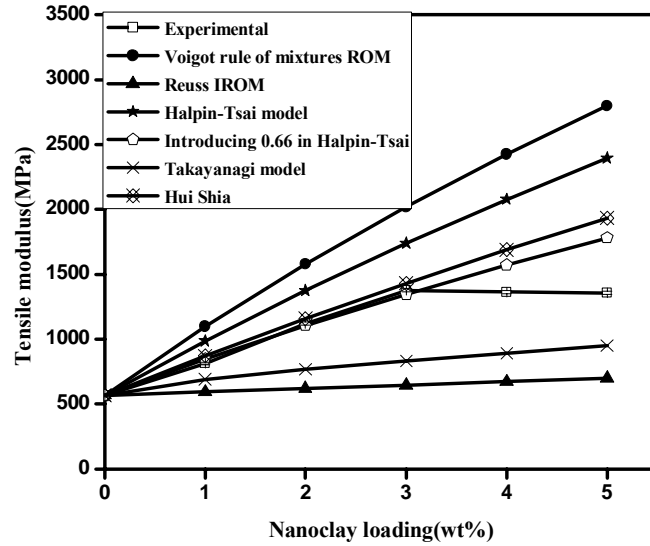


Figure 3.26 Theoretical modeling of tensile modulus as a function of filler loadings using various models of PP/PS/N100Z nanocomposites

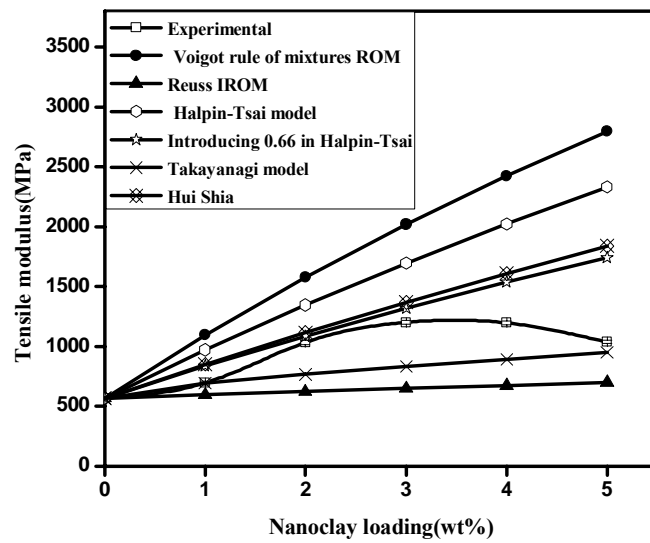


Figure 3.27 Theoretical modeling of tensile modulus as a function of filler loadings using various models of PP/PS/N100V nanocomposites



In the case of PP/PS/N100V nanocomposites (Figure.3.27) the experimentally determined tensile modulus values is converging towards the modified Halpin-Tsai (with a modulus reduction factor) and Hui Shia model but at higher loadings it shows close proximity to the Takayanagi model.

### 3.3.9 Effect of UV aging on the tensile properties

The effect of UV aging on the tensile strength and tensile modulus of PP/PS/clay nanocomposites are given in the Figures 3.28 and 3.29. Figures depict the variation of tensile strength and tensile modulus with nanoclay loading after UV aging. From the figure it is observed that the tensile properties decreases after aging when compared to before aging (Figures 3.20 & 3.21).

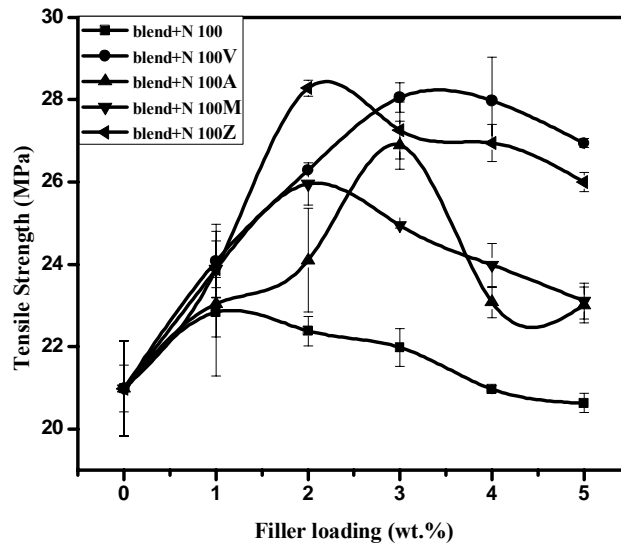


**Figure 3.28 Effect of UV aging on the tensile strength of PP/PS/ clay nanocomposites**

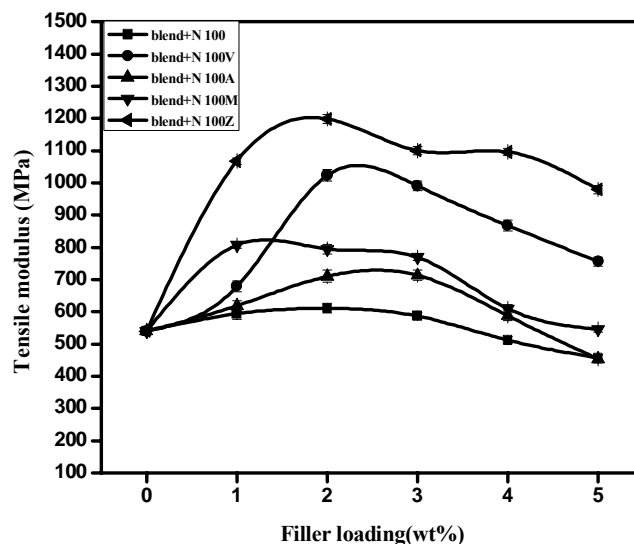


**Figure 3.29** Effect of UV aging on the tensile modulus of PP/PS/clay nanocomposites

The photodegradation of polystyrene is initiated by the absorption of UV radiation by the aromatic ring which results in scission of the C-H bond from the main chain carbon bonded to the aromatic ring. The free radical thus produced has low reactivity due to resonance stabilization. Photodegradation of PS is further accelerated by acetophenone, a chromophore with strong UV absorption which is formed in the primary photodegradation step [62]. Sandrine Morlat *et al.* reported that the photodegradation of polypropylene is by the formation of hydroperoxides, which can decompose to produce alkoxy radicals, which abstract hydrogen on the polymeric backbone or undergo a  $\beta$ -scission [63]. According to Walter *et al.* degradation in polymer blend is very complex depending upon the variety of interactions between the blend components. In PP/PS blend, PS domain acts like a UV radiation trap. Photo degradation of PS is accelerated by acetophenone (formed as a product of primary photo degradation step) and it interacts with PP domains and form more reactive tertiary carbon radicals [64]. In

PP/PS/clay nanocomposites the nanoclay accelerates the photo degradation of PP/PS blend. Generally, nano particles have greater acceleration effect than micro particles due to its smaller size and greater interfacial area [65, 66].

### 3.3.10 Melt Flow Index (MFI)

The measurement of melt flow index (MFI) is a simple way to estimate the chain mobility of polymer materials. Effect of nanoclay type on the MFI value with increasing nanoclay loading is shown in the Figure 3.30. From the figure it is clear that the MFI value of all nanoclay types decreases with increasing clay loading. The clay particles act as fillers causing an increase in viscosity (decrease in MFI value [67]). The N100V and N100Z modified nanocomposites shows low MFI values.

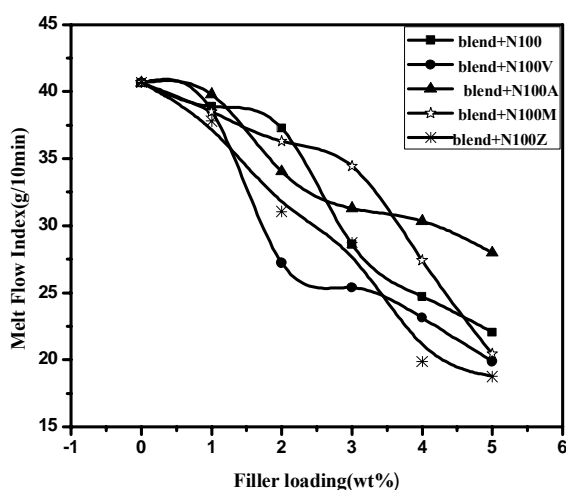


**Figure 3.30 Variation of MFI with nanoclay loadings**

Ke Wang *et al.* suggested that the decrease in MFI with nanoclay loading is also due to the formation of nanoclay network at higher loadings. The orientation and flow of polymer chains would be retarded if the polymer chains were confined in narrow spacing between nanoclay particles, resulting in the decrease of melt fluidity [68].

### 3.4. Conclusions

The effect of kaolin nanoclay modification on the mechanical, thermal and morphological behavior of PP/PS blend is described. In Nanocaliber100V modified nanocomposite system, the clay layers are delaminated as thin platelets in the matrix as evidenced by the shifting of diffraction peaks to lower angle in XRD region and in Nanocaliber100Z modified nanocomposite, there is a reduction of intensity which confirms a partial exfoliation of nanoclay layers in polymer matrix. TEM results show that N100V can be act as an interfacial modifier and N100Z can act as both interfacial modifier and as reinforcing filler and it corroborates the results obtained from XRD. Thermogravimetric analysis shows improved thermal stability of PP/PS/clay nanocomposites caused by the partial exfoliation of the nanoclay in the nanocomposites. The dynamic mechanical analysis reveals higher storage moduli over a temperature range of 40–125°C for nanocomposites, and the extent of increase in the storage modulus is dependent on the type of nanoclay. N100V and N100Z modified nanocomposites show maximum improvement in mechanical properties, suggesting that it provides better interfacial interaction. Hui- Shia and modified Halpin-Tsai models show close proximity to the experimental values till 3 wt%. This confirms the presence of a perfect interface between matrix and nanoclay platelets. SEM photograph shows better dispersion for PP/PS/N100V and for PP/PS/N100Z nanocomposites and the dispersion of the particles in polymer matrix is influenced by the strength of interaction between polymer and filler and also the type of modification. The dispersion of nanoclay particle is also found to improve with proper modification.

## References

- [1]. Liu Xuening, Hu Nan, *Science in China Ser.B chemistry*, 2005, 48(2), 326-333.
- [2]. Qin Zhang, Xiao-lin Gao, Ke Wang ,Qiang Fu, *Chinese Journal of Polymer Science* , 2004,22,(2),175-182.
- [3]. Kyung Yl Kim, Dong Uk Ju, Gi Joon Nam, Jae Wook Lee, *macromolecular symposia*, 2007, 249–250, 283–288.
- [4]. Witold Brostow, Tamara Holijevac Grguric, Oscar Olea-Mejia, Vesna Rek, Jaykumar Unni,e- *Polymers* 2008,33.
- [5]. Chang-jiang You, De-min Jia, *Chinese Journal of Polymer Science*, 2003, 21(4), 443-446.
- [6]. Sani Amril Samsudin, Azman Hassan, Munirah Mokhtar , Syed Mustafa Syed Jamaludin, *Jurnal Teknologi*, 39(A) Keluaran Khas. Dis, 2003, 35-44.
- [7]. Xu-ming Xie ,Xiao Zheng, *Materials and design*, 2001,22,11-14
- [8]. Richard A. Vaia, John F. Maguire, *chemistry of materials*, 2007,1-16.
- [9]. *Deformation Mechanisms in Polymer-Clay Nanocomposites*, PhD Thesis, Amit K. Kaushik, 2010
- [10]. Yun Zhu, Hai-yun Ma, Li-fang Tong, Zheng-ping Fang, *Journal of Zhejiang University Science A*, 2008 9(11) 1614-1620.
- [11]. Kyun yl Kim, Dong Uk Ju, Gi Joon Nam, Jae Wook Lee, *macromolecular symposia*, 2007, 249-250,283-288.
- [12]. Suprakas Sinha Ray, Steve Pouliot, Mosto Bousmina, Leszek A. Utracki, *Polymer*, 2004, 45, 8403-8413.
- [13]. Tamer A.Elbokl, Christian Detellier; *Journal of Physics and Chemistry of Solids*, 2006, 67 950-955.
- [14]. Qian Zhang, Qinfu Liu, James E .Mark, Isao Noda, *Applied clay Science*, 2009, 46, 51-56.

- [15]. Santiago G. Pardo , María J. Abad , Jesús Cano , Luis Barral, *Rheologica acta*, 2010, 49,607–61.
- [16]. G. P. Tandon, G. J. Weng; *Polymer Composites*. 1984, 5,327–333.
- [17]. You-Ping Wu, Qing-Xiu Jia, Ding-Sheng Yu, Li-Qun Zhang, *Polymer Testing*, 2004, 23, 903–909.
- [18]. J. C. Halpin, Affdl, J. L. Kardos, *Polymer Engineering & Science*, 1976, 16, 344-352.
- [19]. Naresh Dayma, Bhabani K. Satapathy, *Materials and Design*, 2012, 33(13), 510-522.
- [20]. Yu Dong , Debes Bhattacharyya, *Polymer* , 2010,51, 816–824.
- [21]. Voigt W. *Über Die Beziehung zwischen den Beiden Elasticitätsconstanten Isotroper Körper*. *Ann phys* 1889; 38:573–87 [in German].
- [22]. Hurang Hu, Landon Onyebueke, Ayo Abatan, *Journal of Minerals & Materials Characterization & Engineering*, 2010, 9(4), 275-319.
- [23]. Reuss A. *Berechnung der fließgrenze von Mischkristallen auf Grund der Plastizitätsbedingung für Einkristalle*. *ZAMM* 1929, 9:49–58 [in German].
- [24]. T.D. Fornes, D.R. Pau, *Polymer*, 2003, 44, 4993–5013.
- [25]. L. Cauvin, D. Kondo, M. Brieu, N. Bhatnagar, *Polymer Testing*, 2010, 29, 245–250.
- [26]. Motowo Tanagiaky, Shixsaku Ueriura, and Shunsuke Minami, *Journal of Polymer Science: Part C*, 5, 113-122.
- [27]. C. Y. Hui, David Shia, *Polymer. Engineering & Science*, 1998, 38(5), 774-782.
- [28]. Naresh Dayma, Bhabani K. Satapathy, *Materials and Design*, 2010, 31, 4693–4703.
- [29]. J.G.Ryu, H.Kim, J.W.Lee, *Polymer Engineering and science*, 2004, 44 (7).

- [30]. T. S. Ellis, D Angelo, J. S. Journal of Applied Polymer Science, 2003, 90, 1639-1647.
- [31]. X. L Jiang, K Sun, Y. X Zhang, Express Polymer Letter, 2007, 1 (5), 283-291.
- [32]. Xingui Zhang, Leslie.s.Loo .Journal of Polymer Science: part B: Polymer Physics, 2008, 46, 2605-2617.
- [33]. J. K Nelson, W Zenger, R. J Keefe, L. S. Schadler Feist, US Pat. no. 7,579,397B2.
- [34]. Sanjay K. Nayak, Smita Mohanty, Sushanta K. Samal, Polymer-Plastics Technology and Engineering, 2009, 48, 976–988.
- [35]. Gopinath Mani, Qinguo Fan, Samuel C. Ugbolue, Yiqi Yang, Journal of Applied Polymer Science, 2005, 97, 218–226.
- [36]. Aswini Kumar Mohapatra , Smita Mohanty & S. K. Nayak, international journal of plastics technology, 2011, 15(2), 174–187.
- [37]. Adam Kiersnowski, Maria Trelinska-Wlazalk, Justyna Dolega , Jacek Piglowski, e- polymers, 2006,.072.
- [38]. S. Sanchez-Valdes, J.Mendez-Nonell, L.F. Ramos de valle, T.Lozano-Ramierz, E. Ramirez-Vargas, M.L. Lopez-Quintanilla, J.M.Gutierrez-Rodriguez, e-Polymers, 2009, 126.
- [39]. S.K. Sharma, S.K. Nayak, Polymer Degradation and Stability, 2009, 94, 132–138.
- [40]. Shahryar Pashaei., Siddaramaiah., Maziar Mansouji Avval., Akheel Ahmed Syed, Chemical Industry & Chemical Engineering. Q, 2011, 17 (2), 141–151.
- [41]. Shahryar Pashaei., Siddaramaiah ., Akheel Ahmed Syed , International Journal of ChemTech Research, 2011, 3(1), 94-103.
- [42]. Jordana Palacios , Rosestela Perera , Carmen Rosales , Carmen Albano, José María Pastor; Polymer Degradation and Stability, 2012, 97, 729-737.

- [43]. Huaili Qin, Shimin Zhang, Chungui Zhao, Meng Feng, Mingshu Yang, Zhongjun Shu, Shousheng Yang; *Polymer Degradation and Stability*, 2004,85,807-813.
- [44]. Maryam Ataefard ;Siamak Moradian, *Polymer plastics technology & Engineering*, 2011, 50, 732–739.
- [45]. Suprakas Sinha Ray.; Masami Okamoto, *Progress in polymer science*, 2003, 28, 1539-1641.
- [46]. Dong Yu, D Bhattacharyya, J P Hunter, *Composites Science and Technology*, 2008, 68, 2864.
- [47]. Yan Zhua, Hai-yun Maa, Li-fang Tonga, Zheng-ping Fang, *Chinese Journal of Polymer Science*, 2008, 26, 783–792.
- [48]. Achmad Chafidz, Mohammad Al-haj Ali, Rabeh Elleithy, *Journal of Material Science*, 2011, 46(18), 6075–6086.
- [49]. Achmad Chafidz, Ilias Ali , M. E. Ali Mohsin, Rabeh Elleithy and Saeed Al-Zahrani, *Journal Polymer Research* ,2012, 19,9906.
- [50]. Naoki hasegawa, Hirotaka Okamoto, Makoto Kato, Arimistu Usuki, *Journal of Applied Polymer Science*,2000,78, 1918–1922 .
- [51]. Weixia Zhong, Xiuying Qiao, Kang Sun, Guoding Zhang, Xiaodong Chen; *Journal of Applied Polymer Science*, 2006, 99, 1523–1529.
- [52]. M.A. Lo'pez-Manchado, M. Arroyo, *Polymer*, 2000, 41, 7761–7767.
- [53]. Chao Ding, Hui He, Baochun Guo, Demin Jia, *Polymer Composites*, 2008, 29(6), 698–701.
- [54]. Weixia Zhong, Xiuying Qiao, Kang Sun, Guoding Zhang, Xiaodong Chen, *Journal of Applied Polymer Science*, 2006, 99, 1523–1529.
- [55]. Jayita Bandyopadhyay, Suprakas Sinha Ray, Mosto Bousmina, J. *Industrial and Engineering Chemistry*, 2007, 13(4) ,614-62.
- [56]. Jaydeep Khedkar, Ioan Negulescu, Efsthios I. Meletis, *Wear*, 2002, 252, 361–369.



- [57]. S. Parijai, S. K. Nayak, S. K. Verma, S. S. Tripathy, *Polymer Composites*, 2004, 25(6).
- [58]. Chao Ding, Demin Jia, Hui He, Baochun Guo, Haoqun Hong, *Polymer Testing*, 2005, 24 , 94–100.
- [59]. Shahryar Pashaei, Siddaramaiah, Ali Souldozi, S. Usman Taqui Syed , Akheel Ahmed Syed, *International Journal of ChemTech Research*, 2011,3 (3).
- [60]. Biplab K. Deka, Tarun K. Maj, *Journal of Applied Polymer Science*, 2012, 124, 2919–2929.
- [61]. Bathija, A.P., 2010. *Elastic Properties of Clays*. Ph.D. Ph.D. Colorado School of Mines, Golden, CO. 234.
- [62]. Kaczmarek H. *European Polymer Journals*, 1995, 31, 1175-84.
- [63]. Sandrine Morlat, Be'ne'dicte Mailhot, David Gonzalez, Jean-Luc Gardette, *Chem. Mater.* 2004, 16, 377-383.
- [64]. Walter R. Waldman, Marco-A. De Paoli, *Polymer Degradation and Stability*, 2008, 93, 273-280.
- [65]. Mustapha Kaci, Cherifa Remili, Stephane Bruzaud, Yves Grohens; *Academic Journal of Manufacturing Engineering*, 2010, 8(1).
- [66]. Cherifa Remili, Mustapha Kaci, Souad Kachbi, Ste' phane Bruzaud, Yves Grohens, *Journal of Applied Polymer Science*, 2009, 112, 2868–2875.
- [67]. Ulku Yilmazer, Gulsum Ozden, *Polymer Composites*, 2006.
- [68]. Ke Wang, Si Liang , Jinni Deng, Hong Yang, Qin Zhang , Qiang Fu, Xia Dong , Dujin Wang, Charles C. Han, *Polymer* ,2006, 47 , 7131-7144.

.....✂.....

**Polypropylene/Polystyrene blends  
reinforced with hybrid Inorganic fillers:  
Effect of modified kaolin nanoclays and  
short glass fibers**

---

**Part A**

**Polypropylene/Polystyrene/E- glass fiber/modified kaolin  
nanoclays hybrid composites**

- 4. A.1 Introduction*
- 4. A.2 Methodology*
- 4. A.3 Results and Discussion*
- 4. A.4 Conclusions*
- 4. A.5 References*

**Part B**

**Polypropylene/Polystyrene/alkali resistant glass fiber/  
modified kaolin nanoclays hybrid composites**

- 4. B.1 Introduction*
  - 4. B.2 Methodology*
  - 4. B.3 Results and Discussion*
  - 4. B.4 Conclusions*
  - 4. B.5 References*
-

## Part – A

### Polypropylene/Polystyrene/E-glass fiber/modified kaolin nanoclays hybrid composites

#### Abstract

*Modified kaolin nanoclays were used as fillers to modify E-glass fiber (EGF) reinforced Polypropylene/Polystyrene blends (PP/PS). Prepared composites were characterized using X-ray diffraction, Scanning Electron Microscopy and Thermogravimetric analysis. Degradation kinetic parameters have been evaluated for the thermal degradation process of composites using three kinetic methods namely Horowitz-Metzger, Broido's and Coats-Redfern. Incorporation of modified kaolin clays into the PP/PS/EGF composites results in the improvement of mechanical properties. A comparison between experimental results (tensile modulus) and various PP/PS/EGF composites are presented. XRD results give credence to the highest degree of exfoliation in the composites. TGA results show an improved thermal stability for the nanocomposite than for the pure blend. The improvement in thermal stability of nanocomposites is confirmed by the increased activation energy ( $E_a$ ).*

#### 4. A.1 Introduction

Short fiber reinforced composites have several attractive characteristics that make them suitable for domestic, electrical and automotive applications where engineering properties such as high stiffness, strength, toughness and thermal resistance are required. Glass fibers show good performance in many applications like playground equipment, recreational items and piping for corrosive chemicals. Fiber reinforced plastics can also be used in aviation industry because the composite materials have the same capabilities as isotropic materials with significant reduction in weight. It is used in construction industry as it offers better bending rigidity, axial stiffness and better environmental resistance than steel.

Enhancement in mechanical properties depends on the fiber concentration, fiber aspect ratio, fiber adhesion to matrix, volume fraction, fiber orientation and its dispersion in the matrix [1, 2]. The degree of reinforcement of glass fiber depends on the aspect ratio, volume fraction of the fiber in the composite, fiber orientation and the adhesion between the fiber and the polymeric matrix [3]. The inclusion of short glass fibers into a plastic matrix at higher volume fraction increases the viscosity of the polymer melt, and so there is a practical limit on the fiber volume fraction at around 40%, which limits the application of such materials as structural composite components [4].

The incorporation of glass fibers increases the tensile modulus of composites, but decreases the strength and toughness. It may be due to the stress concentration, poor fiber–matrix adhesion and confinement of the matrix molecular mobility around the rigid filler phase. Higher filler loading of glass fiber composites causes increased molded part weight, brittleness and processing difficulty. To overcome these drawbacks, hybrid composite with low filler concentration is desirable. Recently, it has been observed that incorporating nanoclay particles into the fiber reinforced polymer composites would give the desired performance for the hybrid composites at low to intermediate filler loadings. The introduction of nanoclay particles into the polymer composite has displayed significant improvements in mechanical, barrier and thermal properties. It is therefore interesting to consider a polymer with reinforcement on two scales; microscopic fiber reinforcement combined with nanoclay.

Hybrid composites are materials made by combining two or more different types of fillers in a common matrix. By careful selection of fillers, the material costs can be reduced. Hybrid composites have wide engineering application where strength to weight ratio, low cost and ease of fabrication are required. In recent years, hybrid composites have been established as highly efficient high performing structural materials and their use is increasing rapidly. The investigation of the novel applications of hybrid composites has been of great interest to the researchers for many years. Hybridization of fibers with fillers has been used to increase the mechanical, thermal and morphological properties of the composites [5]. Kusmono *et al.* examined the effect of clay loading on the morphological and mechanical properties of unsaturated polyester (UP)/ glass fiber (GF) composites. They concluded that the combination of clay and glass fiber had a synergistic effect on the improvement in mechanical properties of UP matrix [6].

Although numerous researchers have investigated individually on PP/PS/GF composites [7] and PP/PS/nanoclay composite systems [8-10], only a few investigations have been done on using nanocomposites as a matrix in advanced fiber-reinforced composites. Many of the works in this area are focused on montmorillonite [11, 12]. Hence in this study low cost kaolin nanoclay is proposed to be used. However, only scarce amount of literature is available on the effect of kaolin nanoclay as reinforcing agent on thermoplastics. Kaolin nanoclay has a wide variety of applications in industry, particularly as filler in paper, plastics, paints and rubber. It has the potential to be an ideal precursor for the preparation of polymer nanocomposites since it is cheaper when compared to montmorillonite clays.

In this part of study the hybrid effect of modified kaolin nanoclays (Nanocaliber 100V and Nanocaliber 100Z) and E- glass fiber on the properties of Polypropylene (PP)/Polystyrene (PS) blends is proposed to be investigated.

## **4. A.2 Methodology**

### **4. A.2.1 Materials**

The details of the polymers and nanoclay types (N100V & N100Z) used for the study are discussed in Chapter 2 (sections 2.1.1, 2.1.2& 2.1.3). E-glass fiber used for the study is discussed in Chapter2 (section 2.1.4).

### **4. A.2.2 Methodology**

#### **4. A.2.2.1 Composite preparation**

Hybrid composites were prepared by melt mixing using an internal mixer (Haake Rheomix 600) at 180°C with a rotor speed of 50 rpm, and a mixing time of 8 min for each sample. PP/PS (80/20) blend was used as the matrix. In the first series of experiments the fiber length was varied (4-10mm) by fixing the fiber content at 10wt %. In the second series, the optimum amount of glass fiber was found by varying the fiber content from 10 to 30 wt% and keeping the fiber length constant.

Hybrid composites were prepared by adding two different types of modified kaolin nanoclays (Nanocaliber 100V-N100V and Nanocaliber 100Z-N100Z) to the PP/PS/glass fiber composite. For the preparation of hybrid composites, glass fiber content was fixed at 20 wt% and nanoclay was varied from 1-5 wt%. The hot mix from the mixing chamber was pressed in a hydraulic press, cut into pieces and the test specimens were

prepared using a DSM Micro 10cc Injection molding machine, with a barrel temperature of 190°C.

#### **4. A.2.2.2 Characterization**

The details of the characterization techniques used for the study are given in the section 2.2.3. The details of the UV degradation study is given in Chapter 3 (section 3.2.2.2). Density of the composites was estimated by the method of displacement of liquid (ASTM D 792).

#### **4. A.2.3 Theoretical background**

##### **4. A.2.3.1 Single fiber models**

The micromechanical models were developed based on the physical characteristics of fiber: whether the composite is made from unidirectional continuous long fibers, random discontinuous fibers or particulate fibers. The advantage of using mathematical model is to reduce cost and time. The accuracy of the model must always be validated in order to accept the final result obtained through analytical approach. Different theoretical models like Parallel and Series model, Hirsch, Halpin-Tsai model, Modified Halpin –Tsai, Halpin – Pagano and Hui-Shia model for the prediction of tensile properties of fiber filled polymers in terms of different parameters like aspect ratio, packing fraction, fiber geometry, fiber distribution and fiber loading are proposed in this study. Aspect ratio is the length/diameter ( $l/d$ ) ratio of the fiber and it is a major parameter that controls the fiber dispersion and fiber-matrix adhesion that gives optimum performance of short fiber polymer composites. Fiber geometry of a composite material includes the length, cross-sectional area and the orientation of the fiber in the matrix. Some common fiber geometries for fiber reinforced composites are aligned fibers, random fibers and woven fibers [13]. The

concentration of fibers and fiber distribution in the matrix plays an important role in determining the mechanical properties of the fiber reinforced polymer composites. At low fiber loading, matrix is not restrained by enough fibers and highly localized strains occur in the matrix at low strain levels causing the bond between fibers and the matrix to break, leaving the matrix diluted by non-reinforcing debonded fibers. At high fiber loading, the matrix is sufficiently restrained and the stress is more evenly distributed. Thus the reinforcement effect outweighs the dilution effect. The concentration of fibers beyond which the properties of the composite improve above the original matrix value is known as optimum fiber concentration. In order to achieve improvement in mechanical properties with short fibers, the matrix is loaded beyond this volume fraction of fiber.

**(a) Parallel and series model**

The rule of mixtures ROM (parallel) can be used to estimate from its constituent properties, the longitudinal modulus,  $E_{11}$  of a unidirectional continuous fiber, when it is loaded in a direction parallel to its fiber. When the laminate is loaded in transverse direction, the transverse modulus of elasticity,  $E_{22}$  can be determined using inverse rule of mixtures (series). In parallel model it is assumed that fibers are uniformly distributed throughout the matrix, which is devoid of loads and having perfect bonding between fibers and the matrix.

According to these models, tensile modulus is calculated using the following equations:



*Parallel model*

$$E_c = E_f \phi_f + E_m \phi_m \dots\dots\dots(4a.1)$$

*Series model*

$$E_c = E_m E_f / E_m \phi_f + E_f \phi_m \dots\dots\dots(4a.2)$$

where  $E_c$ ,  $E_m$  and  $E_f$  are the tensile moduli of composite, matrix and fiber respectively. In parallel model, it is assumed that isostrain conditions exist for both matrix and fiber, whereas in the series model, stress is assumed to be uniform in both matrix and fiber [14].

**(b) Hirsch's model**

Hirsch's model is a combination of parallel and series models [15]. In Hirsch's model it is assumed that the fibers are arranged randomly in the matrix. This model is shown in the Figure 4a.1. According to this model the tensile moduli are calculated using the following equation [5]:

$$E_c = x ( E_m \phi_m + E_f \phi_f ) + (1-x) \frac{E_f E_m}{E_m \phi_f + E_f \phi_m} \dots\dots\dots(4a.3)$$

where  $x$  varies between 0 and 1 and determines the stress-transfer between the fiber and the matrix.

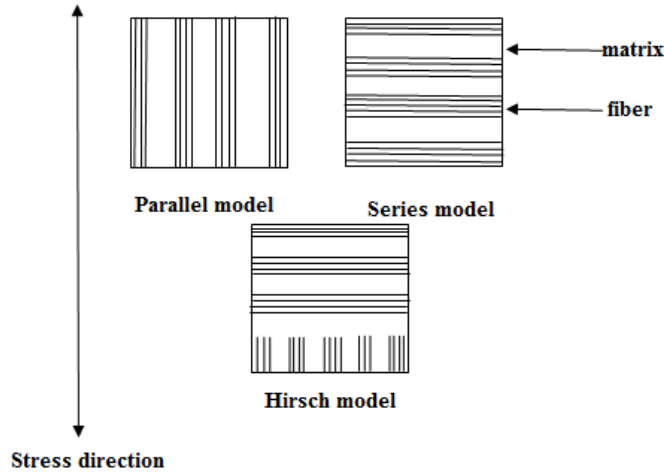


**Figure 4a.1** Schematic representation of parallel, series and Hirsch’s model

**(c) Halpin –Tsai model**

Halpin and Tsai developed a well-known composite theory for predicting the stiffness of unidirectional composites as a function of aspect ratio. Halpin-Tsai equations are widely used to determine the reinforcing effect of filler in the composites. The tensile modulus of composite materials reinforced by fibers can be predicted by Halpin- Tsai equation. According to Halpin-Tsai, tensile moduli of the composite are given by the equations [16, 17]:

$$\frac{E_c}{E_m} = (1 + \xi \eta \phi_f) / (1 - \eta \phi_f) \dots\dots\dots (4a.4)$$

where  $\eta = (E_f/E_m - 1) / (E_f/E_m + \xi) \dots\dots\dots (4a.5)$

$\xi = 2 l/d$  Where  $l$  is the length of the fiber, and  $d$  is the diameter of the fiber.  $\xi$  is the measure of fiber geometry, fiber distribution and fiber loading conditions.

**(d) Modified Halpin-Tsai equation**

Nielson modified the Halpin-Tsai equation by including the maximum packing fraction,  $\phi_{\max}$ , of the reinforcement. According to this [14, 18, 19]:

$$E_c = E_m (1 + \xi \eta \phi_f) / (1 - \eta \psi \phi_f) \dots\dots\dots (4a.6)$$

$$\Psi = 1 + (1 - \phi_{\max} / \phi_{\max}^2) \phi_f \dots\dots\dots (4a.7)$$

$\eta$  is given in Equation 4a.5 and  $\phi_{\max}$  depends upon the particle packing fraction.  $\phi_{\max}$  is maximum packing fraction, and has a value 0.785 for square arrangement of fibers, 0.907 for hexagonal array of fibers and 0.82 for random packing of fibers.

**(e) Halpi-Pagano micromechanical model**

The Halpi-Pagano micromechanical model [20] has been utilized to predict the modulus of composites with randomly oriented short fibers which is given by

$$E_c^{\text{ran}} = 3/8 E_L + 5/8 E_T \dots\dots\dots (4a.8)$$

where  $E_c^{\text{ran}}$  is Young's modulus of random fiber composites,  $E_L$  and  $E_T$  are longitudinal and transverse Young's modulus, respectively, of corresponding uniaxial oriented discontinuous fiber composites. This equation is an averaging procedure for estimating elastic moduli of quasi-isotropic laminates.  $E_L$  and  $E_T$  can be estimated from the following Halpin-Tsai Equations [21, 22]:

$$E_L = E_m [1 + 2(l/d) \eta_L \phi_f / 1 - \eta_L \phi_f] \dots\dots\dots (4a.9)$$

$$E_T = E_m [1 + 2\eta_T \phi_f / 1 - \eta_T \phi_f] \dots\dots\dots (4a.10)$$

where  $\eta_L = (E_f/E_m) - 1 / (E_f/E_m) + (2l/d) \dots \dots \dots (4a.11)$

$$\eta_T = E_f/E_m - 1 / (E_f/E_m) + 2 \dots \dots \dots (4a.12)$$

where  $E_f$  and  $E_m$  are tensile moduli of the fiber and polymeric matrix, respectively;  $\square_f$  and  $l/d$  is volume fraction and aspect ratio , respectively of the fiber in the composites.

**(f) Hui-Shia model (H-S model)**

The Hui-Shia model [23] was developed to predict the tensile modulus of composites with aligned reinforcements with emphasis on fiber-like reinforcements. The H-S model presents the tensile modulus as [24]:

$$E_c/E_m = 1 / \{1 - \square_f / 4 [1/\xi + 3/\xi + A]\} \dots \dots \dots (4a.13)$$

where  $\xi = \square_f + E_m/[E_f - E_m] + 3(1 - \square_f) [\{(1-g)\alpha^2 - g/2\} / \alpha^2 - 1] \dots \dots \dots (4a.14)$

$$g = 1 - [\ln(2\alpha) - 1] / \alpha^2 \quad \alpha \geq 1 \dots \dots \dots (4a.15)$$

$$A = (1 - \square_f) [\{3(\alpha^2 + 0.25)g - 2\alpha^2\} / \alpha^2 - 1] \dots \dots \dots (4a.16)$$

where  $\alpha$  is the inverse aspect ratio of dispersed fillers and  $\alpha = t/l$  for disk-like platelets ( $\alpha \leq 0.1$ ).

**4. A.2.3.2 Multiple filler model**

In order to predict the tensile modulus of the hybrid composites, a hybrid composite is considered as a system consisting of two single composite systems and it is assumed that there is no interaction between the clay and glass fibers.

**(a) Parallel and series model**

In the “parallel” or “rule of mixtures” model, it is assumed that there is equal strain in the matrix and filler phases. The modulus of the hybrid composites can then be evaluated from the rule of mixtures by neglecting the interaction between the two systems by using the equation [25, 26]:

$$E_c = x(E_m\phi_m + E_{f1}\phi_{f1}) + E_{f2}\phi_{f2} \dots\dots\dots (4a.17)$$

where subscript 1 and 2 denote fillers. In this study, 1 and 2 indicate nanoclay and glass fiber phases, respectively.

When assuming uniform stress in the matrix and filler phases, “series” or “inverse rule of mixtures” is proposed. The inverse rule of mixtures (series model) is represented by the equation [27].

$$\frac{1}{E} = \frac{\phi_m}{E_m} + \frac{\phi_1}{E_{f1}} + \frac{\phi_{f2}}{E_{f2}} \dots\dots\dots (4a.18)$$

**(b) Guth model**

Guth considered the interaction between filler particles and the Guth model for two filler system gives [28]:

$$E_c = E_m [1 + 2.5(\phi_{f1} + \phi_{f2}) + 14.1(\phi_{f1} + \phi_{f2})^2] \dots\dots\dots (4a.19)$$

**(c) Paul model**

Yasser Zare *et.al* proposed a model to predict the modulus of multiple filler composites. This equation is a modified form of Paul model. Paul model assumed that consistent stress is applied at the matrix-filler boundary and adhesion is perfect at the interface of a cubic inclusion in a cubic

matrix. When a uniform stress is applied on the boundary, the elastic modulus of the composite is given by equation [28, 29].

$$E_c = E_m [1 + (m_1 + m_2/2 - 1) (\phi_{f1} + \phi_{f2})^{2/3} / 1 + (m_1 + m_2/2 - 1) (\phi_{f1} + \phi_{f2})^{2/3} - (\phi_{f1} + \phi_{f2})] \dots\dots\dots (4a.20)$$

$$m_1 = E_{f1}/E_m \quad m_2 = E_{f2}/E_m$$

**(d) Counto model**

Counto assumed perfect adhesion in the matrix-filler interface and for the two filler phases the model is proposed as [28]:

$$1/E = 1 - (\phi_{f1} - \phi_{f2})^{1/2} / E_m + 1 / \{ [1 - (\phi_{f1} - \phi_{f2})^{1/2}] / (\phi_{f1} - \phi_{f2})^{1/2} E_m + 1/2 (\phi_{f1} + \phi_{f2}) \} \dots\dots\dots (4a.21)$$

**(e) Hirsch model**

In Hirsch's model it is assumed that the fibers are arranged randomly in the matrix. Yasser Zare *et.al* .proposed elastic modulus of the two filler system as [28]:

$$E_c = x [(E_m \phi_m + (E_{f1} + E_{f2})/2 (\phi_{f1} + \phi_{f2})) + (1 - x) [E_m (E_{f1} + E_{f2}) / (E_{f1} + E_{f2}) \phi_m + 2E_m (\phi_{f1} + \phi_{f2})] \dots\dots\dots (4a.22)$$

**(f) Halpin - Tsai**

According to Halpin-Tsai, tensile moduli of the composites are given by the equation [28].

$$E = E_m (1 + \eta_1 \zeta_1 \phi_{f1} + \eta_2 \zeta_2 \phi_{f2} / 1 - \eta_1 \phi_{f1} - \eta_2 \phi_{f2}) \dots\dots\dots (4a.23)$$

$$\eta_1 = E_{f1}/E_m - 1 / E_{f1}/E_m + \zeta_1 \dots\dots\dots (4a.24)$$

$$\eta_2 = E_{f2}/E_m - 1 / E_{f2}/E_m + \zeta_2 \dots\dots\dots (4a.25)$$

#### 4. A.2.4 Determination of fiber aspect ratio

During the manufacturing process (compounding, injection molding etc.) fibers undergo a lot of interaction with machinery. As a result, fiber length may be reduced dramatically. Fiber lengths of the fibers extracted from injection molded composite specimen were measured via optical microscopy. The extracted fibers (diameter=13 $\mu$ m) are obtained by burning the polymer matrix in a muffle furnace at 550 $^{\circ}$ C and then dispersing the fibers in a 10 wt% solution of Polymethyl methacrylate (PMMA) in toluene on glass slide followed by solvent evaporation [30]. The number average fiber length is defined as  $L_n = \frac{\sum N_i L_i}{\sum N_i}$  where  $N_i$  is the number of fibers of lengths  $L_i$ . Figure 4a.2 illustrates typical photograph utilized for determining final fiber length. The average fiber length measured is 0.1278, which gives an aspect ratio ( $l/d$ ) of 9.82.

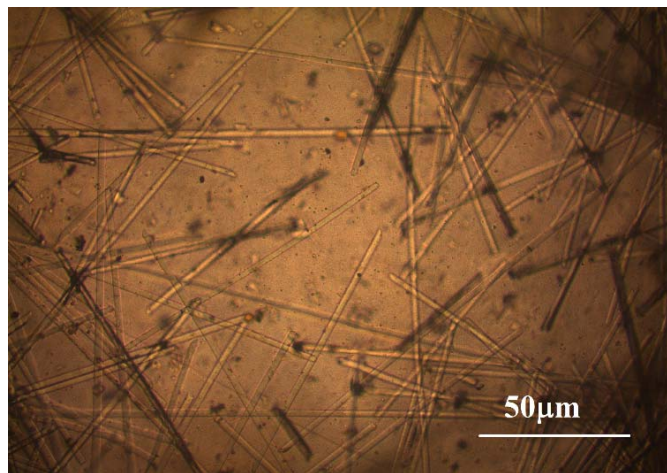


Figure 4a.2 Optical microscopic image of glass fiber for determining fiber length

## 4. A.3 Results and Discussion

### 4. A.3.1 Polypropylene/Polystyrene/E-glass fiber composites

#### 4. A.3.1.1 Effect of fiber length on mechanical properties of PP/PS/ E- glass fiber composites

##### (a) Tensile properties

The variation of tensile strength and tensile modulus as a function of fiber length is plotted in the Figure 4a.3. From the figure it is evident that as the fiber length increases, the tensile properties increase up to an optimum length of 8mm and thereafter show a reverse trend. In the case of fibers shorter than the critical fiber length, the fibers will debone from the matrix resulting in the failure of the composite under low strain. Similarly when the fiber length exceeds the critical fiber length, the tensile properties get decreased. This is because the effective stress transfer is not possible due to fiber curling and fiber bending at high fiber length. The tensile properties of the composites are found to be the maximum at 8 mm length because of the effective stress transfer between the polymer matrix and glass fibers.

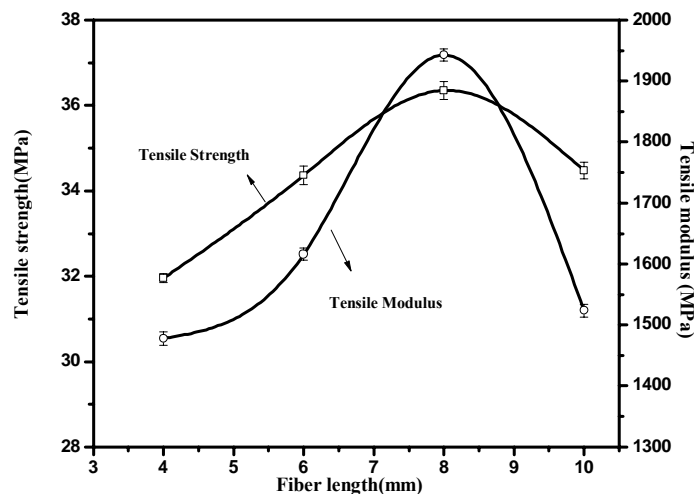


**Figure 4a.3 Variation of tensile properties with fiber length**



**(b) Flexural properties**

The flexural modulus and strength of the composites plotted as a function of glass fiber length is given in the Figure 4a.4. Flexural properties shows similar trend as that of tensile strength. The tensile and flexural tests show good reinforcement at approximately 8 mm length of the glass fiber. Hence 8 mm length is taken as optimum fiber length for further studies.

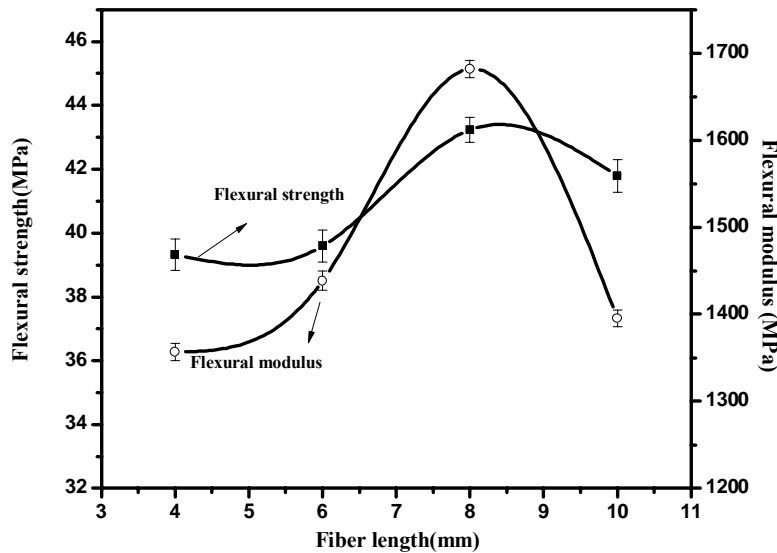


Figure 4a.4 Variation of flexural properties with fiber length

#### 4. A.3.1.2 Effect of fiber loading on mechanical properties of PP/PS/ E-glass fiber composites

**(a) Tensile properties**

The tensile properties of composites as a function of E-glass fiber loading are displayed in the Figure 4a.5. From the figure it is apparent that the tensile properties of the composites are enhanced linearly with increasing fiber concentration but the optimum fiber concentration is obtained at 20 wt %. The tensile strength and modulus increase by 73%

and 298% respectively when compared with the polymer matrix. A significant increase in tensile modulus is also observed. The improvement in tensile properties is due to the efficient stress transfer along glass fiber/matrix interface [31].

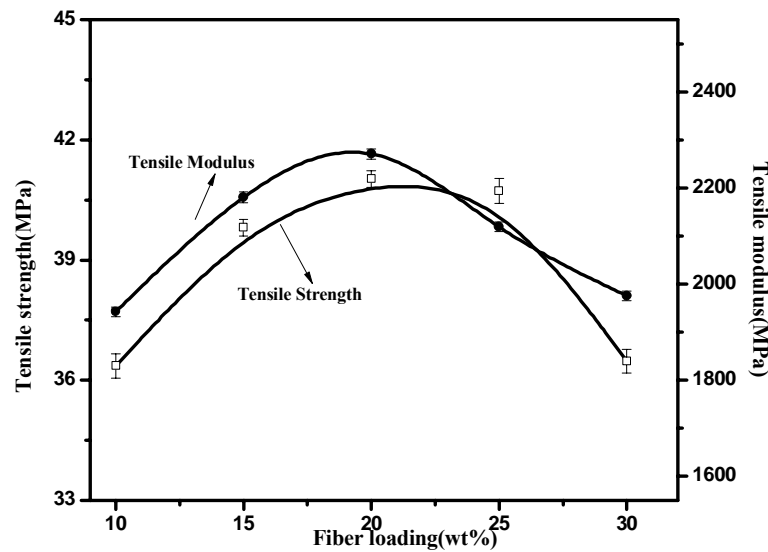


**Figure 4a.5** Variation of tensile properties with fiber loading

The reduction in tensile properties is due to the poor fiber–matrix adhesion and fiber agglomeration in the matrix, which lead to micro-crack formation at the interface under loading and non-uniform stress transfer [32]. Higher percentage of fiber loading also results in formation of voids in the composites because of fiber–fiber accumulation, which also leads to non-uniform stress transfer.

### **(b) Flexural properties**

The flexural modulus and strength of the composites plotted as a function of glass fiber content is illustrated in the Figure 4a.6. Flexural

strength and modulus increases by 29% and 108% respectively [at 20 wt%], as compared to pure polymer matrix.

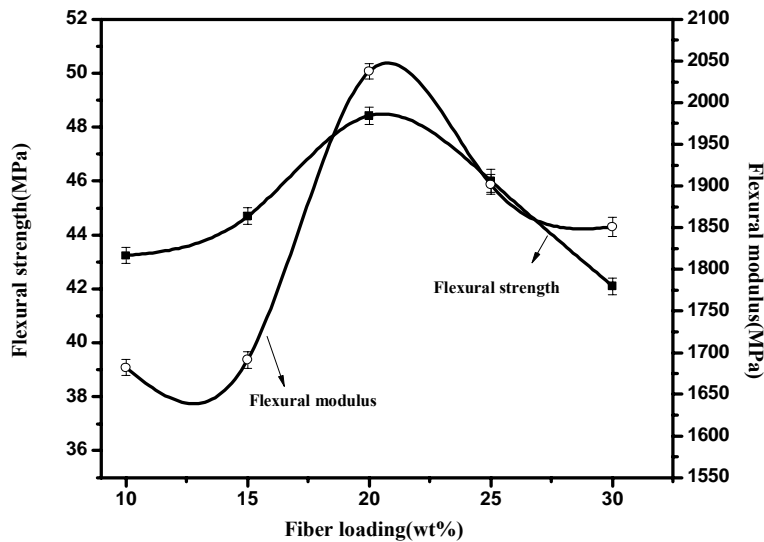
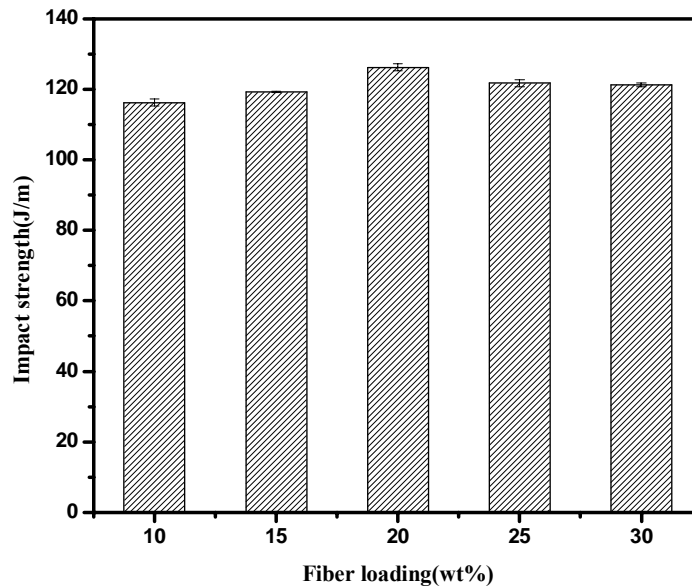


Figure 4a.6 Variation of flexural properties with fiber loading

### (c) Impact strength

Impact strength of a composite is defined as the ability of the material to resist fracture failure under sudden applied force at high speed and is interrelated to the toughness. Figure 4a.7 depicts the variation of impact strength with fiber loading. The impact strength increases with increase in fiber loading up to 20 wt % and then decreases. Fibers resist the crack propagation and act as a load transfer medium. The applied stress is transferred due to the effective interfacial bonding [33]. Decrease in impact strength at higher fiber content is due to the poor fiber/matrix adhesion. The mechanical studies show a good reinforcement at approximately 20wt % of the glass fiber loading. Hence 20 wt % loading is taken as optimum fiber concentration for the further studies. From the studies, it can be concluded

that the 20 wt % of fiber content having a fiber length of 8mm can be considered as the optimum loading for enhancing the mechanical strength of PP/PS blend.



**Figure 4a.7** Variation of impact strength with fiber loading

#### **4. A.3.2 Hybrid effect of E-glass fiber and modified kaolin nanoclays on Polypropylene/Polystyrene blend**

##### **4. A.3.2.1 Effect of nanoclays on the mechanical properties of PP/PS/EGF composites**

###### **(a) Tensile properties**

Tensile properties (tensile strength and modulus) of PP/PS/EGF/modified kaolin nanoclay composites with different levels of nanoclay contents are given in Figures 4a.8 and 4a.9. The maximum improvement in mechanical properties is observed at 20 wt% of fiber content having 8mm fiber length. This composite is selected for nanoclay modification. The tensile strength and modulus of PP/PS/EGF composites at 20wt % EGF

loading containing a variable weight percentage of the two different nanoclay loadings; N100V and N100Z are shown in Figures 4a.8 and 4a.9. From the figures it can be noticed that the tensile strength and modulus of PP/PS/EGF composites increase first and then decrease with increasing nanoclay content from 1 – 5 wt%. The tensile strength and modulus increase by 18 % and 20 % in the case of PP/PS/EGF/N100V (2wt% of N100V) composites and 30 % and 12 % respectively, in the case of PP/PS/EGF/N100Z (3wt% of N100Z) composites when compared to PP/PS/EGF composites. The interfacial adhesion between EGF and polymer matrix increases in the presence of nanoclay hence enhances the tensile properties of the PP/PS/EGF/modified kaolin nanoclay hybrid composites [34]. The nanoclay layers adhere to the surface of glass fiber and improve the interfacial bonding of the resultant hybrid composites resulting in better stress transfer to the glass fibers in the composites.

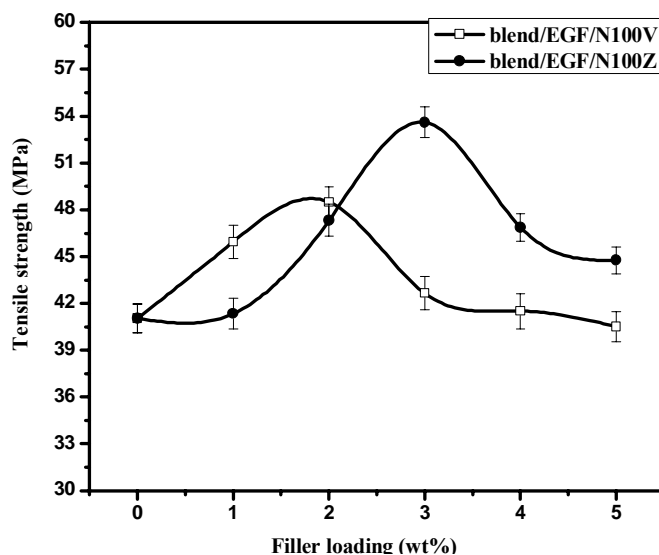
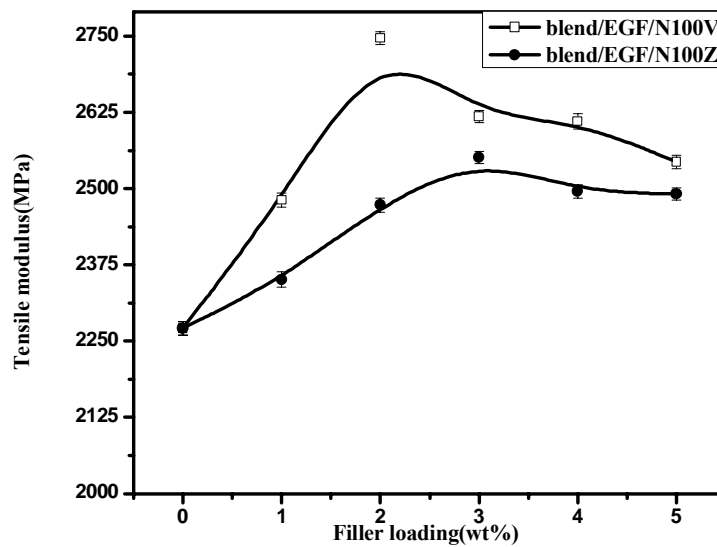


Figure 4a.8 Variation of tensile strength with nanoclay loadings

The improvement is due to the exfoliation of nanoclay particles in the matrix that restricts the mobility of polymer chains under loading. This is in complete agreement with the morphological interpretations from XRD and SEM (sections 4.A.3.7& 4.A.3.8).



**Figure 4a.9** Variation of tensile modulus with nanoclay loadings

At higher nanoclay loading, tensile properties are found to be decreased. This may be due to the agglomeration of clay particles which reduced the interfacial interactions and lowered the strengthening effect of clay in the composites [35]. At higher nanoclay loading, the melt viscosity may be high which hinders the complete dispersion of nanoclays during melt mixing and may have resulted in an improper distribution of nanoclays within the polymer matrix.

**(b) Flexural properties**

Flexural strength and modulus of PP/PS/20wt%EGF composites with varying wt% of N100V and N100Z are plotted in the Figures 4a.10 and 4a.11 respectively. The flexural strength increases by 21 % for PP/PS/EGF/N100V composites (at 2wt %) and by 34% for PP/PS/EGF/N100Z (at 3 wt %). Similarly, flexural modulus increases by 64 % for PP/PS/EGF/N100V at 2 wt % and 85% for PP/PS/EGF/N100Z at 3wt% of nanoclay; compared to PP/PS/EGF composite at the same fiber loading. The increase in the mechanical properties in PP/PS/EGF/modified kaolin nanoclay hybrid composites is due to the synergistic effect caused by nanoclays and glass fiber.

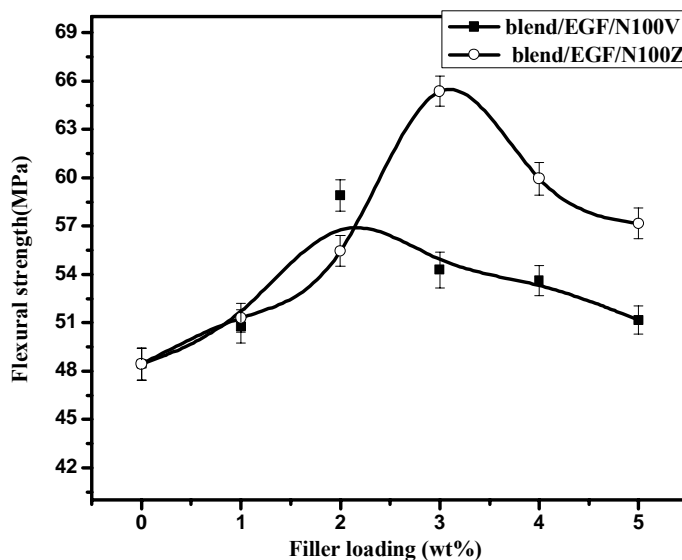
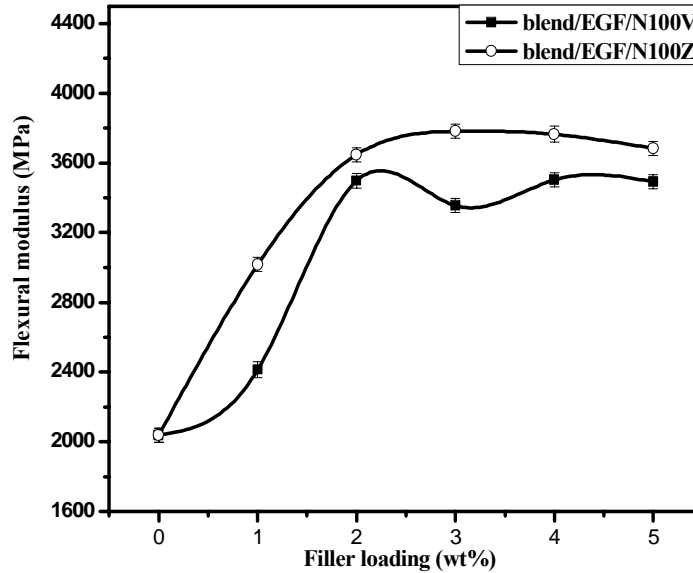


Figure 4a.10 Variation of flexural strength with nanoclay loadings



**Figure 4a.11** Variation of flexural modulus with nanoclay loadings

**(c) Impact strength**

Impact strength of PP/PS/20%EGF composites with varying weight percentage of N100V and N100Z are shown in the Figure 4a.12. It can be observed that the impact strength of PP/PS/EGF/ modified kaolin nanoclay hybrid composites is higher than the PP/PS/EGF composites. The impact strength increases by 12 % in the case of PP/PS/EGF/N100V hybrid composites (2wt % N100V) and by 22 % in the case of PP/PS/EGF/N100Z composites (3wt % N100Z) than the PP/PS/EGF pure composites. The increase in impact strength may be due to the increase in interfacial interaction and synergistical action of nanoclay as an interfacial modifier between the glass fiber and polymer matrix. Besides, the growth of micro-cracks can also be arrested by the nanoclay platelets. The poorly dispersed fillers can easily agglomerate and obstruct stress propagation [35].



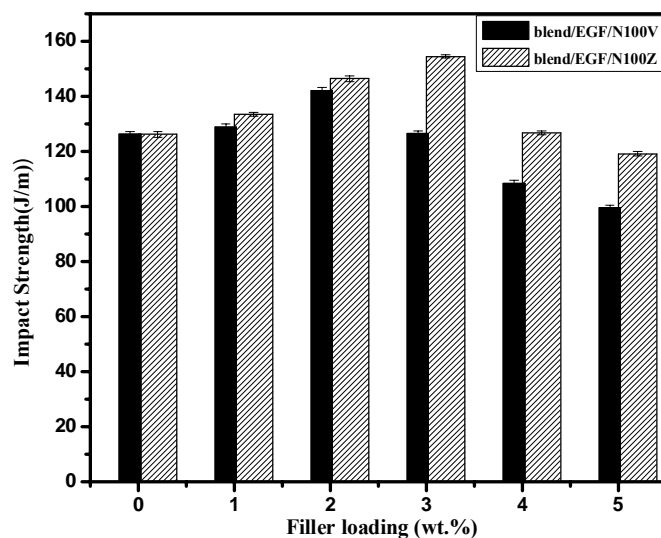
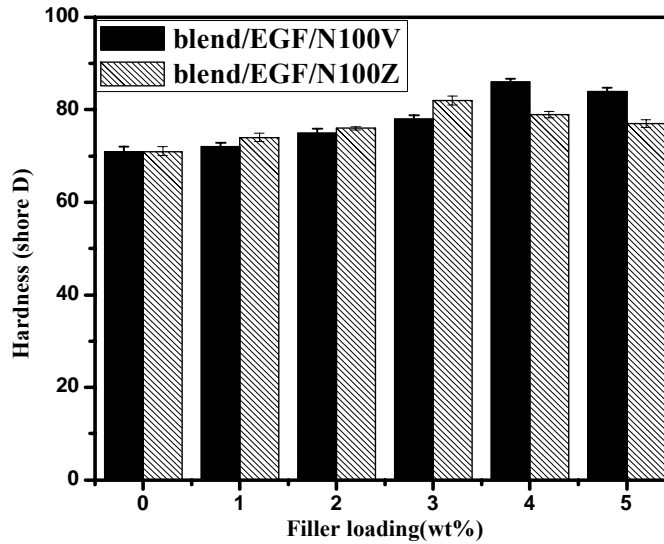


Figure 4a.12 Variation of impact strength with nanoclay loadings

(d) **Hardness**

Hardness of PP/PS/20wt%EGF composites with varying weight percentages of N100V and N100Z are given in the Figure 4a.13. From the figure it is evident that the presence of N100V and N100Z improves the hardness of PP/PS/EGF composites by 21 % (2wt % N100V) and 15 % (3wt % N100Z) compared to pure matrix. The increase in hardness may be due to the higher stiffness of nanoclays and glass fiber. A decreasing trend for the hardness is observed with higher nanoclay addition. The decrease in the hardness value at high nanoclay loading can be attributed to their agglomeration.



**Figure 4a.13** Variation of hardness with nanoclay loadings

#### **4. A.3.3 Theoretical modeling of tensile modulus**

##### **(a) Single fiber model**

Figure 4a.14 gives the comparison between the experimental data and the results provided by various theoretical models (tensile moduli) for PP/PS/EGF composites. Among all the model fits, the predicted moduli based on Hui-Shia and Series show the closest proximity to the experimentally determined tensile modulus values. The curves showing Parallel and Halpin-Tsai models agree least with experimental values. It can also be observed that the values from Halpi-Pagano are deviated away from the experimental values. The values obtained from modified Halpin-Tsai equation (Neilson model) is negatively deviated away from the experimental values. The Hirsch's model also shows the closest proximity to the experimentally determined tensile modulus values. In the case of Hirsch's model, the predicted values converge to experimental values. The better

agreement with the predicted values and the experimental values has been found only when the value of  $x$ , which determines the stress transfer between the matrix and the fiber in equation 4a.3 is 0.05 for randomly oriented composites. The experimental results show close proximity to the Hui Shia model which indicates a perfect interfacial bonding between glass fiber and the polymer matrix as per the assumptions of the model.

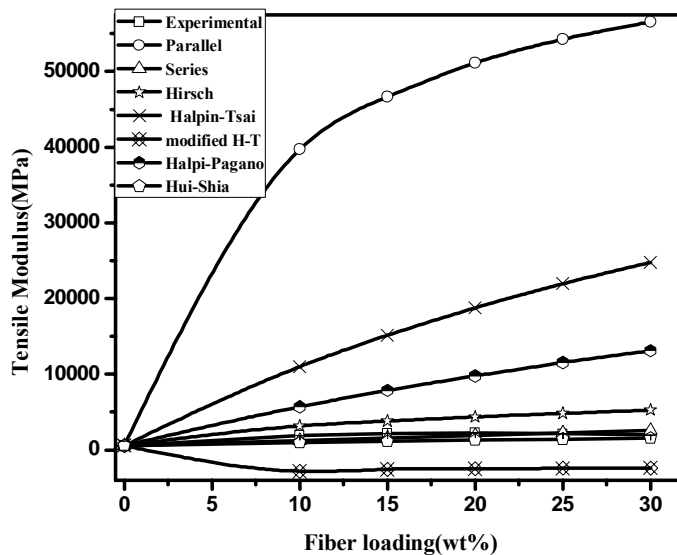


**Figure 4a.14** Theoretical modeling of tensile modulus as a function of glass fiber loadings using various models

The experimental value is in good agreement with Series model which is on the assumption of uniform stress. This can be attributed to the fact that uniform stress is achieved in composites as a result of the better load distribution through the well-dispersed fibers in the matrix. This theoretical analysis indicates that a uniform stress transfer is achieved in the composites due to the better interfacial interaction between glass fiber and the polymer matrix.

**(b) Multiple filler model**

Figures 4a.15 (a) and 4a.15 (b) illustrate the comparison between the experimental data and the results provided by various theoretical models fit tensile moduli for PP/PS/EGF/modified kaolin nanoclay hybrid composites with N100Z and N100V respectively. From the figures it can be seen that both the hybrid composites show similar results on comparison. Among all the model fits, the predicted moduli based on Hirsch and Series shows closest proximity to the experimentally determined tensile moduli values. Paul model and Counto model show close proximity to the experimental values at lower percentage [till 3 wt%] after which the predicted models deviate away from the experimental values for both hybrid composites [PP/PS/EGF/N100Z and PP/PS/EGF/N100V]. Counto model predicts the tensile modulus better than Paul model. Counto model assume that there is a perfect bonding between the fillers and the polymer matrix. Paul model assumes that consistent stress is applied at the matrix-filler boundary and adhesion is perfect at the interface of a cubic inclusion in a cubic matrix. The better prediction of these models (Paul and Counto model) at lower percentages may be due to the presence of nanoclay which increases the interfacial adhesion between the polymer matrix and glass fiber, resulting in better stress transfer at the interface.

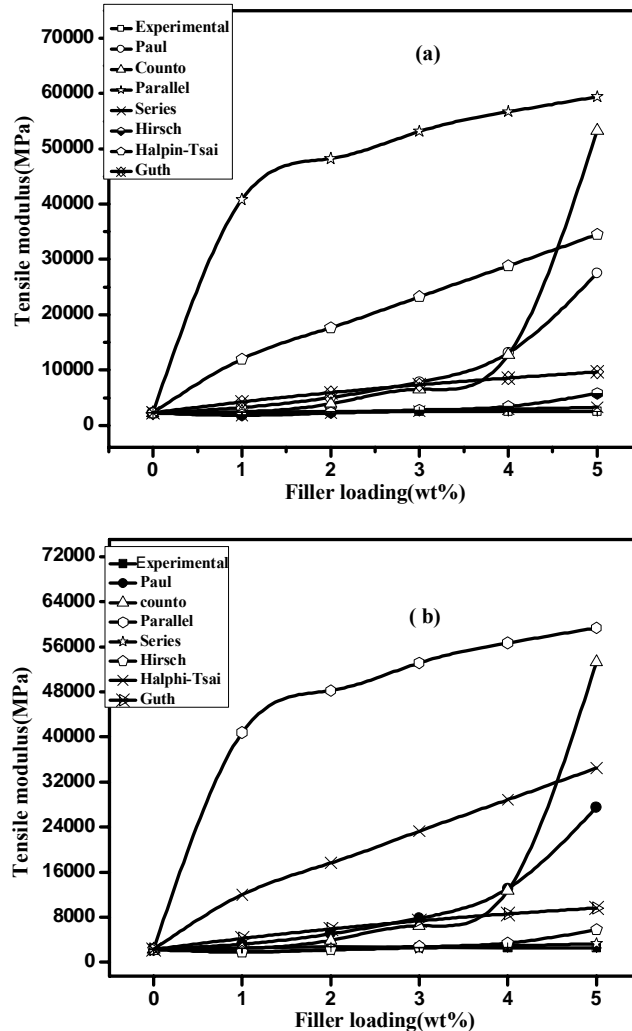


Figure 4a.15 Theoretical modeling of tensile modulus as a function of filler loadings using various models of (a) PP/PS/EGF/N100Z hybrid composite (b) PP/PS/EGF/N100V hybrid composite

The deviation of the models from the experimental values may be due to the agglomeration of nanoclay particles which reduced the interfacial interactions and lowered the strengthening effect of nanoclay in the composites. The predicted data by inverse rule of mixtures (Series model)

are well fitted to the experimental results which assume a uniform stress transfer in the composites. The Hirsch's model also shows the closest proximity to the experimentally determined tensile modulus values. In the case of Hirsch's model, the predicted values converge to experimental values. The better agreement with the predicted values and the experimental values has been found only when the value of  $x$ , which determines the stress transfer between the matrix and the fiber in equation 4a.22 are 0.05 for randomly oriented composites. The curves showing Parallel and Halpin-Tsai models agree the least with experimental values. Guth model shows less deviation from the experimental values.

#### **4. A.3.4 Effect of UV aging on the tensile properties**

Figures 4a.16 (a) & 4a.16 (b) depict the effect of UV aging on the tensile strength and tensile modulus of PP/PS/EGF/modified kaolin nanoclay hybrid composites. After the UV light exposure the tensile properties decrease with nanoclay loading. Increase in photo degradation rates of nanoclay based composites have been reported by many other workers [36-39]. In PP/PS/EGF/modified kaolin nanoclay hybrid composites, the nanoclay particles accelerate the photo degradation of PP/PS blend. Cherifa Remili *et al.* have reported the effect of photo-oxidation under accelerated UV conditions on the structure, the molecular weight and the morphology of polystyrene /organophilic montmorillonite nanocomposites and they found out that the photo-oxidation rates are increased by the catalytic action of nanoclay particles [40].

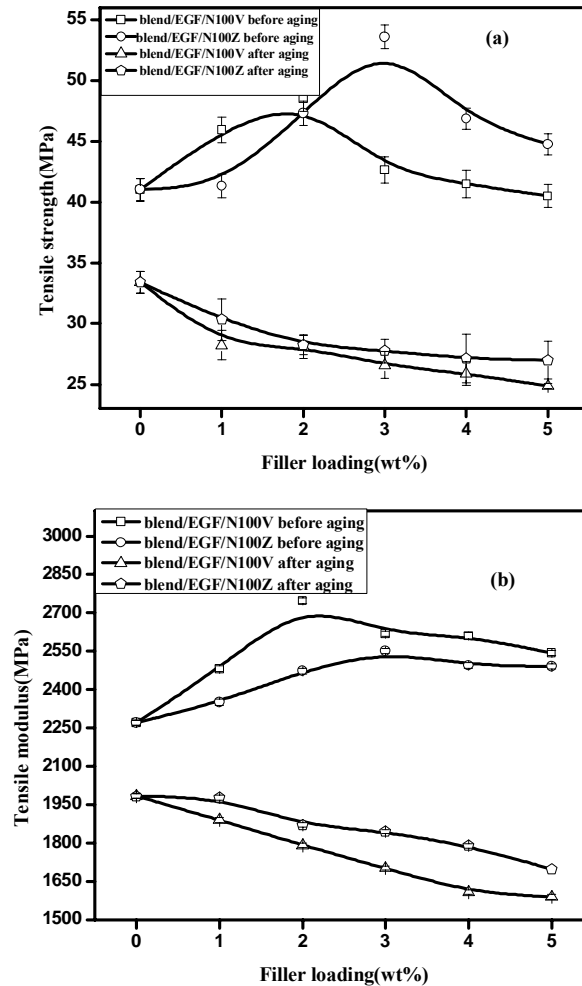


Figure 4a.16 Effect of UV aging on the (a) tensile strength (b) tensile modulus of PP/PS/EGF/ nanoclay hybrid composites

#### 4. A.3.5 Density

Table 4a.1 shows the density of PP/PS/EGF/modified kaolin nanoclay hybrid composites. The density increases with the addition of glass fiber and it further increases with nanoclay content. This may be attributed to the addition of high dense glass fibers and nanoclay particle into the PP/PS blend.

**Table 4a.1 Density of PP/PS/EGF/ nanoclay hybrid composites**

Sample	PP/PS blend	Blend/EGF	Blend/EGF/1%N100V	Blend/EGF/2%N100V	Blend/EGF/3%N100V	Blend/EGF/4%N100V	Blend/EGF/5%N100V
Density (g/cm <sup>3</sup> )	0.9313	0.9339	0.9448	0.9749	0.9825	0.9915	0.9962
Sample	PP/PS blend	Blend/EGF	Blend/EGF/1%N100Z	Blend/EGF/2%N100Z	Blend/EGF/3%N100Z	Blend/EGF/4%N100Z	Blend/EGF/5%N100Z
Density (g/cm <sup>3</sup> )	0.9313	0.9339	0.9432	0.9812	0.9981	0.9991	1.045

#### 4. A.3.6 Melt Flow Index

Figure 4a.17 gives the variation of MFI with nanoclay (N100V& N100Z) loadings in PP/PS/EGF composites. MFI value of the PP/PS/EGF/modified kaolin nanoclay hybrid composites decreases with increasing nanoclay content and this may be attributed to the strong interfacial interaction between polymer matrix and EGF after the addition of nanoclays [41].

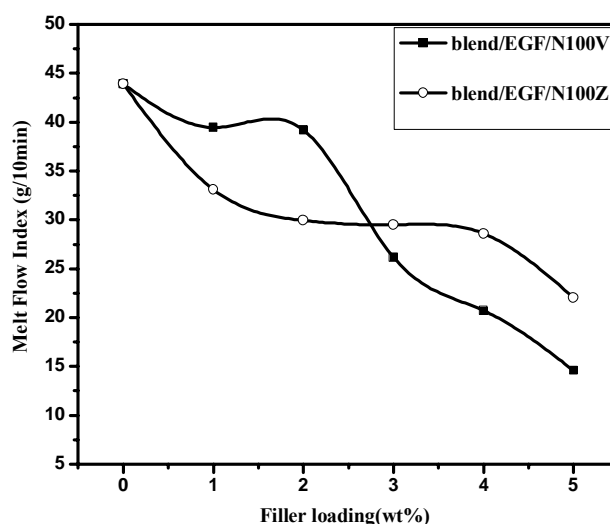


**Figure 4a.17 Variation of MFI with nanoclay loadings**



The nanoclay and glass fiber synergistically influence the reduction of MFI values. This may be due to the increase in interaction of polymer matrix and glass fiber in the presence of nanoclay.

#### 4. A.3.7 X-ray Diffraction

XRD is used to study the dispersibility of nanoclay layers in the polymer matrix [42]. The XRD patterns of N100V, N100Z, PP/PS/EGF, PP/PS/EGF/N100V and PP/PS/EGF/N100Z are given in Figure 4a.18.

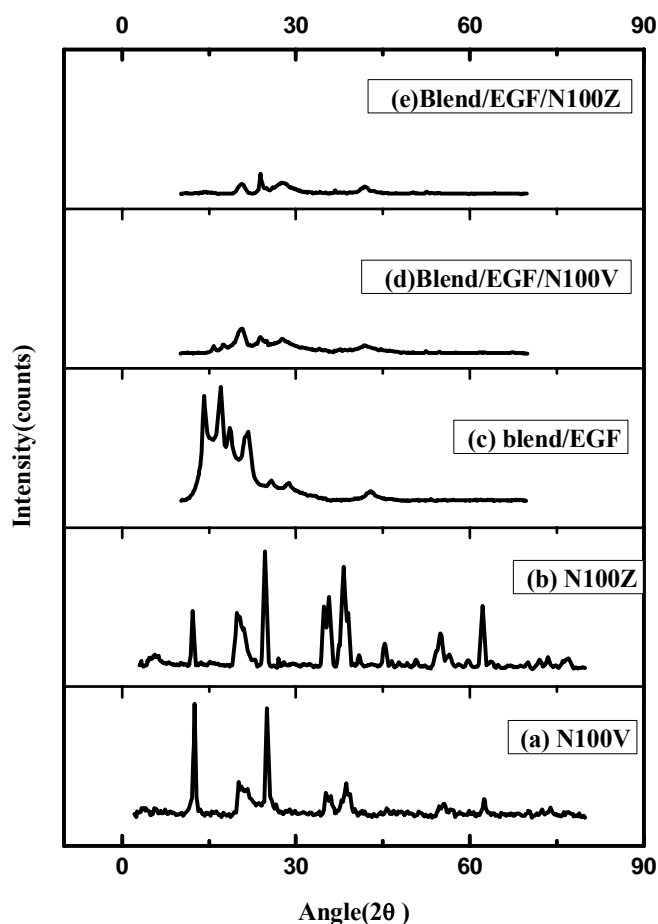
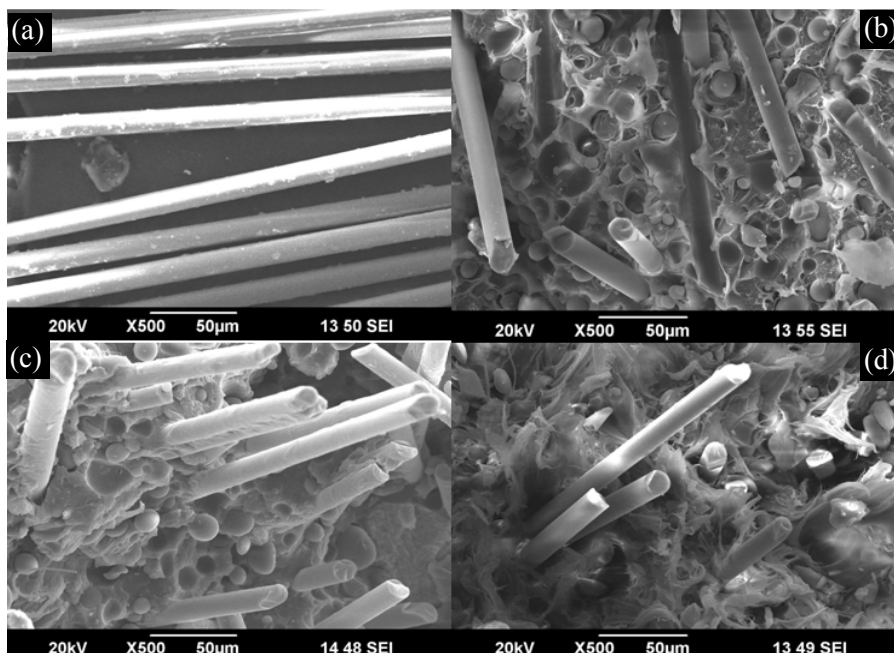


Figure 4a.18 XRD patterns of (a) N100, (b) N100Z, (c) PP/PS blend, (d) PP/PS/EGF/N100V and (e) PP/PS/EGF/N100Z

The original basal reflection peak for N 100V and N100Z is at 12.44° and at 12.18° respectively, which corresponds to an intergallery distance of 7.11 nm and 7.26 nm. Diffraction peaks which appear at  $2\theta = 15- 20^\circ$  in the PP/PS/EGF composite correspond to the monoclinic ‘ $\alpha$ ’ form of the PP [43, 44]. From the XRD curves it is apparent that PP/PS/EGF/N100V and PP/PS/EGF/N100Z hybrid composites exhibit decreased position of characteristic (001) peak. It means that the nanoclay platelets are well dispersed in the hybrid composites. This shows the better interaction between the glass fiber and matrix after the addition of nanoclay [45].

#### **4. A.3.8 Scanning electron microscopy**

Figure 4a.19 exhibits the morphology of glass fiber, PP/PS/EGF composite and PP/PS/EGF/modified kaolin nanoclay hybrid composites. The surface morphology of EGF with diameter 13 $\mu\text{m}$  is shown in the Figure 4a.19 (a). Figure 4a.19 (b) gives the morphology of the tensile fractured surface of PP/PS/EGF composite at the optimum composition (20 wt %). The fractured surface of E-glass fiber composite contains voids mostly at the fiber-matrix interface, which indicates the weak interfacial strength of adhesion between the glass fibers and the polymer matrix. The absence of adhesion between the fibers and the matrix results in debonding and pullout of the fibers at low stress [46, 47].



**Figure 4a.19** SEM photographs of (a) E- glass fiber, (b) PP/PS/EGF, (c) PP/PS/EGF/N100Z and (d) PP/PS/EGF/N100V

Figures 4a.19 (c) and 4a.19 (d) display the tensile fractured surface morphology of 3% N100 Z and 3% N100V filled PP/PS/EGF composites respectively. From the SEM photographs it is apparent that there is a reduction of micro voids in EGF/nanoclay hybrid composites. It can also be observed that the fibers are surrounded and adhered to the matrix. This indicates that the nanoclay particles are dispersed homogeneously in the polymer matrix and the fiber- matrix interfacial adhesion is better in the presence of modified kaolin nanoclays [48].

#### 4. A.3.9 Thermogravimetric analysis

The thermal stability of prepared hybrid composites is measured using TGA measurements. The quantitative value of the onset of degradation temperature ( $T_0$ ), the temperature at which 50% degradation occurs ( $T_{50}$ ), the

maximum degradation temperature ( $T_{max}$ ), the fraction of material which remains at 600 °C, denoted as residue and oxidation index is shown in the Table 4a.2. Figures 4a.20 & 4a.21 show the TG and DTG curves for PP/PS blend and 20 wt % of EGF composites containing various amounts of N100V and N100Z clay nanoparticles (0-5 wt %). The degradation temperature increases with increasing nanoclay content. The hybrid composites show better thermal stability than PP/PS blend.

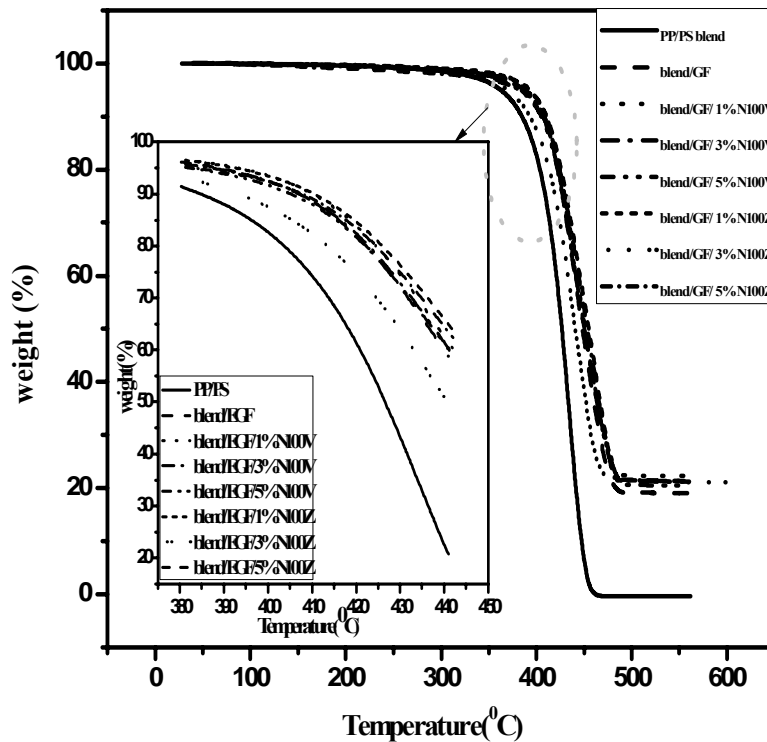


**Figure 4a.20** TG curve of PP/PS blend, PP/PS/EGF composite and PP/PS/EGF/ nanoclay hybrid composites. The inset shows their TG curves in temperature range 375-450°C

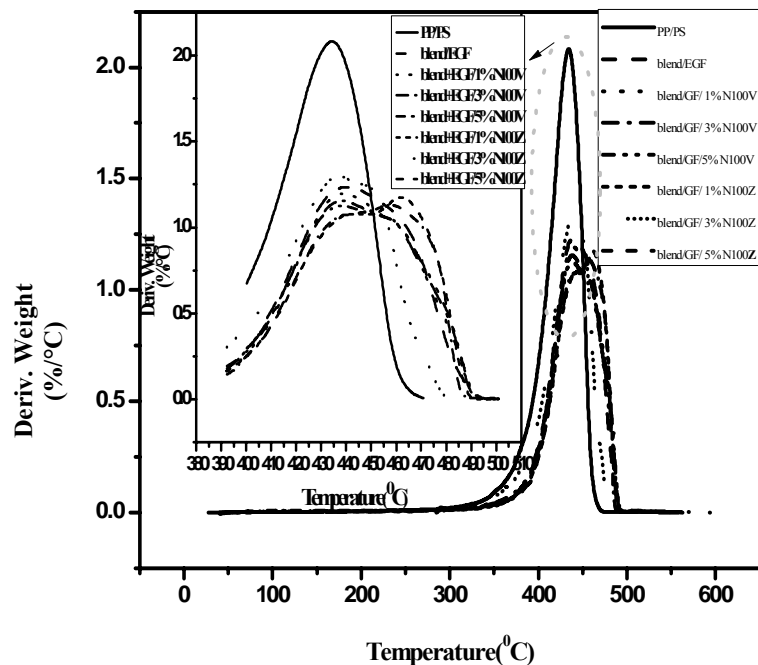


Figure 4a.21 DTG curve of PP/PS blend, PP/PS/EGF composite and PP/PS/EGF/ nanoclay hybrid composites. The inset shows their DTG curves in temperature range 380-510°C

The enhancement in thermal stability is attributed due to the better dispersion of nanoclay platelet which can act as a barrier trapping the volatilizing matrix from escaping into the atmosphere [35].

Higher the values of oxidation index, higher will be the thermal stability. The OI values increases with increase in nanoclay content and lies in the range 0.03-1.54. This study indicates that the clay filled PP/PS/EGF composites are more thermally stable than PP/PS/EGF composites [49].

**Table 4a.2 TGA data of PP/PS blend, PP/PS/EGF composite and PP/EGF/nanoclay hybrid composites**

Samples	Temperature at 50% weight loss (°C)	Onset degradation temperature $T_0$ (°C)	Maximum degradation temperature ( $T_{max}$ ) (°C)	Residue at 600 °C (%)	Oxidation Index (OI)
PP/PS blend	426.6	370.5	434.4	0.456	0.032
Blend /EGF	448.2	378.8	439.7	19.0	1.324
Blend /EGF/1%N100V	450.3	389.4	438.2	20.4	1.423
Blend /EGF/3%N100V	450.2	392.1	438.3	21.1	1.470
Blend /EGF/5%N100V	451.0	393.4	438.5	22.2	1.547
Blend /EGF/1%N100Z	450.8	387.1	436.7	21.1	1.467
Blend /EGF/3%N100Z	453.3	387.5	458.2	21.3	1.479
Blend /EGF/5%N100Z	454.9	394.8	462.1	21.4	1.480

#### 4. A.3.9.1 Kinetic analysis of thermal decomposition

Activation energy was evaluated from the TGA curves using the plots of Horowitz-Metzger, Broido's and Coats Redfern methods. The CR, HM and BR plots for the thermal degradation of PP/PS blend, PP/PS/EGF composite and PP/PS/EGF/modified kaolin nanoclay hybrid composites, from the onset degradation temperature to the maximum degradation temperature are represented in the Figures 4a.22, 4a.23 & 4a.24 respectively. The activation energy ( $E_a$ ) for each method is given in Table 4a.3.

**Table 4a.3 Activation energy (J/mol) calculated by Horowitz-Metzger (HM), Broido's (BR) and Coats-Redfern (CR) methods of PP/PS pure blend, PP/PS/EGF and PP/PS/EGF/ nanoclay hybrid composites**

Sample	Coats –Redfern	Broido's	Horowitz- Metzger
PP/PS blend	174	181	175
Blend/EGF	178	190	199
Blend/EGF/1%N100V	182	188	198
Blend/EGF/3 %N100V	186	191	200
Blend/EGF/5%N100V	189	196	202
Blend/EGF/1 %N100Z	180	189	197
Blend /EGF/3 %N100Z	183	194	209
Blend /EGF/5 %N100Z	186	197	212

The Coats Redfern plots of PP/PS blend, PP/PS/EGF composites, PP/PS/EGF/N100V and PP/PS/EGF/N100Z hybrid composites are presented in the Figure 4a.22. The  $E_a$  values of PP/PS blend, PP/PS/EGF composites and PP/PS/EGF/modified nanoclay hybrid composites calculated from the slopes of the plots of  $\log(-\log(1-\alpha)/T^2)$  verses  $1/T$  are summarized in the Table 4a.3. The  $E_a$  values of PP/PS/EGF/modified kaolin nanoclay hybrid composites are higher than that of PP/PS blend. The hybrid composites reinforced with N100Z show better thermal stability. The improvement in the thermal stability of hybrid composites with the introduction of nanoclay particles is explained by the effective function of clay particles as physical barriers both to retard the thermal decomposition of volatile components and to prevent the transport of volatile decomposed products in the hybrid composites [50].

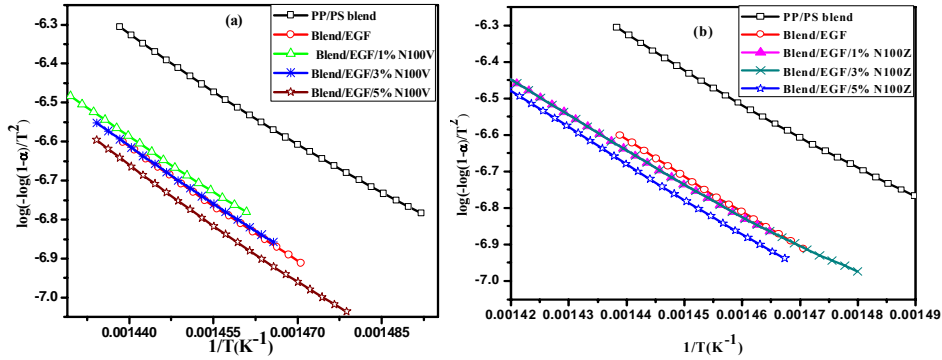


**Figure 4a.22 Kinetic plots for the determination of activation energy of PP/PS blend, PP/PS/EGF, (a) PP/PS/EGF/N100V and (b) PP/PS/EGF/N100Z composites using CR equation**

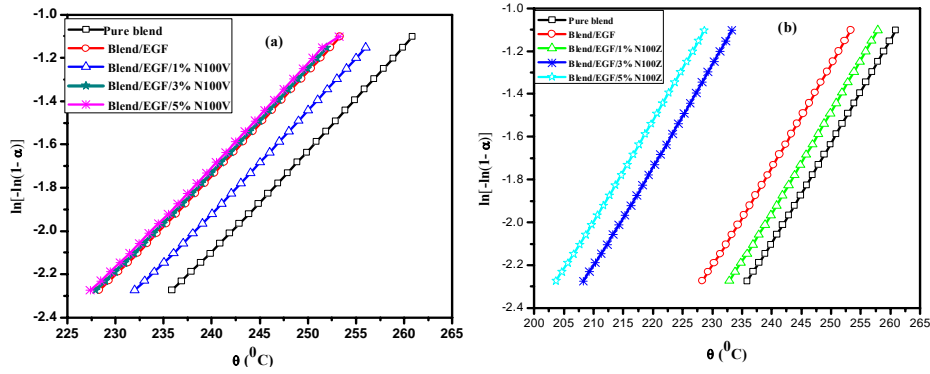


**Figure 4a.23 Kinetic plots for the determination of activation energy of PP/PS blend, PP/PS/EGF, (a) PP/PS/EGF/N100V and (b) PP/PS/EGF/N100Z composites using HW equation**

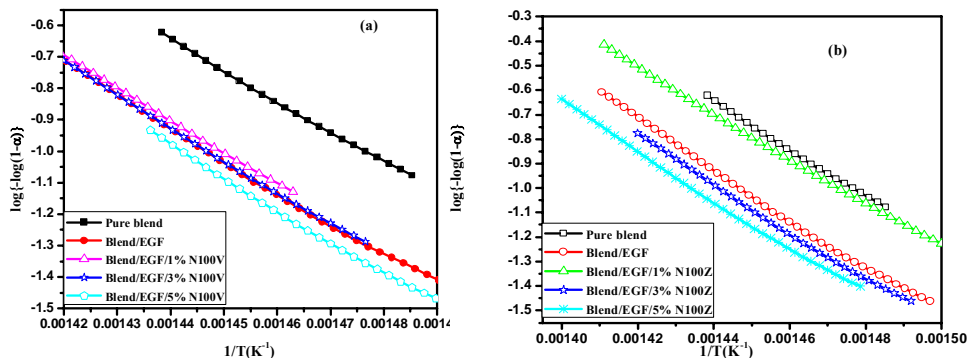


**Figure 4a.24 Kinetic plots for the determination of activation energy of PP/PS blend, PP/PS/EGF, (a) PP/PS/EGF/N100V and (b) PP/PS/EGF/N100Z composites using BR method**



The plot  $\ln [-\ln (1- \alpha)]$  verses  $\theta$  gives a straight line and the  $E_a$  values using Horowitz-Metzger of PP/PS blend, PP/PS/EGF and PP/PS/EGF/N100V and PP/PS/EGF/N100Z hybrid composites calculated from the slopes are summarized in the Table 4a.3. The Horowitz-Metzger plot of PP/PS/EGF/modified clay [Figure 4a.22] composites exhibited a good linear relationship indicating that the method was effective in describing the thermal decomposition kinetics of hybrid composites. The  $E_a$  values of PP/PS/EGF/modified nanoclay hybrid composites are higher than that of pure blend.

The Broido's plots of PP/PS blend, PP/PS/EGF composites, PP/PS/EGF/N100V and PP/PS/EGF/N100Z hybrid composites are shown in the Figure 4a.24. The  $E_a$  values of PP/PS blend, PP/PS/EGF and PP/PS/EGF/modified nanoclay hybrid composites calculated from the slopes of the plots of  $\log \{-\log (1-\alpha)\}$  verses  $1/T$  are summarized in the Table 4a.3.

Comparing the three models, the  $E_a$  values obtained from the Broido's method were slightly larger than that of the Horowitz-Metzger and Coats-Redfern analysis, whereas the three models revealed similar trend of the  $E_a$  values with the introduction of nanoclay particles. The kinetic analysis suggests that an enhanced thermal stability of hybrid composites is associated with the increase in the activation energy of their degradation process. At higher temperature the thermal behavior of EGF becomes predominant and an increase in the thermal stability of the EGF composite (PP/PS/EGF) is observed. This may explain why the values of maximum degradation temperature of PP/PS/EGF are higher than those values for composites with increasing nanoclay loading [51].

#### **4.A.3.10 Dynamic mechanical analysis**

In order to investigate the reinforcing effect of nanoclays and E-glass fiber in PP/PS blend, dynamic mechanical analysis (DMA) has been carried out at a fixed frequency of 1Hz in the temperature range of 40 to 125°C. The storage modulus for PP/PS blend, PP/PS/EGF composite, EGF reinforced PP/PS blend with 3 wt % N100V and 3 wt % N100Z are depicted in the Figure 4a.25. Table 4a.4 shows the storage moduli, glass transition temperatures ( $T_g$ ) and interaction parameter (B) values of the PP/PS blend, PP/PS/EGF and PP/PS/EGF/modified kaolin nanoclay hybrid composites. The storage modulus of the glass fiber composites is higher than that of virgin matrix. This behavior is due to the reinforcing effect imparted by the fibers that allows a greater degree of stress transfer at the interface [52]. The storage modulus is further increased by the addition of modified kaolin nanoclays and is due to the hybrid effect caused by the presence of glass fiber and nanoclay. The storage modulus of pure blend increases by 163 % at 80°C with the incorporation of 20wt % EGF. There is an increase of 32% by the addition of 3 wt% N100V into the PP/PS/EGF composites and 42% increase is shown after the addition of 3wt% N100Z. This improvement is attributed to the mobility restriction of polymer chains by the nanoclay particles [46] and also due to the better interaction between the polymer matrix and glass fibers by the addition of nanoclay layers which leads to better interfacial interaction and better stress transfer [53].

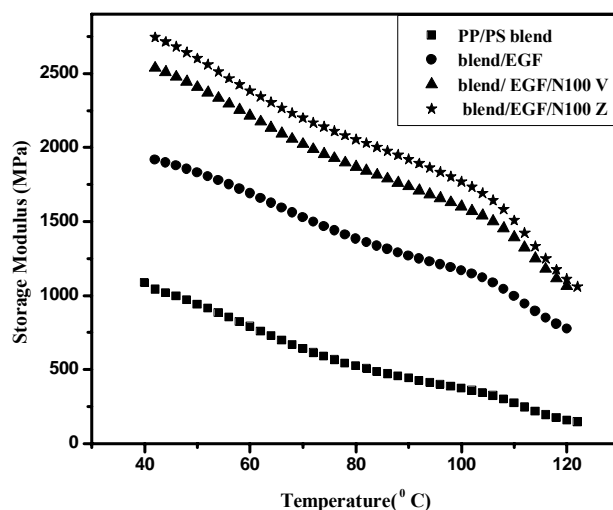
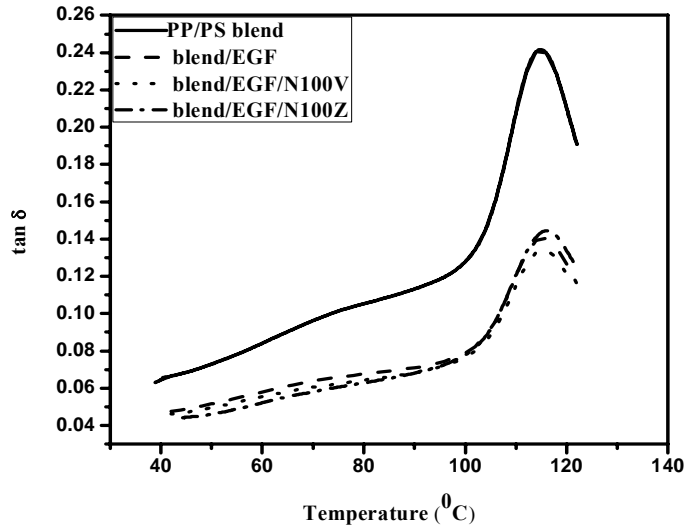


Figure 4a.25 Storage modulus curves of PP/PS blend, PP/PS/EGF and PP/EGF/ nanoclay hybrid composites

Table 4a.4 Storage moduli,  $T_g$  and interaction parameter values of PP/PS blend, PP/PS/EGF, PP/PS/EGF/ nanoclay hybrid composites

Samples	Storage modulus				$T_g$ (°C) from tan $\delta$ value	Interaction Parameter (B)
	45 °C	80 °C	100 °C	120 °C		
PP/PS blend	1007	525.3	374.1	159	115.0	0
Blend/EGF	1889	1384	1171	778	115.4	0.68
Blend/EGF/3%N100V	2496	1871	1603	1063	115.5	2.97
Blend/EGF/3%N100Z	2699	2056	1770	1112	115.9	2.51

Tan $\delta$  curves for PP/PS blend, PP/PS/EGF composite, EGF reinforced PP/PS blend with 3 wt % N100V and 3 wt % N100Z are evidenced in the Figure 4a.26. From Table 4a.4, it can be noticed that  $T_g$  increases slightly with the addition of glass fiber and nanoclays. The slight increase in  $T_g$  is due to the immobilization of polymer molecules due to the molecular interaction caused by EGF and modified kaolin nanoclays. As the interaction between the polymer matrix and the glass fiber increases the mobility of macromolecular chain is reduced and  $T_g$  shifts to higher temperature.



**Figure 4a.26** Tan  $\delta$  curves of PP/PS blend, PP/PS/EGF and PP/PS/EGF/ nanoclay hybrid composites

Interfacial interaction between two phases can be determined using DMA. The relationship of the loss tangent value between the filled polymer and the unfilled polymer matrix can be calculated using the following equation [54,55].

$$\tan \delta = \tan \delta_m / (1 + 1.5B \Phi) \dots\dots\dots (4a. 26)$$

where  $B$  is an interaction parameter, the larger the value, the stronger the interfacial interaction between the polymer matrix and filler;  $\Phi$  is the volume fraction of filler;  $\tan \delta$  and  $\tan \delta_m$  represent the loss tangent value of the filled polymer and the unfilled polymer matrix respectively. Interaction parameter ( $B$ ) is higher for PP/PS/EGF/modified nanoclay composites, which suggests a strong interfacial interaction between the nanoclay and PP/PS/EGF composite.

#### 4.A.3.10.1 Cole-Cole Plot analysis

Figure 4a.27 depicts Cole–Cole plot where the loss modulus ( $E''$ ) data are plotted as a function of storage modulus ( $E'$ ) for PP/PS/EGF/modified kaolin nanoclay hybrid composites. A Cole-Cole plot is used to predict the nature of a composite, whether it is homogeneous or heterogeneous and also to understand the phase behavior and structural changes taking place after the addition of nanofiller to polymeric systems. Homogeneous systems are reported to show semicircular curve, whereas a heterogeneous system exhibits an irregular curve (imperfect semicircle). In this plot, a drift from a semicircle represents immiscibility and the shape of the curve points up to the relatively good fiber/matrix adhesion [56, 57]. The shape of the curve shows the heterogeneous systems with relatively good clay–polymer and fiber interaction. Thus, it can be concluded that the nanoclay loadings do not affect the morphological state of fiber-reinforced nanocomposites.

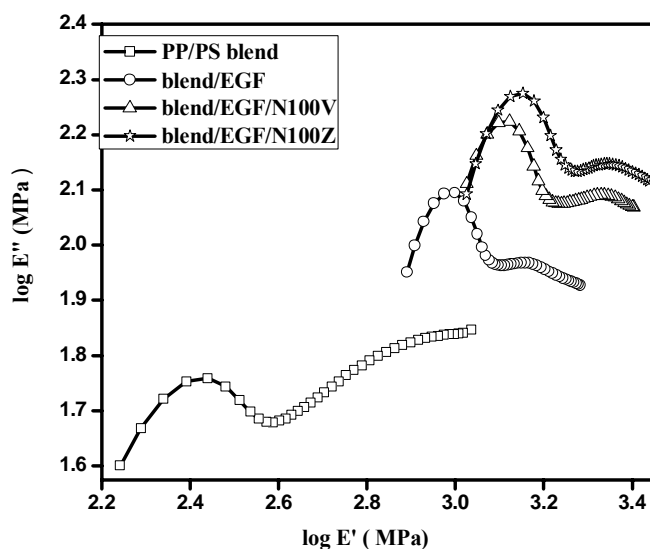


Figure 4a.27 Cole-Cole plot of PP/PS blend, PP/PS/EGF composite and PP/PS/EGF/nanoclay hybrid composites

Cole-Cole plot of PP/PS/EGF and PP/PS/EGF/modified kaolin nanoclay hybrid composites deviated from scaling  $\log G'$  versus  $\log G''$  of the unreinforced polymer blends. The addition of EGF and nanoclay particles into PP/PS blends has enhanced the interfacial adhesion, increased the elasticity and improved the properties of the composites.

#### **4. A.3.11 Differential scanning calorimetry**

The crystallization temperature ( $T_c$ ), the apparent melting temperature ( $T_m$ ) and the corresponding enthalpies are given in the Table 4 a.5, whereas the Figure 4a.28 presents the DSC melting and cooling curves for PP/PS blend, PP/PS/EGF composites and EGF reinforced PP/PS blend with 3 wt % N100V and 3 wt % N100Z. Crystallization temperature of the PP/PS blend increases after the addition of nanoclay particles. These higher  $T_c$  values of the hybrid composites with respect to the pure blend indicate that the crystallization rate of composites increased after the addition of clay particles. The increase in  $T_c$  could be considered to be due to the nucleation.

**Table 4a.5 Thermal characteristics of PP/PS blend, PP/PS/EGF and PP/PS/EGF/nanoclay hybrid composites**

<b>Samples</b>	<b><math>T_c</math> (°C)</b>	<b><math>\Delta H_c</math> (J/g)</b>	<b><math>T_m</math> (°C)</b>	<b><math>\Delta H_m</math> (J/g)</b>
PP/PS pure blend	111.9	61.1	158.4	32.4
Blend/EGF	113.7	56.8	158.2	35.8
Blend/EGF/N100V	117.0	58.8	158.8	37.3
Blend/EGF/N100Z	115.6	57.4	158.7	37.7

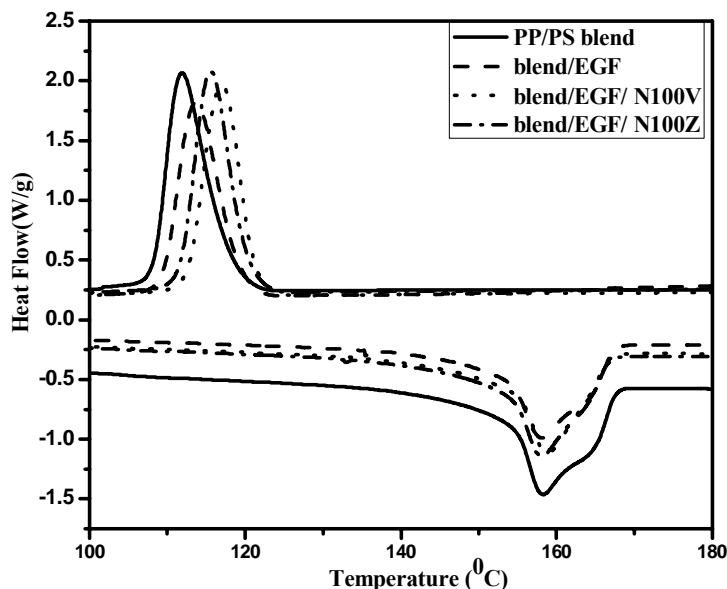


**Figure 4a.28** DSC melting and crystallization curves of PP/PS pure blend, PP/PS/EGF, PP/PS/EGF/nanoclay hybrid composites

In the glass fiber composites (PP/PS/EGF) the crystallization enthalpy,  $\Delta H_c$  is found to be decreased. The molecular motion of the polymer matrix could be restricted by the addition of E-glass fibers, resulting in a decrease of crystallization [58]. There is an increase in  $\Delta H_c$  after the addition of nanoclay particles into the PP/PS/EGF composites which may be due to the nucleating effect of nanoclays [59]. The melting temperatures ( $T_m$ ) of the studied samples are shown in the Table 4a.5.  $T_m$  is not significantly affected by the addition of either EGF or clay particles. The increase in  $\Delta H_m$  values of the hybrid composites from that of the neat polymer matrix indicates the higher thermal stability of the composites [60].

#### **4.A.4 Conclusions**

The study shows that modified kaolin nanoclays and E-glass fiber can synergistically reinforce PP/PS composites. The optimum fiber content that gives maximum mechanical properties of composites is about 20 wt%. The addition of modified nanoclays improves the mechanical properties of the PP/PS/EGF composites. A comparison between experimental results (tensile modulus) of various models of PP/PS/EGF composites has been presented. The predicted moduli based on Series and Hirsch model, show the closest proximity to the experimentally determined elastic moduli values and Paul and Counto model shows close proximity at lower percentage. The results predict better dispersion of clay particles in PP/PS/EGF composites at lower percentage. XRD patterns reveal a partial nanoclay exfoliation in dialkyl modified and vinyl modified kaolin nanoclay reinforced PP/PS/EGF composites. DMA studies show that incorporation of nanoclay into the composites increase the storage modulus of the hybrid composites over the entire range of temperature studied. SEM photographs show a reduction of microvoids in prepared hybrid composites and also show a better adhesion between glass fiber and polymer matrix in the presence of modified kaolin nanoclays. TGA studies show an increase in the thermal stability after the addition of modified nanoclay. The activation energy increases with the addition of organoclays confirming higher thermal stability.



## References

- [1]. Quynh T. Nguyen , Phuong Tran, Tuan D. Ngo, Phong A. Tran, Priyan Mendis, *Composites: Part B* , 2014,62 , 218–229.
- [2]. *Structural Analysis of Fiber Reinforced Composite Materials*, Cesar Augusto Rojas, The University Of Texas At Arlington, Master of Science in Mechanical Engineering, 2006.
- [3]. N. M. L. Mondadori, R. C. R. Nunes, A. J. Zattera, R. V. B. Oliveira, L. B. Canto, *Journal of Applied Polymer Science*, 2008, 109, 3266–3274.
- [4]. Mike J. Clifford, Tong Wan, *Polymer*, 2010, 51, 535–539.
- [5]. Yi-Hua Cui, Xin-Xin Wang, Zhi-Qi Li, Jie Tao, *Journal of Vinyl and Additive Technology*, 2010, 16(3), 189–194.
- [6]. Kusmono, Zainal Arifin Mohd Ishak, *International Journal of Polymer Science*, 2013, Article ID 797109, 7.
- [7]. J. P. F Inberg, P. H Hunse, Andr. J. Gaymans, *Polymer Engineering and Science*, 1999, 39(2), 340-346.
- [8]. Kyung Y Kim, Dong Uk Ju, Gi Joon Nam, Jae Wook Lee, *Macromolecular Symposia*, 2007, 249–250 (1): 283–288.
- [9]. Suprakas Sinha Raya, Steve Pouliota, Mosto Bousminaa, Leszek A. Utracki, *Polymer*, 2004, 45 (25), 8403–8413.
- [10]. Yan Zhu, Hai-Yun Ma, Li-Fang Tong, Zheng-Ping Fang, *Chinese Journal of Polymer Science*, 2008, 26(6), 783–792.
- [11]. Youngjae Yoo, M.W.Spencer, D.R Paul, *Polymer*, 2011, 52(1), 180-190.
- [12]. Mazlan Norkhairunnisa, Abu Bakar azhar, Chow Wen Shyang, *Polymer International*, 2007, 56(4), 512-517.
- [13]. James E. Bell, *ARS Journal*, 1961, 31(9), 1260-1265.
- [14]. G. Kalaprasad, K. Joseph, S. Thomas, *Journal of Materials Science*, 1997, 32, 4261- 4267.

- [15]. M.S. Sreekala, Jayamol George, M.G. Kumaran, Sabu Thomas, *Composites Science and Technology*, 2002, 62, 339–353.
- [16]. J. C. Halpin, Affdl, J. L. Kardos, *Polymer Engineering and Science*, 1976, 16 (5), 344-351.
- [17]. J. C. Halpin, *Journal of composite materials*, 1969, 3, 732.
- [18]. L. E. Nielson, Marcel Dekker, *J Polym Sci Pol Lett*, 13, 120-121(1974).
- [19]. L. E. Nielson, *Rheological Acta*, 1974, 13(1), 86-92.
- [20]. S.W Tsai, N.J Pagano, *Invariant Properties of Composite Materials*. Defense Technical Information: Fort Bellvoir, VA, USA, 1968.
- [21]. Runzhou Huang, Xinwu Xu , Sunyoung Lee , Yang Zhang, Birm-June Kim, Qinglin Wu. *Materials*, 2013, 6, 4122-4138.
- [22]. Srikanth Pilla, Shaoqin Gong, Eric O'Neill, Roger M. Rowell, Andrzej M. Krzysik, *Polymer Engineering and Science*, 2008, 48(3), 578–587.
- [23]. C. Y. Hui, David Shia, *Polymer Engineering and Science*, 1998, 38(5), 774-782.
- [24]. Hurang Hua, Landon Onyebueke, Ayo Abatan, *Journal of Minerals & Materials Characterization & Engineering*, 2010, 9(4), 275-319.
- [25]. M. R. Mansor, S. M. Sapuan, E. S. Zainudin, A. A. Nuraini, and A. Hambali, *Journal of Polymeric Materials*, 2013, 30(3), 321-334.
- [26]. Jamal Mirbagheri, Mehdi Tajvidi, Ismaeil Ghasemi, C.John Hermanson. *Iran Polymer Journal*, 2007, 16 (4), 271-278.
- [27]. Jeremiah Paul Konell, *Characterization and Tensile Modulus Modeling of Conductive Resins*, Ph.D thesis, 2002.
- [28]. Yasser Zare, Hamid Garmabi, *Journal of Applied Polymer Science*, 2012, 123(4), 2309–2319.
- [29]. J. Malzbender, J.M.J. Den Toonder, A.R. Balkenende, G.De, *Materials Science and Engineering. R*, 2002, 36(2), 47- 103.
- [30]. T.D. Fornes, D.R. Paul, *Polymer* , 2003 , 44(17), 4993–5013.

- [31]. Moe Thwe, Kin Liao, *Composite Science and Technology*, 2003, 63 (3-4), 375–387.
- [32]. Normasmira Abd. Rahman, Aziz Hassan, Rosiyah Yahya, R.A. Lafia-Araga and Peter R. Hornsby, *Journal of Reinforced Plastics and Composites*, 2012, 31(4), 269–281.
- [33]. P. Amuthakkannan, V. Manikandan, J.T. Winowlin Jappes, M. Uthayakumar, *Materials Physics and Mechanics*, 2013, 16, 107-117.
- [34]. Normasmira A. Rahman, Aziz Hassan, R. Yahya, R.A. Lafia-Araga, *Sains Malaysiana*, 2013, 42(4), 37–546.
- [35]. N H Mohd. Zulfli, A Abu Bakar, W. S Chow, *Malaysian Polymer Journal*, 2012, 7 (1), 8-15.
- [36]. L. Botta, N.Tz. Dintcheva, F.P. La Mantia, *Polymer Degradation and Stability*, 2009, 94, 712–718.
- [37]. Ping Wei, Sergio Bocchini, Giovanni Camino, *European Polymer Journal*, 2013, 49 , 932–939.
- [38]. Huaili Qin, Shimin Zhang, Huiju Liu, Shaobo Xie, Mingshu Yang, Deyan Shen, *Polymer*, 2005, 46 , 3149–3156.
- [39]. Huaili Qin, Chungui Zhao, Shimin Zhang, Guangming Chen, Mingshu Yang, *Polymer Degradation and Stability* ,2003,81 ,497–500.
- [40]. Cherifa Remili, Mustapha Kaci, Souad Kachbi, Stephane Bruzard, Yves Grohens , *Journal of Applied Polymer Science*, 2009, 112, 2868–2875 .
- [41]. Sevdalina Turmanova, Svetlana Genieva, Lyubomir Vlaev, *International Journal of Chemistry*, 2012, 4(4).
- [42]. J G Ryu, H Kim, J W Lee, *Polymer Engineering and Science*, 2004, 44, 1198-1204.
- [43]. Jinge Li , Huayi Li , Chunhong Wu, Yucai Ke , Dujin Wang, Qian Li, Liaoyun Zhang , Youliang Hua, *European Polymer Journal*, 2009, 45,2619.

- [44]. S.Thomas Ellis, S. Joseph D'Angelo, Journal of Applied Polymer Science, 2003, 90, 1639.
- [45]. Jan Golebiewski , Andrzej Galeski, Composite Science and Technology, 2007, 67, 3442.
- [46]. Ishak Ahmad, Ramli Ismail, Ibrahim Abdullah, Polymer Engineering and Science, 2011, 51,419.
- [47]. SunanTiptipakorn, SarawutRimduisit, Siriporn Damrongsakkul, Takeshi Kitano, Engineering journal, 2009, 13,125.
- [48]. Jia-Lin Tsai, Ming-Daw Wu, Journal of Composite Materials, 2008,42, 553.
- [49]. Shahryar Pashaei, Siddaramaiah, Maziar Mansouji Avval, Akheel Ahmed Syed, Chemical Industry & Chemical Engineering Quarterly, 2011, 17 (2), 141–151.
- [50]. V. S. Aigbodio, S. B. Hassan , C. U. Atuanya, Journal of Materials and Environmental Science,2012, 3 (6), 1027-1036.
- [51]. Normasmira Abd. Rahman, Aziz Hassan, Rosiyah Yahya, R.A. Lafia-Araga, Peter R. Hornsby, Journal of Reinforced Plastics and Composites ,31(4) 269–281.
- [52]. K.Sushanta Samal, Smita Mohanty, K.Sanjay Nayak, Journal of Reinforced Plastics and Composites, 2008, 28, 2729.
- [53]. F.Rezaei, R.Yunus, N.A. Ibrahim, Materials and Design, 2009, 30, 260.
- [54]. Shao-jian He, Yi-qing Wang, Yi-ping Feng, Qing-sheng Liu, Li-qun Zhan, Nanotechnology, 2010, 21, 7.
- [55]. D. Ziegel, A. Romanov, Journal of Applied Polymer Science, 1973, 17, 1119.
- [56]. Sherely Annie Paul, Christoph Sinture, Kuruvilla Joseph, G.D. Gem Mathew, Laly A. Pothan, Sabu Thomas, Polymer Engineering and Science, 2010, 50, 384–395.

- [57]. L Uma Devi, S S Bhagawan ,S Thomas , Polymer Composites ,2010, 31, 956–965.
- [58]. Seung-Hwan Lee, Siqun Wang, Composites: Part A, 2006, 37, 80–91.
- [59]. Chen- Jui Hung, Hung-Yang Chuang, Feng –Chih Chan, Journal of Applied Polymer Science, 2008, 107,831-839.
- [60]. Jaydeep Khedkar, Ioan Negulescu, Efstathios I. Meletis, Wear, 2002, 252, 361–369.

## Part – B

### **Polypropylene/Polystyrene/alkali resistant glass fiber/modified kaolin nanoclays hybrid composites**

#### **Abstract**

*Polypropylene/ Polystyrene/alkali resistant glass fiber (PP/PS/ARGF) composites with different modified kaolin nanoclay contents were prepared by melt mixing in a Thermo Haake Rheocord mixer. Prepared composites were characterized using X-ray diffraction, Scanning Electron Microscopy and Thermogravimetric analysis. The use of two types of fillers leads to synergetic effect on the mechanical properties of the hybrid composites. A comparison between experimental results (tensile modulus) and various models of PP/PS/ARGF composites has been presented. The predicted moduli based on Series and Hirsch model show the closest proximity to the experimentally determined elastic modulus. Paul and Counto model show close proximity at lower percentage up to 4wt%. XRD reveals better nanoclay dispersion in hybrid composites. TGA results show an improved thermal stability for hybrid composite than for the pure blend.*

- 1) Effect of alkali-resistant glass fiber on Polypropylene/Polystyrene blends: modeling and characterization ; Asha Krishnan K, Anjana R, K.E. George, Polymer Composites, DOI: 10.1002/pc.23193

#### **4. B.1 Introduction**

Fiber reinforced composites have been widely used in many structural applications such as marine, automobile, civil engineering etc due to their excellent strength-to-weight ratio, chemical and weather resistance, mechanical, thermal and electrical properties. Fibers can enhance the stiffness, strength and fracture resistance of fiber reinforced composites and this enhancement depends on factors like the fiber concentration, fiber aspect ratio, fiber adhesion to matrix, fiber orientation and its dispersion in the matrix. Fiber reinforced composites with 30 to 50 wt % loadings are quite familiar. Higher fiber loading leads to increased specific gravity, decreased melt flow and increased brittleness, making the processing and

molding of the composite difficult [1,2]. Alkali resistant glass fiber has been used for reinforcing polymer in this study. Alkali resistant (AR) glass fibers are composed of alkali zirconium silicates, generally used in cement substrates and concrete. M. Enamul Hossain studied four fiber glass-reinforced plastic materials (i.e., AR-glass, boron free E-glass, C-glass, and E-glass) in acidic and alkaline environments. The results showed that AR-glass was corrosion resistant at high temperature and highly acidic and alkaline environments and could be used in the petroleum industry [3].

Traditionally, automotive applications employ glass or mineral filled systems with higher loadings. The processing of the composites becomes difficult with high filler loading and this inevitably leads to heavier products. Recently, it has been observed that by incorporating filler particles into the matrix of fiber reinforced composites would give materials of desired properties at low to intermediate filler loadings. T.P Mohan and K. Kanny examined the effect of nanoclays on the processing, mechanical and wearing properties of Polypropylene/short glass fiber composites. The results suggest that the addition of nanoclay enhances the mechanical and rheological properties of PP/GF composites [4]. Mike J. Clifford and Tong Wan studied the effect of nanoclay and glass fibers on the mechanical properties of polyamide composites and the study showed that the nano particles of clay with micro-scale glass fibers synergistically enhanced the mechanical properties [5].

In this part of study the effect of modified kaolin nanoclays (Nanocaliber 100V-N100V and Nanocaliber 100Z-N100Z) on the properties of alkali resistant glass fiber reinforced Polypropylene (PP)/Polystyrene (PS) blends is proposed to be studied.

## **4. B.2 Methodology**

### **4. B.2.1 Materials**

The details of the polymers and nanoclay types used for the study are discussed in Chapter 2 (sections 2.1.1, 2.1.2& 2.1.3). The alkali resistant glass fiber used for the study is discussed in Chapter 2 (section 2.1.4).

### **4. B.2.2 Methodology**

Short glass fiber reinforced PP/PS blends (PP/PS/ARGF) were prepared in a Haake Rheomix 600. In the first series of experiments the fiber length was varied (4-10mm) by fixing the fiber content at 10 wt%. In the second series of experiments the optimum amount of glass fiber was found by varying the fiber content (10-30wt. %) and keeping the fiber length constant.

Hybrid composites were prepared by melt mixing using an internal mixer (Haake Rheomix 600) at 180°C with a rotor speed of 50 rpm, and the mixing time of 8 min for each sample. PP/PS (80/20) blend was used as the matrix. For the preparation of hybrid composites glass fiber content was fixed at 15 wt% and nanoclays were varied from 1-5 wt. %. The hot mix from the mixing chamber was pressed in a hydraulic press, cut into pieces and the test specimens were prepared using a DSM Micro 10cc Injection Molding Machine, with a barrel temperature of 190°C. Figure 4b.1 shows the schematic representation of PP/PS/ARGF/modified kaolin nanoclay hybrid composite. The tensile properties, flexural properties, impact strength, hardness, dynamic mechanical properties, thermal properties and morphological properties were analyzed according to various standards as described in Chapter 2 (section 2.23). Modeling of the



tensile modulus was done according to the equations described in section 4. A.2.3.

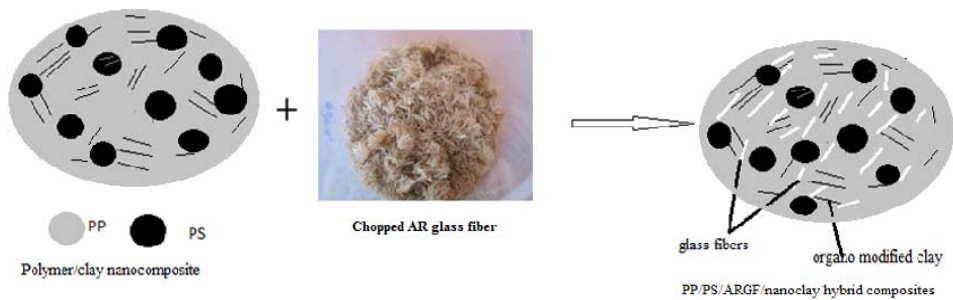


**Figure 4b.1 Schematic diagram showing PP/PS/ARGF/nanoclay hybrid composites**

#### 4. B.2.3 Determination of aspect ratio of glass fiber

Fiber lengths in composites were measured by analyzing optical micrographs of the fibers extracted from injection molded specimen. The sample preparation for the optical microscopy is discussed in Chapter 4 Part A section 4. A.2.4 [6].



**Figure 4b.2 Optical microscopic images of glass fiber for determining fiber length**

Figure 4b.2 is a typical photograph utilized for determining final fiber length. The average fiber length measured is 439.89 $\mu\text{m}$  which gives an aspect ratio (l/d) of 43.

## 4. B.3 Results and Discussion

### 4. B.3.1 Polypropylene/Polystyrene/alkali-resistant glass fiber composite

#### 4. B.3.1.1 *Effect of fiber length on mechanical properties of PP/PS /AR glass fiber composites*

##### a) Tensile properties

Variation of tensile strength and tensile modulus of the composite as a function of glass fiber length is plotted in Figure 4b.3. The results show an increase in tensile strength and tensile modulus at 6 mm fiber length and then show a decline in values.

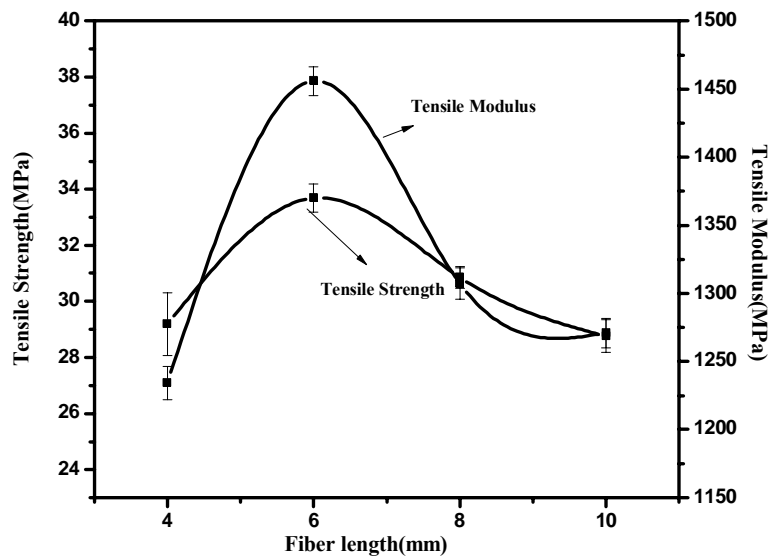
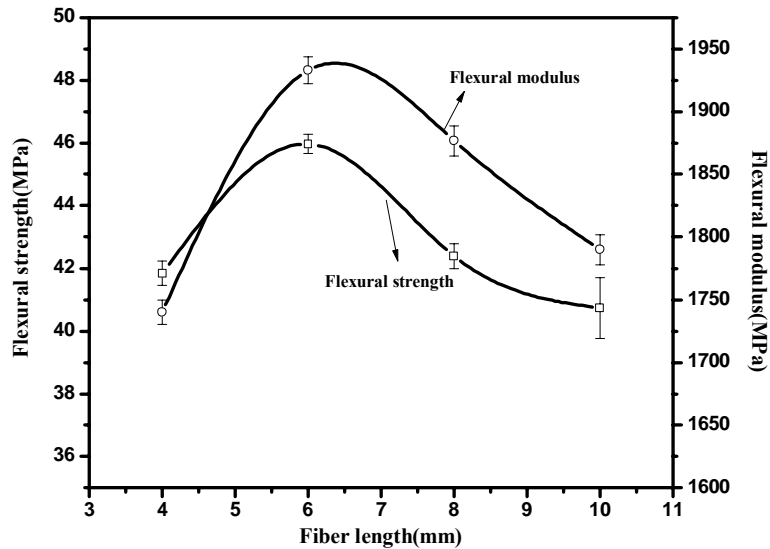


Figure 4b.3 Variation of tensile properties with fiber length

In short glass fiber polymer composites, the stress along the fiber is not uniform. A definite fiber length is required for the effective stress transfer between fiber and matrix. In order to attain maximum stress in the fiber, the fiber length must be at least equal to the critical fiber length. The critical fiber length is defined as the minimum fiber length at which the extent of load transfer is high. If fiber length is lower than critical fiber length (here 4 mm), tensile properties decline which is due to the fact that length may not be enough for proper distribution of load and may debond from the polymer matrix resulting in failure of composite under low strain. And also short fibers will create more fiber ends, which act as stress concentration points where failure often occurs. Similarly, decrease in tensile properties at higher fiber length (greater than the critical fiber length) is observed, because the effective stress transfer is not possible due to fiber curling and bending. The decrease in tensile properties is due to the presence of defects, such as voids and also weak interface bonding between matrix and fibers [7-9]. The long fibers may undergo entanglement with each other causing aggregate lumps of fibers which act as stress concentrated points, as a result the stressed composite leads to brittle failure.

**(b) Flexural properties**

The trend in variation of flexural modulus and strength of the composites plotted as a function of glass fiber length is given in the Figure 4b.4. The maximum mechanical properties are observed for the composites prepared with 6 mm fibers. Hence 6 mm length is taken as optimum fiber length for further studies.



**Figure 4b.4** Variation of flexural properties with fiber length

#### **4. B.3.1.2** *Effect of fiber loading on mechanical properties of PP/PS/AR glass fiber composites*

##### **(a) Tensile properties**

The variation of tensile strength and tensile modulus of the blend as a function of glass fiber content is shown in Figure 4b.5. The tensile properties of the composites increase with increase in alkali resistant glass fiber (ARGF) content and reach a maximum peak at 15 wt%. The improvement of the mechanical properties points to an efficient stress transfer from the matrix to the fiber. The reduction in tensile properties is an indication of poor fiber –matrix adhesion [10, 11].

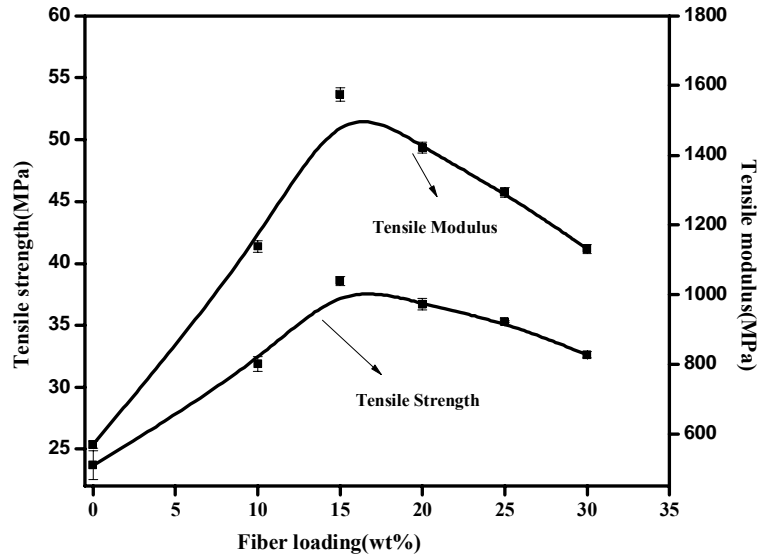


Figure 4b.5 Variation of tensile properties with fiber loading

(b) Flexural properties

The flexural strength and flexural modulus of the composites plotted as a function of glass fiber content is depicted in Figure 4b.6.

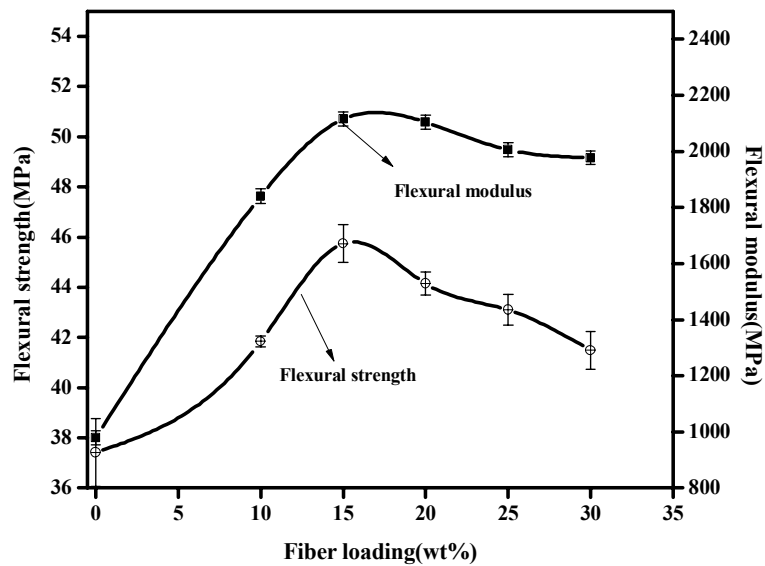
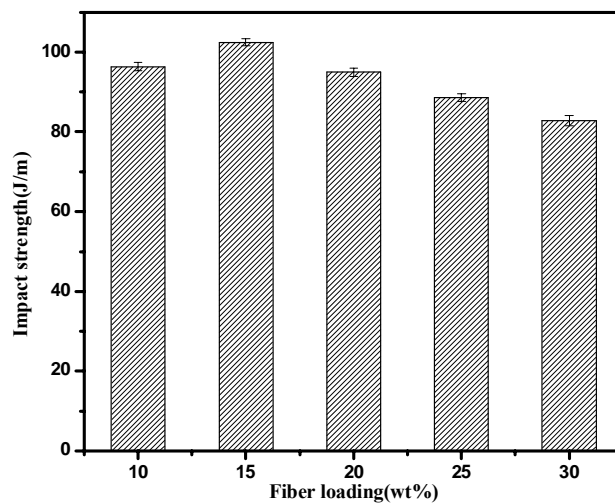


Figure 4b.6 Variation of flexural properties with fiber loading

There is a significant increase in the flexural modulus and strength as in the case of the tensile properties.

**(c) Impact strength**

Impact resistance of a composite is the measure of total energy dissipated in the material before it fails. Figure 4b.7 illustrates the variation of impact strength with fiber loading. The impact strength increases with increase in fiber loading up to 15 wt. %. The impact strength of a composite depends upon many factors like toughness of the reinforcing filler, nature of the interfacial region, and frictional work involved in pulling out the fiber from the matrix. When the polymer matrix is subjected to an impact loading, a large number of crazes will form and upon further loadings some crazes turn into cracks and break down the specimen. Fibers play an important role in the impact resistance of the composites as they resist the crack propagation and act as a load transfer medium. The applied stress is transferred effectively due to effective interfacial bonding strength [8, 12].



**Figure 4b.7 Variation of impact strength with fiber loading**

The improvement in mechanical properties is more pronounced at 15 wt. % of the glass fiber loading. Deterioration in mechanical properties at higher fiber content is due to the poor fiber/matrix adhesion and therefore due to lack of stress transfer capability of the fiber

From the above observations, it can be concluded that the 15 wt % of fiber content having a fiber length of 6mm can be considered as the optimum loading for the enhanced mechanical strength of PP/PS blend.

#### **4. B.3.2 Hybrid effect of alkali-resistant glass fiber and modified kaolin nanoclays on Polypropylene/Polystyrene blend**

##### **4. B.3.2.1 *Effect of nanoclays on the mechanical properties of PP/PS/ARGF composites***

###### **(a) Tensile properties**

Since maximum improvement in mechanical properties is obtained at 15 wt% of fiber content with 6mm length, this composite is selected for nanoclay modification. The change in tensile strength and tensile modulus of PP/PS/ARGF composites at 15wt. % ARGF loading containing a variable weight percentage of the two different nanoclay loadings; N100V and N100Z are given in Figures 4b.8 and 4b.9 respectively. The tensile strength of PP/PS/ARGF composites increases at first, reaches a maximum value, thereafter decreases. The improvement in tensile properties is due to the better stress propagation between the matrix and the ARGF in the presence of modified nanoclays.

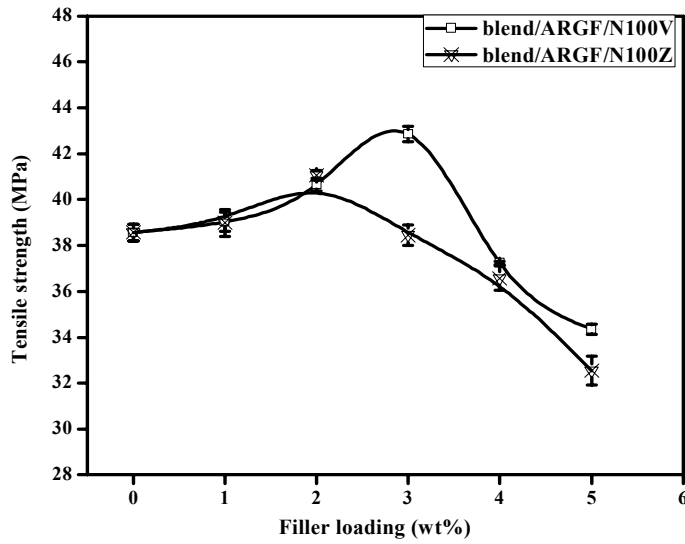


**Figure 4b.8** Variation of tensile strength with nanoclay loadings

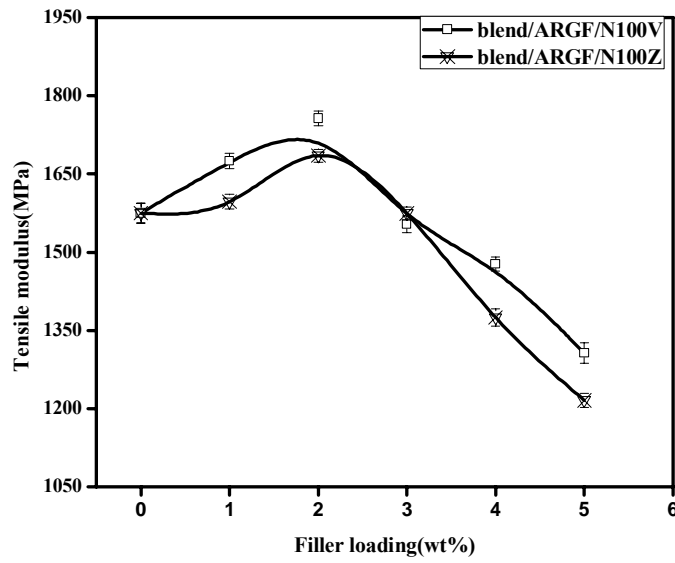


**Figure 4b.9** Variation of tensile modulus with nanoclay loadings



**(b) Flexural properties**

The change in flexural strength and flexural modulus of PP/PS/15wt% ARGF composites with varying weight percentage of N100V and N100Z are evinced in the Figures 4b.10 and 4b.11 respectively. The flexural strength increases by 11 % for PP/PS/ARGF/N100V composites and by 9% for PP/PS/ARGF/N100Z. Similarly, flexural modulus increases by 7 % for PP/PS/ARGF/N100V and 32% for PP/PS/ARGF/N100Z at 3wt% of nanoclays; compared to PP/PS/ARGF composite at the same fiber loading. The incorporation of nanoclay gives improvement in the flexural modulus of the PP/PS/ARGF composites, which is attributed to the stiffness and rigidity of the clay nanoparticles. Effective stress transfer due to the enhanced interfacial interaction increases the mechanical properties of fiber composites based on nanocomposite matrix [4, 13]. Modified kaolin nanoclays act as a molecular bridge gripping the glass fiber on to the polymer matrix.

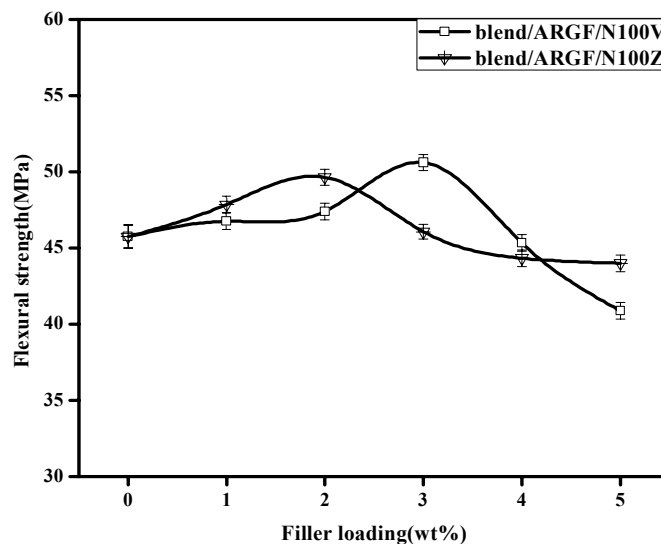


**Figure 4b.10** Variation of flexural strength with nanoclay loadings

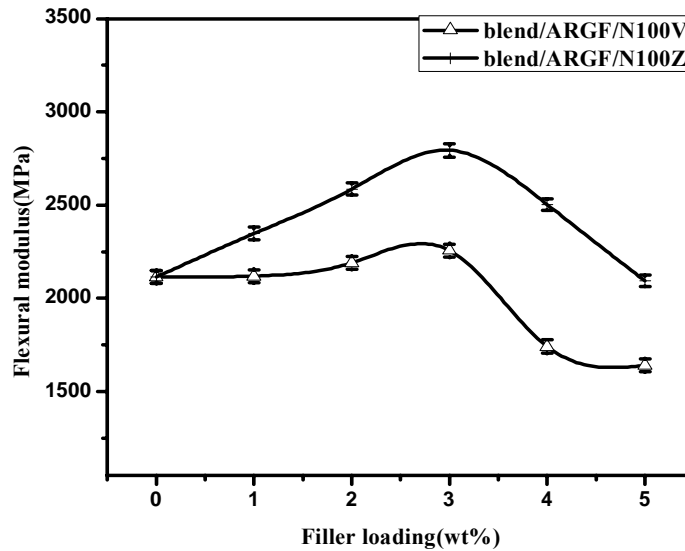


**Figure 4b.11** Variation of flexural modulus with nanoclay loadings

**(c) Impact strength**

The change in impact strength of glass fiber reinforced composites with varying weight percentage of N100V and N100Z are exhibited in the Figure 4b.12. The impact strength of PP/PS/ARGF/modified kaolin nanoclay hybrid composites is higher than the PP/PS/ARGF composites as evidenced from the figure. The enhancement in the impact strength is attributed to the interfacial adhesion between nanoclays and polymer matrix. It is clear that more energy is needed for the fiber debonding. Since the fibers can act as stress transferring medium and interact with the crack formation in the matrix during crack propagation, the impact strength of the hybrid composite increases. The growth of micro-cracks can also be stopped by the nanoclay platelets [14]. However, a decreasing trend is observed for the impact strength with higher nanoclay addition (Figure 4b.12).

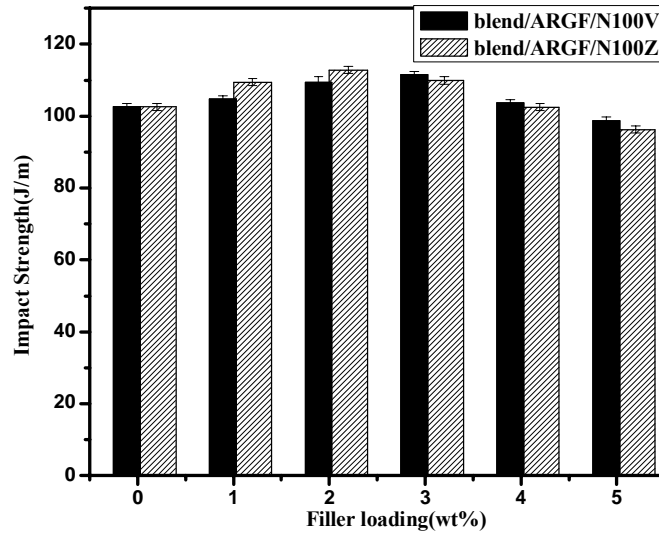


Figure 4b.12 Variation of impact strength with nanoclay loadings

(d) **Hardness**

Hardness is the measure of the degree of deformation of a material under an applied force. Hardness of PP/PS/ARGF composites with varying weight percentage of N100V and N100Z are revealed in the Figure 4b.13.

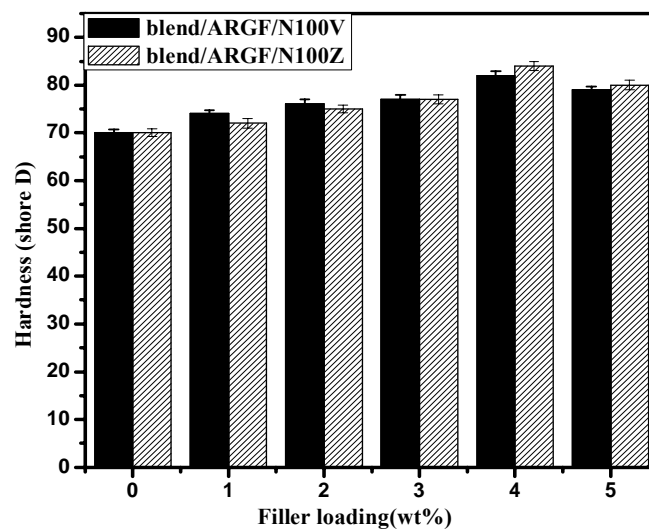


Figure 4b.13 Variation of hardness with nanoclay loadings

From the figure it is observed that the presence of N100V and N100Z improves the hardness of PP/PS/ARGF composites by 17% and 20% compared to pure matrix. The presence of hybrid fillers effectively restricts the indentation and increases the hardness of the composites [15].

The decrease in mechanical properties at higher nanoclay loadings is probably due to the presence of un-exfoliated aggregates and voids.

#### **4. B.3.3 Theoretical modeling of tensile modulus**

##### **(a) Single fiber model**

Figure 4b.14 depicts the comparison between the experimental data and the results provided by various theoretical models (tensile moduli) for PP/PS/ARGF composites. Among all the model fits the predicted moduli based on Hui-Shia and Series models show the closest proximity to the experimentally determined tensile modulus values. The Hirsch's model also shows the closest proximity to the experimentally determined tensile modulus values. The better agreement with the predicted values and the experimental values has been found only when the value of  $x$  which determines the stress transfer between the matrix and the fiber in equation 4a.3 is 0.05 for randomly oriented composites. The curves showing Parallel and Halpin-Tsai models agree the least with experimental values. It can also be evident that the values from Halpi-Pagano are deviated away from the experimental values. The values obtained from modified Halpin-Tsai equation (Neilson model) is negatively deviated away from the experimental values. This theoretical analysis indicates that, a uniform stress transfer is achieved in the composites due to the better interfacial interaction between glass fiber and the polymer matrix.

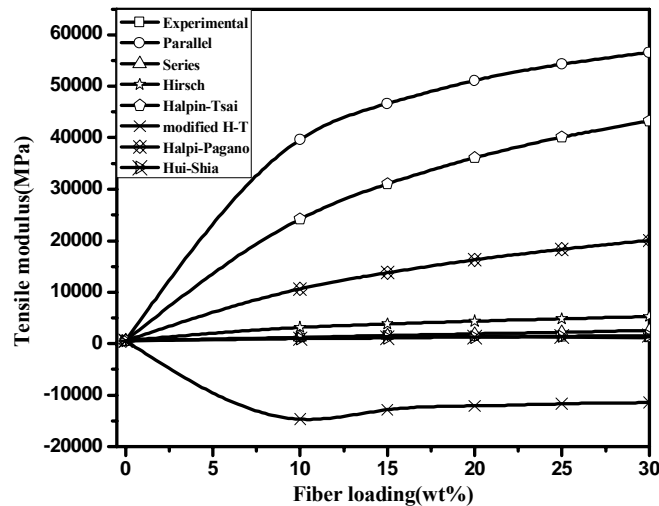
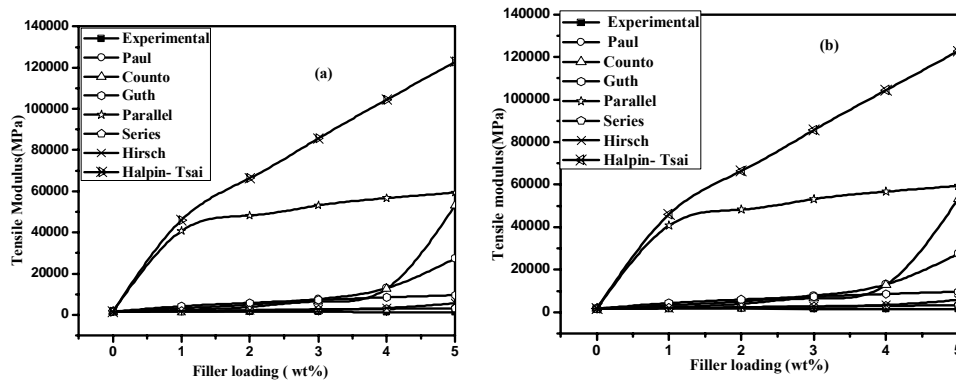


Figure 4b.14 Theoretical modeling of tensile modulus as a function of glass fiber loadings using various models

#### (b) Multiple filler model

Figure 4b.15 (a) and 4b.15 (b) present the comparison between the experimental data and the results provided by various theoretical models (tensile moduli) for PP/PS/ARGF/modified kaolin nanoclay hybrid composites with N100Z and N100V respectively. Both the hybrid composites show similar results on comparison. Among the entire model fits, the predicted moduli based on Hirsch and Series models show the closest proximity to the experimentally determined elastic modulus values. Paul model and Counto model show close proximity to the experimental values at lower percentage till 4 wt%, thereafter the predicted models deviate away from the experimental values for both hybrid composites. The better prediction of the models (Paul and Counto model) at lower percentage [up to 4wt%] is attributed to the increase in interfacial adhesion between the polymer matrix and glass fiber due to the presence of modified kaolin

nanoclays which results in better stress transfer at the interface. The deviation of the models from the experimental values may be due to the agglomeration of clay particles, reduced interfacial interactions and lowered strengthening effect of clays in the composites. The predicted data by Series model are well fitted to the experimental results which assume a uniform stress transfer in the composites. The Hirsch's model also shows the closest proximity to the experimentally determined elastic modulus values. In the case of Hirsch's model, the predicted value is converging to experimental values. The better agreement with the predicted values and the experimental values has been found only when the value of  $x$  which determines the stress transfer between the matrix and the fiber in equation 4a.22 is 0.05 for randomly oriented composite. The curves showing Parallel and Halpin-Tsai models agree the least with experimental values. Guth model shows less deviation from the experimental values.



**Figure 4b.15** Theoretical modeling of tensile modulus as a function of filler loadings using various models of (a) PP/PS/ARGF/N100Z hybrid composite (b) PP/PS/ARGF/N100V hybrid composites.

#### 4. B.3.4 Effect of UV aging on the tensile properties

The effect of UV aging on the tensile strength and tensile modulus of PP/PS/ARGF/modified kaolin nanoclay hybrid composites is given in the Figures 4b.16 (a) & 4b.16 (b). From the figure it is apparent that the tensile properties decrease with nanoclay loading. In PP/PS/ARGF/modified kaolin nanoclay hybrid composites the nanoclay particles accelerate the degradation of PP/PS blend [16].

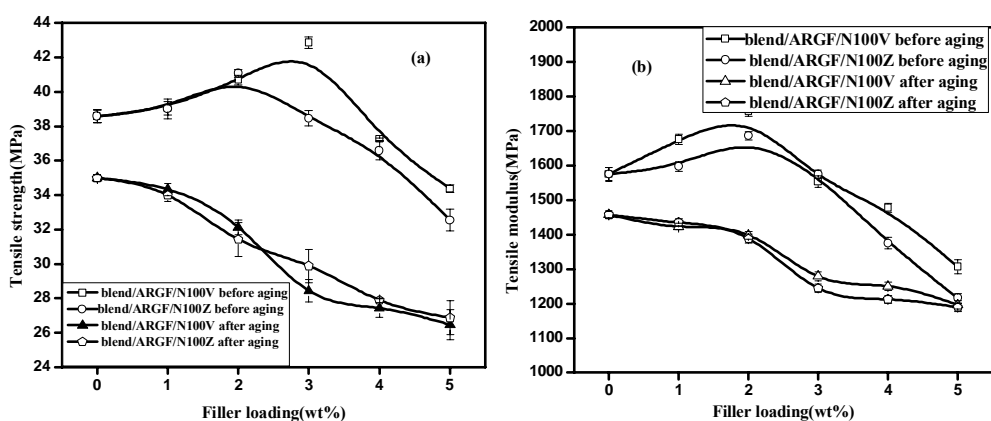


Figure 4b.16 Effect of UV aging on the (a) tensile strength (b) tensile modulus of PP/PS/ARGF/ nanoclay hybrid composites

#### 4.B.3.5 Density

Table 4b.1 shows the density of PP/PS/ARGF/modified kaolin nanoclay hybrid composites. From the table it is clear that pure PP/PS blend has a density of  $0.9313 \text{ g/cm}^3$ . After incorporating the glass fiber the density increases slightly. There is a marked increase in density after the incorporation of glass fiber and nanoclays. Density of composites depends on the relative proportion of matrix and reinforcing materials.

**Table 4b.1 Density of PP/PS/ARGF/ nanoclay hybrid composites**

Sample	PP/PS blend	Blend/ ARGF	Blend/ ARGF/ 1% N100V	Blend/ ARGF/ 2% N100V	Blend/ ARGF/ 3% N100V	Blend/ ARGF/ 4% N100V	Blend/ ARGF/ 5% N100V
Density (g/cm <sup>3</sup> )	0.93	0.94	0.95	0.99	0.99	1.00	1.01
Sample	PP/PS blend	Blend/ ARGF	Blend/ ARGF/ 1%N100Z	Blend/ ARGF/ 2%N100Z	Blend/ ARGF/ 3%N100Z	Blend/ ARGF/ 4% N100Z	Blend/ ARGF/ 5% N100Z
Density (g/cm <sup>3</sup> )	0.93	0.94	0.95	0.96	0.98	0.99	1.10

#### 4. B.3.6 Melt Flow Index

Figure 4b.17 exhibits the variation of MFI with nanoclay loadings (N100V& N100Z) in PP/PS/ARGF composites.

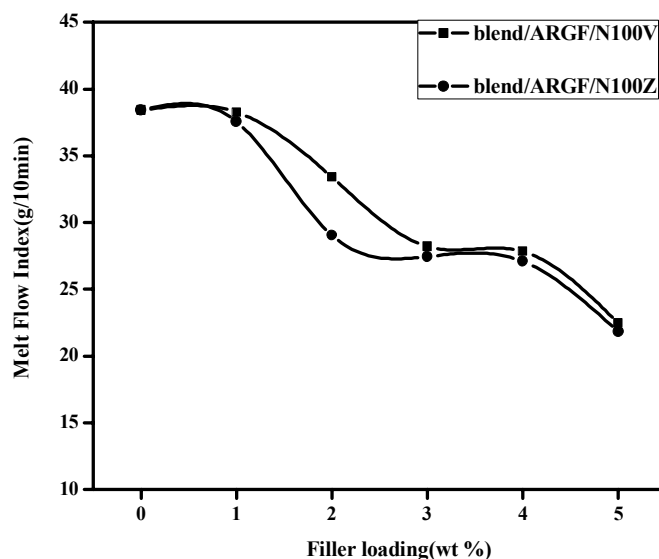


**Figure 4b.17 Variation of MFI with nanoclay loadings**

The MFI in the PP/PS/ARGF/nanoclay hybrid composites decreases with increasing clay content. The generation of strong interfacial interaction between polymer matrix and ARGF after the addition of nanoclays decreases the MFI of



hybrid composites [17, 18]. It should be emphasized that presence of organoclay reduces MFI of PP/PS blend but comparing the results obtained from samples with and without ARGF, the presence of ARGF has synergistic effects on reduction of MFI. This may be due to increase in interfacial adhesion between polymer matrix and glass fiber in the presence of nanoclay.

#### 4.B.3.7 X-ray Diffraction (XRD)

X-ray diffraction provides information on the changes of the inter-layer spacing of the nanoclay [19, 20].

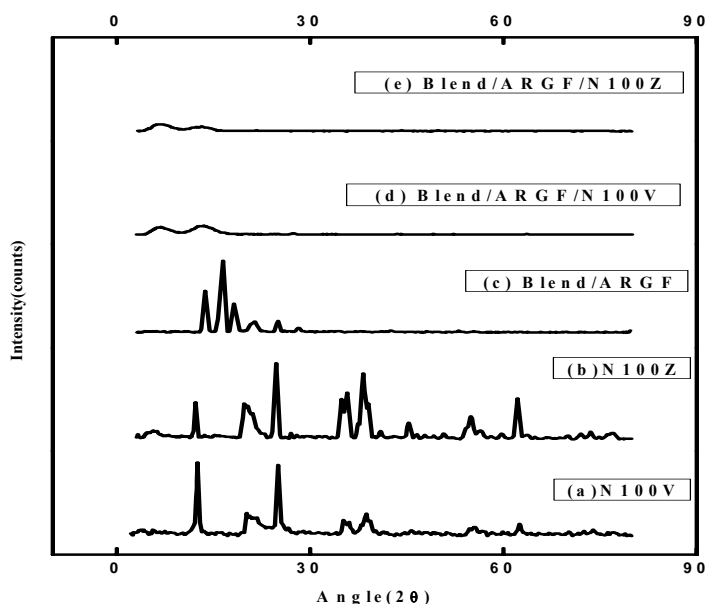


**Figure 4b.18** XRD patterns of (a) Nanocaliber 100 V (N100 V), (b) Nanocaliber 100 Z (N100Z), (c) PP/PS/ARGF, (d) PP/PS/ARGF/N100V and (e) PP/PS/ARGF/N100Z

The Figure 4b.18 exhibits the XRD patterns of N100V, N100Z, PP/PS/ARGF, PP/PS/ARGF/N100V and PP/PS/ARGF/N100Z. The original basal reflection peak for N 100V and N100Z is at  $12.44^\circ$  and at  $12.18^\circ$  respectively, which corresponds to an intergallery distance of 7.11 nm and 7.26 nm. Diffraction

peaks which appear at  $2\theta = 15- 20^\circ$  in the PP/PS/ARGF composite corresponds to the monoclinic ‘ $\alpha$ ’ form of the PP [21, 22]. The intensity of the characterization peaks of nanoclay have reduced in PP/PS/ARGF/N100V and PP/PS/ARGF/ N100 Z hybrid composites and this suggests the disorder and loss of regularity of nanoclay layers [23, 24].

#### **4. B.3.8 Scanning electron microscopy**

The morphology of alkali resistant glass fiber (ARGF), PP/PS/ARGF composite and PP/PS/ARGF/modified kaolin nanoclay hybrid composites are illustrated in the Figure 4b.19. The surface morphology of ARGF with diameter  $10\mu\text{m}$  is shown in the Figure 4b.19 (a). Figure 4b.19 (b) gives the morphology of the tensile fractured surface of PP/PS/ARGF composite at the optimum composition (15 wt %). Figures 4b.19 (c) and 4b.19 (d) show the tensile fractured surface morphology of 3% N100Z and 3% N100V filled PP/PS/ARGF composites respectively.

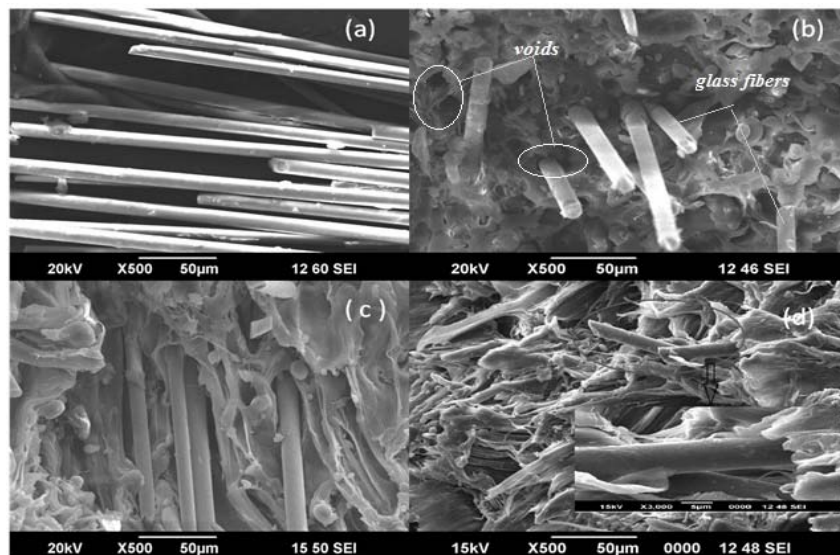


**Figure 4b.19 SEM photographs of (a) AR glass fiber, (b) PP/PS/ARGF, (c) PP/PS/ARGF/N100Z and (d) PP/PS/ARGF/N100V**

The fractured surface of glass fiber reinforced polymer matrix shows voids and the fiber surface retain low amount of matrix indicating poor fiber/matrix adhesion while in the case of hybrid composites, the fibers are surrounded and adhered to the matrix [12, 25].

This indicates that the adhesion of the ARGF with polymer matrix is better in the presence of modified kaolin nanoclays [26].

#### **4.B.3.9 Thermogravimetric analysis**

TGA measurements were used to obtain information on the thermal stability of the prepared hybrid composites. The results obtained from the DTG curve is given in the Table 4b.2. Figures 4b.20 & 4b.21 show the TG and DTG curves for PP/PS (80/20) and 15wt.% ARGF composites containing various amounts of N100V and N100Z clay nanoparticles (0-5 wt %). Table 4b.2 depicts an increase in onset degradation temperature after the addition of nanoclays. The results suggest that the increase of decomposition at the onset temperature is due to the improvement of barrier properties by the intercalated composites, in which nanoclay act as a barrier to decrease the permeability of degradation compounds [27, 28]. At higher temperatures the thermal behavior of ARGF becomes predominant and an increase in thermal stability may occur. This may be the reason for the increase in the decomposition temperature of the hybrid composites [13].

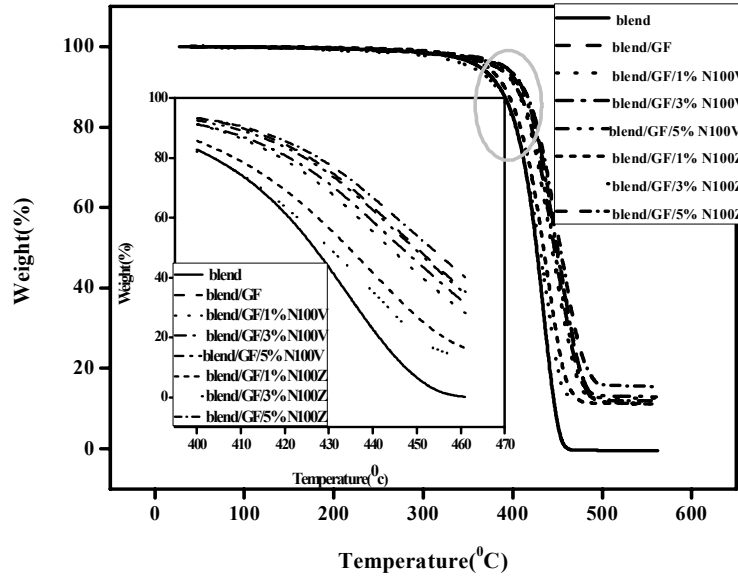


**Figure 4b.20** TG curve of PP/PS blend, PP/PS/ARGF and PP/PS/ARGF/nanoclay hybrid composites. The inset shows their TG curves in temperature range 380–470°C

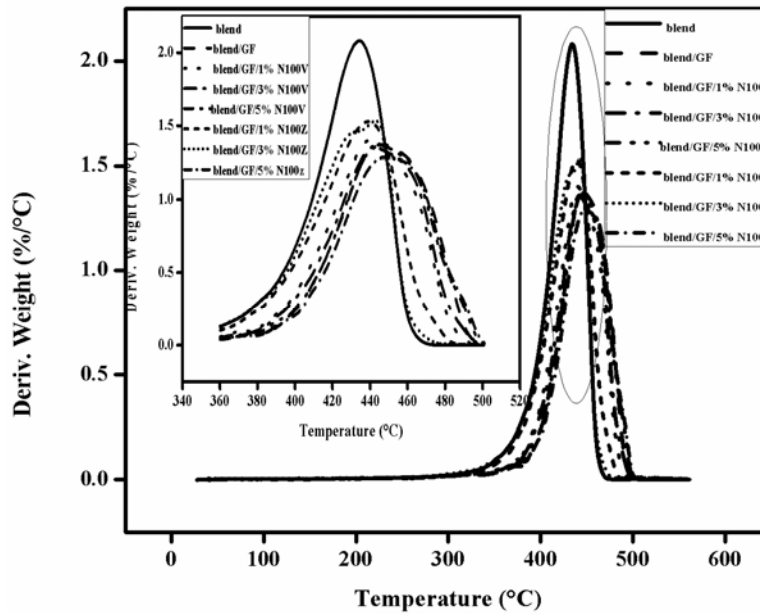


**Figure 4b.21** DTG curve of PP/PS blend, PP/PS/ARGF and PP/PS/ARGF/nanoclay hybrid composites. The inset shows their DTG curves in temperature range 340–520°C

The OI values increases with increase in clay content and it lies in the range 0.03-1.07. This study indicates that the nanoclay filled PP/PS/ARGF composites are more thermally stable than PP/PS/ARGF composites [29].

**Table 4b.2 TGA data of PP/PS blend, PP/PS/ARGF and PP/ARGF/ nanoclay composites**

Samples	Temperature at 50% weight loss (°C)	Onset degradation temperature ( $T_0$ (°C))	Maximum degradation temperature ( $T_{max}$ )(°C)	Residue at 600°C (%)	Oxidation Index(OI)
PP/PS blend	426.6	370.5	434.4	0.456	0.032
Blend/ARGF	449.8	382.3	446.1	11.1	0.769
Blend/ARGF/1%N100V	443.8	386.9	440.2	11.2	0.778
Blend/ARGF/3%N100V	446.4	389.2	442.0	12.5	0.872
Blend/ARGF/5%N100V	449.2	392.8	445.6	12.9	0.901
Blend/ARGF/1%N100Z	430.0	382.8	438.9	11.1	0.775
Blend/ARGF/3%N100Z	434.5	385.8	442.8	11.8	0.822
Blend/ARGF/5%N100Z	453.1	392.0	447.9	15.5	1.078

#### 4. B.3.9 .1 Kinetic analysis of thermal decomposition

Kinetic parameters were evaluated from the TGA curves using the plots of Horowitz-Metzger, Broido's and Coats Redfern methods. The CR, BR & HW plots for the thermal degradation of PP/PS/ARGF/modified nanoclay hybrid composites from the onset degradation temperature to the maximum degradation temperature are exhibited in the Figures 4b.22, 4b.23 and 4b.24 respectively. The activation energy ( $E_a$ ) for each method is given in Table 4b.3.

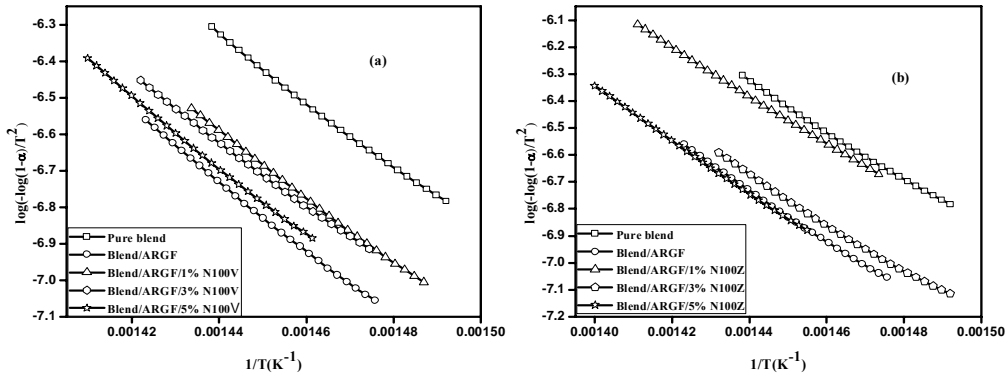


Figure 4b.22 Kinetic plots for the determination of activation energy of PP/PS blend, PP/PS/ARGF (a) PP/PS/ARGF/N100V and (b) PP/PS/ARGF/N100Z composites using Coats-Redfern equation

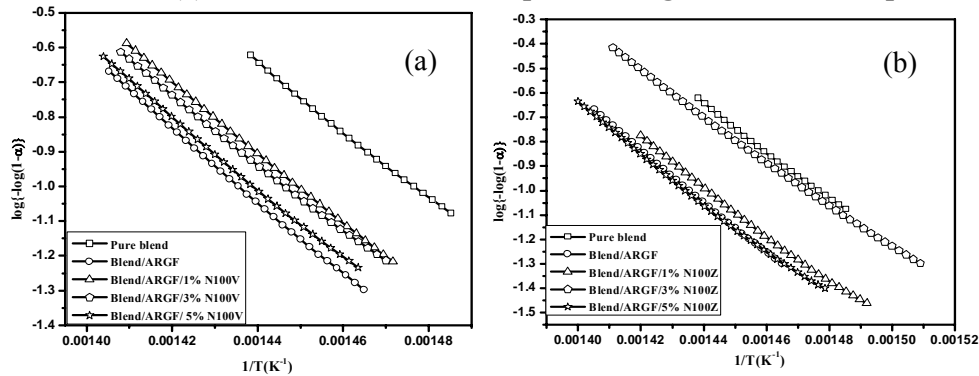


Figure 4b.23 Kinetic plots for the determination of activation energy of PP/PS blend, PP/PS/ARGF (a) PP/PS/ARGF/N100V and (b) PP/PS/ARGF/N100Z composites using Broido's method

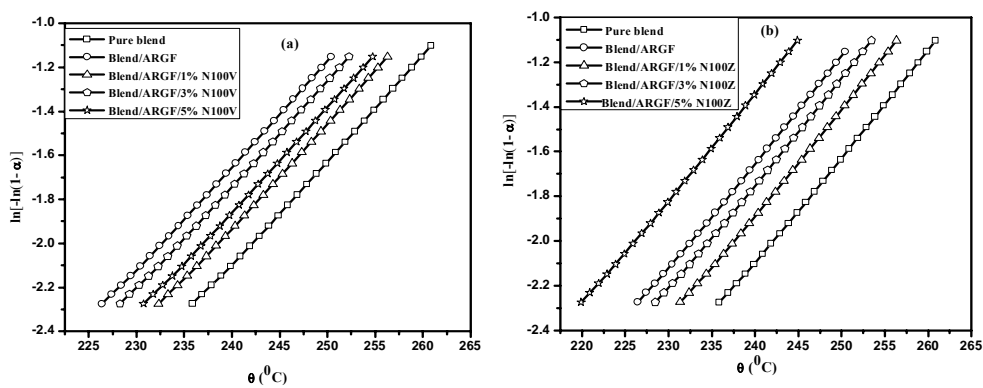


Figure 4b.24 Kinetic plots for the determination of activation energy of PP/PS blend, PP/PS/ARGF, (a) PP/PS/ARGF/N100V and (b) PP/PS/ARGF/N100Z composites using Horowitz-Metzger equation

The plots of  $\log (-\log (1-\alpha)/T^2)$  versus  $1/T$  (CR),  $\log \{-\log (1-\alpha)\}$  versus  $1/T$  (BR) and  $\ln [-\ln (1-\alpha)]$  versus  $\theta$  (HM), and for PP/PS/ARGF/N100V and PP/PS/ARGF/N100Z hybrid composites are displayed in Figures 4b.22, 4b.23 and 4b.24 respectively. Activation energy increases with increase in clay content. The improvement in thermal stability and activation energy in the hybrid composites are attributed to the good dispersion of nanoclay particles in the polymer matrix that restricts the easy diffusion of volatiles from the bulk [30].

**Table 4b.3** Activation energy (J/ mol) calculated by Horowitz-Metzger (HM), Broido's (BR) and Coats-Redfern (CR) methods of PP/PS blend, blend/ARGF and PP/PS/ARGF/ nanoclay composites

Sample	Coats -Redfern	Broido's	Horowitz-Metzger
PP/PS blend	174	181	175
Blend/ARGF	187	194	180
Blend/ARGF/1%N100V	178	187	177
Blend/ARGF/3 %N100V	182	192	181
Blend/ARGF/5%N100V	192	195	184
Blend/ARGF/1 %N100Z	175	185	176
Blend/ARGF/3 %N100Z	181	187	183
Blend/ARGF/5 %N100Z	194	196	189

#### 4. B.3.10 Dynamic mechanical analysis (DMA)

Dynamic mechanical analysis (DMA) is a powerful technique for studying the viscoelastic behavior of polymer based materials. Table 4b.4 gives the storage moduli,  $T_g$  and interaction parameter values of the PP/PS blend, PP/PS/ARGF and PP/PS/ARGF/modified kaolin nanoclay hybrid composites, estimated by DMA. The storage modulus for pure PP/PS blend, PP/PS/ARGF composite, ARGF reinforced PP/PS blend with 3 wt % N100V

and 3 wt % N100Z are given in the Figure 4b.25. By the addition of glass fiber, the modulus of the virgin matrix increases [10]. The dynamic mechanical properties are affected by the presence of modified kaolin nanoclays (N100V & N100Z). PP/PS/ARGF/modified kaolin nanoclay hybrid composites exhibit higher storage moduli over the entire temperature range of the study (40°C to 125°C). The storage modulus of pure blend increases by 107% at 80°C with the incorporation of 15 wt% ARGF. This reflects the effectiveness of the stress transfer occurring between the fiber and the matrix. There is an increase of 8% by the addition of 3 wt % N100V into the PP/PS/ARGF composites and 25% increase after the addition of 3% N100Z. It depicts that with the addition of nanoclay, the storage modulus of the PP/PS/ARGF composite increases not only due to the mobility restriction of polymer chain by the nanoclay platelets but also due to the better interfacial interaction, and hence better stress transfer [12, 31].

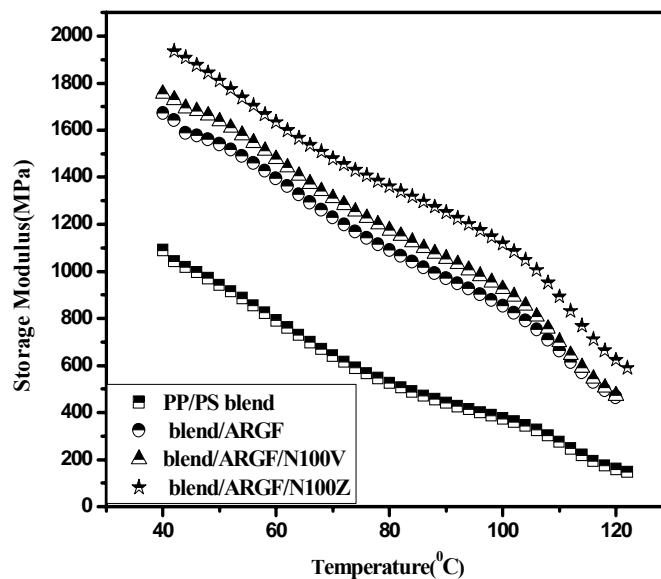


**Figure 4b.25** Storage modulus curves of PP/PS blend, PP/PS/ARGF and PP/ARGF/ nanoclay hybrid composites



Tan  $\delta$  is useful in determining the occurrence of molecular mobility transitions such as  $T_g$ . From the Figure 4b.26 it is observed that  $T_g$  increases slightly with the addition of glass fiber and nanoclays. The PP/PS blend shows a  $T_g$  at 114.95°C and the addition of 15 wt% glass fiber shifts it to 115.30°C [11]. For N100V  $T_g$  shifts to 115.40°C and in the case of N100Z,  $T_g$  is at 115.53°C. The slight increase in  $T_g$  is due to the immobilization of polymer molecules in the presence of ARGF and modified kaolin nanoclays.

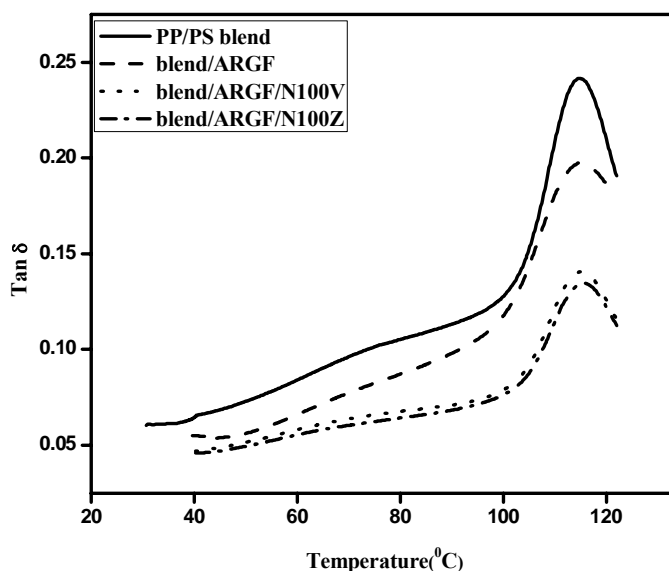


**Figure 4b.26** Tan  $\delta$  curves of PP/PS blend, PP/PS/ARGF and PP/PS/ARGF/ nanoclay hybrid composites

Interfacial interaction between the two phases can be determined using DMA. The detailed description of interaction parameter is given in Chapter 4 Part A section 4. A.3.10. Interaction parameter (B) is higher for PP/PS/ARGF/ modified kaolin nanoclay composites and it proposes a strong interfacial interaction between the glass fiber and polymer matrix in the presence of nanoclay particles [32-44].

**Table 4b.4 Storage moduli,  $T_g$  & interaction parameter values of the PP/PS blend, PP/PS/ARGF and PP/ARGF/nanoclay hybrid composites**

Samples	Storage modulus				Tg(°C) from tan $\delta$ value	Interaction Parameter (B)
	45°C	80°C	100°C	120°C		
PP/PS blend	1007	525.3	374.1	159	114.95	0
Blend/ARGF	1583	1089	852.3	466.1	115.30	3.29
Blend/ARGF/3%N100V	1688	1174	925.7	473.1	115.40	4.49
Blend/ARGF/3%N100Z	1893	1363	1118	623.8	115.53	4.98

**4. B.3.10 .1 Cole-Cole Plot analysis**

Figure 4b.27 shows Cole–Cole plot where the loss modulus ( $E''$ ) data are plotted as a function of storage modulus ( $E'$ ) for PP/PS/ARGF/modified

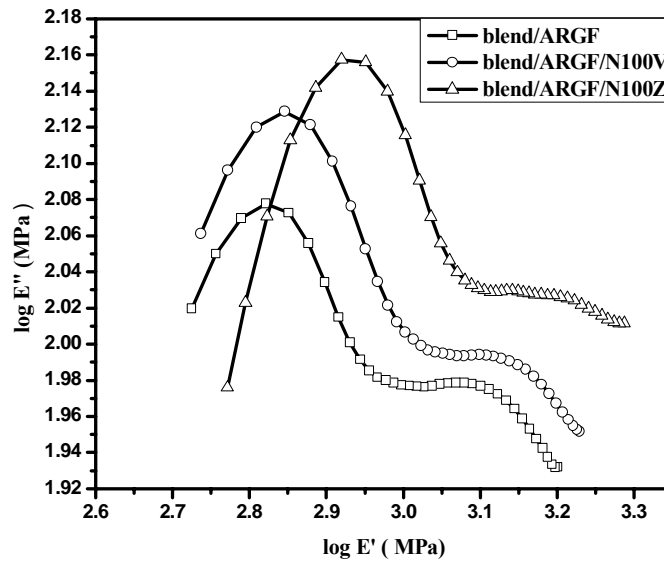


**Figure 4b.27 Cole-Cole plot of PP/PS/ARGF/nanoclay hybrid composites**

kaolin nanoclay hybrid composites. In this plot, a drift from a semicircle shows immiscibility. However, the shape of the curve point up to relatively

good fiber/matrix adhesion [35- 37]. The shape of the curve shows the heterogeneous system with relatively good clay–polymer and fiber interaction.

#### 4.B.3.11 Differential scanning calorimetry (DSC)

The effect of hybrid fillers on the crystallization behavior of PP/PS/ARGF/modified kaolin nanoclay hybrid composites was analyzed using DSC experiments. The crystallization temperature ( $T_c$ ), the apparent melting temperature ( $T_m$ ) and the corresponding enthalpies are shown in the Table 4b.5. The DSC melting and cooling curves for PP/PS blend, PP/PS/ARGF composites, PP/PS/ARGF/3wt% modified nanoclays (N100V and N100Z) hybrid composites are shown in the Figure 4b.28.

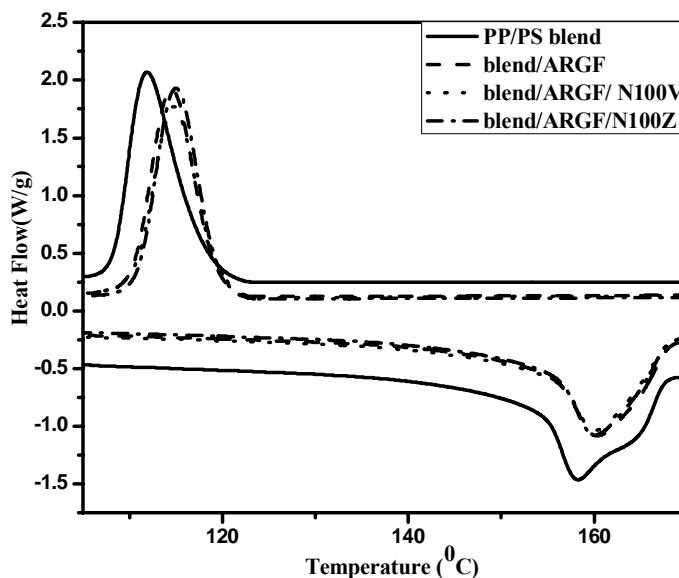


**Figure 4b.28** DSC melting and crystallization curves of PP/PS blend, PP/PS/ARGF and PP/PS/ARGF/ nanoclay hybrid composites

All the hybrid composites have a higher melting temperature ( $T_m$ ), compared to neat PP/PS blend. The crystalline peak temperature ( $T_c$ ) of the hybrid composites is shown in Table 4b.5. The  $T_c$  values show small increment with nanoclay in PP/PS/ARGF composites. This increment in crystallization temperature may be due to the nucleating effect of nanoclay particles. The decrease in crystallization enthalpy in PP/PS/ARGF composites is due to the restriction of molecular mobility after the addition of glass fibers.

**Table 4b.5 Thermal characteristics of PP/PS/ARGF/nanoclay hybrid composites**

<b>Samples</b>	<b><math>T_c</math> (°C)</b>	<b><math>\Delta H_c</math> (J/g)</b>	<b><math>T_m</math> (°C)</b>	<b><math>\Delta H_m</math> (J/g)</b>
PP/PS blend	111.9	61.1	158.4	32.4
Blend/ARGF	114.5	54.8	160.4	41.1
Blend/ARGF/N100V	114.8	55.5	160.2	33.6
Blend/ARGF/N100Z	115.0	57.2	160.2	34.2

The melting temperatures( $T_m$ ) and melting enthalpies ( $\Delta H_m$ ) of the PP/PS/ARGF is higher than that of PP/PS blend and this may be due to the increase in thermal stability of the composites.  $T_m$  is not significantly affected by the addition of nanoclay particles. The melting enthalpies ( $\Delta H_m$ ) of the hybrid composites are found to be decreased with the addition of nanoclay particles. This is because of the strong interfacial interaction between polymer matrix and glass fibers with nanoclay particles, confining polymer chain orientation [38, 39].

#### **4. B.4 Conclusions**

PP/PS/ARGF/modified kaolin nanoclay hybrid composites were prepared by melt intercalation. Two modified kaolin nanoclays (Nanocaliber 100V and Nanocaliber 100Z) were introduced into PP/PS/ARGF composites. The study shows that modified kaolin nanoclays and glass fiber can synergistically reinforce PP/PS composites. The glass fiber at 6mm length and 15 wt% shows maximum mechanical property. A comparison between experimental results (tensile modulus) and various models of PP/PS/ARGF composites has been presented. The predicted moduli based on Series and Hirsch model shows closest proximity to the experimentally determined tensile modulus values and Paul and Counto model shows close proximity at lower percentage upto 4wt%. The results point to better dispersion of nanoclay particles in PP/PS/ARGF composites at lower percentage. XRD shows an increase in the degree of dispersion of dialkyl modified and vinyl modified kaolin reinforced PP/PS/ARGF composites. The dynamic properties are improved with the addition of modified clays and ARGF. The thermal stability of the composites is enhanced by the addition of nanoclays and glass fiber. Kinetic studies reveal that the activation energies increase with the addition of modified kaolin nanoclays confirming higher thermal stability.

## References

- [1]. Vajihesadat Mortazavi1, Mohammad Atai, Mohammadhossein Fathi, Solmaz Keshavarzi, Navid Khalighinejad , Hamid Badrian, Journal of Dental Research, 2012, 9(3), 273–280.
- [2]. Sinto Jacob, K K Suma, Jude Mendez, K E George, Materials Science and Engineering B, 2010, 168(3), 245-249.
- [3]. M. Enamul Hossain, Journal of Composite Materials ,45(20) 2133–2144
- [4]. TP Mohan and K Kann , Journal of Reinforced Plastics and Composites, 30(2), 152–160 .
- [5]. Mike J. Clifford, Tong Wan, Polymer, 2010, 51, 535–539.
- [6]. T.D. Fornes, D.R. Paul, Polymer, 2003, 44(17), 4993–5013.
- [7]. K. N. Indira, Jyotishkumar Parameswaranpillai, Sabu Thomas, Hindawi Publishing Corporation, Polymer Science, 2013, 8.
- [8]. P. Amuthakkannan, V. Manikandan, J.T. Winowlin Jappes, M. Uthayakumar, Materials Physics and Mechanics, 2013, 16, 107-117.
- [9]. Raghavendra.S, Dr. P. Balachandrashetty, Dr. P. G Mukunda. Dr. K. G. Sathyanarayana International Journal of Engineering Research & Technology (IJERT), 1 (6), ISSN: 2278-0181.
- [10]. Sushanta K. Samal, Smita Mohanty, Sanjay K. Nayak, Journal of Reinforced Plastics and Composites, 2008, 28(22), 2729-2747.
- [11]. Manoranjan Biswal, Smita Mohanty, Sanjay K. Nayak, Journal of Applied Polymer Science, 2009, 114(6), 4091–4103.
- [12]. Ishak Ahmad, Ramli Ismail, Ibrahim Abdullah, Polymer Engineering and Science, 2011.
- [13]. Normasmira Abd. Rahman, Aziz Hassan, Rosiyah Yahya, R.A. Lafia-Araga, Peter R. Hornsby, Journal of Reinforced Plastics and Composites, 2012,31 (4),269–281.

- [14]. N H Mohd. Zulfli, A Abu Bakar, W S Chow, Malaysian Polymer Journal, 2012, 7 (1), 8-15.
- [15]. Irina Turku, Timo Karki, European Journal of Wood and wood Products, 2014, 72, 73–79.
- [16]. K. J. Singala, A. A. Mungray, A. K. Mungray, Industrial & Engineering Chemistry Research, 2012, 51, 10557–10564.
- [17]. Sevdalina Turmanova, Svetlana Genieva, Lyubomir Vlaev, International Journal of Chemistry, 2012, 4(4).
- [18]. Ayswarya E. P, Beena T. Abraham, Eby Thomas Thachil, Journal of Applied Polymer Science, 2012, 24, 1659–1667.
- [19]. J G Ryu, H Kim, J W Lee, Polymer Engineering and Science, 2004, 44(7), 1198–1204.
- [20]. Maryam Ataefard, Siamak Moradian, Polymer-Plastic Technology, 2011, 50(7), 732-739.
- [21]. Jinge Li , Huayi Li , Chunhong Wu, Yucai Ke , Dujin Wang, Qian Li, Liaoyun Zhang, Youliang Hua., European Polymer Journal, 2009, 45(9), 2619–2628.
- [22]. Thomas S. Ellis, Joseph S. D'Angelo, Journal of Applied Polymer Science, 2003, 90(6), 1639–1647.
- [23]. Jan Golebiewski, Andrzej Galeski, Composite Science and Technology, 2007, 67 (15-16), 3442–3447.
- [24]. Sanjay K. Nayak, Smita Mohanty, Sushanta K. Samal. Polymer Plastic Technology and Engineering, 2009, 48(9), 976 -988.
- [25]. SunanTiptipakorn, Sarawut Rimdusit, Siriporn Damrongsakkul , Takeshi Kitano. Engineering journal, 2009, 13 (3), 125-8281.
- [26]. Jia-Lin Tsai, Ming-Daw Wu, Journal of Composite and Materials, 2008, 42( 6), 553.

- [27]. S Y Lee, I A Kang I. A, Doh. G. H., Kim W. J, Kim J. S, Yoo. H. G Wu Q, eXPRESS Polymer Letters, 2008, 2(2), 78–87.
- [28]. Asha K. Krishnan, Tresa Sunitha George, R. Anjana, Newly Joseph, K. E. George, Journal of Applied Polymer Science, 2013, 127, 1409.
- [29]. Shahryar Pashaei, Siddaramaiah, Maziar Mansouji Avval, Akheel Ahmed SyedChemical Industry & Chemical Engineering Quarterly, 2011,17 (2), 141–151.
- [30]. Jordana Palacios, Rosestela Perera , Carmen Rosales, Carmen Albano, José María Pastor, Polymer Degradation and Stability, 2012, 97, 729-737.
- [31]. F Rezaei, R Yunus, N A Ibrahim, Materials and Design, 2009, 30(2), 260–263.
- [32]. Shao-jian He, Yi-qing Wang, Yi-ping Feng, Qing-sheng Liu, Li-qun Zhang, Nanotechnology, 2010, 21, 7.
- [33]. D. Ziegel, A. Romanov, Journal of Applied Polymer Science, 1973, 17, 1119-1131.
- [34]. K. D. Ziegeland , Romanov, 1973, 17,1133-1142.
- [35]. Manoranjan Biswal, Smita Mohanty and Sanjay K. Nayak, Journal of Thermoplastic Composite Materials, 2012, 25 (6), 765-790.
- [36]. Young Jin Kim, Cui Sook Shin, In Tae Lee, And Byunc Kyu Kim, Journal of Applied Polymer Science, 1993, 47, 295-304.
- [37]. L. Uma Devi, S.S. Bhagawan, S. Thomas, Polymer Composites, 2010, 31(6), 956–965.
- [38]. Seung-Hwan Lee, Siqun Wang, Composites: Part A, 2006, 37, 80–91.
- [39]. Jaydeep Khedkar, Ioan Negulescu, Efstathios I. Meletis, Wear, 2002, 252, 361–369.

.....✂.....



**Polypropylene/Polystyrene/clay  
nanocomposites: Effect of  
vinyltriethoxysilane modification**

---

<i>Contents</i>	<b>Part A</b>
	<b>Modification and characterization of nanokaolin clay using vinyltriethoxysilane</b>
	<i>5. A.1 Introduction</i>
	<i>5. A.2 Methodology</i>
	<i>5. A.3 Results and Discussion</i>
	<i>5. A.4 Conclusions</i>
	<b>Part B</b>
	<b>Polypropylene/Polystyrene/Vinyltriethoxysilane modified clay nanocomposites</b>
	<i>5. B.1 Introduction</i>
	<i>5. B.2 Methodology</i>
<i>5. B.3 Results and Discussion</i>	
<i>5. B.4 Conclusions</i>	

---

## Part -A

### Modification and characterization of kaolin nanoclay using vinyltriethoxysilane

#### Abstract

*Functionalization of kaolin clay with vinyltriethoxysilane (VTES) was reported in this study. The intercalation was achieved using kaolin-Dimethylsulfoxide (DMSO) intercalate as a starting material. FTIR shows that VTES effectively displaced DMSO from the clay mineral interlayer. The resulting material was characterized by X-ray diffraction, thermal analysis and Infra-Red Spectroscopy. The X-ray diffractograms reveals the intercalation of DMSO, and subsequently by VTES. The thermogravimetric curves of the kaolin clay functionalized with VTES indicates that the material was thermally stable up to 515 °C.*

- 1) Mechanical and morphological properties of Organomodified kaolin/ Polypropylene/ Polystyrene nanocomposites; Asha Krishnan K, Tresa Sunitha George; K.E. George; Pauline Journal of research and studies; Vol.1.No.1(2013)

#### 5. A.1 Introduction

Polymer-clay nanocomposites are a class of hybrid materials composed of organic polymer matrix in which layered inorganic particles with nanoscale dimension is distributed. As a result of the nanometer-scale dispersion, nanocomposites exhibit markedly improved mechanical, thermal and physicochemical properties, decreased gas and water vapor permeability, resistance to flammability and thermal degradation as compared with the conventional composites [1-3]. These nanocomposites synergistically integrate the advantages of organic polymers and those of the inorganic filler.

Clays are commonly used as fillers because they are composed of layered silicates that can intercalate organic molecules. The clay consists of

stacked aluminosilicate layers that can be separated and are held together by electrostatic forces which cannot be broken into separate layers by simple shear. Thus, organic modification of the clay is required to achieve the separation of the stacked clay layers [4]. Clay minerals interact with organic compounds by adsorption, intercalation and cation exchange. Many of the work in this area have focused on montmorillonite (MMT) clays. Montmorillonite is a valuable mineral used for industrial applications because of their high cation exchange capacities, large surfaces areas, surface reactivities, and adsorptive properties. Organic modifiers such as alkyl ammonium cations make them organophilic, which further extend their applications [5]. The aspect ratio of MMT is about 10-1000 and the surface area is in the range of 750 m<sup>2</sup>/g.

Kaolin clay which is found in hydrothermal, residual and sedimentary deposits is less studied as its cation exchange capacity (CEC) is less than 0.1 meq/g. Now there is an increasing interest on organo modified nanokaolin as filler in polymer to reinforce the mechanical properties and to reduce the cost. Kaolin clay is a 1:1 dioctahedral aluminosilicate with two distinct basal layers. One of them consists of a tetrahedral siloxane surface formed by very chemically inert -Si-O-Si- bonds, while the other is constituted by an octahedral gibbsite sheet, Al(OH)<sub>3</sub>. The neutral layered 1:1 structure can be disrupted and the broken bonds have the ability to accommodate -OH groups [6]. Because of the hydrophilic properties of kaolin and hydrophobic character of polymer, the modification of kaolin is necessary.

Kaolin nanoclay can interact with organic molecules by intercalation. The reactive guest molecules enter the interlamellar space, break up the

hydrogen bonds and form new ones resulting in a nano-layered material. The kind of guest species intercalated between the layers of kaolin is limited due to the hydrogen bonding between the octahedral side and tetrahedral side. Limited number of polar guest species such as N-methylformamide (NMF) [7], Urea [8], DMSO [9] can be directly intercalated. Intercalation of kaolin with guest species can be done by displacement reactions. The separation of kaolin results in particle size reduction and an increase of the specific surface area. A good kaolin clay modification results in better intercalation between filler and polymer matrix.

Weiss *et.al* classified the guest molecules as (a) Compounds that form strong hydrogen bonds with the silicate layers e.g.: urea, formamide etc. (b) Compounds form strong dipole interaction with silicate layers e.g. DMSO and (c) Alkali salts of strong fatty acids for e.g. acetic acid. Non-reactive molecules enter into the clay layers by displacing reactive guest molecules. Reactive molecules can be used as precursors for the intercalation of non-reactive organic molecules via the displacement of intercalated molecules. In addition to the formation of organo-clay nano-hybrid materials, intercalation can lead to the covalent grafting of organic molecules [10, 11]. Hence in this study guest-displacement method is used to modify the kaolin nanoclay.

## **5. A.2 Methodology**

### **5. A.2.1 Modification of kaolin nanoclay**

Kaolin nanoclay is characterized by two types of interlayer surfaces: a gibbsite type surface covered by aluminol groups and a siloxane surface. Adjacent layers are linked by Van der Waals and H-bonds, which induce restricted access to the interlamellar aluminol groups. The strong interaction

between the nanoclay layers prevents the insertion of most substances; a preceding expansion step is required. Kaolin can be expanded by intercalating small and highly polar molecules such as dimethylsulfoxide (DMSO). Modification of kaolin nanoclay is done in two steps. First step involves the intercalation of kaolin nanoclay by dimethylsulfoxide in order to expand the interlayer space. Second step involves the displacement of DMSO by vinyltriethoxysilane (VTES). Figure 5a.1 shows the schematic representation of the modification of kaolin nanoclay.

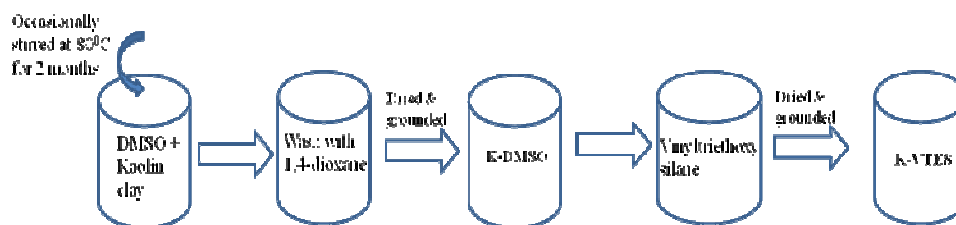


**Figure 5a.1 Schematic representation of the modification of kaolin nanoclay**

#### **5. A.2.1.1 Intercalation of kaolin nanoclay by dimethylsulfoxide (DMSO) as precursor**

The modification of kaolin nanoclay is done by guest displacement method. Kaolin was modified by treatment in solution with DMSO. 10 g of the clay fraction was suspended in DMSO, and the mixture was occasionally stirred at 80°C, using a magnetic stirrer for two months. After two months, the clay–DMSO complex was washed with 1,4-dioxane to remove excess DMSO. The contents were filtered using vacuum in a Buchner funnel. The filter cake was dried in an oven at 70°C. The dried clay was ground using a mortar and pestle to get a fine powder of DMSO intercalated kaolin (K-DMSO). The guest molecules enter the interlayer space and move apart the

silicate layers. Figure 5a.2 shows the intercalation of DMSO into the kaolin layers.

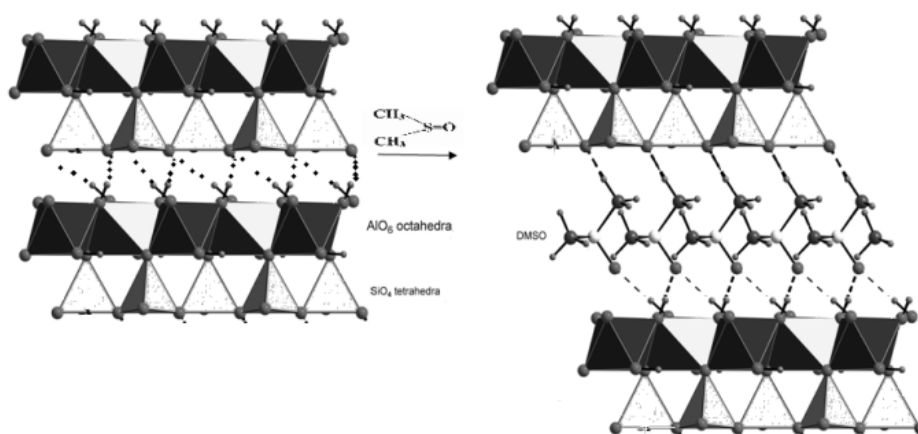


**Figure 5a.2 Schematic representation of the intercalation of DMSO into the kaolin layers.**

#### 5. A.2.1.2 Modification by vinyltriethoxysilane

The nanoclay was modified by hydrolysis followed by condensation reaction of vinyltriethoxysilane. The DMSO intercalated clay particles were sonicated (10g/100ml of methanol-water mixture) for 1 hour to get a homogeneous aqueous dispersion. The dispersion was acidified (3-5 pH) with 2N HCl and triethoxy vinyl silane (vinyltriethoxysilane in the methanol-water mixture) was added slowly. Then the mixture was stirred for 3 min at 70°C for the hydrolysis reaction. NaOH solution (7-9 pH) was then added and the mixture was further stirred for 1 hour at 60°C for condensation reaction. Reaction of the vinyltriethoxysilane with nanoclay is shown in the Figure 5a.3. Silanetriols are most stable at pH 3-6, but condense rapidly at pH 7-9 [12]. This was then filtered, washed with distilled water and dried to get fine particles of vinyltriethoxysilane modified kaolin nanoclay (K-VTES).

Schematic representation of the possible reactions between nanoclay and vinyltriethoxysilane is shown in the Figure 5a.4.

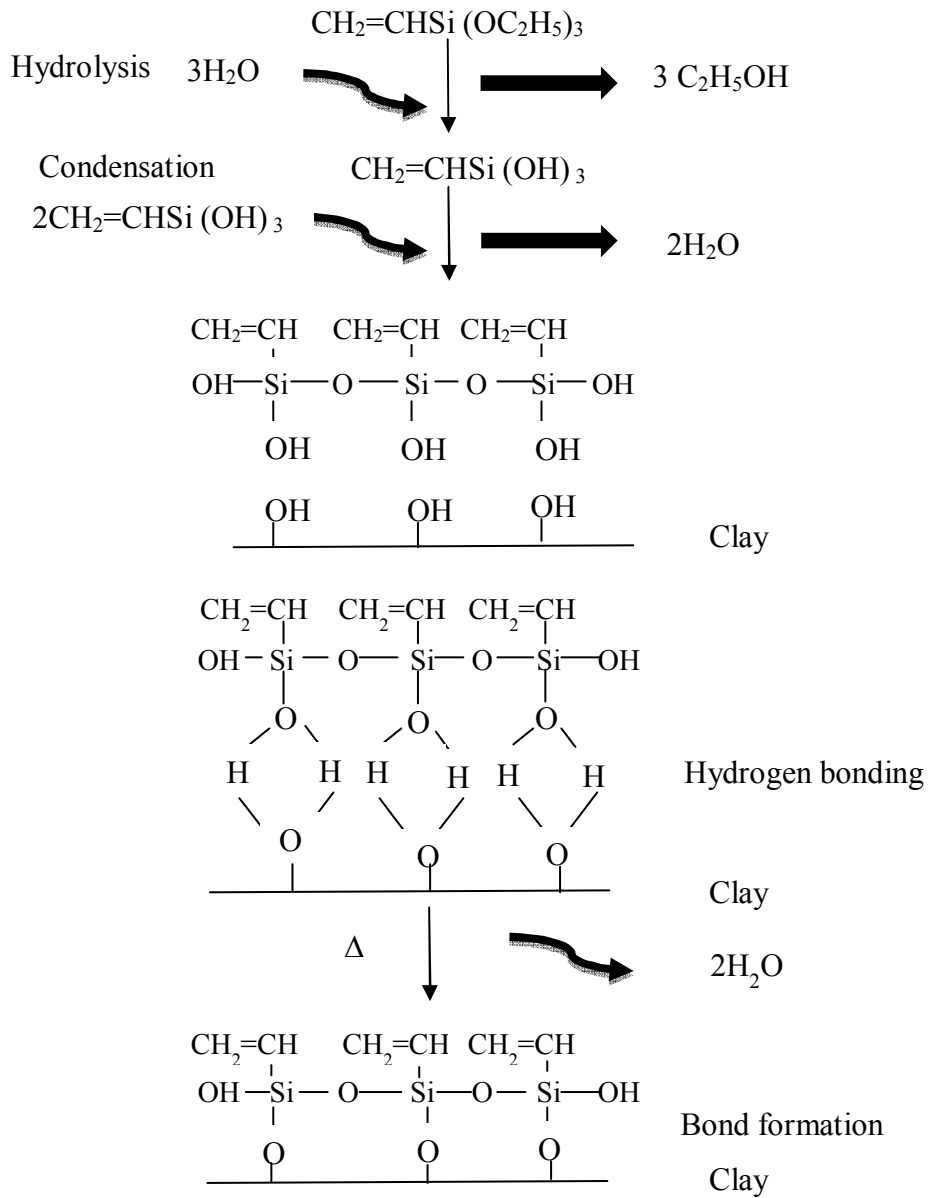


**Figure 5a.3** Reaction process of vinyltriethoxysilane with nanoclay

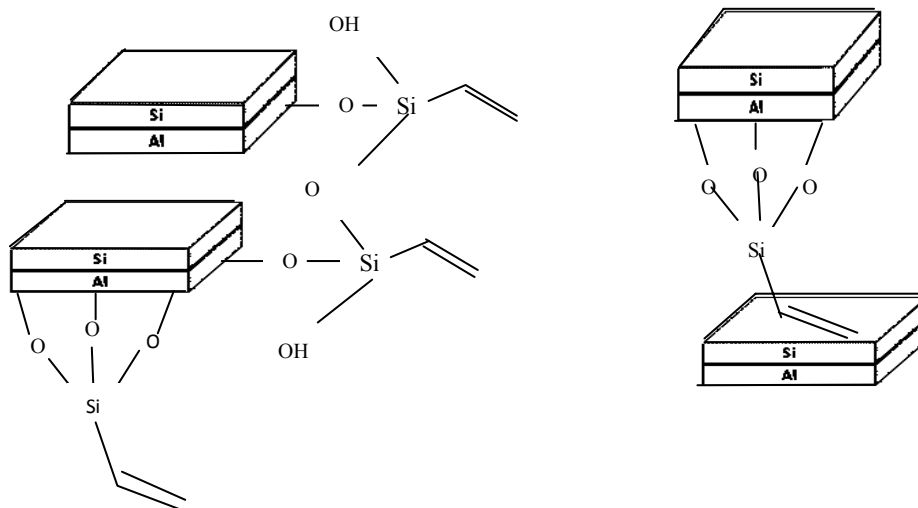


**Figure 5a.4** Schematic representation of the possible reactions between the nanoclay and the vinyltriethoxysilane

### 5. A.2.2 Characterization

The modified kaolin nanoclay was characterized by using various techniques such as SEM, XRD, FTIR and TGA. Surface area, bulk density and particle size of the vinyltriethoxysilane modified kaolin clay was determined using the procedure given below.

#### (a) BET studies

Surface area of vinyltriethoxysilane modified kaolin clay was measured using BET method. Measurements were carried out under nitrogen atmosphere using Autosorb iQ Station 1, surface area and porosity analyser, Surface area was determined using the equation,

$$S_{\text{BET}} = 4.353 V_m$$

Where  $S_{\text{BET}}$  is the surface area in  $\text{m}^2/\text{g}$  and  $V_m$  is the molar volume of adsorbate gas ( $\text{N}_2$ ) at STP.



(b) *Bulk density*

The bulk density of the material was determined as per ASTM D 1895-96. Bulk density is defined as the weight per unit volume of a material. It is primarily used for powders or pellets. The test can provide a gross measure of particle size and dispersion, which can affect material flow consistency.

Procedure

The small end of the funnel is closed with hand or a suitable flat strip and  $115 \pm 5 \text{ cm}^3$  of samples are poured into the funnel. Open the bottom of the funnel quickly and allow material to flow freely into the cup. If caking occurs in the funnel, the material may be loosened with a glass rod. After the material has passed through the funnel immediately scrape of the excess on the top of the cup with a straight edge without shaking the cup. Weigh the material nearest to 0.1 g and determine the bulk density.

(c) *Particle size analysis*

Particle size analysis of the vinyltriethoxysilane modified kaolin clay was carried out in a particle size analyzer (Nanotrak equipment from Microtrac). The sample was sonicated prior to analysis.

### **5.A.3 Results and Discussion**

#### **5.A.3.1 Fourier transform infrared spectroscopy**

The infrared absorption spectra of unmodified kaolin clay, DMSO modified kaolin nanoclay (KDMSO) and vinyltriethoxysilane modified kaolin

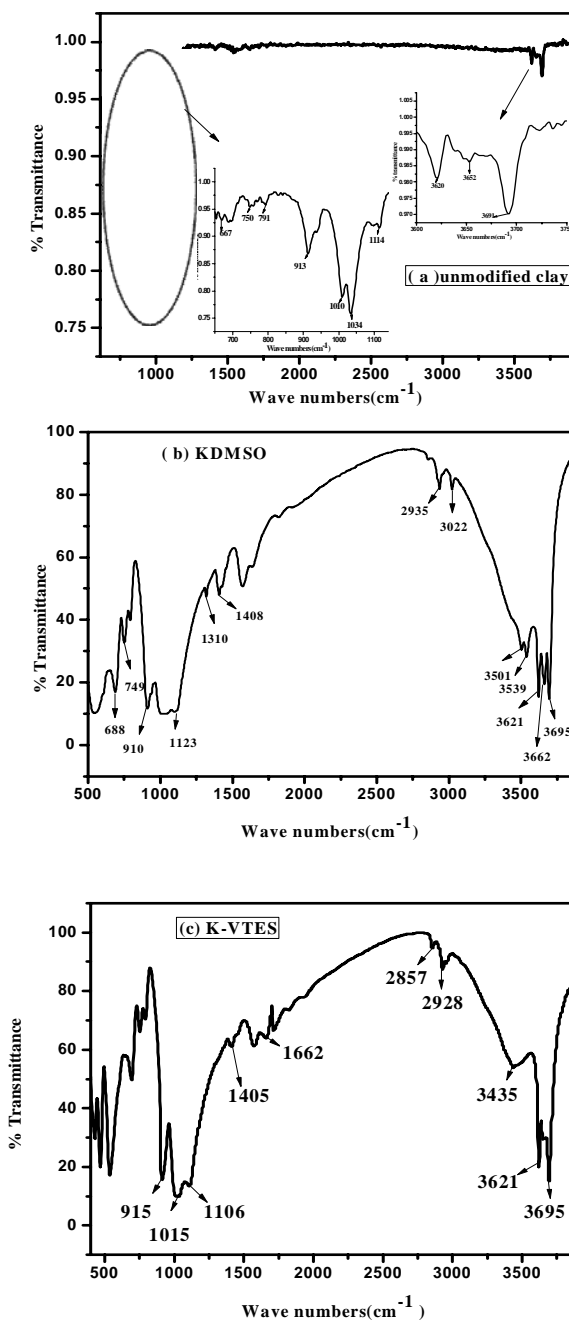


Figure 5a.5 FTIR spectrum of (a) Unmodified kaolin nanoclay (b) KDMSO (c) Vinyltriethoxysilane modified kaolin nanoclay (K-VTES)

(K-VTES) are given in the Figure 5a.5. Kaolin nanoclay (Figure 5a.5 (a)) consists of three kinds of hydroxyl groups that is, inner-surface hydroxyl, inner hydroxyl, and absorbed water hydroxyl. Bands observed at 3691 and 3620  $\text{cm}^{-1}$  are attributed to the phase vibration of the inner-surface hydroxyl and inner hydroxyl respectively, and the band at 3652  $\text{cm}^{-1}$  is the characteristic vibration band of absorbed water [13]. The bands at 1134, 1034 and 910 $\text{cm}^{-1}$  are attributed to the Si-O stretching vibrations [14]. The bands at 791, 750, and 667 $\text{cm}^{-1}$  are due to the O-Al-OH stretching vibrations [15].

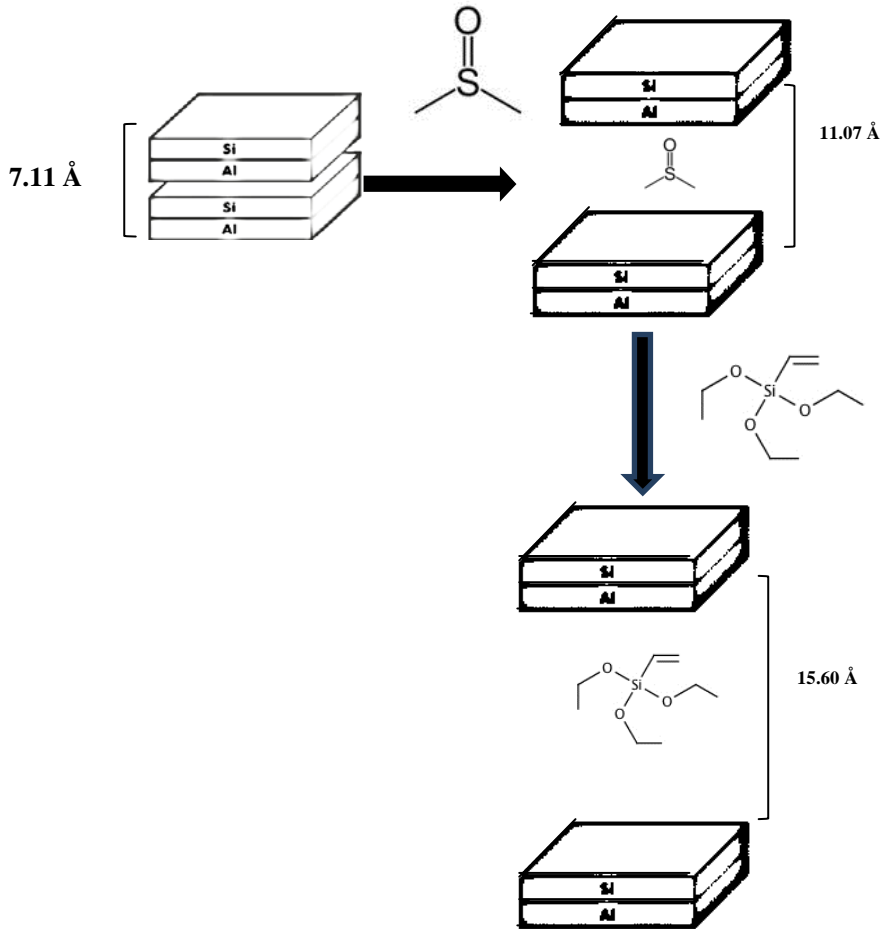
Kaolin nanoclay is modified by guest displacement method in which new guest species can be intercalated by displacing previously intercalated species. After the intercalation of kaolin with DMSO (Figure 5a.5 (b)), the additional bands at 3539 and 3501  $\text{cm}^{-1}$  are observed, which are attributed to intercalation of DMSO molecules through hydrogen bonding with the interlamellar hydroxyls of the nanoclay (Si=O-OH). The vibrational band of kaolin clay at 3620  $\text{cm}^{-1}$  has not been affected but the bands at 3691  $\text{cm}^{-1}$  is shifted to 3695 $\text{cm}^{-1}$  after the intercalation of DMSO. New bands appear at 2935 and 3022  $\text{cm}^{-1}$  are assigned to the vibrations of the DMSO C-H groups. The band of 3662  $\text{cm}^{-1}$  is attributed to the hydroxyl stretching vibration of inner-surface hydroxyl groups that are hydrogen bonded to the -S=O group of DMSO. The band at 910 $\text{cm}^{-1}$  are due to the Si-O stretching vibrations and the O-Al-OH stretching vibrations at 667 $\text{cm}^{-1}$  is shifted to 688 $\text{cm}^{-1}$ [16,17].

Figure 5a.5(c) shows two peaks at 2857 and 2928  $\text{cm}^{-1}$  which are due to the vibrations of C-H bonds introduced by the organic modifier. Peaks at

2928  $\text{cm}^{-1}$ , due to  $\text{CH}_3$  asymmetric stretching, and at 2857  $\text{cm}^{-1}$ , due to  $\text{CH}_3$  and  $\text{CH}_2$  asymmetric stretching confirm the presence of silane in modified kaolin clay. In the region of 3700–3200  $\text{cm}^{-1}$ , a number of sharp peaks at 3695, and 3620  $\text{cm}^{-1}$  are observed due to O–H stretching vibration of silanol groups. The predominant peak at 1015–1080  $\text{cm}^{-1}$  is due to the siloxane bonds (Si–O–Si). The peak observed at 915  $\text{cm}^{-1}$  is accredited to the Al–OH stretching vibrations. The peak observed at 1662  $\text{cm}^{-1}$  is ascribed to the C=C stretching vibrations. The absorption band observed at 1405  $\text{cm}^{-1}$  is due to the C –  $\text{CH}_3$  symmetric bending vibration [18, 19].

### 5. A.3.2 X-ray Diffraction

The schematic representation of the functionalization of kaolin clay is shown in the Figure 5a.6. The XRD patterns of unmodified clay, DMSO modified kaolin clay (K-DMSO), vinyltriethoxysilane modified kaolin nanoclay (K-VTES) are depicted in the Figure 5a.7. The characterization peak for unmodified clay exhibit a  $d_{001}$  reflection at  $2\theta = 12.44^\circ$  having a basal spacing of 7.11 Å. After the intercalation of kaolinite with DMSO, the original peak of kaolin at  $2\theta = 12.44^\circ$  is shifted to 7.961 $^\circ$ . The basal spacing of KDMSO expands from 7.11 Å to 11.07 Å. Thereafter intense intercalation of VTES is confirmed by the typical increase of d spacing from 11.07 Å to 15.60 Å with a corresponding decrease in  $2\theta$  value to 5.66 $^\circ$ . VTES displaced the guest molecule (DMSO), as shown by XRD patterns (Figure 5a.7) [16].



**Figure 5a.6 Schematic representation of the functionalization of kaolin nano clay**

Crystallite thickness of the vinyltriethoxysilane modified kaolin clay can be calculated by using the Scherrer equation [20]:

$$t = (K \times \lambda) / B \cos \theta \dots\dots\dots (5a.1)$$

where

t = crystallite thickness

K = a constant (0.91 for clay)

$\lambda$  = X-ray wavelength

B = Full width half max (FWHM) of the diffraction peak

$\theta$  = diffraction angle

The crystallite size found using the equation 5a.1 is 15.26 nm.

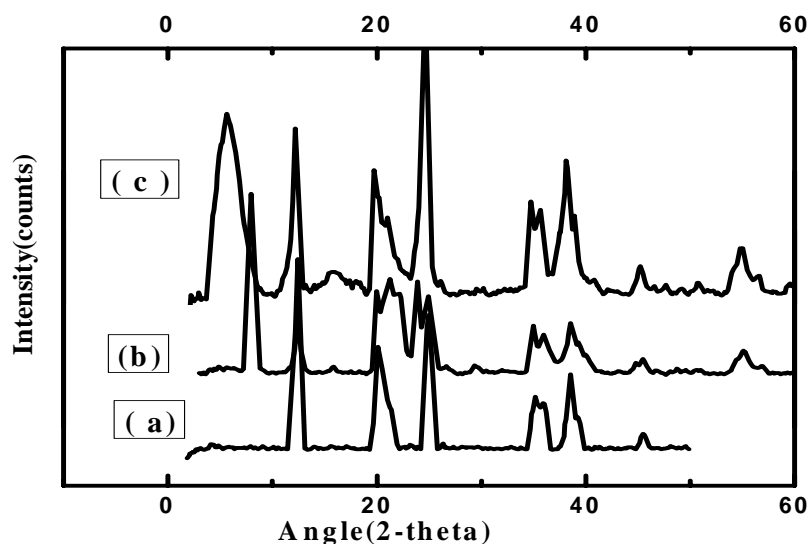
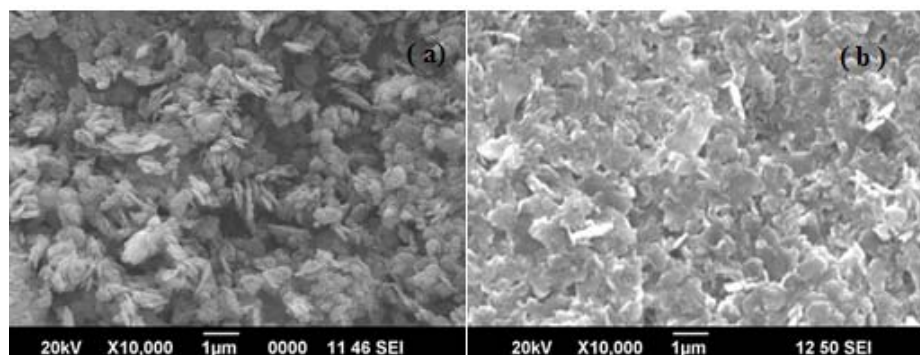


Figure 5a.7 XRD patterns of (a) unmodified clay (b) KDMSO and (c) K- VTES

### 5. A.3.3 Scanning electron microscopy

Figures 5a.8 (a) & 5a.8 (b) illustrate the surface morphology of commercial vinyl silane modified nanoclay and vinyltriethoxysilane modified kaolin nanoclay. Commercial kaolin SEM photograph reveal the platelet hexagonal structure of the kaolinite crystals. The vinyltriethoxysilane modified kaolin shows individual plates. The vinyltriethoxysilane modified kaolin exhibits a compact platelet morphology with delaminated layers which shows the presence of organic modification in kaolin nanoclay.



**Figure 5a.8 SEM images of (a) Commercial vinyl silane modified nanoclay (b) Vinyltriethoxysilane modified nanoclay**

#### **5A.3.4 BET surface area**

The surface area obtained for different samples by BET adsorption method are given in Table 5a.1. Vinyltriethoxysilane modified nanoclay has higher surface area than that of commercial vinyl silane modified nanoclay.

**Table 5a.1 Surface area of kaolin nanoclay samples**

<b>Samples</b>	<b>Surface area(m<sup>2</sup>/g)</b>
Commercial vinyl silane modified nanoclay	30.00
Vinyltriethoxysilane modified nanoclay	46.29

The surface area of the nanoclay particles is found to be higher as particle size decreases. The above table shows that vinyltriethoxysilane modified kaolin nanoclay has lower particle size than the commercial nanoclay. This confirms that the presence of vinyl silane group on the surface of nanoclay particles which decreases the adsorption of nitrogen. This indicates that nanoclay surface is effectively modified by vinyltriethoxysilane.

#### **5A.3.5 Bulk density**

The bulk density values of vinyltriethoxysilane modified nanoclay are compared with commercial vinyl silane modified nanoclay (Table 5a.2).

Bulk density of vinyltriethoxysilane modified nanoclay is found to be higher than the commercial vinyl silane modified nanoclay. This is due to the smaller particle size of vinyltriethoxysilane modified kaolin nanoclay compared to that of the other.

**Table 5a.2 Bulk densities of kaolin nanoclay samples**

Samples	Bulk density(g/cm <sup>3</sup> )
Commercial vinyl silane modified nanoclay	0.2
Vinyltriethoxysilane modified nanoclay	0.5

### 5. A.3.6 Particle size analysis

For both commercial vinyl silane modified nanoclay (Figure 5a.9 (a)) and vinyltriethoxysilane modified nanoclay (Figure 5a.9 (b)) the finest fraction lies < 0.5  $\mu\text{m}$  in size. Particle size analysis data shows that volume weighted mean D of the commercial vinyl silane nanoclay is 283 nm and for vinyltriethoxysilane modified kaolin nanoclay is 253 nm.

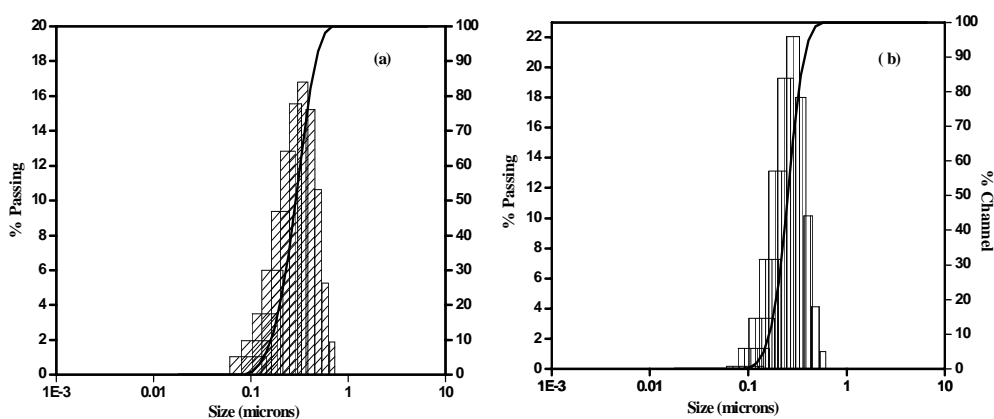


**Figure 5a.9 Particle Size Distribution of (a) Commercial vinyl silane modified nanoclay (b) Vinyltriethoxysilane modified nanoclay**



### 5.A.3.7 Thermogravimetric analysis

The thermal decomposition of unmodified clay, KDMSO and K-VTES in nitrogen atmosphere is shown in the Figure 5a.10. Figures 5a.10 (a) & 5a.10 (b) depict the TG and DTG curves for unmodified clay, KDMSO, K- VTES. Thermogravimetry can be used as a proof of interactions between organic medium and inorganic nano platelet's surface. The unmodified clay shows a maximum degradation temperature at 507.9°C. It corresponds to dehydroxylation of kaolinite and the formation of metakaolinite. The kaolin intercalated with DMSO (KDMSO) exhibits two mass losses in the TG curve, accompanied with two endotherms centered at about 154.3°C and 510.4°C. The former is attributed to the loss of the organic moiety, and the latter is due to the usual dehydroxylation step of kaolinite [13]. The vinyltriethoxysilane modified kaolin (K-VTES) depicts a degradation peak at 515.3 °C. Maximum degradation peak increased from 507.9°C to 515.3 °C. This shows that thermal stability of kaolin nanoclay is increased by the addition of vinyltriethoxysilane.

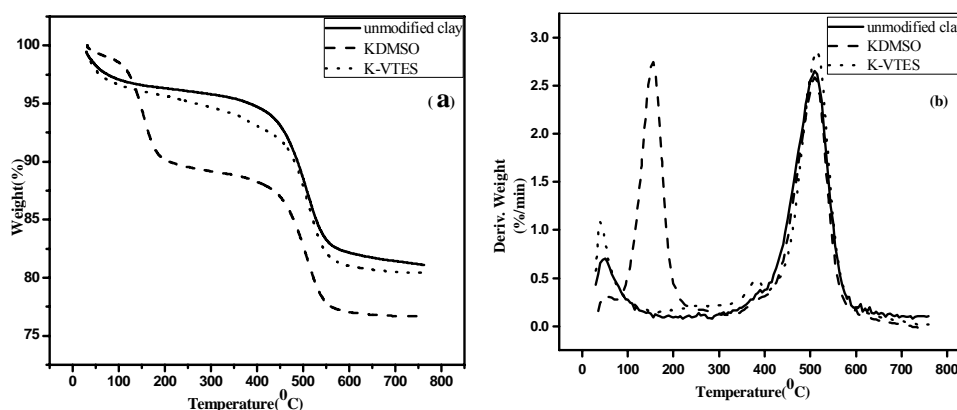


**Figure 5a.10 (a) TG and (b) DTG curves for unmodified clay, KDMSO, K- VTES**

## 5A.4 Conclusions

The basal spacing of kaolin is expanded with the intercalation of DMSO into the interlayer sheets of kaolin. KDMSO is successfully displaced with vinyltriethoxysilane in the interlayer spaces of kaolin. XRD shows an increase in d-spacing of kaolin nanoclay from 7.11 Å to 15.60 Å after the addition of vinyltriethoxysilane. Further the evidence for the delamination of kaolin nanoclay by DMSO with subsequent substitution of vinyltriethoxysilane is also displayed in FTIR spectra. Thermal analysis shows that the modified nanoclay is thermally stable up to 515°C. The bulk density and surface area of vinyltriethoxysilane modified kaolin nanoclay is higher than that of commercially available vinyl silane nanoclay and this confirms the presence of modifying group on the surface of kaolin nanoclay.

## References

- [1]. Liu Xuening, HuNan, Science in China Ser. B chemistry, 2005, 48(2), 326-333.
- [2]. Qin Zhang, Xiao-lin Gao, Ke Wang, Qiang Fu, Chinese Journal of Polymer Science, 2004, 22(2), 175-182.
- [3]. Kyung YI Kim, Dong Uk Ju, Gi Joon Nam, Jae Wook Lee, Macromolecular. Symposia, 2007, 249–250, 283–288.
- [4]. Yasemin Turhan, Mehmet Dogan, Mahir Alkan, Industrial & Engineering Chemistry Research, 2010, 49, 1503–1513.
- [5]. Kathleen A. Carrado Applied Clay Science, 2000, 17, 1–23.

- [6]. Sadok Letaief, Tamer A. Elbokl, Christian Detellier, *Journal of Colloid and Interface Science*, 2006, 302, 254–258.
- [7]. B. P. Kelleher, D. Sutton, T. F. ODwyer, *Journal of Colloid and Interface Science*, 2002, 255, 219–224.
- [8]. Eva Mako, Janos Kristof, Erzsebet Horvath, Veronika Vagvolgyi, *Journal of Colloid and Interface Science*, 2009,330, 367–373.
- [9]. James J. Tunney, Christian Detellier, *Chemistry of Materials*, 1996, 8, 927-935.
- [10]. G. Lagaly, *Phil. Trans. R. Sco. Lond. A*, 1984, 311,315-332.
- [11]. A. Weiss, W Thieleppe, H Orth, *Proc.int. Clay conf. Jerusalem*, Jerusalem, Israel University Press, 1966, 1,277-293.
- [12]. A Silane Primer: Chemistry and Applications of Alkoxy Silanes, Gerald L. WituckiDow Corning Corporation, *A Journal of Coatings Technology Reprint* .
- [13]. Yasemin Turhan, Mehmet Dog'an, Mahir Alkan, *Industrial & Engineering Chemistry Research*, 2010, 49, 1503–1513.
- [14]. Clay surfaces: Fundamentals and applications, Fernando Wypych kestr Gundappa Satyanarayana, Academic press publisher, 2004.
- [15]. Bo Zhang, Yanfeng Li, Xiaobing Pan, Xin Jia, Xiaolong Wang, *Journal of Physics and Chemistry of Solids* ,2007,68 , 135–142.
- [16]. Lilian R. Avila, Emerson H. de Faria , Katia J. Ciuffi , Eduardo J. Nassar, Paulo S. Calefi, Miguel A. Vicente, Raquel Trujillano, *Journal of Colloid and Interface Science*, 2010, 341 , 186–193.
- [17]. E.H. de Faria , K.J. Ciuffi , E.J. Nassar , M.A. Vicente , R. Trujillano , P.S. Calefi, *Applied Clay Science* ,2010,48 , 516–521.
- [18]. Sudip Raya, Anil K. Bhowmicka, K.S.S. Sarmab, A.B. Majalib, V.K. Tikku ; *Radiation Physics and Chemistry*,2002, 65 ,627–640.

- [19]. Weld line behaviour of modified PP, HDPE and their blend, PhD Thesis, Cochin University of Science and Technology, 2011.
- [20]. Sanjay K. Nayaka, Smita Mohantya, Sushanta K. Samala, *Polymer-Plastics Technology and Engineering*, 2009, 48, 976–988.

## **Part -B**

### **Polypropylene/Polystyrene/Vinyltriethoxysilane modified clay nanocomposites**

#### **Abstract**

*Polypropylene (PP)/Polystyrene (PS)/clay nanocomposites were prepared by melt mixing in a Thermo Haake Rheochord mixer. The effect of vinyltriethoxysilane modified nanoclay on the properties of PP/PS (80/20) blend was studied. The major objective was to examine the static and dynamic mechanical properties of the nanocomposites. The clay mineral layer exfoliation in nanocomposites was monitored by XRD and SEM. Evaluation of thermal degradation kinetics of nanocomposites by three kinetic methods namely Coats Redfern, Broido's and Horowitz Metzger was also a focus of the present study. XRD results reveal the exfoliation of both PP and PS in nanoclay galleries. TGA results show an improved thermal stability for nanocomposites than the pure blend.*

#### **5. B.1 Introduction**

Polymer blend/clay nanocomposites represent a new class of hybrid materials that emerged as a subject of enormous scientific interest. This is because the compounding leads to a new kind of high performance material, combining the advantages of polymer blends and polymer nanocomposites. A great deal of work has been focused on studying the modifying effect of nanoclay in the immiscible polymer blends [1]. The use of nanoclay for enhancement of properties is possible only if agglomeration between the particles is reduced and good interfacial bonding between particle surfaces and polymer matrix is ensured. Much of the work in this area is focused on montmorillonite [2,3]. So kaolin nanoclay with a chemical composition  $\text{Al}_2\text{Si}_2\text{O}_5(\text{OH})_4$  and 1: 1 type layered structure is proposed to be used in this study.

Individual layers of kaolin nanoclay consists of both tetrahedral sheets and octahedral in which one tetrahedral sheet linked through oxygen atoms to one octahedral sheet of alumina. The hydrophilic character of the kaolin nanoclay makes it ineffective for absorption of aliphatic and relatively hydrophobic substances [4]. Modification of nanoclay minerals with organic intercalates changes the hydrophilic nature of nanoclay mineral to hydrophobic and increases the interlayer distance [5]. They ensure better dispersion in the organic polymer matrix by virtue of expanded interlayer space.

The kind of guest species intercalated between the layers of kaolin is limited due to the hydrogen bonding between the octahedral side and tetrahedral side. Limited number of polar guest species such as N-methylformamide (NMF) [6], Urea [7], Dimethylsulfoxide (DMSO) [8] can be directly intercalated. Intercalation of kaolinite with guest species can be done by displacement mechanisms. Yasemin Turhan *et al.* studied the effect of modified kaolin clay in Poly (vinyl chloride). In their study kaolin clay was modified using succinimide by replacing DMSO. They found that the incorporation of nanoparticles in polymer results in an increase in thermal stability and UV transparency [9]. Rugmini Sukumar *et al.* modified the kaolin clay with sodium salt of rubber seed oil (SRSO) and studied the effect of modified kaolin clay in natural rubber. They observed that the mechanical properties is increased, indicating the probable role of SRSO-modified kaolin as a nanofiller in NR [10].

Organo functional alkoxy silanes like aminoalkoxy silane [11], methacrylate alkoxy silane [12] are employed for the functionalization

of kaolin clay. Ignas K. Tonlé *et al.* have reported the grafting of 3-aminopropyltriethoxysilane (APTES) onto the kaolin clay [13].

Organosilane compounds contain two kinds of reactive groups (inorganic and organic) in a single molecule. A chemical reaction between the functional groups (such as -OH) of filler and the alkoxy groups of silane is expected to occur, creating a silane-functionalized surface [14]. The chemical reactions between the functional groups of the silane-modified clay and the polymer matrix enhance the interaction between the components of the polymer/ clay nanocomposites.

In this study, vinyltriethoxysilane has been used as a modifier of kaolin nanoclay which replaces a DMSO intermediate. The effect of modified filler on the mechanical, thermal and morphological properties of PP/PS blend is proposed to be studied.

## **5. B.2 Methodology**

### **5. B.2.1 Materials**

The details of the polymers used for the study are discussed in Chapter 2 (sections 2.1.1 & 2.1.2).

### **5. B.2.2 Nanocomposite preparation**

PP/PS (80/20) and vinyltriethoxysilane modified kaolin nanoclay (K-VTES) in varying amounts (1-5 wt %) were prepared by melt mixing using an internal mixer (Haake Rheomix 600) at 180 °C with a rotor speed of 50 rpm, and a mixing time of 8 min for each sample. After mixing the melt is pressed in a hydraulic press, cut into pieces and injection moulded in DSM Micro 10cc Injection Molding Machine, with a barrel temperature of

190°C. The tensile properties, flexural properties, impact strength, hardness, dynamic mechanical properties, thermal properties and morphology of the nanocomposites were analyzed according to various standards as described in Chapter 2 (section 2.2.3). The details of the UV aging studies are described in Chapter 3 (section 3.2.2.2).

## 5. B.3 Results and Discussion

### 5. B.3.1 X-ray diffraction

The XRD patterns of vinyltriethoxysilane modified kaolin nanoclay (K-VTES) and PP/PS/modified clay nanocomposite (3wt %) is given in the Figure 5b.1

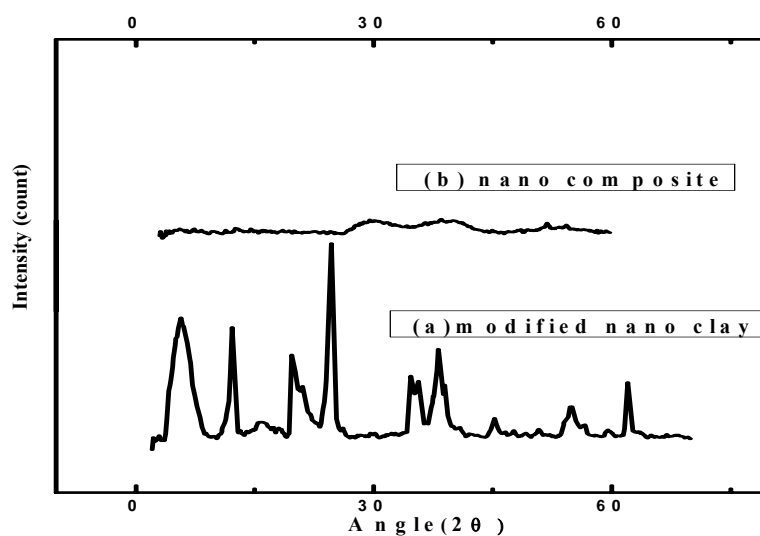


**Figure 5b.1 XRD patterns of (a) K- VTES (b) PP/PS/3wt% K-VTES modified nanocomposite**

The characterization peak for K- VTES appears at 15.69 Å with a 2θ value of 5.66°. Reduced peak intensity at (001) plane of nanocomposite is attributed to the reduced number of layers in clay stacks. The shear of



mixing process is capable of opening the basal plane of nanoclay in order to intercalate polymer chains into the nanoclay layers. This observation suggests a better dispersion and lower tactoid for the modified kaolin nanoclay in polymer matrix.

### **5. B.3.2 Scanning electron microscopy**

The morphology of tensile fracture surface of PP/PS blend and PP/PS/modified clay nanocomposites (1, 3 and 5 wt % nanoclay) is given in Figure 5b.2. PP/PS blend (Figure 5b.2 (a)) exhibits a morphology in which spherical domains of PS phase are surrounded by the continuous PP phase. When PP is mixed with PS, the polymer blend is characterized by phase separation due to the high immiscibility. Addition of 1 wt % of K-VTES (Figure 5b.2(b)) improves the adhesion between two components giving a more homogeneous structure at some regions indicating good but not complete intercalation of the modified nanoclay. After the addition of 3wt % vinyltriethoxysilane modified kaolin nanoclay (K-VTES) (Figure 5b.2 (c)) the adhesion between the two components is improved to form a homogeneous morphology throughout with a better degree of intercalation. This is also evidenced by mechanical properties (section 5.B.3.6) and the XRD measurements (section 5.B.3.1). Figure 5b.2 (d) depicts the surface morphology of PP/PS blend with 5wt% vinyltriethoxysilane modified kaolin nanoclay. The composite shows a weak interface between the dispersed phase (PS) and the continuous phase (PP) resulting in inferior properties. At higher clay content, melt viscosity is high which can hinder the complete dispersion of nanoclays during melt mixing resulting in improper distribution of nanoclays in the interface.

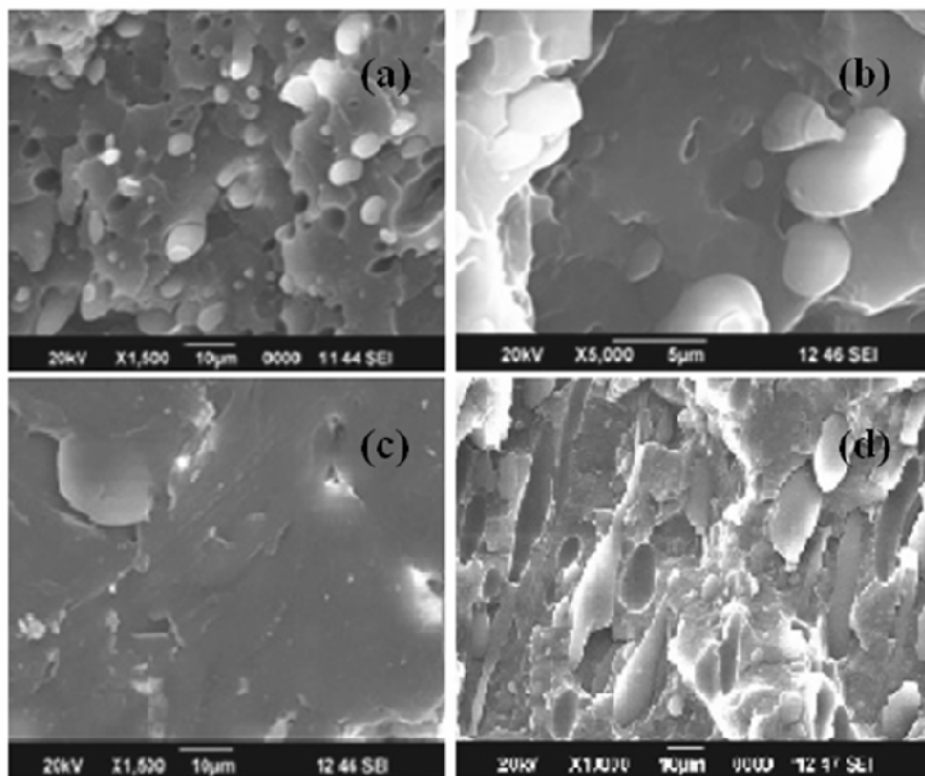


**Figure 5b.2 SEM images of (a) PP/PS pure blend (b) PP/PS/1wt% K-VTES modified nanocomposite (c) PP/PS/3wt% K-VTES modified nanocomposite (d) PP/PS/5 wt% K-VTES modified nanocomposite**

### 5. B.3.3 Thermogravimetric analysis

The thermal stability of the nanocomposites in nitrogen atmosphere has been investigated using TGA. Table 5b.1 gives the results from the DTG curves of PP/PS/modified clay nanocomposites. Figure 5b.3 shows the TG and DTG curves for PP/PS pure blend and PP/PS clay nanocomposite with 1, 3 & 5 wt% of vinyltriethoxysilane modified nanoclay.

**Table 5b.1 Thermal characteristics of PP/PS/clay nanocomposites**

Samples	50% mass loss( °C)	T <sub>max</sub> ( °C)	T <sub>onset</sub> ( °C)	Residue 600 °C (%)	Oxidation Index(OI)
PP/PS blend	426.6	434.4	370.5	0.46	0.032
Blend+1wt% modified clay	443.0	441.5	371.6	0.75	0.052
Blend+3wt% modified clay	443.6	460.2	373.9	1.02	0.071
Blend+5wt% modified clay	454.9	462.1	399.5	2.92	0.203

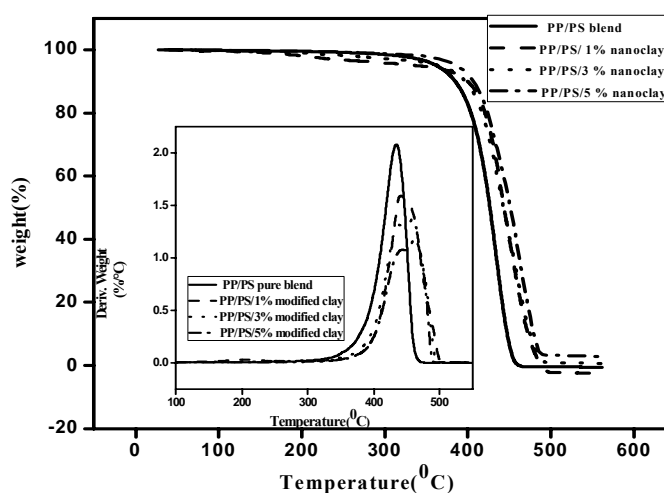


**Figure 5b.3 TG curves of PP/PS pure blend, 1, 3 & 5 wt. % modified clay nanocomposites. The inset shows their respective DTG curves**

Pure blend shows a maximum degradation temperature ( $T_{max}$ ) of 434.4°C. The addition of 1, 3 & 5 wt % of vinyltriethoxysilane modified nanoclay has shifted this temperature to 441.5, 460.2 & 462.1°C respectively. Nanoclay when incorporated into the polymer matrix is found to improve the thermal stability by acting as a superior insulator and mass transport barrier to the volatile products generated during combustion. It results in the formation of highly charred carbonaceous silicate cumulating on the surface of

nanocomposite [15]. The OI values show increment with increase in the clay content and it indicates that the PP/PS/clay nanocomposites are more thermally stable than PP/PS blend.

### 5. B.3.3 .1 Kinetic analysis of thermal decomposition

Kinetic parameters for the thermal degradation of PP/PS blend and PP/PS/clay nanocomposites were evaluated from the TGA curves using Horowitz-Metzger (HM) method, Broido's method (BR) and Coats Redfern (CR) methods.

**Table 5b.2** Activation energy (J/mol) calculated by Horowitz-Metzger, Broido's and Coats-Redfern methods of PP/PS/clay nanocomposites

Samples	Coats – Redfern	Broido's	Horowitz-Metzger
PP/PS blend	174	181	175
Blend+1wt% modified clay	177	185	180
Blend+3wt% modified clay	180	189	191
Blend+5wt% modified clay	185	192	198

The plots of  $\ln [-\ln (1-\alpha)]$  verses  $\theta$  (HM),  $\log [-\log (1-\alpha)/T^2]$  verses  $1/T$  (CR) and  $\log [-\log (1-\alpha)]$  verses  $1/T$  (BR) for vinyltriethoxysilane modified clay nanocomposites are exhibited in the Figure 5b.4 a-c. The activation energy for each method is given in Table 5b.2. PP/PS/clay nanocomposites show higher  $E_a$  than PP/PS blend. Thus, the addition of clay nanoparticles slows down the release rate of the decomposed byproducts and hence enhances the thermal stability of the nanocomposites [16].

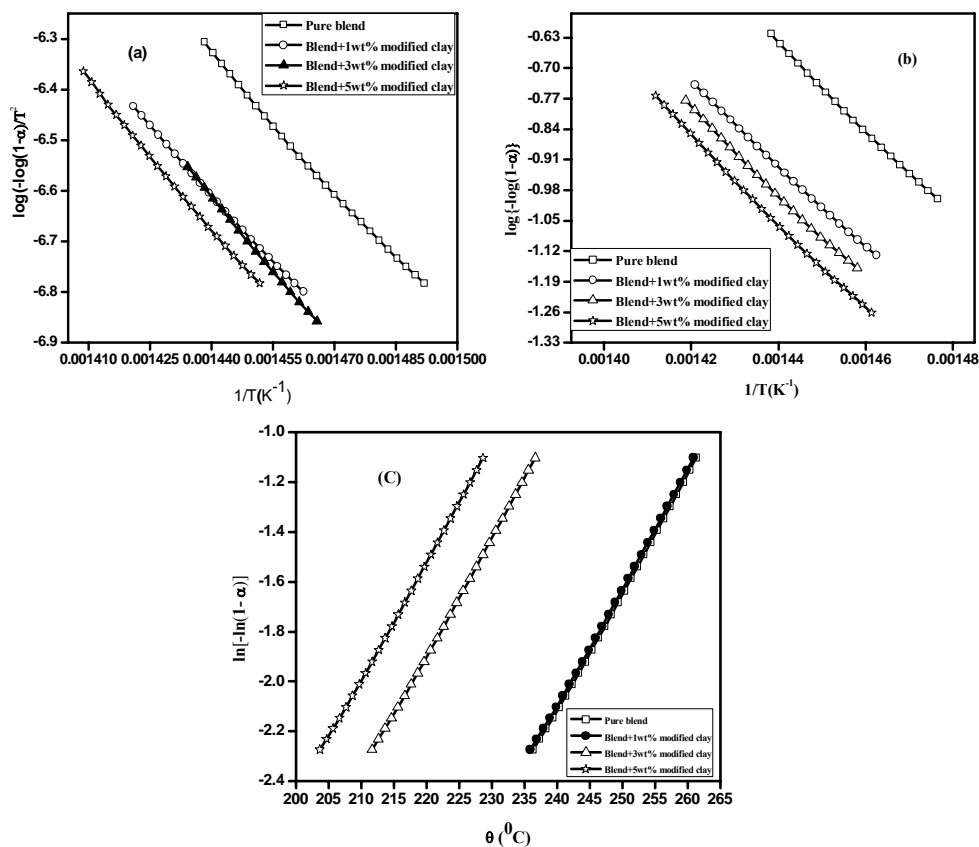


**Figure 5b.4** Kinetic plots for the determination of activation energy of PP/PS blend and nanocomposites (1, 3 & 5 wt %) using (a) Coats-Redfern equation (b) Broido's method and (c) Horowitz-Metzger equation

Lower activation energy of pure blend is due to the presence of different kinds of polymer di-radicals produced during the bond scission and unzipping processes occurring at degradation stage. In the nanocomposites the clay platelets restrain the radicals produced and prevent the decomposition reaction [17].

### 5. B.3.4 Dynamic mechanical analysis

Figures 5b.5 & 5b.6 depict the temperature dependence of storage modulus and  $\tan\delta$  for pure PP/PS blend and PP/PS/clay nanocomposites (1,

3 & 5 wt %). Table 5b.3 gives the  $T_g$  values obtained for the pure PP/PS blend and the modified nanocomposites from the  $\tan \delta$  curves. PP/PS/clay nanocomposites show higher storage modulus than pure blend. This observation clearly indicates the effect of intercalation of the polymer in nanoclay layers, leading to dispersion of nanoclay platelets in the polymer matrix [18]. After the addition of 5 wt % of nanoclay particles there is a slight decrease in storage modulus and this may be due to the agglomeration of nanoclay particles at higher loading.

**Table 5b.3 Storage moduli and  $T_g$  values of PP/PS blend and PP/PS/nanoclay composites.**

Samples	Storage modulus				$T_g$ (°C) from $\tan \delta$ curve
	45 °C	80 °C	100 °C	120 °C	
PP/PS blend	1007	525.3	374.1	159.0	114.95
PP/PS/1% modified clay	1144	618.7	445.2	194.8	113.79
PP/PS/3% modified clay	1196	661.8	481.7	199.8	113.77
PP/PS/5% modified clay	1055	583.7	411.6	171.3	113.73

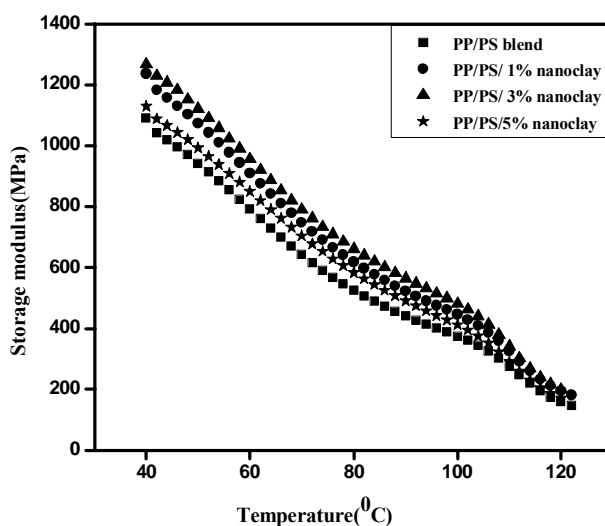


**Figure 5b.5 Storage modulus curves of PP/PS blend and PP/PS/clay nanocomposites**

The  $\tan \delta$  curves represent the ratio of dissipated energy to stored energy and relates to the  $T_g$  of the polymer.  $\tan \delta$  is useful in determining the occurrence of molecular mobility transitions such as  $T_g$ . The Figure 5b.6 clearly illustrates that there is a slight decrease in  $T_g$  with the addition of nanoclay. This reduction is attributed to the plasticizing action of the surfactant of organically modified clay which is responsible for the improved mobility of polymer chains [15].

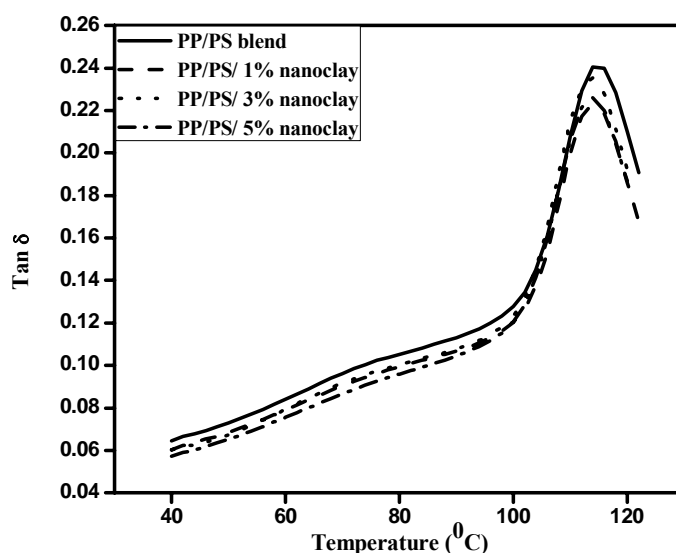


**Figure 5b.6**  $\tan \delta$  curves of PP/PS blend and PP/PS/clay nanocomposites

The relative storage moduli of PP/PS/vinyltriethoxysilane modified kaolin clay nanocomposites to those of PP/PS blend ( $E'_{PP/PS/clay}/E'_{PP/PS}$ ) are plotted in Figure 5b.7. The relative storage moduli of PP/PS/clay nanocomposites are higher than those of PP/PS blend at all temperature range. Nanocomposite with 3 wt % nanoclay shows the highest relative storage modulus and it increases with temperature. There are “hump like curves” at higher loadings and these may be attributed to the hindrance of

polymer chain movement due to the presence of clay nanoparticles [19, 20]. These “hump like curves” show the resistance to the applied stress as a result of development of polymer-nanoclay network. This network resistance increases with the nanoclay loadings and the size of the “hump” also increases.

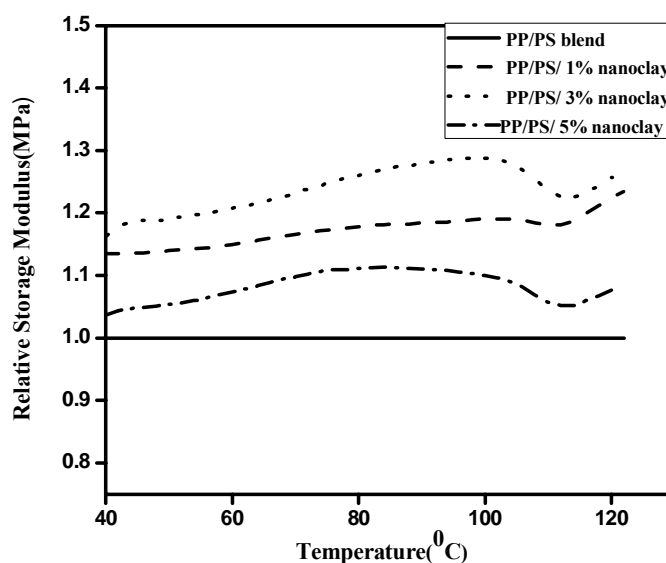


**Figure 5b.7** Relative Storage modulus curves of PP/PS blend and PP/PS/clay nanocomposites

### 5. B.3.5 Differential scanning calorimetry

DSC measures the amount of heat energy absorbed or released when the material is heated, cooled or maintained at a constant temperature. Figure 5b.8 illustrates the melting and cooling curves for PP/PS blend and blend containing 1, 3 & 5 wt % of modified nanoclay. The crystallization temperature ( $T_c$ ), the apparent melting temperature ( $T_m$ ) and the corresponding enthalpies are shown in the Table 5b.4. The  $T_m$  and  $T_c$  values for



nanocomposites are shifted towards the higher temperature range. The  $\Delta H$  values are also increased as compared to the pure polymer matrix (Table 5b.4). The significant change in  $T_c$  is due to the effective nucleating action of clay nanoparticles [1, 21].

$T_m$  and  $\Delta H_m$  follows the same trend as  $T_c$  and  $\Delta H_c$ . Figure 5b.8 also shows that there is a slight increase in melting temperature ( $T_m$ ) with increase in filler loading. This increase in  $T_m$  values signifies that the crystal structure in nanocomposites is more perfect than in polymer matrix [22]. The results show that  $\Delta H_m$  values of the nanocomposites are significantly greater than that of the neat polymer matrix. This indicates a higher thermal stability for the nanocomposites [23].

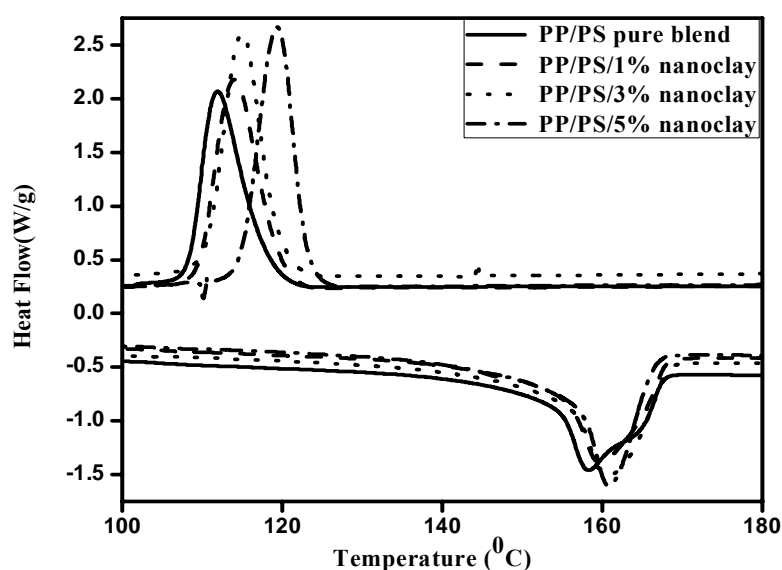


**Figure 5b.8 DSC curves for melting and crystallization curves of PP/PS/clay nanocomposites**

Table 5b.4 DSC parameters of PP/PS/clay nanocomposites

Samples	$T_c$ (°C)	$\Delta H_c$ (J/g)	$T_m$ (°C)	$\Delta H_m$ (J/g)
PP/PS blend	111.9	61.1	158.4	32.4
PP/PS/1% modified clay	114.0	71.5	159.9	38.7
PP/PS/3% modified clay	114.9	76.9	160.7	40.1
PP/PS/5% modified clay	119.3	77.0	160.9	41.0

### 5. B.3.6 Mechanical properties

#### (a) Tensile properties

The tensile strength and tensile modulus as a function of clay loadings are plotted in the Figure 5b.9. The tensile properties increases initially, reach a maximum and then fall at higher nanoclay loadings. After the addition of clay particles, the interfacial tension is lowered and results in the enhancement of interfacial adhesion of the compatibilized blends giving more efficient stress transfer between the phases during fracture [1].

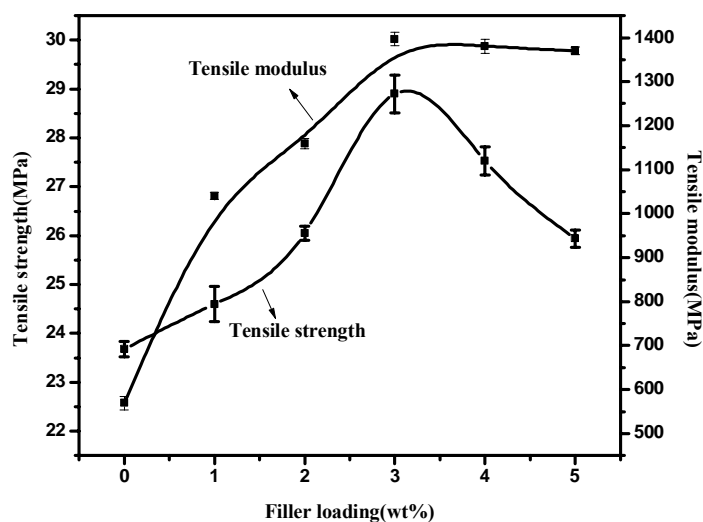


Figure 5b.9 Variation of tensile properties with nanoclay loadings

The resistance exerted by nanoclay layers against plastic deformation of the polymer and the stretching resistance of polymer chains with an extended conformation in the nanoclay gallery also contributes to the enhancement of modulus in clay nanocomposites [24].

### (b) Flexural properties

Effect of organoclay loadings on flexural properties of nanocomposites is presented in Figure 5b.10. The change of flexural strength of the samples with respect to organoclay content shows resemblance to tensile strength change. The increase in flexural strength and modulus indicates that the nanocomposites have become more rigid and less flexible.

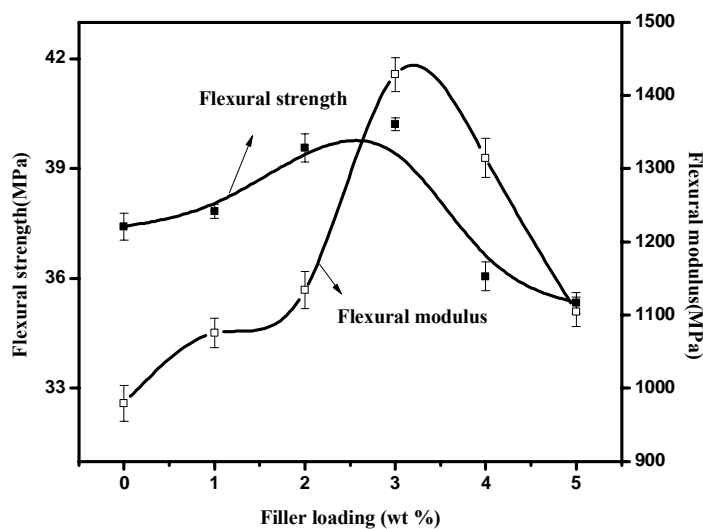
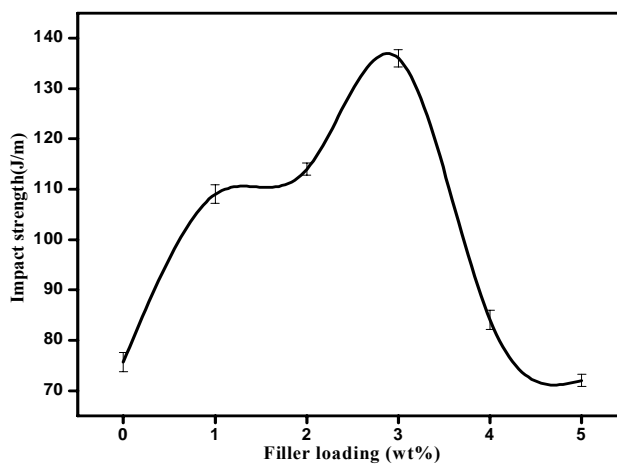


Figure 5b.10 Variation of flexural properties with nanoclay loadings

### (c) Impact strength

Figure 5b.11 depicts the change in impact strength with nanoclay loading. The maximum impact strength is found to be at 3 wt% of modified

nanoclay. The improvement is attributed to the increase in toughness of the composite with increasing nanoclay content.



**Figure 5b.11** Variation of impact strength with nanoclay loadings

The increase in impact strength of the nanocomposites is due to the interdiffusion of polymer matrix through the interlayer galleries of the modified kaolin nanoclay.

#### **(d) Hardness**

The effect of nanoclay loadings on hardness is shown in Figure 5b.12. An improvement of 33% in the hardness has been achieved by adding 3 wt % clay loading. The uniformly distributed clay layers improved the stiffness of nanocomposites. The presence of nanoclay platelets restricts the indentation and improves the hardness [25, 26].

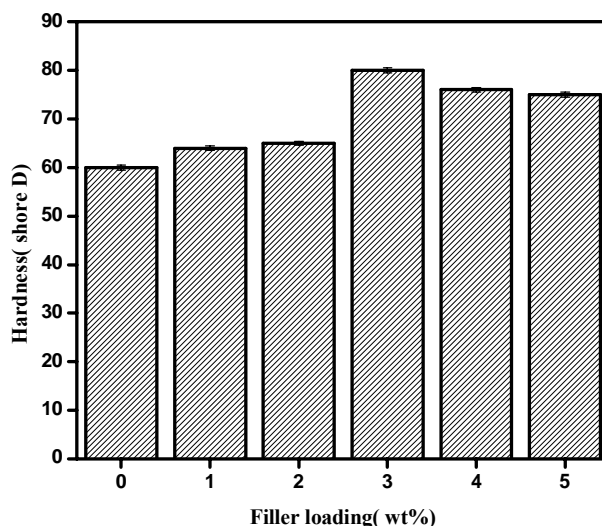


**Figure 5b.12 Variation of hardness with nanoclay loading**

The decrease in mechanical properties at higher loadings is due to the agglomeration of nanoclay particles within the polymer matrix.

#### **5. B.3.7 Effect of UV aging on the tensile properties of PP/PS/clay nanocomposite**

Figure 5b.13 displays the effect of UV aging on tensile properties of PP/PS/clay nanocomposites. Figures 5b.13 (a) & 5b.13 (b) shows the variation of tensile strength and tensile modulus with nanoclay loading before and after UV aging. From the figure it is observed that the tensile properties decrease after aging.

The polymer blend degradation study is very complex in view of the variety of interactions between the blend components. Walter *et al.* reported that in PP/PS blend, PS domain acted like a UV radiation trap. Photo degradation of PS is accelerated by acetophenone (formed as a product of

primary photodegradation step) and it interacts with the PP domains and form more reactive tertiary carbon radicals.

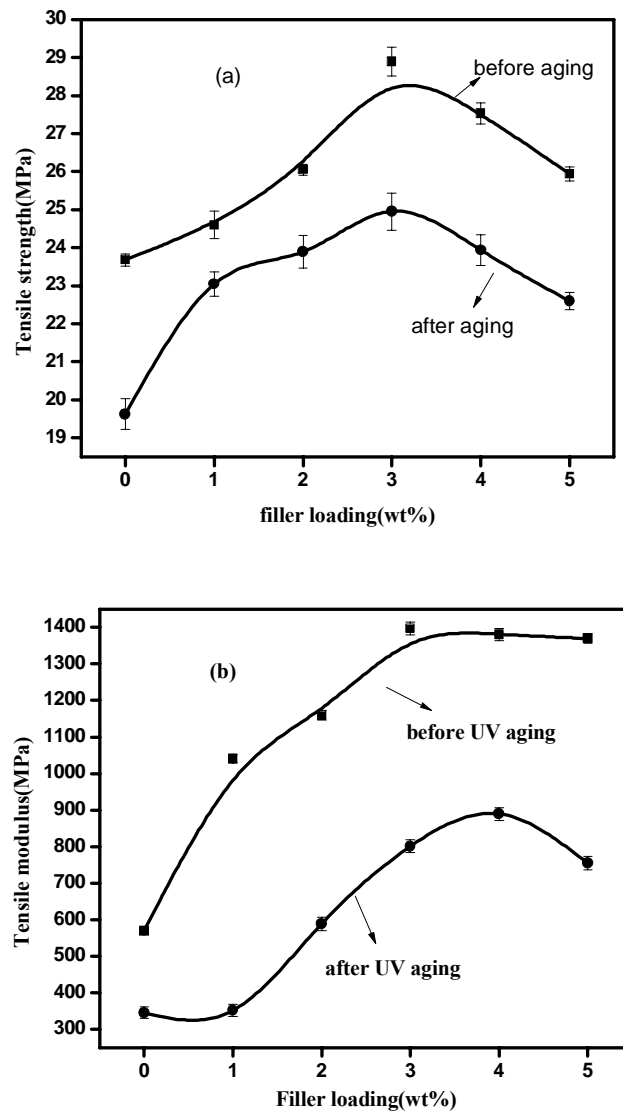
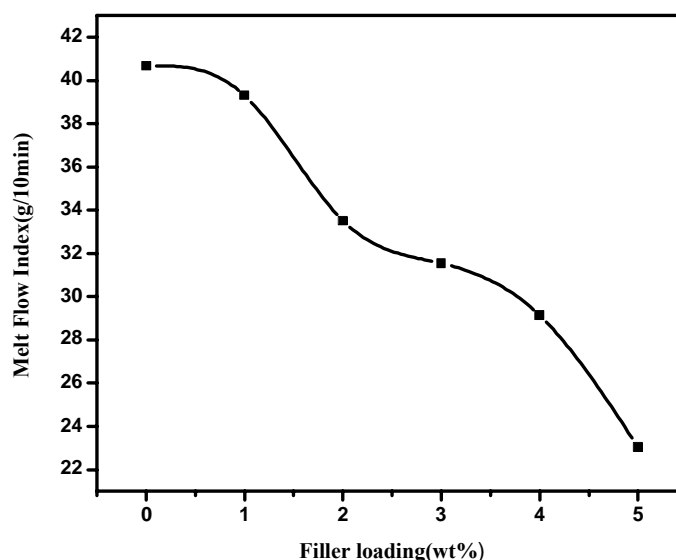


Figure 5b.13 Effect of UV aging on the (a) tensile strength (b) tensile modulus of PP/PS/clay nanocomposites

In PP/PS/clay nanocomposites, the nanoclay particles accelerate the photodegradation of PP/PS blend. Generally, nano particles had greater acceleration effect than micro particles due to its smaller size and greater interface area [27]. Several studies have been reported about the catalytic activities of nanoclays [28-30].

### **5. B.3.8 Melt Flow Index**

The variation of MFI with nanoclay loading is given in Figure 5b.14. It is clear from the figure that MFI values decrease with increasing nanoclay content. Low melt flow index indicates higher melt viscosity. The influence of nanoclay particles on MFI values can be envisaged by taking into consideration of two aspects and they are (i) the nanoclay particles act as fillers causing an increase in viscosity (ii) the dispersed nanoclay particles further prevent the flow of the polymer chains.



**Figure 5b.14** Variation of MFI with nanoclay loadings

## 5. B.4 Conclusions

The study shows that vinyltriethoxysilane modified kaolin nanoclay can act as a modifier for PP/PS blend. XRD patterns reveal a partial nanoclay exfoliation in PP/PS blend. Crystallinity and thermal stability of PP/PS blend increases by the incorporation of vinyltriethoxysilane modified kaolin nanoclay. Three kinetic methods namely Horowitz-Metzger, Broido's and Coats-Redfern are used to study the thermal degradation kinetics of PP/PS/clay nanocomposites. The studies show that activation energies increase with the addition of organo clays confirming higher thermal stability. The dynamic mechanical analysis reveals higher storage moduli for the modified clay nanocomposites over the entire temperature range (40-125<sup>0</sup>C). Mechanical properties are found to be maximum at loading of 3 wt% modified kaolin nanoclay.

## References

- [1]. Chen-Jui Hung, Hung-Yang Chuang, Feng-Chih Chang, *Journal of Applied Polymer Science*, 2008,107, 831–839.
- [2]. Joung Sook Hong, Yong Kyoung Kim, Kyung Hyun Ahn, Seung Jong Lee, *Journal of Applied Polymer Science*, 2008,108, 565–575.
- [3]. Anup K. Dhibar, Jin Kon Kim, Bhanu B. Khatua, *Journal of Applied Polymer Science*, 2011, 119, 3080–3092.
- [4]. Influence of kaolinite modification on the PVC composites properties Jitka Zykova, Alena Kalendova, Vlastimil Matejka, Petr Zadraba, Jiri Malac; *Advances in sensors, signals and materials–conference 2010*, University of Algarve, Faro, Portugal.



- [5]. Melia Guessoum, Sorya Nekkaa, Franc,oise Fenouillot-Rimlinger, Nacerddine Haddaoui, *International Journal of Polymer Science*, 2012, Article ID 549154, 9.
- [6]. B. P. Kelleher, D. Sutton, T. F. O'Dwyer, *Journal of Colloid and Interface Science*, 2002, 255, 219–224.
- [7]. Eva Mako, Janos Kristof, Erzsebet Horvath , Veronika Vagvolgyi, *Journal of Colloid and Interface Science*,2009, 330 , 367–373
- [8]. James J. Tunney, Christian Detellier, *Chemistry of Materials*, 1996, 8, 927-935.
- [9]. Yasemin Turhan, Mehmet Dog'an, Mahir Alkan, *Industrial & Engineering Chemistry Research*, 2010, 49, 1503–1513.
- [10]. Rugmini Sukumar, A. R. R. Menon, *Journal of Applied Polymer Science*, 2008, 107, 3476–3483.
- [11]. O. Turunc, M.V. Kahraman, Z.S. Akdemir, N. Kayaman-Apohan, A. Gungor, *Food Chemistry*,2009, 112 ,992.
- [12]. D. Hua, J. Tang, J. Jiang, Z. Gu, L. Dai, X. Zhu, *Materials Chemistry & Physics*, 2009,114, 402.
- [13]. Ignas K. Tonlé, Thomas Diaco, Emmanuel Ngameni, Christian Detellier; *Chemistry of Materials*, 2007, 19, 6629–6636.
- [14]. Lilian R. Avila,, Emerson H. de Faria , Katia J. Ciuffi , Eduardo J. Nassar a, Paulo S. Calefi, Miguel A. Vicente , Raquel Trujillano, *Journal of Colloid and Interface Science*,2010, 341 , 186–193.
- [15]. Adam Kiersnowski, Maria Trelinska-Wlazalk, Justyna Dolega , Jacek Piglowski, *e- polymers*, 2006,.072.
- [16]. Jordana Palacios , Rosestela Perera , Carmen Rosales , Carmen Albano , José María Pastor, *Polymer Degradation and Stability*, 2012,97, 729-737.

- [17]. Shahryar Pashaei, Siddaramaiah, Maziar Mansouji Avval, Akheel Ahmed Syed, *Chemical Industry & Chemical Engineering Quarterly* , 2011, 17 (2), 141–151.
- [18]. Yan Zhua., Hai-yun Maa., Li-fang Tonga , Zheng-ping Fang, *Chinese Journal of Polymer Science*,2008, 26 ,783–792.
- [19]. Achmad Chafidz, Ilias Ali , M. E. Ali Mohsin, Rabeh Elleithy , SaeedAl-Zahrani, *Journal of Polymer Research* , 2012, 19,9906.
- [20]. Naoki hasegawa, Hirotaka Okamoto, Makoto Kato, Arimistu Usuki, *Journal of Applied Polymer Science*, 2000, 78, 1918–1922.
- [21]. Jayita Bandyopadhyay, Suprakas Sinha Ray, Mosto Bousmina; *Journal of Industrial Engineering Chemistry*, 2007, 13(4), 614-623.
- [22]. N.A. Jamal, H. Anuar, S.B.A. Razak; *IIUM Engineering Journal*, 2010, 11(2).
- [23]. Jaydeep Khedkar, Ioan Negulescu, Efstathios I. Meletis, *Wear* 252 (2002) 361–369.
- [24]. Sanjay K. Nayaka, Smita Mohantya, Sushanta K. Samala, *Polymer-Plastics Technology and Engineering*, 2009, 48,976–988.
- [25]. Shahryar Pashaei, Siddaramaiah, Ali Souldozi1, S. Usman Taqui Syed, Akheel Ahmed Syed, *International Journal of ChemTech Research*, 2011, 3(3).
- [26]. Biplab K. Deka, Tarun K. Maj, *Journal of Applied Polymer Science*, 2012, 124, 2919–2929.
- [27]. Walter R. Waldman, Marco-A. De Paoli, *Polymer Degradation and Stability*, 2008, 93, 273-280.
- [28]. Mustapha Kaci, Cherifa Remili, Stephane Bruzard and Yves Grohens, *Academic Journal of Manufacturing Engineering*, 2010, 8(1).

- [29]. Cherifa Remili, Mustapha Kaci, Souad Kachbi, Ste'phane Bruzaud, Yves Grohens, *Journal of Applied Polymer Science*, 2009, 112, 2868–2875.
- [30]. J. Singala, A. A. Mungray, A. K. Mungray, *Industrial & Engineering Chemistry Research*, 2012, 51, 10557–10564.

.....✂.....

## Chapter 6

---

# **Polypropylene/ Polystyrene/ clay nanocomposites: Effect of compatibilizers**

---

<i>Contents</i>	<b>Part A</b>
	<b>Polypropylene/ Polystyrene/Itaconic acid /modified kaolin clay nanocomposites</b>
	6. A.1 Introduction
	6. A.2 Methodology
	6. A.3 Results and Discussion
	6. A.4 Conclusions
	<b>Part B</b>
	<b>Polypropylene/ Polystyrene/Dimethyl itaconate/modified kaolin clay nanocomposites</b>
	6. B.1 Introduction
	6. B.2 Methodology
6. B.3 Results and Discussion	
6. B.4 Conclusions	

---

**Part-A****Polypropylene/ Polystyrene/Itaconic acid /modified kaolin clay nanocomposites****Abstract**

*Itaconic acid compatibilized Polypropylene/Polystyrene clay nanocomposites were prepared by melt blending technique. The effect of modified clays and compatibilizer on the properties of nanocomposites was investigated. The degree of dispersion and morphology of nanocomposites were investigated by X-ray diffraction, Transmission Electron microscopy and Scanning electron microscopy. The prepared nanocomposites were characterized using DSC and TGA. Thermogravimetric analysis shows improved thermal stability for compatibilized PP/PS/clay nanocomposites. The dynamic mechanical analysis reveals higher storage moduli over a temperature range of 40–125 °C for nanocomposites. The XRD and TEM results show the increased distribution of nanoclay layers, indicating enhanced compatibility between the polymer and nanoclay with the addition of compatibilizer.*

**6. A.1 Introduction**

Polymer clay nanocomposites have attracted great interest in research and industry, as they exhibit enhanced mechanical, thermal, and barrier properties. PP and PS used in this study are immiscible and modified kaolin nanoclay is used as an interfacial modifier. Depending upon the hydrophilic/hydrophobic balance of a polymer, the polymer chains could enter into the interlayer space of the nanoclay and form either tactoid, intercalated or exfoliated nanocomposites. It can be seen that the extent of intercalation and exfoliation of the clay platelets by the polymer chains determines the degree of enhancement of mechanical, thermal and barrier properties. Due to the strong hydrophilic nature of the nanoclays, adhesion between clays and non-polar polymers is low and the dispersibility of nanoclay layers in polymer

matrix is limited. In order to improve dispersibility of nanoclay in polymer matrices grafted polymers are used as compatibilizers. Compatibilizer containing polar groups can be intercalated between the nanoclay layers by hydrogen bonding. This increases the interlayer spacing of clay gallery and weakens the interaction between the layers. Dispersion of clay layers in polymer matrix can be improved by subjecting to high shearing forces [1, 2]. In a study by Yan Zhu *et al.* [3], the degree of dispersion of Na-montmorillonite in PP/PS blend prepared by melt intercalation was improved by the addition of maleic anhydride and sulfonic group as compatibilizers on modified PP and PS phase respectively. Oana M. Istrate *et al.* used maleated PP as the compatibilizer for PS/PP blend and showed that in the compatibilized PS/PP blend the nanoclay particles were located in both the phases resulting in improved mechanical properties [4].

In this part of study itaconic acid (IA), a non oil- based dicarboxylic acid monomer is used as a compatibilizer for PP/PS blend. Itaconic acid is obtained through large-scale fermentation of agricultural wastes such as molasses, a sub-product of sugar industry. Due to its double functionality, IA and its derivatives offer interesting possibilities as polar functional monomers for the modification of nonpolar polymers [5]. Better dispersion is likely to be achieved using itaconic acid as compatibilizer, which can enhance the intercalation of the polymer chains within the nanoclay gallery. Mehrdad Yazdani –Pedram *et al.* compared the effect of two compatibilizers, maleic anhydride (MA) and itaconic acid (IA) as a coupling agent in the preparation of mineral filled PP composites and they found that the PP-g-IA compatibilized nanocomposites showed enhancement in mechanical properties than PP-g-MA compatibilized nanocomposites[6]. Similar results

were obtained for Edwin Moncada *et al.* and the studies indicated that IA-grafted PP was far more efficient as compatibilizer for the formation of nanocomposites than commercially available maleic anhydride-grafted PP [5]. In this study IA is added directly into PP/PS clay nanocomposites. The hydroxyl group of clay reacts with IA and disperses the nanoclay well within polymer matrix through in situ compatibilization. The compatibilizer was prepared by grafting reaction of IA onto PP/PS blend in the presence of dicumyl peroxide (DCP) initiator. The aim of this study is to determine the effect of the [Polypropylene/Polystyrene]-g-itaconic acid ([PP/PS]-g-IA) as a compatibilizer in the mechanical, thermal and morphological properties of PP/PS/clay nanocomposite.

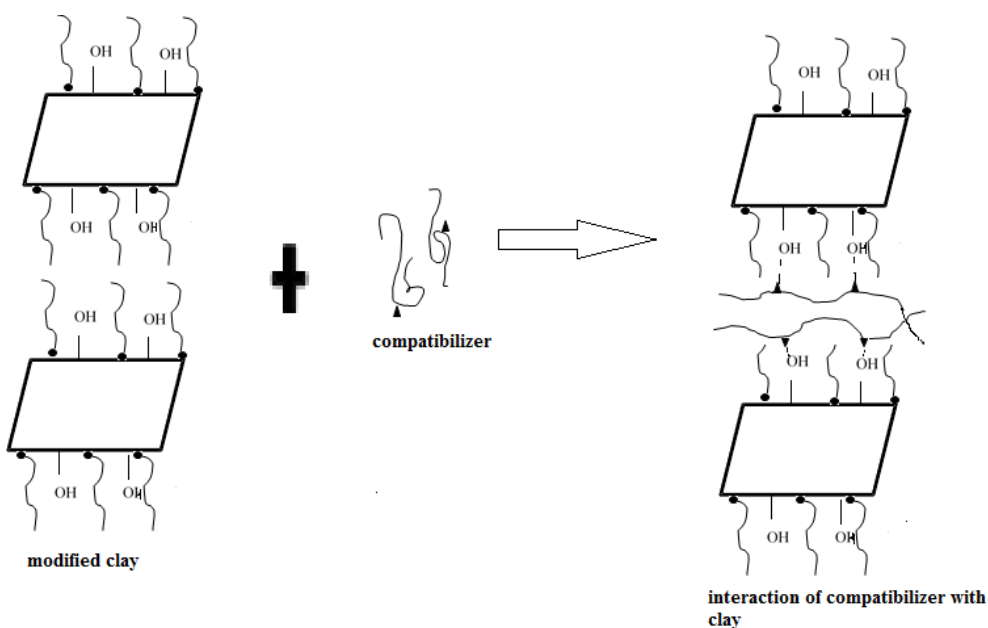


**Figure 6a.1** Schematic representation for the interaction of modified kaolin nanoclay with [PP/PS]-g-IA

## **6. A.2 Methodology**

### **6. A.2.1 Materials**

The details of the polymers and nanoclay types used for the study are discussed in Chapter 2 (sections 2.1.1, 2.1.2& 2.1.3). The details of itaconic acid used for the study are discussed in section 2.1.6.

### **6. A.2.2 Preparation of the compatibilized blend and its characterization**

The compatibilizer was prepared by grafting reaction between IA and PP/PS blend in the presence of DCP initiator at 170 °C at 50 rpm for 8 min by melt mixing in a Thermo Haake PolyLab system equipped with roller rotors. PP and PS were allowed to melt for 2 min initially. In the first series of experiment the concentration of DCP was varied (0.03-0.9wt %) and the concentration of itaconic acid (IA) was kept constant at 1 wt%. In the second series of experiments the optimum amount of IA was found by varying the concentration of IA (1, 2, 3,4,5,7,9,11 wt %) and keeping the concentration of DCP constant. The grafting reaction was monitored using soxhlet extraction. Samples were compressed into thin films, cut into small pieces, and then put in contact with acetone using soxhlet apparatus for 16 h to remove the unreacted IA. It was finally dried in a vacuum oven at 70 °C for 12 h. The product before and after soxhlet extraction was weighed, percentage of grafting was determined.

### **6. A.2.3 Nanocomposite preparation**

PP/PS (80/20) blends were mixed with modified kaolin nanoclays and the compatibilizer using a Thermo HAAKE PolyLab system equipped with roller rotor operating at 180 °C and 50 rpm for 8 min. The resulting compounds



were hot pressed into sheets and cut into pieces. The material was then injection molded at 190 °C. Figure 6a. 1 shows the interaction of modified kaolin nanoclay with compatibilizer. The tensile properties, flexural properties, impact strength, hardness, dynamic mechanical analysis, thermal properties and morphological properties were analyzed according to various standards as described in Chapter 2(section 2.2.3).

#### *Fourier Transform Infrared Spectroscopy (FTIR)*

The grafting of IA on the blend was confirmed by the FTIR spectra recorded on a Thermo Nicolet FTIR Spectrometer Model Avatar 370. Samples in the form of thin films  $\approx$  1 mm thickness were employed.

### **6. A.3 Results and Discussion**

#### **6.A.3.1 Effect of initiator (DCP) concentration on the mechanical properties of PP/PS/blend**

##### **(a) Tensile properties**

The variation of tensile properties with initiator loading is presented in Figures 6a.2 & 6a.3. The initiator concentration is one of the most important parameter affecting grafting reaction. The radical formed by the decomposition of the initiator activates the polymer by transferring the radical to the polymer chain. The results show an increase in tensile strength and tensile modulus from 0 to 0.5 wt % DCP after that the values decrease with further increase of DCP concentration. The free radical concentration increases with increasing DCP loading. These radicals abstract hydrogen from PP and PS macromolecule and form active sites on the backbone. These active chains undergo chain transfer reaction resulting in the formation of new active sites. Thus grafting increases with chain transfer and hydrogen abstractions resulting in increase of tensile properties [7, 8].

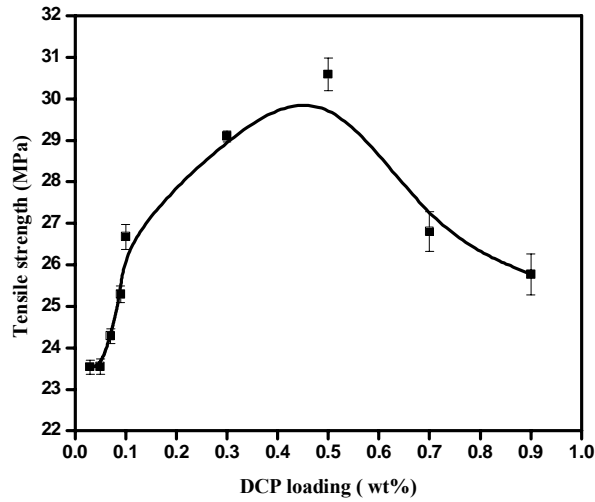


Figure 6a.2 Variation of tensile strength with DCP loading

However increase of DCP concentration above 0.5wt% increases the radical concentration to such an extent that termination reactions also increase. This leads to a decrease in properties of the composite. Similar results were reported by Isiklan *et al.* in their study [9].

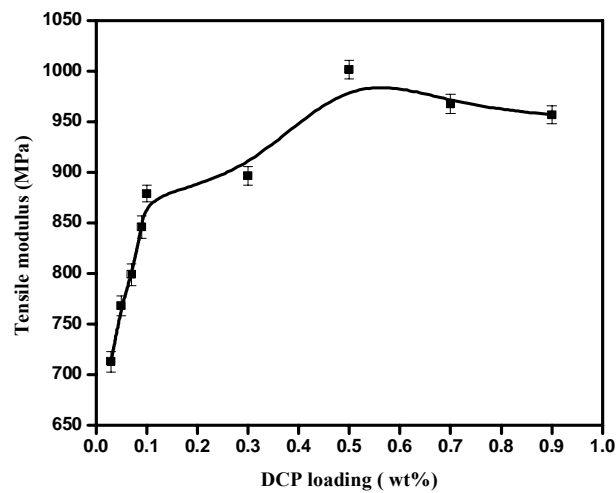


Figure 6a.3 Variation of tensile modulus with DCP loading

**(b) Flexural properties**

Variation of flexural strength and flexural modulus of the composites as a function of DCP loading is plotted in Figures 6a.4 & 6a.5. There is a significant increase in the flexural modulus and strength as in the case of the tensile properties. Hence 0.5wt% is taken as optimum DCP loading for the further studies.

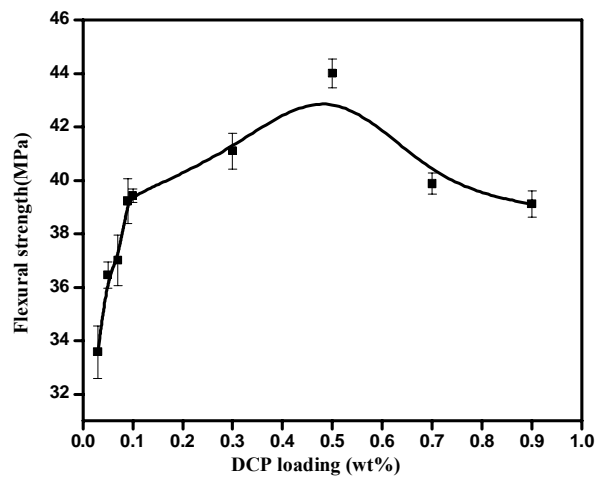


Figure 6a.4 Variation of flexural strength with DCP loading

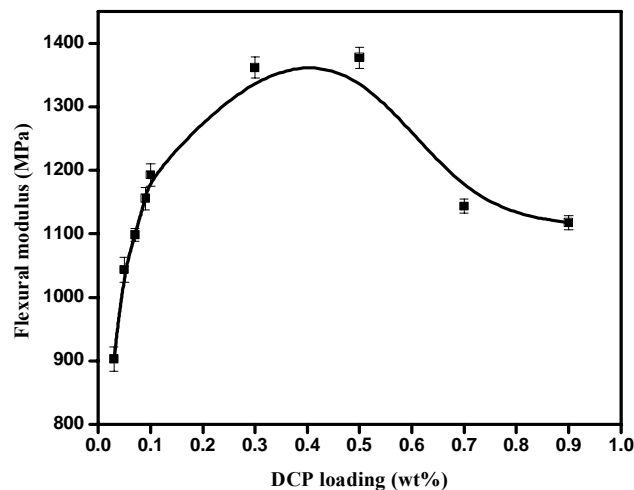


Figure 6a.5 Variation of flexural modulus with DCP loading

### 6.A.3.2 Evidence of grafting IA onto PP/PS blend

#### 6.A.3.2.1 Fourier Transform Infrared Spectroscopy

The existence of grafted IA in PP/PS was confirmed by FTIR spectroscopy. Figure 6a.6 illustrates the FTIR spectrum of PP/PS blend and IA functionalized PP/PS blend. FTIR spectrum of the PP/PS grafted with IA {[PP/PS]-g-IA} showed two absorption bands in the carbonyl region which is absent in the spectrum of PP/PS blend. The absorption band at  $1705\text{ cm}^{-1}$  is due to stretching vibrations of the carbonyl groups of the carboxylic acid of the itaconic acid. The second absorption band at  $1788.53\text{ cm}^{-1}$  is due to a carbonyl absorption band coming from itaconic acid grafted as anhydride during the grafting reaction [10].

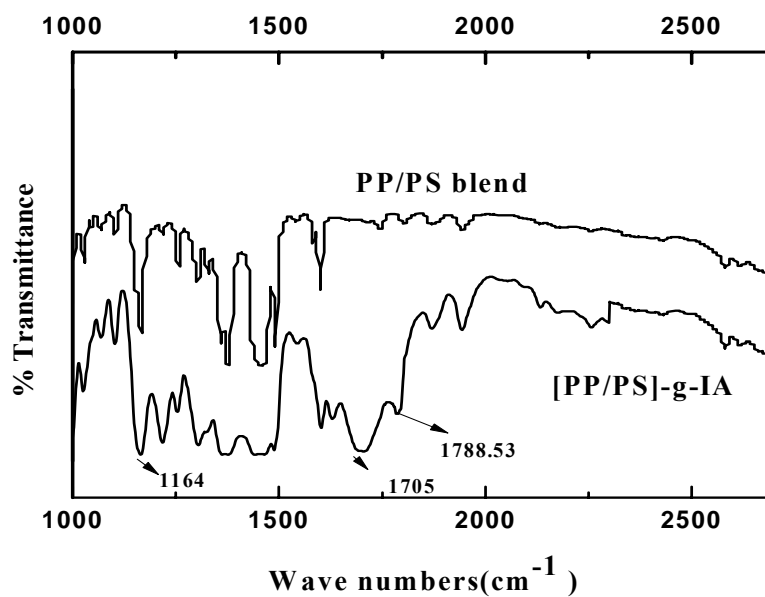


Figure 6a.6 FTIR spectrum of PP/PS blend and IA functionalized PP/PS blend

### 6. A.3.3 Effect of itaconic acid concentration on the mechanical properties of PP/PS blend

#### (a) Tensile properties

Figures 6a.7 & 6a.8 displays the variation of tensile properties with itaconic acid (IA) loading at 0.5wt% DCP content. From the figure it is noticed that the increase in IA concentration leads to an increase in tensile properties up to 3 wt % and then shows a decline in values. The maximum tensile properties occur at 3wt % loading and grafting yield is found to be 2.5%. With increase in IA concentration, hydrogen abstraction from PP and PS backbone also increases leading to higher grafting efficiency and increase in properties. Further increase in IA concentration, increases the concentration of Poly (Itaconic acid) [PIA] macroradicals leading to homopolymerization of IA [9, 11].

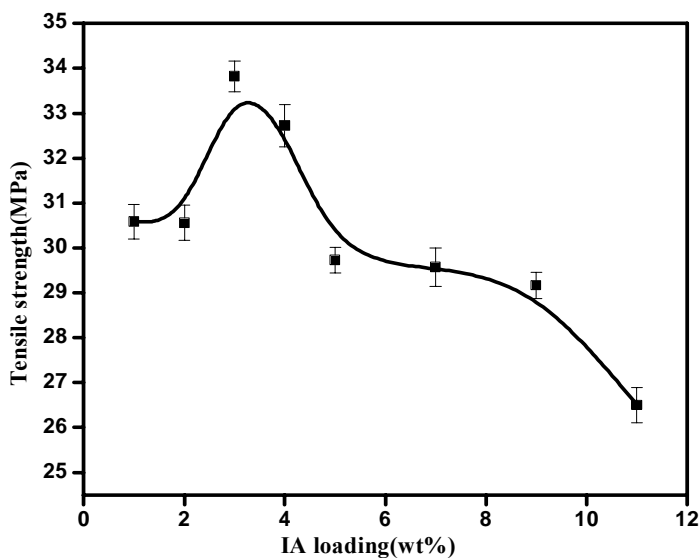
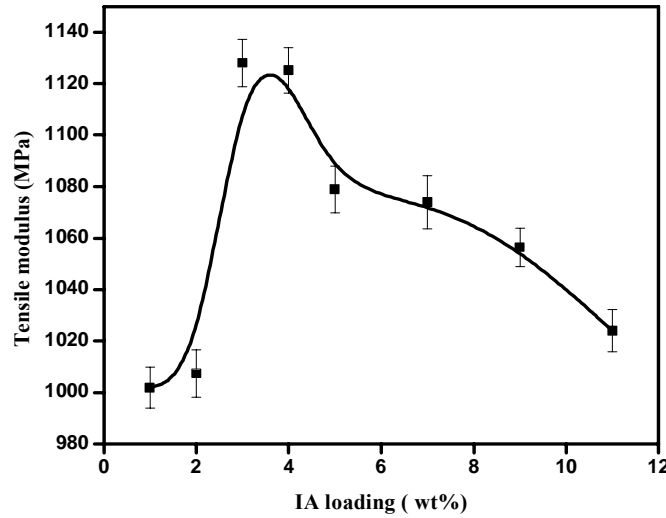


Figure 6a.7 Variation of tensile strength with IA loading



**Figure 6a.8 Variation of tensile modulus with IA loading**

**(b) Flexural properties**

Variation of flexural strength and flexural modulus of the composites are plotted as a function of IA content is given in Figures 6a.9 & 6a.10.

Flexural properties reach a maximum at 3 wt %.

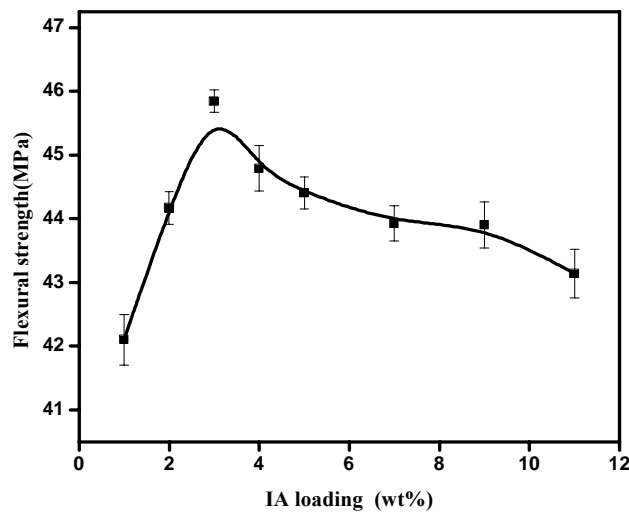


**Figure 6a.9 Variation of flexural strength with IA loading**

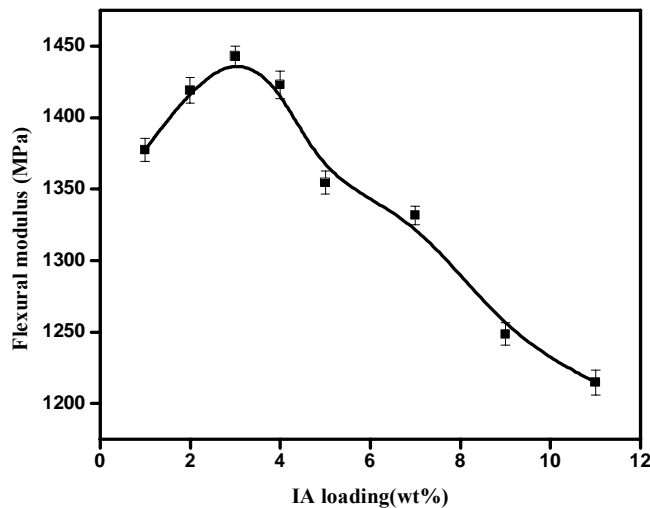
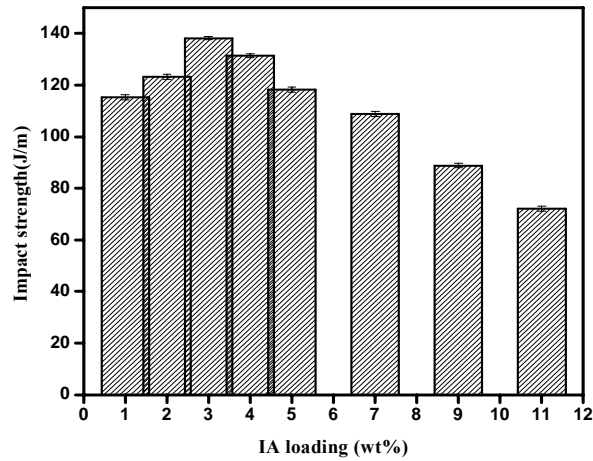


Figure 6a.10 Variation of flexural modulus with IA loading

### (c) Impact strength

PP/PS blend used in this study is immiscible as evidenced by large solubility parameter differences that lead to poor interfacial adhesion. Such non-bonded interfaces are excellent crack deflection sites that can deflect fast propagating cracks in brittle polymers such as polystyrene. Deflection generates tortuous crack path through the composite, increasing the work of fracture and toughness. The non-bonded interfaces prevent load transfer across the interface and thus results in weakening of the material. So in order to improve the properties compatibilizers are used. The impact strength of the composites is plotted as a function of IA content in Figure 6a.11. From the figure it is evident that the maximum improvement of impact strength is obtained at 3 wt% of IA loading. Hence 3 wt% was taken as optimum IA content for further studies. Thus itaconic acid has a compatibilizing effect on the interface between PP and PS, and thus increases energy absorption mechanisms and impact resistance.



**Figure 6a.11 Variation of impact strength with IA loading**

#### **6. A.3.3.1 Melt Flow Index (MFI)**

Figure 6a.12 indicates the variation of MFI value with itaconic acid loading. It is clear from the figure that the MFI values increases with increasing itaconic acid. The melt flow index is a measure of the ability of the material to flow, and thus, grafted PP has a higher flow speed in the molten state, which indicates a lower viscosity of the material [12, 13].

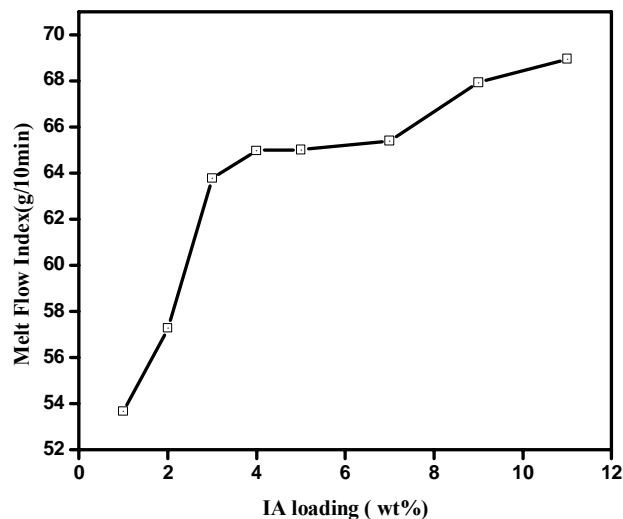


**Figure 6a.12 Variation of MFI with IA loading**



### 6. A.3.4 Effect of itaconic acid (IA) grafting on the properties of PP/PS/ clay nanocomposites

#### (a) Tensile properties

Tensile strength and tensile modulus of [PP/PS]-g-IA/modified kaolin clay composite with different levels of nanoclay contents are illustrated in Figures 6a.13 & 6a.14. Since maximum improvement in mechanical properties are obtained at 3 wt% of IA content and 0.5wt% DCP content, this composite is selected for nanoclay modification.

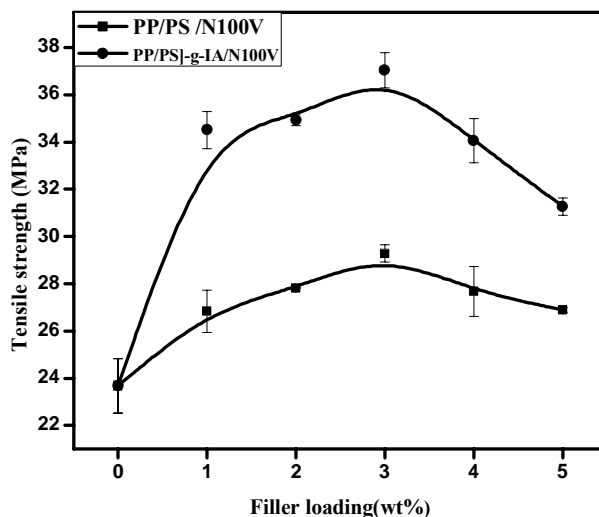
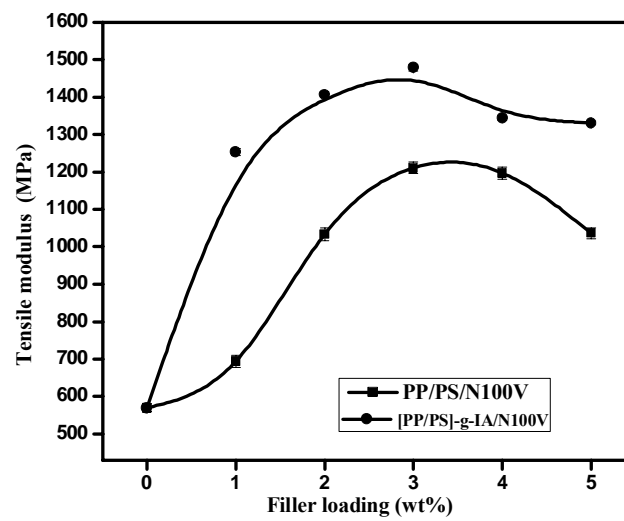


Figure 6a.13 Variation of tensile strength with filler loading

Comparing PS/PP/N100V with [PP/PS]-g-IA/N100V nanocomposite, it is observed that the tensile strength and moduli increased by 26 and 22%, attesting to the uniform dispersion of the stiff nanoclay. This improvement may be due to better stress transfer and increased interfacial interaction. A homogeneous dispersion of nanoclay layers in a polymer matrix will give maximum reinforcement via load transfer and deflection of cracks resulting

from an applied load. The improvement in mechanical properties is due to better dispersion of nanoclay particles when [PP/PS]-g-IA is used as the compatibilizer. Thus the addition of [PP/PS]-g-IA promoted more interaction between nanoclay–polymer and thus significantly increased the stiffness of the PP/PS/clay nanocomposites.



**Figure 6a.14** Variation of tensile modulus with filler loading

**(b) Flexural properties**

Figures 6a.15 & 6a.16 gives the effect of [PP/PS]-g-IA on the flexural strength and flexural modulus of PP/ PS/clay nanocomposites reinforced with N100V. The flexural strength and modulus increases by 3 % and 1.45 % in the case of [PP/PS]-g-IA/N100V composites when compared to PP/PS/N100V nanocomposites. The degree of dispersion of nanoclay particles is improved by the addition of [PP/PS]-g-IA and results in better stress transfer due to improved interfacial adhesion. The improvement in flexural properties could be attributed to the high stiffness and aspect ratio of

silicate layers. This is attributed to the compatibilizing effect of [PP/PS]-g-IA which improved the interfacial adhesion and promoted the degree of exfoliation of nanoclay layers in the PP/PS matrix [14].

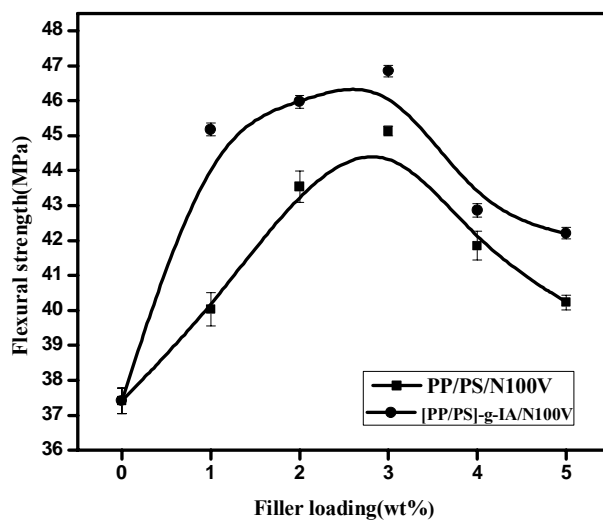


Figure 6a.15 Variation of flexural strength with filler loading

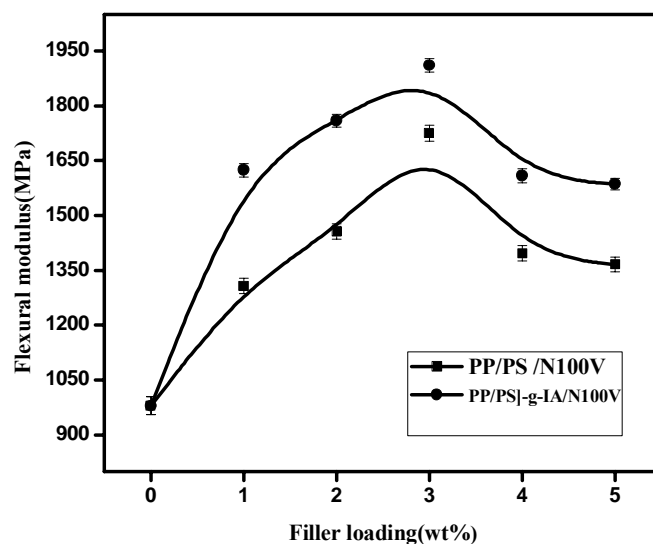


Figure 6a.16 Variation of flexural modulus with filler loading

**(c) Impact strength**

From the Figure 6a.17 it is clear that the incorporation of itaconic acid leads to an increase in impact strength of PP/PS blend i.e. increased by 64 % ([PP/PS]-g-IA/N100V) than the corresponding nanocomposites. The enhanced impact strength may be attributed to the improved interfacial adhesion between PP/PS due to the presence of compatibilizer and modified nanoclays. This substantial improvement shows the ability of [PP/PS]-g-IA to act as an impact modifier and compatibilizer. The presence of organoclay platelets, especially in the compatibilized systems allows deforming to larger strain before crack propagation takes place [15]. After reaching a maximum the impact strength shows a reverse trend. However at higher clay loadings the embrittlement and weak resistance of crack propagation plays a major role. Shanti V. Nair *et al.* studied the fracture initiation and fracture propagation toughening of polyamide 6,6 (PA-66) polymers with different types of layered silicate clay having nanoscale (fully dispersed) or multiscale (mixed nanoscale/microscale) structure. According to Nair, the reduction in toughness of polyamide 6,6/clay nanocomposites is due to the formation of micro cracks in the crack-tip region in the vicinity of reinforcement– matrix interfaces, which enhance the local stress fields in the crack-tip region and tend to reduce toughness [16]. Thus it is of interest to note that the nanocomposites containing grafted polymers show higher toughness without a reduction in strength and stiffness.

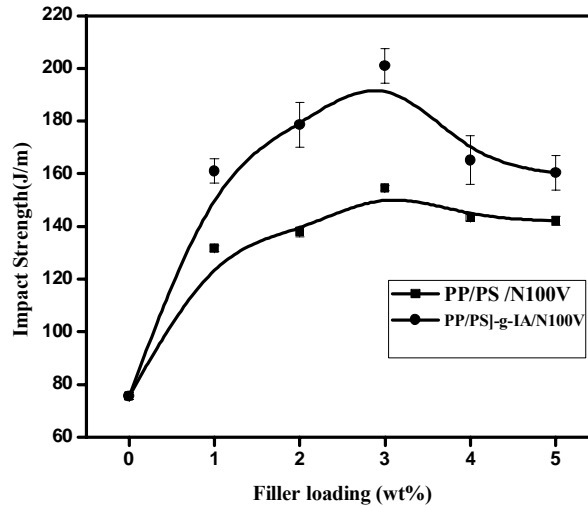


Figure 6a.17 Variation of impact strength with filler loading

(d) Hardness

Figure 6a.18 reveals the variation of hardness with increasing nanoclay loading in the presence of itaconic acid. The surface hardness of the compatibilized nanocomposites increases with nanoclay content reaches a maximum and then decreases.

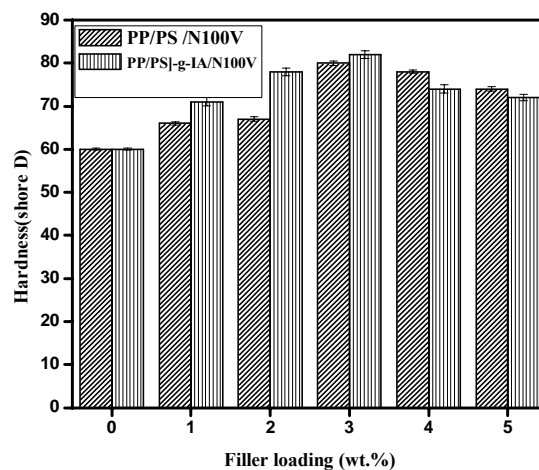


Figure 6a.18 Variation of hardness with filler loading

The increase in hardness in polymer clay nanocomposites is due to the improvement in interfacial adhesion in the presence of compatibilizer.

### 6. A.3.5 Melt Flow Index (MFI)

Figure 6a.19 illustrates the variation of MFI with filler loading. From the figure it is evident that MFI decreases with increasing nanoclay loadings. The increase in viscosity increases with nanoclay loading. The degree of dispersion of nanoclay particle in the matrix increases with the addition of itaconic acid, which may be attributed to the interaction between the nanoclay and the polymer matrix

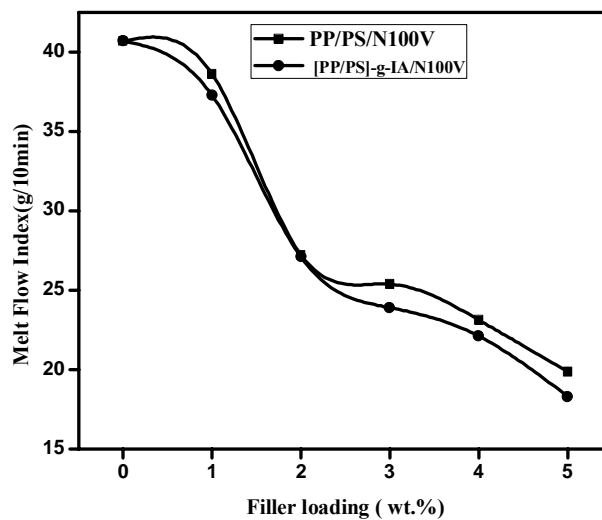
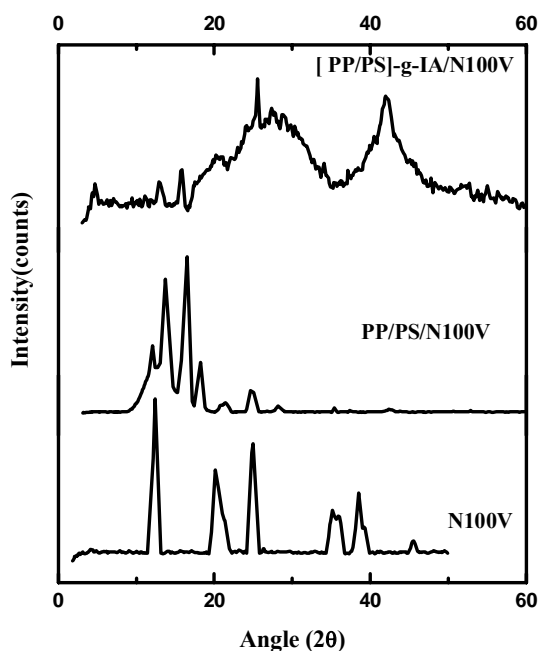


Figure 6a.19 Variation of MFI with filler loading

### 6. A.3.6 X-ray Diffraction

XRD is used to analyze the morphology of [PP/PS]-g-IA/clay nanocomposite. Figure 6a.20 exhibits the XRD patterns of Nanocaliber 100V, PP/PS/N100V and [PP/PS]-g-IA/clay nanocomposite (3wt%). N100V has its characteristic peak at  $12.44^\circ$  with an intergallery spacing of

7.11 nm. The shifting of clay peak position to lower  $2\theta$  region increases the d-spacing to 7.32 nm in the PP/PS/N100V nanocomposite. This indicates the intercalation of polymer chains into the nanoclay galleries.



**Figure 6a.20 XRD patterns of Nanocaliber100V, PP/PS/N100V and [PP/PS]-g-IA/clay nanocomposite (3wt %)**

There is a broadening of peak and reduction of intensity in IA compatibilized nanocomposites which shows a good dispersion of clay layers in the polymer matrix. This confirms a high degree of intercalation or partial exfoliation of nanoclay in the nanocomposite. The [PP/PS]-g-IA contain two acid carbonyl groups as well as anhydride carbonyl groups capable of forming a greater number of hydrogen bonds with hydroxyl groups of the nanoclay surface [5]. This enhances the dispersion of nanoclay particles in polymer matrix [17]. The improvement in properties is due to the increase in polarity of the matrix which enhances the interactions and improves the dispersion.

### 6. A.3.7 Transmission electron microscopy

TEM bright field image of IA compatibilized clay nanocomposite at 1 $\mu$ m and 20 nm is shown in the Figures 6a.21(a) and 6a.21(b). The bright phase of the picture is the matrix phase, and the dark phase is the particle phase. The dark entities are the cross section of intercalated nanoclay layers.

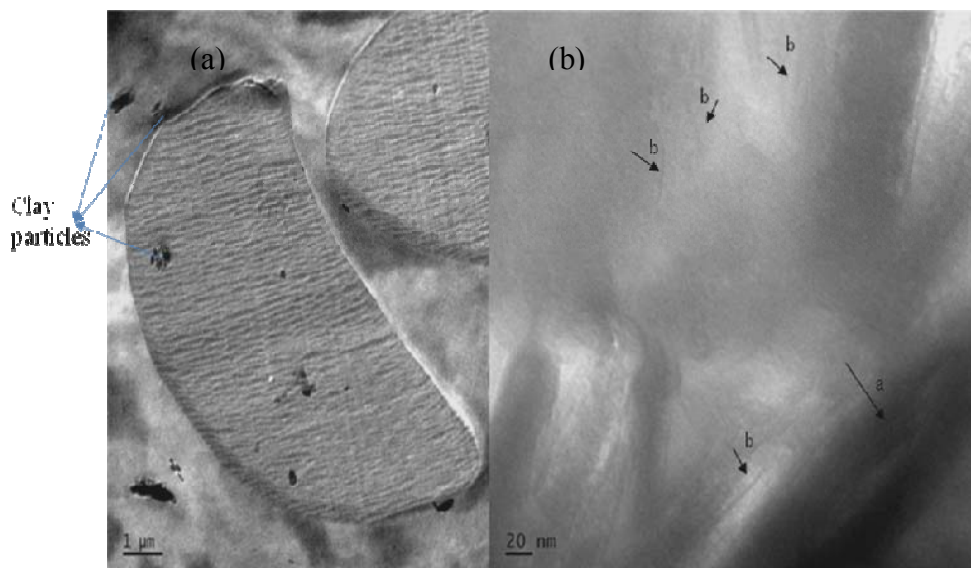


**Figure 6a.21 Transmission electron microscopic bright field images of IA compatibilized nanocomposite at (a) 1  $\mu$ m and at (b) 20 nm (intercalated and exfoliated structure present in the microstructure of nanocomposite is marked by 'a' and 'b')**

TEM microscopic photographs of PP/PS/N100V are shown in Chapter 3 (Section 3.3.2, Figure 3.5 & 3.8). In the compatibilized polymer nanocomposite the clay particles are randomly distributed throughout the polymer matrices as evidenced from Figure 6a.21(a). It is clear from the Figure 6a.21(b) that nanoclay particles are well dispersed in the polymer matrix in the presence of compatibilizer. High magnification TEM images revealed that although there is intercalated nanoclay layers present marked



by 'a', single exfoliated layers is also prevalent in some areas near the intercalated layers indicated by 'b'.

#### 6. A.3.8 Scanning electron microscopy (SEM)

The typical morphology of tensile fractured cross-section of IA grafted PP/PS/clay nanocomposite reinforced with N100V is presented in Figure 6a.22.

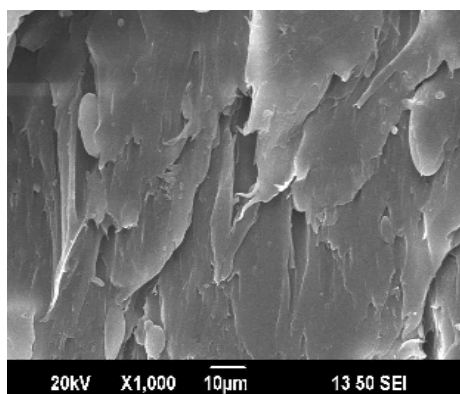


**Figure 6a.22 SEM photographs of PP/PS]-g-IA/N100V nanocomposite**

From the SEM photographs it is discernible that blends containing grafted polymers show a homogeneous morphology revealing a better exfoliation. Figure clearly illustrates that [PP/PS]-g-IA is very efficient as a coupling agent for nanoclay particles and polymer matrix. Therefore, the improved homogeneity increases the tensile and flexural properties.

#### 6. A.3.9 Thermogravimetric Analysis

TG analysis gives the effect of N100V and the compatibilizer (IA) in the thermal degradation of PP/PS blend. Figure 6a.23 shows the TG curves for PP/PS blend, PP/PS/N100V and [PP/PS]-g-IA/3wt%N100V nanocomposites.

Table 6a.1 presents the results obtained from DTG curves of [PP/PS]-g-IA/clay nanocomposites

**Table 6a.1 Thermal characteristics of IA compatibilized clay nanocomposites**

Samples	50% mass loss (°C)	Tonset (°C)	Tmax (°C)	Residue at 600 °C (%)	OI
PP/PS Pure blend	426.6	370.5	434.4	0.456	0.032
PP/PS/ N100V	446.4	397.3	460.7	1.77	0.124
[PP/PS]-g-IA/3%N100V	448.8	389.1	462.2	1.88	0.131

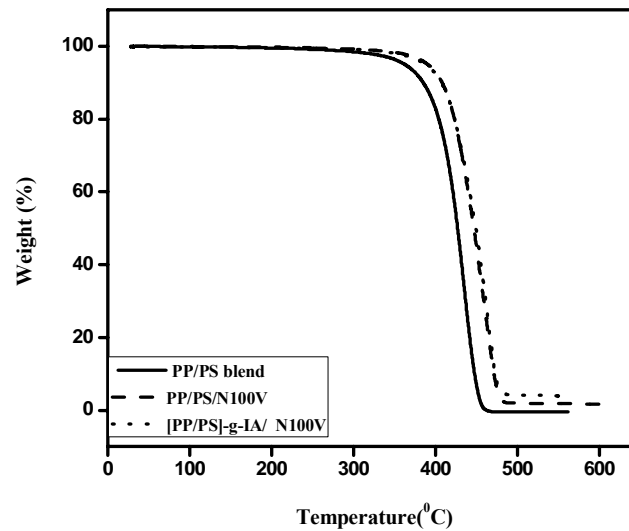


**Figure 6a.23 TG curves of PP/PS blend, PP/PS/N100V and [PP/PS]-g-IA/N100V nanocomposites**

Addition of compatibilizer (3 wt %) to the PP/PS/clay nanocomposites increases the thermal stability. This increase in thermal stability is due to the adsorption of volatile products on the nanoclay and it indicates that the dispersion of nanoclay particles is improved by the addition of compatibilizer in polymer [18]. It is apparent from the Table 6a.1 that the

oxidation index values for [PP/PS]-g-IA/clay nanocomposites is higher than that of pure blend; hence higher thermal stability.

#### 6. A.3.9.1 Kinetic analysis of thermal decomposition

The Coats Redfern (CR), Broido's (BR) and Horowitz-Metzger (HM) plots for the thermal degradation of itaconic acid grafted PP/PS/clay nanocomposites from the onset degradation temperature to the maximum degradation temperature are presented in the Figure 6a.24. The activation energy for each method is given in Table 6a.2.

**Table 6a.2 Activation energy (J/mol) calculated by Horowitz-Metzger (HM), Broido's (BR) and Coats-Redfern (CR) methods of IA grafted PP/PS/clay nanocomposite**

Samples	Coats – Redfern	Broido's	Horowitz-Metzger
PP/PS blend	174	181	175
PP/PS/N100V	196	228	196
[PP/PS]-g-IA/N100V	199	229	202

The IA grafted PP/PS/clay nanocomposite show higher activation energy  $E_a$  than that of PP/PS blend. The dispersion of clay particles in the polymer matrix is improved in the presence of IA. The enhanced thermal stability of the nanocomposites is credited to strong interaction between the polymer matrix and nanoclay surface through chemical linkage between compatibilizer and nanoclays, which in turn arbitrates the surface polarity of nanoclay and polymer/nanoclay interface. The organoclay delays volatilizations of the products generated during carbon-carbon bond scission of the polymer matrix.

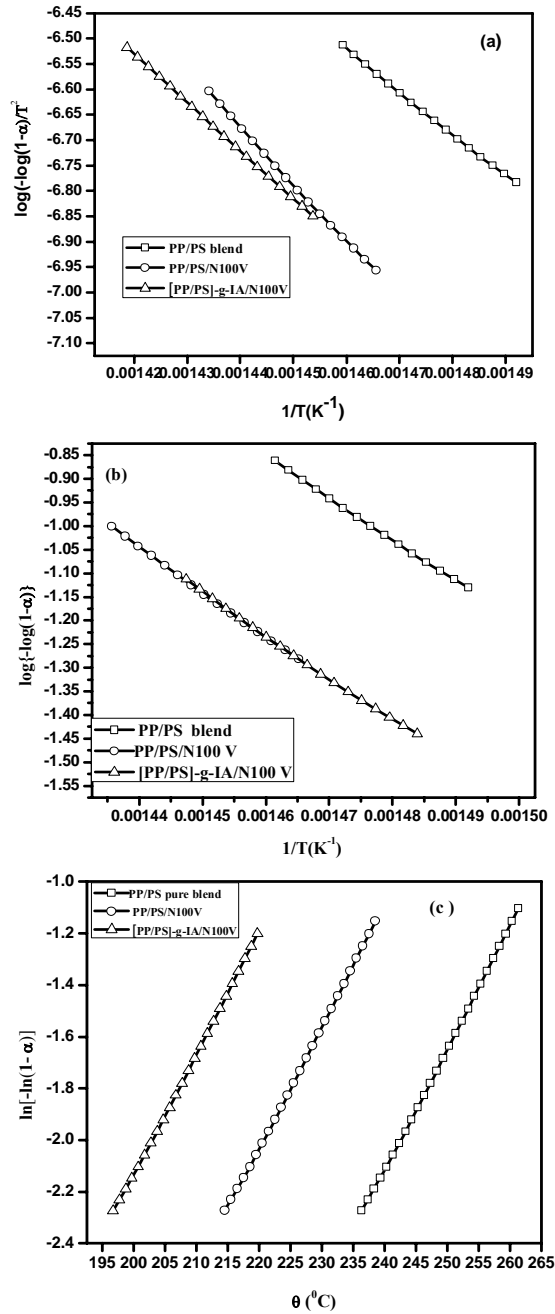
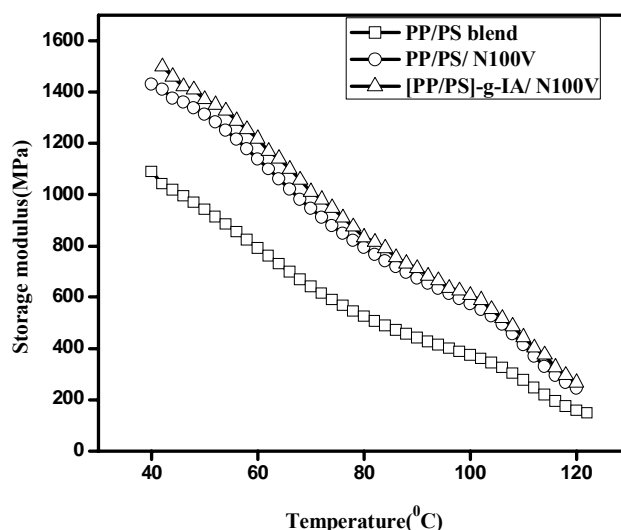


Figure 6a.24 Kinetic plots for the determination of activation energy of PP/PS blend, PP/PS/N100V and IA grafted PP/PS clay nanocomposites using (a) Coats-Redfern equation (b) Broido's method and (c) Horowitz-Metzger equation

### 6.A.3.10 Dynamic mechanical analysis

The dynamic mechanical properties of IA compatibilized clay nanocomposites at 3 wt% are studied over a wide temperature range from 40 to 125 °C and the results are reported in Table 6a.3. Figure 6a.25 shows the storage modulus curve for compatibilized clay nanocomposites. The storage modulus of compatibilized nanocomposites is higher than uncompatibilized clay nanocomposites. Incorporation of nanoclay and compatibilizer in the samples increases the modulus more significantly compared to the samples without compatibilizer.



**Figure 6a.25** Storage modulus curves of PP/PS blend, PP/PS/N100V and [PP/PS]-g-IA/N100V nanocomposites

The increase in storage modulus is attributed to the better dispersion of nanoclay particles within the polymer matrix after the addition of compatibilizer. The number of active groups present in the compatibilizer will govern the extent of intercalation of nanoclay particles within the

polymer matrix [19]. The presence of compatibilizer increase the interaction between nanoclay layers and IA group through hydrogen bonding and this will increase the intercalation of nanoclay particles within the polymer matrix and increase the stress transfer [20].

Figure 6a.26 exhibits the variation of  $\tan \delta$  [ratio of loss to storage modulus ( $E''/E'$ )] plotted as a function of temperature. From the Table 6a.3 it is apparent that the presence of nanoclay and compatibilizers does not influence the  $T_g$  value. A slight decrease can be observed due to the plasticizing action of surfactant on nanoclay particles.

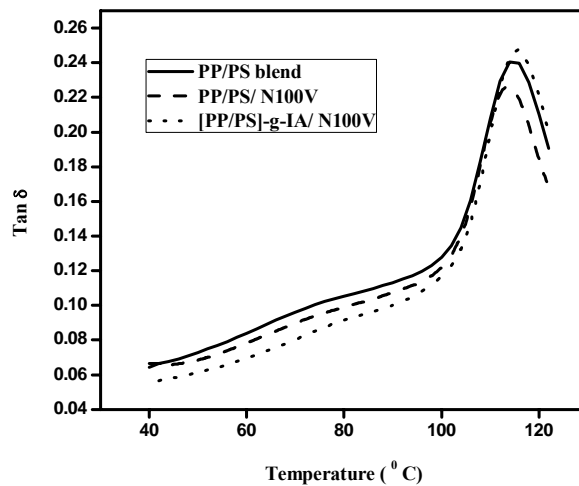


**Figure 6a.26**  $\tan \delta$  curves of PP/PS blend, PP/PS/N100V and [PP/PS]-g-IA/N100V nanocomposites

**Table 6a.3** Results obtained from DMA curves of PP/PS blend, PP/PS/N100V and [PP/PS]-g-IA/N100V nanocomposites

Samples	Storage modulus (MPa)				Tg( °C) from $\tan \delta$ value
	45 °C	80 °C	100 °C	120 °C	
PP/PS blend	1007	525	374	159	114.95
PP/PS/ N100 V	1369	792.7	573.6	245.6	114.35
[PP/PS]-g-N100V	1445	833	606	267	113.22

### 6.A.3.11 Differential scanning calorimetry

The crystallization temperature ( $T_c$ ), the apparent melting temperature ( $T_m$ ) and the corresponding enthalpies ( $\Delta H$ ) are illustrated in Table 6a.4. Figure 6a.27 shows the DSC melting and cooling curves for PP/PS blend and IA compatibilized clay nanocomposite with modified kaolin nanoclay at 3 wt %.

**Table 6a.4 DSC parameters of PP/PS (80/20), PP/PS/N100V and [PP/PS]-g-IA/N100V nanocomposites**

Samples	$T_c$ (°C)	$\Delta H_c$ (J/g)	$T_m$ (°C)	$\Delta H_m$ (J/g)
PP/PS pure blend	111.9	61.1	158.4	32.4
PP/PSN100V	114.4	63.3	160.2	40.0
[PP/PS]-g-N100V	119.2	68.2	161.6	37.7

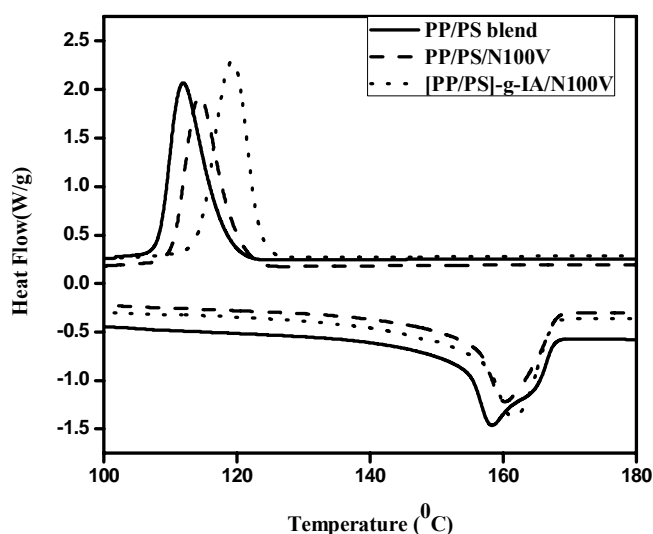


**Figure 6a.27 DSC melting and crystallization curves of PP/PS blend, PP/PS/N100V and [PP/PS]-g-IA/N100V nanocomposites**

The compatibilized clay nanocomposite has slightly higher crystallization temperatures and  $\Delta H_c$  compared to uncompatibilized nanocomposite as

displayed in Table 6a.4. These results show that the addition of nanoclay has a nucleating role and the extent of change is higher in the presence of IA [21- 23]. This increase in melting temperature shows that the crystal structure in nanocomposites is more perfect than in polymer matrix.

#### **6.A.4 Conclusions**

The grafting reaction of itaconic acid on to PP/PS blend is confirmed by FTIR. The compatibilized nanocomposites show improved mechanical properties compared to uncompatibilized clay nanocomposites and this is due to the improved interfacial adhesion between PP and PS in presence of compatibilizer and modified nanoclays. XRD and TEM results reveal better dispersion of the clay particles in polymer matrix in the presence of compatibilizer. The storage modulus of compatibilized blends is greater than the modulus of neat matrix. Thermal stability is improved by the addition of compatibilizer and this is attributed to the dispersion of nanoclay particles in the polymer matrix that restricts the easy diffusion of volatiles from the bulk. SEM photographs which indicates that blends containing grafted polymers. DSC results show that nanoclay can act as a nucleating agent in compatibilized clay nanocomposites.

#### **References**

- [1]. Yu-Qing Zhang, Joong-Hee Lee, Han-Jong Jang, Chang-Woon Nah, *Composites: Part B*, 2004, 35, 133–138.
- [2]. Maria Pilar Villanueva, Luis Cabedo, Jose Maria Lagaron, Enrique Gimenez, *Journal of Applied Polymer Science*, 2010, 115, 1325–1335.



- [3]. Yan Zhu, Yuzhen Xu, Lifang Tong, Zhongbin Xu, Zhengping Fang , Journal of Applied Polymer Science, 2008, 110, 3130–3139.
- [4]. Oana M. Istrate, Micheal A. Gunning, Clement L. Higginbotham, Biqiong Chen, Journal of Polymer Science Part B: Polymer Physics 2012, 50, 431–441.
- [5]. Edwin Moncada, Raul Quijada, Ingo Lieberwirth, Mehrdad Yazdani-Pedram, Macromolecular Chemistry and Physics, 2006, 207, 1376–1386.
- [6]. Use of Grafted Polypropylene With Itaconic Acid As Compatibilizer: Influence On The Mechanical Properties Of Polyolefin Micro- And Nano-Composites , Mehrdad Yazdani-Pedram , Raúl Quijada , Patricio Toro; CONAMET/SAM 2006.
- [7]. Ramazan Coskun, European Polymer Journal 2007, 43, 1428–1435.
- [8]. R. Coskun, M. Sacak, M. Karakısla, Journal of Applied Polymer Science, 2005, 97(5), 10.
- [9]. Isıklan, Fatma Kursun, Murat Inal, Carbohydrate Polymers, 2010, 79, 665–672.
- [10]. M. Yazdani-Pedram, J. Bruna, R. Quijada, B. Gonzalez, Proceeding of the 8th Polymers for Advanced Technologies International Symposium, Budapest, Hungary, 13-16 September 2005.
- [11]. J. Bruna M. Yazdani-Pedram , R. Quijada , J.L. Valenti'n , M.A. Lo'pez-Manchado, Reactive & Functional Polymers,2005, 64 ,169–178.
- [12]. M. A. López-Manchado, J. M. Kenny, R. Quijada, M. Yazdani-Pedram, Macromolecular Chemistry and Physics, 2001,202(9),1909-1918.
- [13]. S. S. Pesetskii, B. Jurkowski, O. A. Makarenko, Journal of Applied Polymer Science, 2002, 86, 64–72.

- [14]. Kusmono, Z. A. Mohd Ishak, W. S. Chow, T. Takeichi, Rochmadi, *eXPRESS Polymer Letters*, 2008, 2(9), 655–664.
- [15]. Waraporn Rattanawijan, Taweechai Amornsakchai, Pornsawan Amornsakchai, Pinsupha Petiraksakul, *Journal of Applied Polymer Science*, 2009,113, 1887–1897.
- [16]. Shanti V. Nair, Lloyd A. Goettler, Bruce A. Lysek, *Polymer Engineering and Science*, 2002, 42(9).
- [17]. S. Sánchez-Valdes, E. Ramírez-Vargas, M.C. Ibarra-Alonso, L.F. Ramos de Valle, J. Méndez-Nonell, F.J. Medellín-Rodríguez, J.G. Martínez-Colunga, S. Vazquez-Rodriguez, R. Betancourt-Galindo, *Composites: Part B*, 2012,43 ,497–502.
- [18]. S. Y. Lee, I. A. Kang, G. H. Doh, W. J. Kim, J. S. Kim, H. G. Yoon, Q. Wu, *eXPRESS Polymer Letters*, 2002, 2(2), 78–87.
- [19]. Yeh Wang, Feng-B. Chen, Yann-C. Lib, Kai-C. Wu, *Composites: Part B*, 2004, 35, 111–124.
- [20]. Sangeeta Hambir, Neelima Bulakh and J. P. Jog *Polymer Engineering & Science* ,2002, 42(9),1800–1807.
- [21]. Maria Pilar Villanueva, Luis Cabedo, Jose, Maria Lagaron, Enrique Giménez; *Journal of Applied Polymer Science*, 2010, 115, 1325–1335.
- [22]. S. K. Sharma, Ajay K. Nema, S. K. Nayak, *Journal of Applied Polymer Science*, 2010, 115, 3463–3473.
- [23]. Jaydeep Khedkar, Ioan Negulescu, Efstathios I. Meletis, *Wear*, 2002, 252, 361–369.

**Part B****Polypropylene/ Polystyrene/Dimethyl itaconate/modified kaolin clay nanocomposites****Abstract**

*Dimethyl itaconate compatibilized Polypropylene/ Polystyrene/clay nanocomposites were prepared by melt blending technique. The effect of compatibilizer on the mechanical, thermal and morphological properties of Polypropylene/ Polystyrene/ clay nanocomposites has been studied. Thermogravimetric analysis shows improvement in the thermal stability for compatibilized clay nanocomposites. The widening of peaks observed in XRD studies confirms the penetration of polymer matrix into the nanoclay galleries. SEM photographs reveal that blends containing grafted polymers show a better exfoliation.*

**6. B.1 Introduction**

Polymer/clay nanocomposites (PCNs) have attracted significant academic and industrial interest in recent years. The nano-sized-layer-filed polymers can exhibit dramatic improvements in mechanical and thermal properties at low clay contents because of the strong synergistic effects between the polymer and the clay on both the molecular or nanometric scale [1]. Nanocomposites based on Polypropylene/Polystyrene (PP/PS) blend have been studied extensively by many researchers [2-4]. Because of the strong hydrophilic nature of the nanoclays, adhesion between clays and non-polar polymers is low and the dispersibility of clay layers in polymer matrix is limited. In order to increase the dispersibility of nanoclays within the polymer matrices grafted polymers are used as compatibilizers. Yan Zhu *et al.* increased the polarities of PS and PP by sulfonation and by introduction of polar maleic anhydride group, respectively reported that the higher polarity of the polymer generates higher interaction between clay and polymer components, and hence results in stronger preferential intercalating ability [5].

In this part of study dimethyl itaconate (DMI) is prepared by grafting reaction is used as a compatibilizer. M. Yazdani-Pedram *et al.* used DMI for the functionalization of PP and they reported that crystallization temperature is increased for the functionalized polymers than the pure PP [6]. Here DMI is added directly into PP/PS/clay nanocomposites. The hydroxyl groups of nanoclay react with DMI and disperse the nanoclay well within polymer matrix through in-situ compatibilization. The compatibilizer is proposed to be prepared by grafting reaction between DMI and PP/PS blend in the presence of a DCP initiator. The aim of this study is to determine the effect of the [PP/PS]-g-DMI as a compatibilizer in the mechanical, thermal and morphological properties of PP/PS/clay nanocomposites.

## **6. B.2 Methodology**

### **6. B.2.1 Materials**

The details of the polymers and nanoclay types used for the study are discussed in Chapter 2 (sections 2.1.1, 2.1.2& 2.1.3). The details of dimethyl itaconate used for the study are discussed in section 2.1.7.

### **6. B.2.2 Preparation of the compatibilized blend and its characterization**

The compatibilizer was prepared by grafting reaction between DMI and PP/PS blend in the presence of DCP initiator at 170 °C at 50 rpm for 8 min by melt mixing in a Thermo Haake PolyLab system equipped with roller rotors. Initially PP and PS were allowed to melt for 2 min. In the first series of experiment the DCP was varied (0.03-0.9wt %) fixing the concentration of dimethyl itaconate (DMI) at 1 wt. %. In the second series of experiments the optimum amount of DMI was found by varying the concentration of DMI (1, 2,

3,4,5,7,9,11 wt %) and keeping the concentration of DCP constant. The grafting reaction was monitored using soxhlet extraction. Samples were compressed into thin films, cut into small pieces, and then put in contact with acetone using soxhlet apparatus for 16 h to remove the unreacted DMI. It was finally dried in a vacuum oven at 70 °C for 12 h. The product before and after soxhlet extraction, was weighed and percentage of grafting was determined.

### **6. B.2.3 Nanocomposite preparation**

PP/PS (80/20) blends were mixed with modified kaolin nanoclays and the compatibilizer (DMI) using a Thermo HAAKE Polylab system equipped with roller rotor operating at 180 °C and 50 rpm for 8 min. The resulting compounds were hot pressed into sheets and cut into pieces. The material was then injection molded at 190 °C. The tensile properties, flexural properties, impact strength, hardness, dynamic mechanical analysis, thermal properties and morphological properties were analyzed according to various standards as described in Chapter 2(section 2.2.3). The details of FTIR used are described in section 6.A.2.3.

## **6. B.3 Results and Discussion**

### **6. B.3.1 Effect of initiator (DCP) concentration on the mechanical properties of PP/PS/blend**

#### **(a) Tensile properties**

Figures 6b.1 & 6b.2 illustrate the variation of tensile strength and tensile modulus respectively with initiator loading. In this study concentration of DMI is fixed at 1 wt. %. Tensile properties are found to be maximum at 0.7 wt. % of DCP.

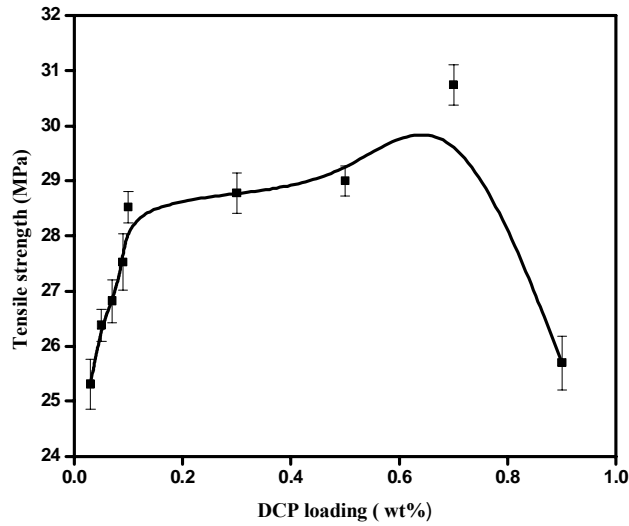


**Figure 6b.1** Variation of tensile strength with initiator loading

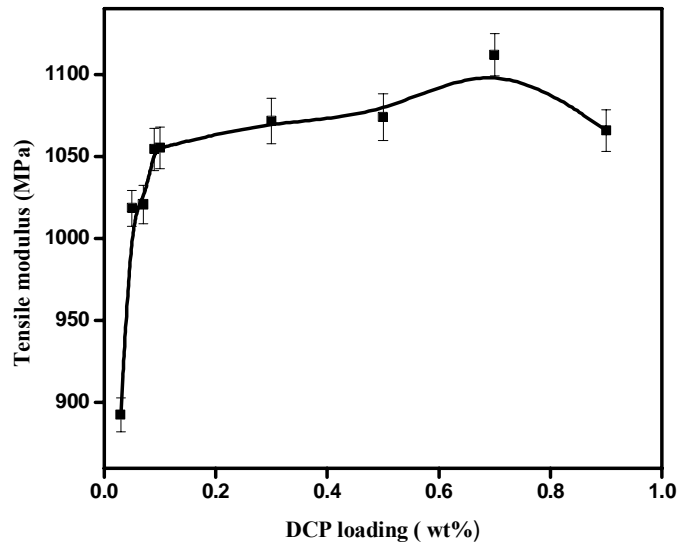


**Figure 6b.2** Variation of tensile modulus with initiator loading

**(b) Flexural properties**

The flexural strength and flexural modulus of the nanocomposites are plotted as a function of DCP loading in Figures 6b.3 & 6b.4 respectively. There is a significant increase in flexural modulus and flexural strength with increase in DCP loading. 0.7wt% is taken as optimum DCP loading for further studies.

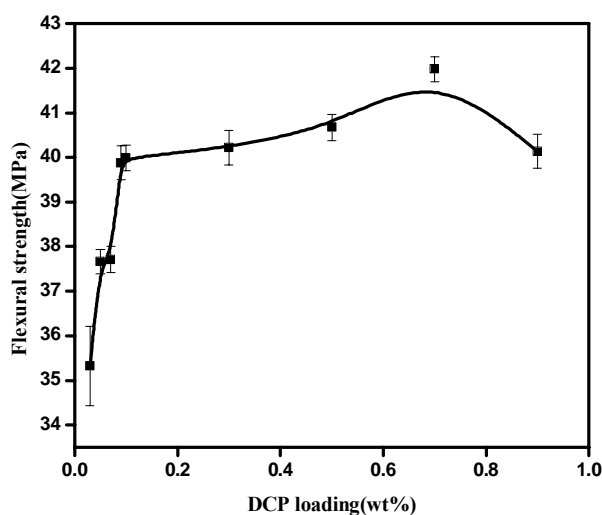


Figure 6b.3 Variation of flexural strength with initiator loading

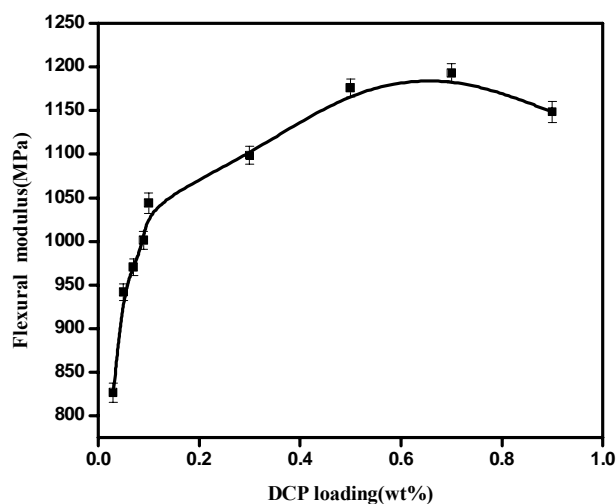
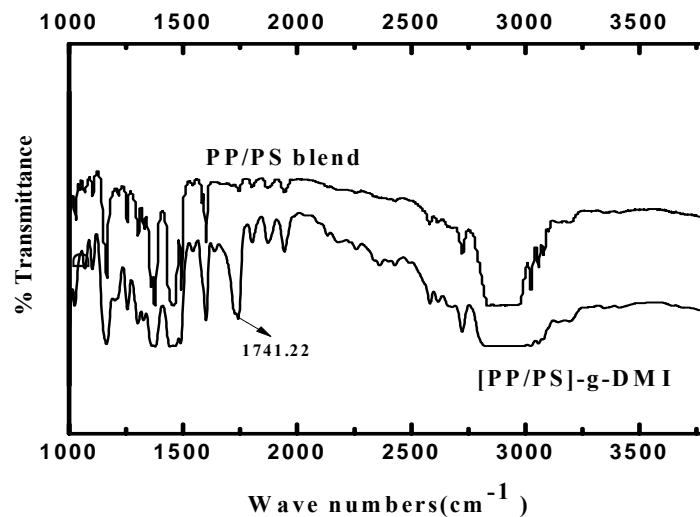


Figure 6b.4 Variation of flexural modulus with initiator loading

### **6. B.3.2 Evidence of grafting DMI onto PP/PS blend**

#### **6. B.3.2.1 Fourier Transform Infrared Spectroscopy**

The existence of grafted DMI in PP/PS blend was confirmed by FTIR spectroscopy. Figure 6b.5 reveals the FTIR spectrum of PP/PS blend and DMI functionalized PP/PS blend. FTIR spectrum of the PP/PS grafted with DMI {[PP/PS]-g-DMI} exhibited an absorption band at  $1741\text{cm}^{-1}$  and is due to the carboxyl group of the ester linkage of DMI. Thus it confirms the incorporation of this monomer into the PP/PS chains [7].



**Figure 6b.5 FTIR spectrum of PP/PS blend and DMI functionalized PP/PS blend.**

### **6. B.3.3 Effect of dimethyl itaconate (DMI) concentration on the mechanical properties of PP/PS blend**

#### **(a) Tensile properties**

Variation of tensile properties with dimethyl itaconate (DMI) loading at a fixed DCP loading (0.7wt%) is given in the Figures 6b.6 & 6b.7



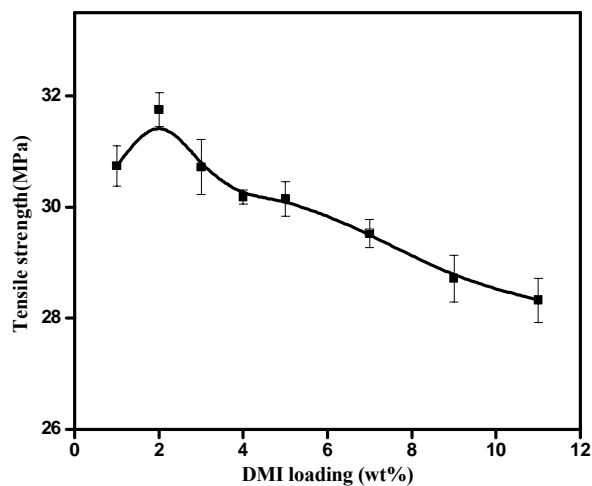


**Figure 6b.6** Variation of tensile strength with DMI loading

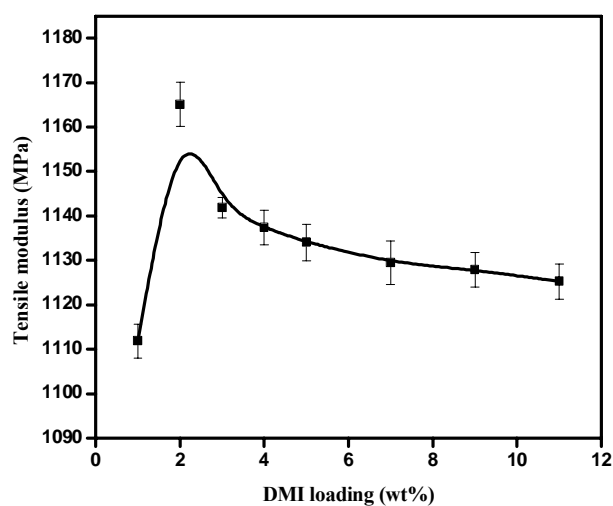


**Figure 6b.7** Variation of tensile modulus with DMI loading

Maximum tensile properties occur at 2wt % DMI loading and grafting yield is found to be 2.11%. Further increase in concentration of DMI leads to decrease in tensile properties. This decrease may be due to the partial homopolymerization of DMI. Similar results were reported by M. Yazdani – Pedram [6].

**(b) Flexural properties**

The flexural strength and flexural modulus of the nanocomposites are plotted as a function of DMI content are depicted in the Figures 6b.8 & 6b.9. Flexural properties increases up to 2 wt % and thereafter declined.

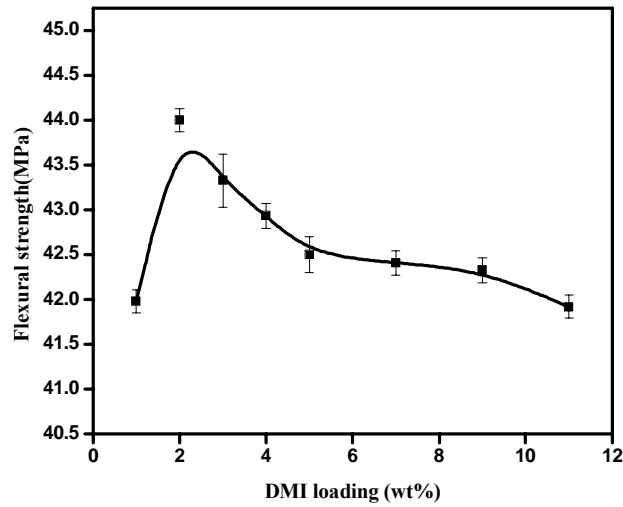


**Figure 6b.8** Variation of flexural strength with DMI loading

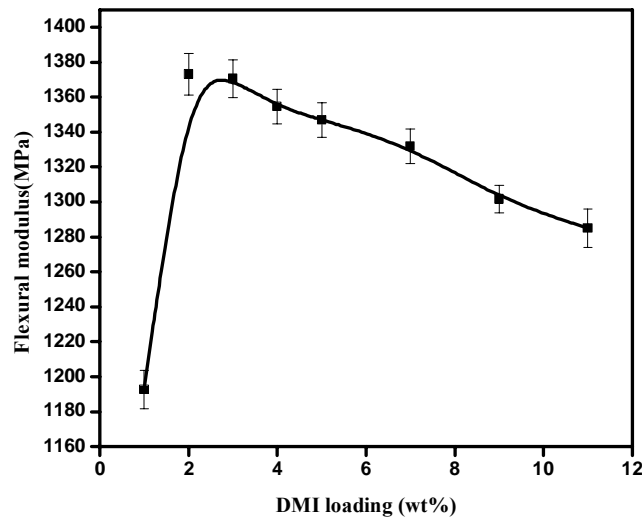


**Figure 6b.9** Variation of flexural modulus with DMI loading

### (c) Impact strength

The impact strength of the nanocomposites is plotted as a function of DMI content is indicated in the Figure 6b.10. The increase in DMI concentration leads to an increase in impact strength up to 2 wt% and thereafter shows a reverse trend.

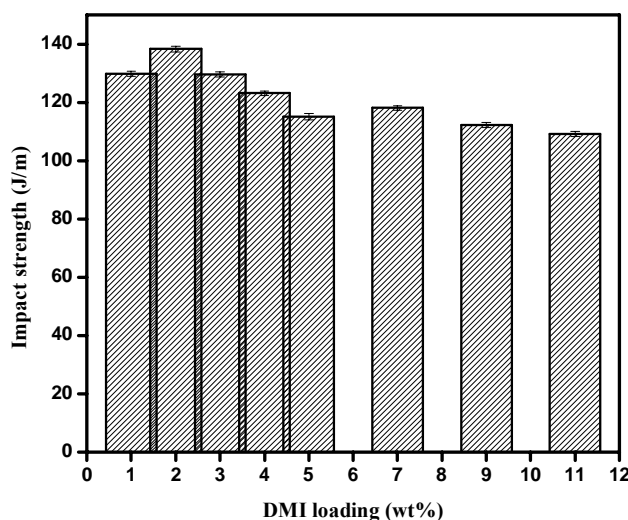


**Figure 6b.10** Variation of impact strength with DMI loading

The maximum mechanical properties were obtained at 2 wt% DMI loading. Hence 2 wt% is taken as optimum DMI content for the further studies.

#### 6. B.3.3.1 Melt Flow Index

Figure 6b.11 reveals the variation of MFI with DMI concentration. The MFI values increases with increasing DMI concentration. This indicates a lower viscosity of the material and confirms the higher ease of processing of the compatibilized blends, which may be due to degradation of polymer chains.

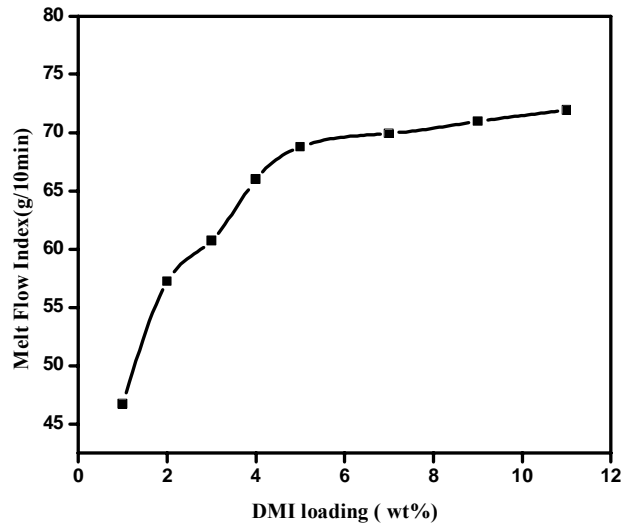


**Figure 6b.11** Variation of MFI with DMI loading

#### **6. B.3.4 Effect of dimethyl itaconate (DMI) grafting on the properties of PP/PS/clay nanocomposites**

##### **(a) Tensile properties**

Tensile strength and tensile modulus of [PP/PS]-g-DMI/modified kaolin nanoclay composite with different levels of nanoclay contents are shown in Figures 6b.12 and 6b.13 respectively. Grafted PP/PS blend having 2 wt. % DMI loading with 0.7 wt. % DCP is selected for nanoclay modification as it exhibits maximum improvement in mechanical properties. The tensile strength and tensile modulus increases by 21 % and 14 % in the case of [PP/PS/]-g-DMI/N100V composites when compared to PP/PS/N100V nanocomposite.

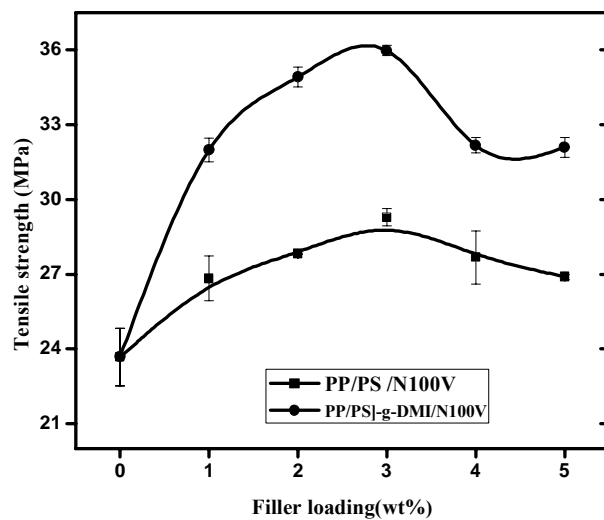


Figure 6b.12 Variation of tensile strength with filler loading

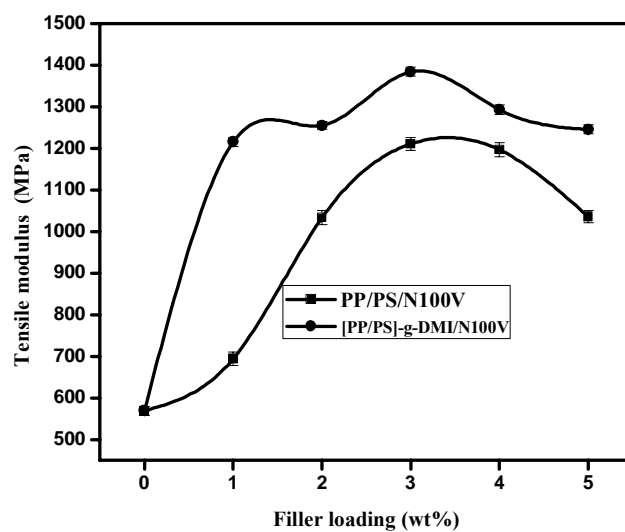


Figure 6b.13 Variation of tensile modulus with filler loading

Increase in tensile properties reveals the improvement in interfacial adhesion between PP, PS and nanoclay particles in presence of the compatibilizer. Moreover the presence of the compatibilizer improves the

dispersion of nanoclay in the polymer matrix. This is further confirmed by XRD analysis (section 6. B.3.6). Similar results were reported by Kusmono *et al.* in their study when using PP-g-MA as a compatibilizer for PA6/PP/OMMT nanocomposites [8].

**(b) Flexural strength**

Figures 6b.14 & 6b.15 show the flexural strength and flexural modulus of the DMI compatibilized PP/PS clay nanocomposites.

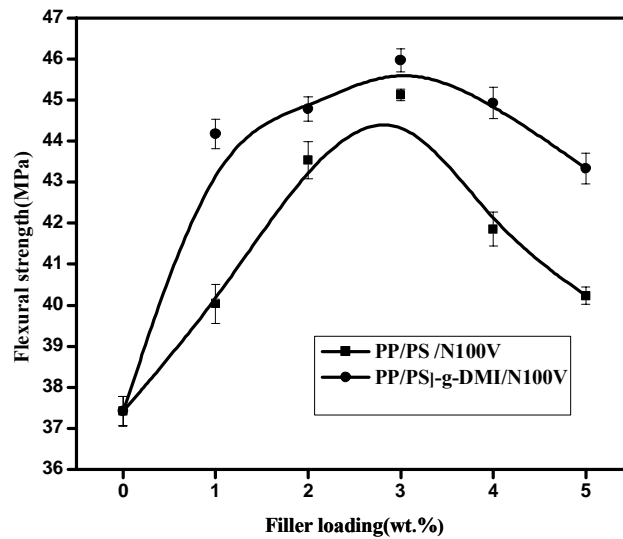


**Figure 6b.14 Variation of flexural strength with filler loading**

The addition of DMI increased the flexural modulus and strength of PP/PS/clay nanocomposites. This may be attributed to the compatibilizing effect of DMI, which improves the interfacial adhesion and promotes the degree of dispersion of nanoclay particles in the PP/PS matrix.

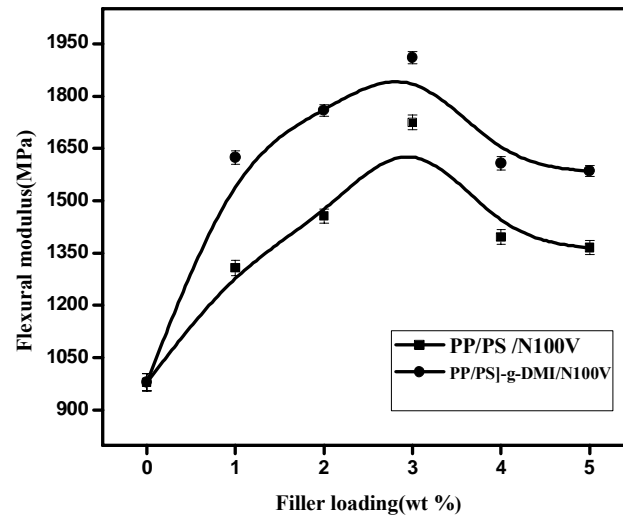


Figure 6b.15 Variation of flexural modulus with filler loading

(c) Impact strength

From the Figure 6b.16 it can be noted that the incorporation of DMI led to an increase in impact strength of the PP/PS/clay nanocomposites.

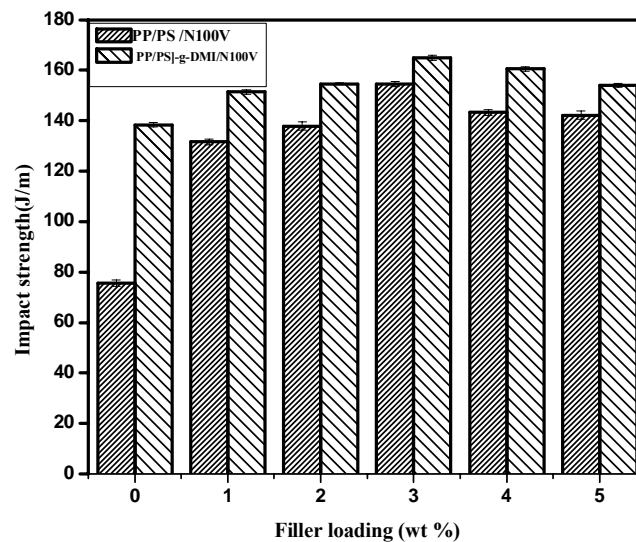
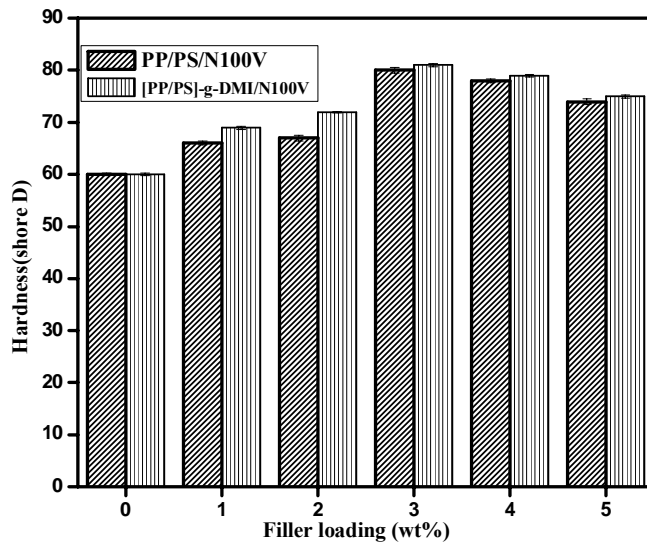


Figure 6b.16 Variation of impact strength with filler loading

The enhanced impact strength is attributed to the improved interfacial adhesion. After reaching a maximum the impact strength begins to decrease. The reduction in toughness may be attributed to the lack of the crack front deflection [8].

**(d) Hardness**

Figure 6b.17 displays the increase in hardness with filler loading. The improvement in the hardness is due to the presence of intercalated and exfoliated nanoclay platelets in polymer matrix in the presence of compatibilizer. The intercalated or exfoliated nanoclay platelets restrict indentation and increase the hardness of the nanocomposites.



**Figure 6b.17 Variation of hardness with filler loading**

**6. B.3.5 Melt Flow Index**

Figure 6b.18 shows the variation of MFI with filler loading. MFI decreases with increasing nanoclay loadings and this is due to the increase



in degree of intercalation and exfoliation of nanoclay particle in the matrix with the addition of dimethyl itaconate.

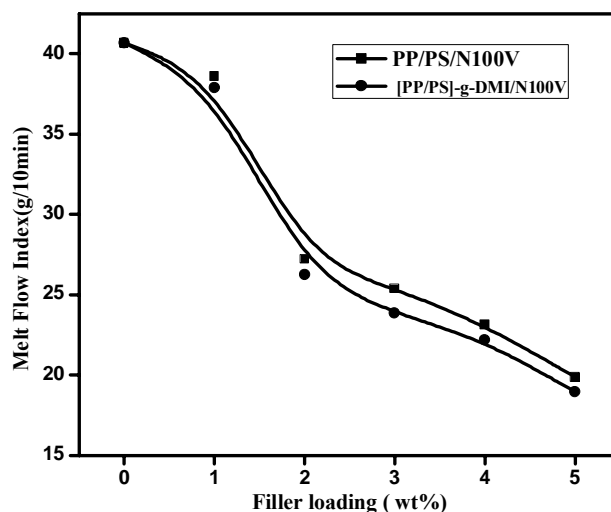


Figure 6b.18 Variation of MFI with filler loading

### 6. B.3.6 X-ray Diffraction

XRD patterns of Nanocaliber 100V, PP/PS/N100V and [PP/PS]-g-DMI/clay nanocomposite (3wt %) are illustrated in Figure 6b.19. The expansion of intergallery distance of the nanoclay particles is governed by the interaction between nanoclay treatment and compatibilizer. The characteristic diffraction peak  $d_{001}$  for N100V is located around  $12.44^\circ$  corresponding to an intergallery spacing of 7.11nm. For the PP/PS/N100V nanocomposite, the characteristics peak of N100V is shifted to  $2\theta = 12.08^\circ$  having a d-spacing of 7.32 nm. The shifting of the diffraction peaks to higher d-spacing designates the expansion of inter-gallery spacing, which is attributed to the intercalation of polymer chains in the nanoclay layers.

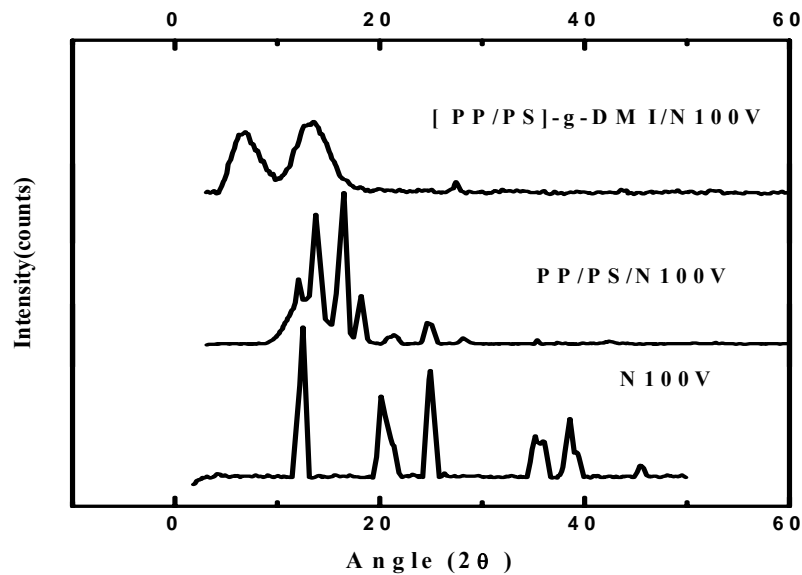
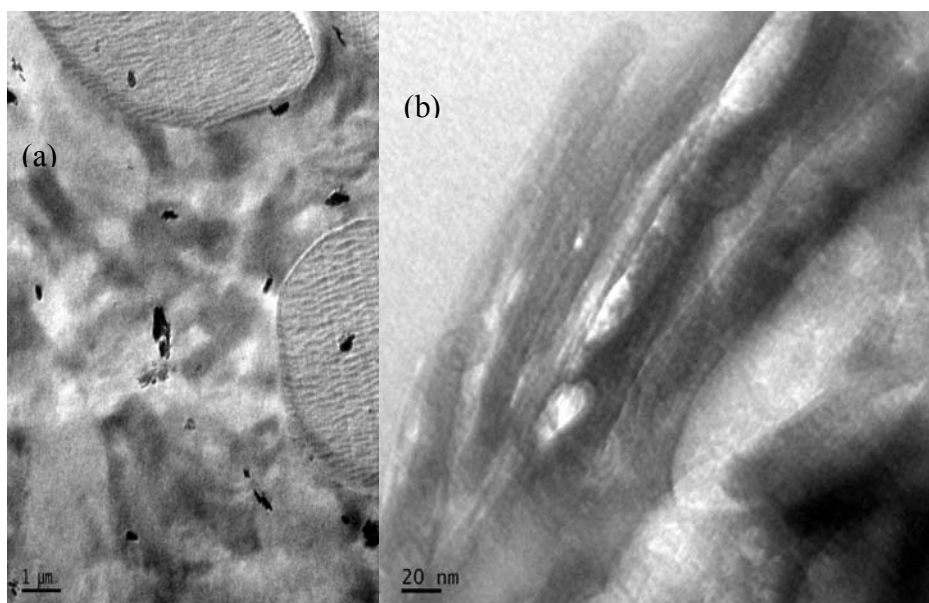


Figure 6b.19 XRD patterns of Nanocaliber 100 V, PP/PS/N100V and [PP/PS]-g-DMI/N100V nanocomposite (3wt %)

On addition of compatibilizer the nanoclay is partially exfoliated in polymer matrix i.e. the widening of peak and reduction of intensity is observed in DMI compatibilized nanocomposite.

### 6. B.3.7 Transmission electron microscopy

TEM bright field image of DMI compatibilized clay nanocomposite at  $1\mu\text{m}$  and  $20\text{ nm}$  is shown in the Figures 6b.20 (a) and 6b.20 (b). The bright phase of the picture is the matrix phase, and the dark phase is the particle phase. The dark entities are the cross section of intercalated nanoclay layers. TEM microscopic photographs of PP/PS/N100V are shown in Chapter 3 (Section 3.3.2, Figure 3.5& 3.8).



**Figure 6b.20** Transmission electron microscopic bright field images of DMI compatibilized nanocomposite at (a) 1  $\mu\text{m}$  and at (b) 20 nm

In DMI compatibilized nanocomposites the clay particles are distributed throughout the polymer matrix (Figure 6b.20 (a)). It is clear from figure 6b.20(b) that the presence of compatibilizer significantly improves the dispersion of nanoclay in the polymer matrix when compared to that of uncompatibilized nanocomposite.

#### **6. B.3.8 Scanning electron microscopy (SEM)**

The SEM photographs of fractured cross section of the tensile sample of DMI grafted PP/PS/clay nanocomposite reinforced with N100V (3 wt %) is given in the Figure 6b.21.

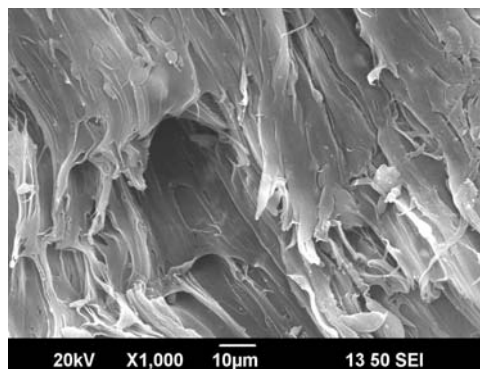


**Figure 6b.21 SEM photographs of [PP/PS]-g-DMI/N100V nanocomposite**

A homogeneous morphology reveals a better dispersion of nanoclay particles within the polymer matrix in presence of compatibilizer. This is further evidenced by the XRD analysis (section 6. B.3.6) and improvement in mechanical properties (section 6. B. 3. 4).

### **6. B.3.9 Thermogravimetric analysis**

The effect of the nanofiller and the compatibilizer on the thermal stability of the composites was studied by means of thermogravimetric experiments carried out in N<sub>2</sub> atmosphere.

**Table 6b.1 Thermal characteristics of DMI compatibilized clay nanocomposites**

Samples	50% mass loss (°C)	Tonset (°C)	Tmax (°C)	Residue at 600 °C (%)	OI
PP/PS blend	426.6	370.5	434.4	0.456	0.032
PP/PS/ N100V	446.4	397.3	460.7	1.77	0.124
[PP/PS]-g-DMI/3%N100V	451.3	399.5	462.5	2.97	0.207

Figure 6b.22 presents the TG curves for PP/PS blend, PP/PS/N100V and [PP/PS]-g-DMI/3 wt%N100V nanocomposites. Table 6b.1 gives the thermal characteristics of the different samples. Presence of nanoclay with

high thermal stability and better barrier properties prevents quick heat transmission and limits the continuous decomposition of PP/PS/ N100V nanocomposite [9], increasing the onset degradation temperature. Thermal stability of DMI compatibilized clay nanocomposites is higher than that of PP/PS/N100V. The strong hydrogen bonding between DMI and hydroxyl group of the silicate layer as well as the shear force exerted on nanoclay during melt blending can produce the driving force necessary for the better intercalation. The presence of compatibilizer improves the dispersion of nanoclay particles within the polymer matrix and hence promotes the thermal stability of the nanocomposites. It is apparent from the Table 6b.1 that the oxidation index values for [PP/PS]-g-DMI/clay nanocomposites are higher than that of uncompatibilized clay nanocomposites.

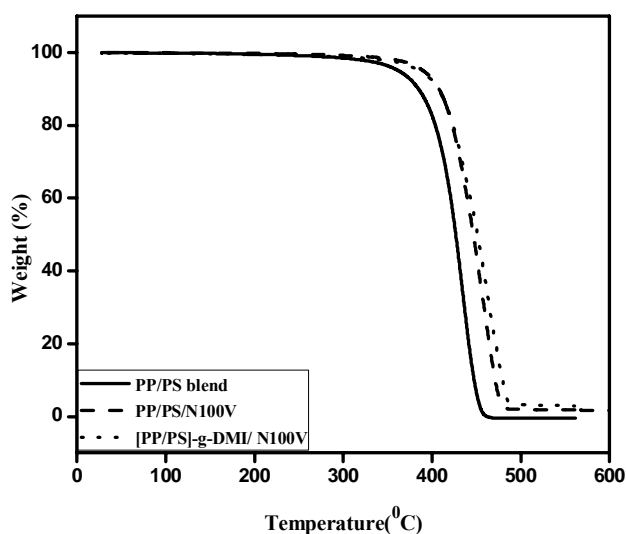


**Figure 6b.22** TG curves of PP/PS blend, PP/PSN100V and [PP/PS]-g-DMI/N100V nanocomposite

### 6. B.3.9.1 Kinetic analysis of thermal decomposition

The Coats Redfern (CR), Broido's (BR) and Horowitz-Metzger (HM) plots for the thermal degradation of dimethyl itaconate grafted PP/PS/ clay nanocomposite from the onset degradation temperature to the maximum degradation temperature are displayed in Figure 6b.23. The activation energy ( $E_a$ ) for each method is given in Table 6b.2.

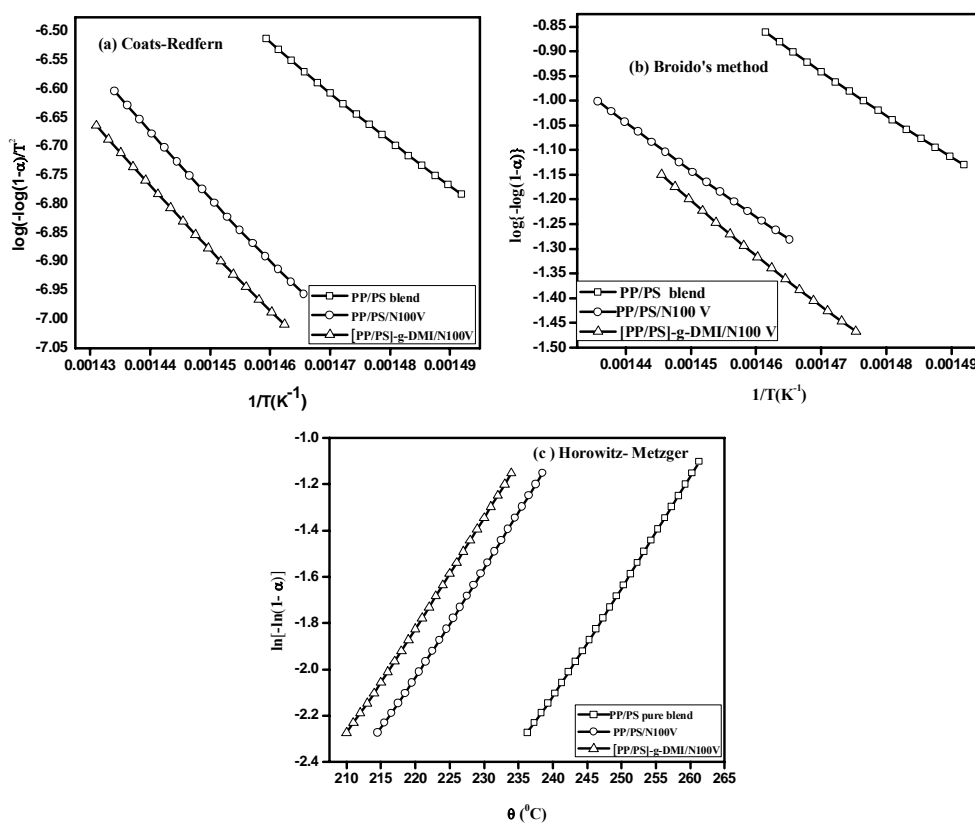


**Figure 6b.23** Kinetic plots for the determination of activation energy of PP/PS blend, PP/PSN100V and [PP/PS]-g-DMI/N100V nanocomposite using (a) Coats-Redfern equation (b) Broido's method (c) Horowitz-Metzger equation

**Table 6b.2** Activation energy (J/mol) calculated by Horowitz-Metzger (HM), Broido's (BR) and Coats-Redfern (CR) methods for DMI grafted PP/PS/clay nanocomposites

Samples	Coats –Redfern	Broido's	Horowitz- Metzger
PP/PS blend	174	181	175
PP/PS/N100V	196	228	196
[PP/PS]-g-DMI/N100V	198	231	213

DMI grafted PP/PS/clay nanocomposite show higher  $E_a$  value than that of uncompatibilized nanocomposite. The thermal stability and activation energy of the nanocomposites is enhanced in the presence of compatibilizer.

### 6. B.3.10 Dynamic mechanical analysis

DMA is used to study the relaxations in polymers. The analysis of storage modulus and  $\tan \delta$  curves are used to ascertain the performance of a sample under stress and temperature. Figures 6b.24 & 6b.25 depict the storage modulus and  $\tan \delta$  curves for DMI compatibilized PP/PS/clay reinforced with N100V (3 wt %), while Table 6b.3 illustrates the results obtained from the DMA curves.

**Table 6b.3** Results obtained from DMA curves of PP/PS blend, PP/PS/N100V and [PP/PS]-g-DMI/N100V nanocomposite

Samples	Storage modulus ( MPa)				$T_g$ ( °C) from $\tan \delta$ value
	45 °C	80 °C	100 °C	120 °C	
PP/PS blend	1007.0	525.0	374.0	159.0	114.95
PP/PS/ N100 V	1369	792.7	573.6	245.6	114.35
[PP/PS]-g-DMI/N100V	1427	874.8	676.6	347.3	115.02

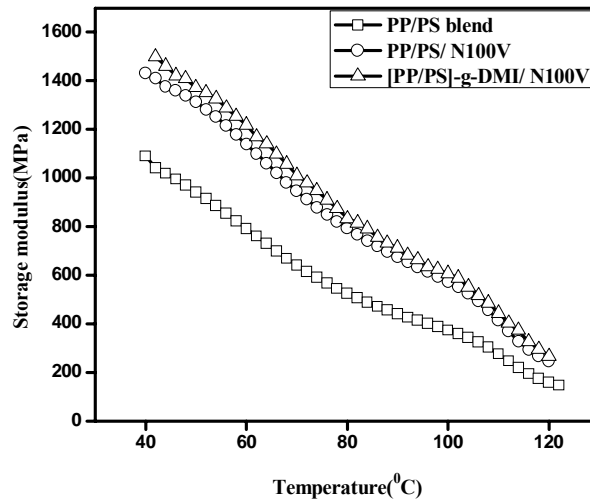
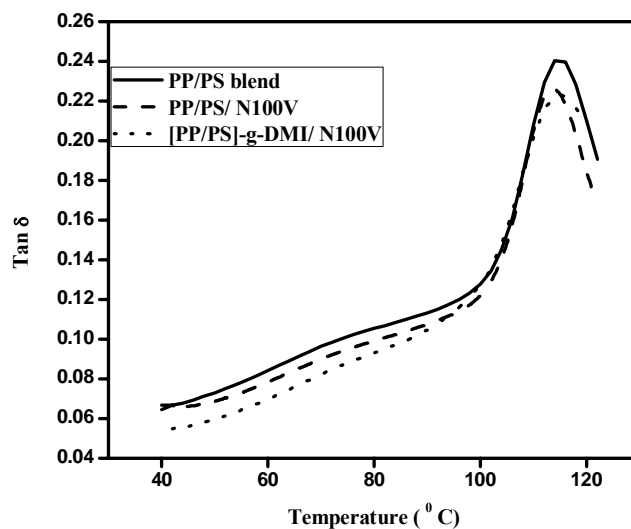


Figure 6b.24 Storage modulus curves of PP/PS blend, PP/PS/N100V and [PP/PS]-g-DMI/N100V nanocomposites

The storage modulus of DMI compatibilized clay nanocomposite is higher than that of uncompatibilized clay nanocomposite. It depicts that the inclusion of nanoclay in polymer matrix results in higher storage modulus of the nanocomposite. These results indicate that the addition of clay particles into the DMI compatibilized polymer matrix enhances stiffness [10]. When the nanoclay particles diffuse into the compatibilized clay nanocomposites, a bond is formed between the [PP/PS]-g-DMI and the nanoclay particles. It will result in increase in dispersion of nanoclay particles in the polymer matrix [11].





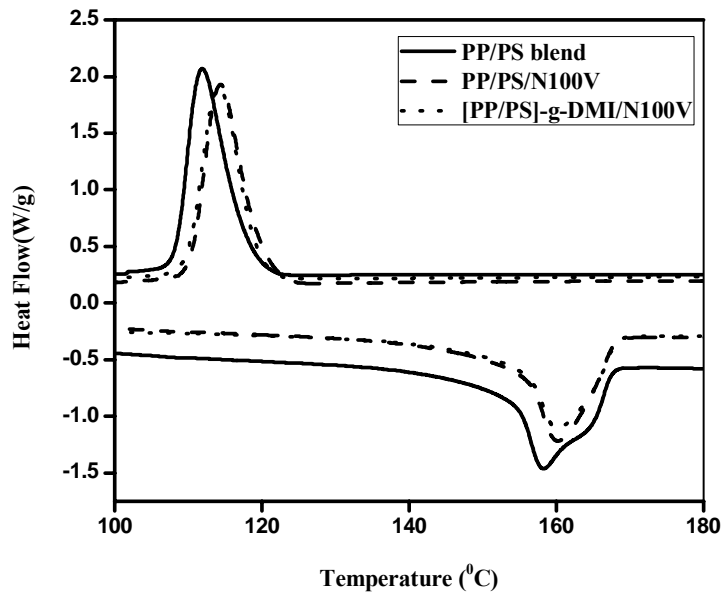
**Figure 6b.25** Tan  $\delta$  curves of PP/PS blend, [PP/PS]-g-DMI/N100V and [PP/PS]-g-DMI/N100Z nanocomposites

Figure 6b.25 shows the variation of  $\tan\delta$  [ratio of loss to storage modulus ( $E''/E'$ )] plotted as a function of temperature. From the table it is clear that the presence of modified nanoclays and compatibilizer does not influence the  $T_g$  value.

### 6. B.3.11 Differential scanning calorimetry

DSC analysis provides a better quantitative evaluation of the crystallization behavior of the compatibilized clay nanocomposites. The crystallization temperature ( $T_c$ ), the apparent melting temperature ( $T_m$ ) and the corresponding enthalpies ( $\Delta H$ ) are exhibited in the Table 6b.4, whereas the Figure 6b.26 shows the DSC melting and cooling curves for PP/PS blend, PP/PS/N100V and DMI compatibilized clay nanocomposite with modified kaolin nanoclay at 3wt %. The crystallization temperature increases after the addition of nanoclay particle. This result indicates that nanoclays and [PP/PS]-g-DMI can act as nucleating agent [12]. This increase in

$T_m$  values indicates that the crystal structure in nanocomposites is more perfect than in polymer matrix [13]. There is no change in the temperature of crystallization and melting for the compatibilized nanocomposite.



**Figure 6b.26** DSC melting and crystallization curves of PP/PS blend, PP/PS/N100V and [PP/PS]-g-DMI/N100V nanocomposites

**Table 6b.4** DSC parameters of PP/PS blend, PP/PS]-g-DMI/N100V and [PP/PS]-g-DMI/N100Z nanocomposites

Samples	$T_c$ (°C)	$\Delta H_c$ (J/g)	$T_m$ (°C)	$\Delta H_m$ (J/g)
PP/PS blend	111.88	61.13	158.43	32.43
PP/PSN100V	114.4	63.3	160.2	40.0
[PP/PS]-g-DMI/N100V	114.2	59.8	160.3	48.1

## 6. B.4 Conclusions

The grafting of dimethyl itaconate on to PP/PS blend is confirmed by FTIR. The compatibilized PP/PS/clay nanocomposites give better mechanical properties compared to uncompatibilized nanocomposites. The addition of dimethyl itaconate improves the toughness of all blends while retaining their strength and stiffness. XRD results reveal good dispersion of nanoclay particles in polymer matrix in the presence of compatibilizer. The storage modulus and thermal stability of compatibilized blends is greater than the modulus of uncompatibilized clay nanocomposite. SEM photographs show that blends containing grafted polymers have a homogeneous morphology and reveals better exfoliation.

## References

- [1]. Effects of Clay Modification and Compatibilizers on the mechanical, morphological, and thermal properties of Polyamide 6/ Polypropylene Nanocomposites, Kusmono, Ph.D. thesis, November 2008.
- [2]. Yun ZHU, Hai-yun MA, Li-fang TONG, Zheng-ping FANG, Journal of Zhejiang University Science A ,2008, 9(11) , 1614-1620.
- [3]. Kyun yl Kim, Dong Uk Ju, Gi Joon Nam, Jae Wook Lee, Macromolecuar symposia,2007,249-250,283-288.
- [4]. Suprakas Sinha Ray, Steve Pouliot, Mosto Bousmina, Leszek A. Utracki, Polymer, 2004, 45, 8403-8413.
- [5]. Yan Zhu, Yuzhen Xu, Lifang Tong, Zhongbin Xu, Zhengping Fang, Journal of Applied Polymer Science, 2008,110, 3130–3139.
- [6]. Yazdani-Pedram, H. Vega, R. Quijada, Polymer, 2001, 42, 4751-4758.

- [7]. M.A.Lopez-Manchado; J.M.Kenny, R.Quijada, M. Yazdani- Pedram, *Macromolecular Chemistry and Physics*, 2001, 202(9), 1909-1918.
- [8]. Kusmono, Z. A. Mohd Ishak, W. S. Chow, T. Takeichi, Rochmadi, *eXPRESS Polymer Letters*, 2008, 2(9) 655–664.
- [9]. Sangeeta Hambir, Neelima Bulakh, J. P. Jog, *Polymer Engineering and Science*, 2002, 42(9), 1800-1807.
- [10]. Joong-Hee Lee , Daeseung Jung ,Chang-Eui Hong , Kyong Y. Rhee, Suresh G. Advani , *Composites Science and Technology*,2005, 65, 1996–2002.
- [11]. Mónica A. Pérez, Bernabé L. Rivas , Saddys M. Rodríguez, Álvaro Maldonado, Carola Venegas, *Journal of Chilean Chemical. Society*, 2010, 55(4).
- [12]. S. Y. Lee, I. A. Kang, G. H. Doh, W. J. Kim, J. S. Kim, H. G. Yoon, Q. Wu, *eXPRESS Polymer Letters*,2008, 2(2 ), 78–87
- [13]. N.A. Jamal, H. Anuar ,S.B.A. Razak, *IIUM Engineering Journal*, 2010, 11( 2)

.....✂.....

**Polypropylene/ Polystyrene/ Sisal Cellulose  
nano fiber composites**

---

**Part A**

**Isolation of cellulose nano fibers from Sisal**

- 7. A.1 Introduction
- 7. A.2 Methodology
- 7. A.3 Results and Discussion
- 7. A.4 Conclusions

**Part B**

**Polypropylene/Polystyrene/Cellulose nano fiber composites**

- 7. B.1 Introduction
  - 7. B.2 Methodology
  - 7. B.3 Results and Discussion
  - 7. B.4 Conclusions
-

**Part-A**  
**Isolation of cellulose nano fibers from Sisal**

**Abstract**

*In this work, cellulose nano fibers were extracted from sisal leaves using steam explosion technique. The chemical composition, morphology and thermal properties of the nano fibers and their intermediate products were characterized. The progressive removal of noncellulosic constituents is confirmed by FTIR studies. X-ray diffraction reveals that crystallinity increased with successive chemical treatments. Characterization of the fibers by SEM and TEM gives evidence for the formation of cellulose nano fibers. TGA results shows that the cellulose nano fibers exhibit enhanced thermal properties over the untreated fibers.*

### 7. A.1 Introduction

Cellulose nano fibers based on plants have attracted significant interest in the last few decades due to sustainability, availability and characteristics such as high surface area-to-volume ratio, high Young's modulus and tensile strength, low coefficient of thermal expansion, better electrical and thermal properties as compared with other commercial fibers. Nowadays cellulose nano fibers and their composites offer attractive research and industrial applications. The term “nano-fibers” are the elementary assemblies of distinct polymer units (based on glucopyranose in the case of cellulose nanofibrils) that have diameters in the order of tens of nanometers [1].

Cellulose is the main component of several natural fibers such as cotton, flax, sisal etc. It is the world's most abundant natural, renewable, biodegradable polymer. Cellulose is a polydispersed linear polymer of  $\beta$

(1, 4)-D -glucose with a syndiotactic configuration. In cell walls, cellulose nano fibers are embedded in matrix substances such as hemicellulose and lignin and the removal of the matrix substances has been performed before the fibrillation process.

Different raw materials used for production of cellulose nano fibers are banana (pseudo stem), jute (stem), pineapple (leaf) [2], Kenaf bast fibers [3], coconut husk fibers [4], oil palm empty-fruit-bunch [5], and hemp fibers [6]. In this part of the study sisal leaves were used for the isolation of cellulose nano fibers. Sisal fiber is obtained from the leaves of the plant *Agave sisalana*, which was originated from Mexico. It is grouped under the broad heading of the “hard fibers” in which sisal is placed second to manila in durability and strength [7]. Juan I. Moran *et al.* has been reported that sisal fibers are composed of cellulose (50–74%), lignin (8–11%), hemicellulose (10–14%), pectin (1%) and wax (2%) [8]. Cellulose extraction from sisal fibers could lead to high yield of nano fibers due to its high cellulose content.

Several methods are used to extract cellulose nano fibers from the plant cell wall [9, 10]. They are generally based on chemical and mechanical treatments. Wenshuai Chen *et al.* isolated nano fibers from four different sources (wood, bamboo, wheat straw and flax fibers) by a chemical-ultrasonic treatment [11]. S. Panthapulakkal and M. Sain reported the isolation of cellulose nano fibers from wood pulp fibers by mechanical defibrillation [12]. M. Paakko *et al.* prepared nanoscale cellulose fibrils by enzymatic pre-treatment methods [13]. Farah Fahma *et al.* isolated cellulose nano fibers from oil palm empty-fruit-bunch using sulfuric acid hydrolysis [5].

The steam explosion technique includes saturating the sisal leaves with steam at elevated pressure and temperature followed by sudden release of pressure, during which the flash evaporation of water exerts a thermo mechanical force causing the material to rupture. The steam explosion process was first introduced by Mason in 1927. He used the technique to defibrate wood into fiber for board production [14]. Bibin Mathew Cherian *et al.* reported that steam explosion process lead to the hydrolysis of glycosidic bonds in hemicellulose and cleavage of hemicellulose –lignin bonds. It also resulted in an increased solubilization of hemicellulose in water and increased the solubility of lignin in alkaline or organic solvents [15]. In this study it is proposed to isolate cellulose nano fibers from sisal leaves using steam explosion technique.

## **7. A.2 Methodology**

### **7. A.2.1 Isolation of cellulose nano fibers (CNF)**

Sisal leaves were peeled and chopped into short length of about 0.5–1 cm and treated with 2 wt% NaOH in an autoclave and kept under 137 Pa pressure for one hour. Then the pressure was released immediately and subsequently washed with water. The fibers were then dried in an air oven at 50 °C for 2 h. The immersion of sisal fibers in dilute alkaline medium facilitates the removal of adhesive nature of the fiber surface by extracting non-cellulosic constituents and causes the separation of structural linkages between lignin and carbohydrate and the disruption of lignin structure [14]. The fibers were then bleached using a mixture of sodium hydroxide, acetic acid and 1:3 sodium hypochlorite solution. Each bleaching took 1 h and the process was repeated six times. After bleaching, the fibers were washed in



distilled water until the smell of the bleaching agent was removed and then dried.

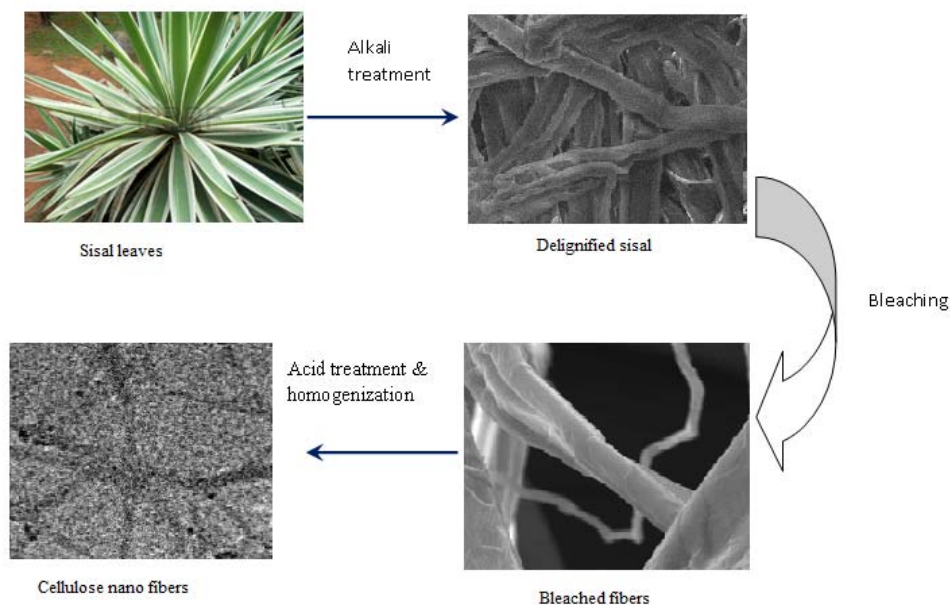


**Figure 7a.1 Schematic representation for the isolation of cellulose nano fiber**

The bleaching process in the presence of sodium hypochlorite solution helps to remove majority of the lignin component. The bleached fibers were treated with 10% oxalic acid in an autoclave under pressure of 25 psi for 15 min. The combined acid and steam treatments remove the traces of hemicellulose and lignin remaining after the bleaching process [15]. The pressure was released immediately facilitating the separation of nanofibrils. The process was repeated eight times. The fibers were suspended in water and subjected to continuous stirring with a mechanical stirrer of type RQ-1.27 A and 9000 R.P.M for 4 h. The suspension was kept in an oven at 90°C till it was fully dried. Figure 7a.1 gives the schematic representation for the isolation of cellulose nano fibers. The chemical composition,

morphology, crystalline behavior and thermal stability of the isolated nano fibers were characterized by means of chemical analysis, SEM, TEM, FTIR, XRD and TGA.

## **7. A.3 Results and Discussion**

### **7. A.3.1 Chemical Analysis**

Table 7a.1 depicts the chemical composition of raw fiber, alkali treated fiber and bleached fiber. It is clear from the table that the raw fiber has the highest content of hemicellulose and lignin naturally showing lowest percentage of  $\alpha$ -cellulose. When the raw fiber is subjected to alkali treatment followed by steam explosion, partial hydrolysis of hemicellulose and depolymerization of lignin occur giving rise to sugars and phenolic compounds. Lignin has an alkali soluble character while hemicellulose is a water soluble polysaccharide. Jiebing Li *et al.* reported that the steam explosion process resulted in hydrolysis of glycosidic bonds in the hemicellulose and it will lead to the cleavage of hemicellulose – lignin bonds [16]. B Xiao *et al.* have reported that the high solubility of lignin and hemicellulose is due to the cleavage of the  $\alpha$ -ether linkages between lignin and hemicellulose during alkali treatment [17]. It is apparent from the Table 7a.1 that the complete removal of lignin and hemicellulose does not take place. There is a decrease in percentage of lignin and hemicellulose content and a corresponding increase in percentage of  $\alpha$ -cellulose after the bleaching process. The trace amounts of hemicellulose and lignin components even after the bleaching process are also confirmed from the FTIR analysis. Increase in percentage of cellulose content after steam explosion of sisal fibers increases the number of available hydroxyl groups which in turn leads to the enhanced moisture absorption [14].

**Table 7a.1 Chemical composition of treated and untreated sisal fibers**

Sample	$\alpha$ -cellulose (%)	Hemicellulose (%)	Lignin (%)	Moisture content (%)
Raw fiber	74±2.8	12±0.5	9±0.7	10.43±0.5
Alkali treated fiber	86±1.2	8±0.6	4±0.6	10.50±0.32
Bleached fiber	95±1.5	0.54±.01	1.6±0.3	10.56±0.34

### 7. A.3.2 Fourier transform infrared spectroscopy

Sisal fibers in various forms were analyzed using FTIR to know about the various chemical constituents present in them. Figure 7a.2 depicts the FTIR spectra of raw fiber, alkali treated fiber, bleached fiber and cellulose nano fiber. The FTIR peaks reflected in the broad absorption band in the 3700-3100  $\text{cm}^{-1}$  region is related to the -OH groups present in their main components. The peaks in the area of 3424  $\text{cm}^{-1}$  arise due to O-H stretching vibrations of hydrogen bonded hydroxyl (-OH) group. The peaks around 2916  $\text{cm}^{-1}$  are due to the aliphatic saturated C-H stretching vibration in cellulose and hemicellulose. In the cellulose nano fiber, the peak around 1643  $\text{cm}^{-1}$  may be due to the absorbed water. The peak around 1730-1700  $\text{cm}^{-1}$  is due to the acetyl and uronic ester groups of residual hemicellulose or the ester linkage of carboxylic group of the ferulic and *p*-coumaric acids of lignin. This peak is absent in the case of cellulose nano fiber.

The 1635-1515  $\text{cm}^{-1}$  region in the raw fiber and alkali treated fiber corresponds to aromatic C = C stretch from lignin components [18, 19]. The peak in the range 1270-1032  $\text{cm}^{-1}$  shows C-O stretch and deformation bands in cellulose, hemicelluloses and lignin, while the peak at 897  $\text{cm}^{-1}$  is due to  $\beta$ -glycosidic linkages of glucose ring of cellulose [15].

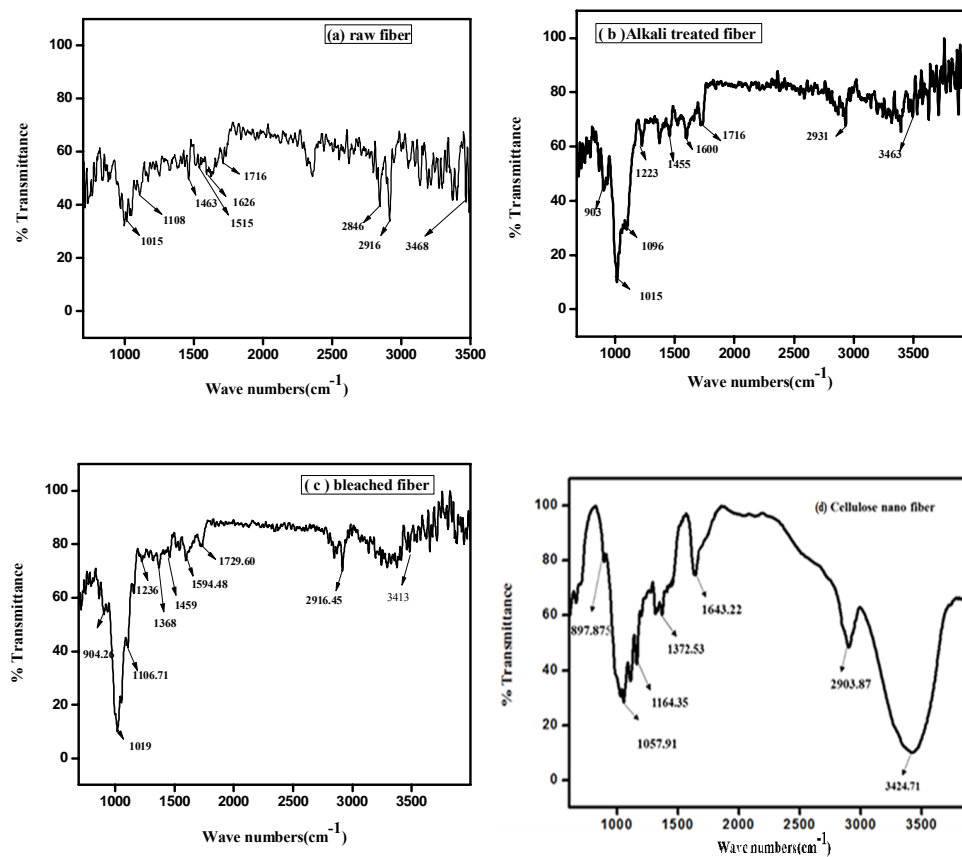


**Figure 7a.2 FTIR spectra of (a) Raw fiber (b) Alkali treated fiber (c) Bleached fiber and (d) Cellulose nano fiber**

The band at 1057 cm<sup>-1</sup> is assigned to ether linkage (C-O-C) from lignin or hemicellulose [15]. The absence of the absorption bands related to aromatic ring vibrations (1635-1515cm<sup>-1</sup>) from the spectra of cellulose nano fiber gives evidence for the removal of lignin. The absorbance at 1372, 1164, 1057 and 897cm<sup>-1</sup> (Figure.7a.2 (d)) is associated with the typical values of cellulose [8, 20, 21].

### 7. A.3.3 X-ray Diffraction

XRD is used to analyze the crystallinity of nano fibers. Figure 7a.3 illustrates the X-ray diffraction peaks for raw sisal fiber, alkali treated fiber, bleached fiber and cellulose nano fiber. The cellulose is present in the form of cellulose I, not as cellulose II and so there is no doublet in the intensity of the main peak. Similar result was reported by Juan I. Moran *et.al* [8]. The crystalline nature of the treated sisal fiber can be observed from XRD studies. Figure 7a.3 (a) exhibits the XRD pattern of untreated sisal fiber. From the pattern, it is evident that the fiber is almost amorphous with very little crystallinity in it. Figure 7a.3 (b) shows the XRD pattern of alkali treated fiber, where slight crystallinity is revealed by a relatively intense peak at  $2\theta = 22.73^\circ$ . The XRD pattern of bleached fiber (Figure 7a.3(c)), in which the crystallinity is increased, gives a relatively intense peak at  $2\theta = 22.5^\circ$ . The XRD pattern of cellulose nano fiber (Figure 7a.3 (d)) shows an intense peak at  $2\theta = 22.42^\circ$ . The sharp peak in the XRD pattern of the cellulose nano fiber shows higher crystallinity due to the more efficient removal of non cellulosic polysaccharides and dissolution of amorphous zones.

The crystallinity index ( $X_c$ ) of the cellulose can be determined by the equation [22]:

$$X_c = [I_{crystalline} - I_{amorphous}] / I_{crystalline} * 100 \dots\dots\dots (7a.1)$$

Where  $I_{crystalline}$  is the intensity at a  $2\theta$  angle close to  $22^\circ$  representing crystalline material and

$I_{\text{amorphous}}$  is the intensity at a  $2\theta$  angle close to  $18^\circ$  representing amorphous material in the cellulosic fiber.

**Table 7a.2 Crystallinity index of the fibers**

Samples	Raw Fiber	Alkali treated fiber	Bleached fiber	Cellulose nano fiber
Xc (%)	12.35	54.43	71.59	84.07

The values of the crystallinity index obtained are shown in Table 7a.2. Both bleaching and preparation conditions affects the degree of crystallinity of cellulose nano fiber. In the case of raw sisal fiber, crystalline cellulose components are oriented in a matrix of lignin, hemicellulose, pectin, etc. During chemical treatment, this matrix is dissolved and the remaining pure crystalline particles are isolated.

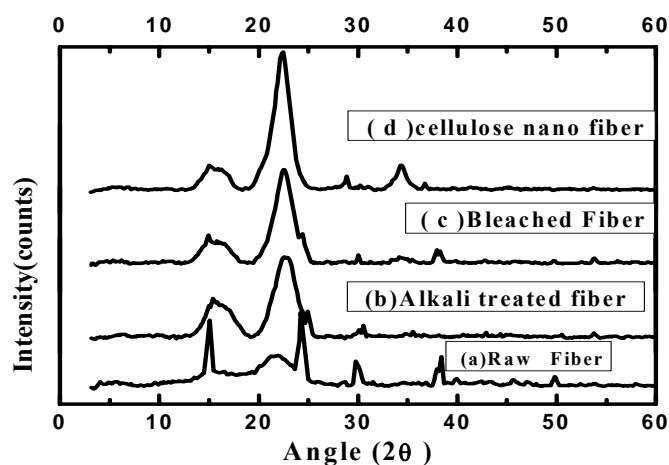


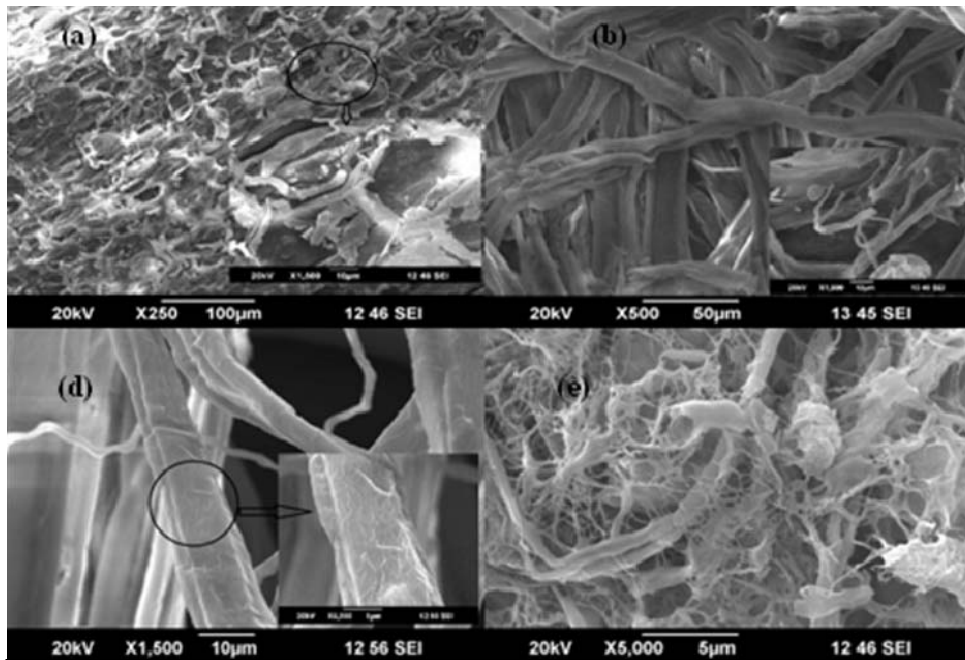
**Figure 7a.3 XRD of (a) Raw fiber (b) Alkali treated fiber (c) Bleached fiber and (d) Cellulose nano fiber**

These particles show increasing orientation along a particular axis, due to their similarity in shape. So the alkali treatment will lead to an increase in

percentage of crystallinity. The crystallinity index is further increased by the bleaching treatment. This confirms that the non-cellulosic amorphous polysaccharides were removed by the treatment. During the acid treatment, the hydronium ions can penetrate into the amorphous regions of cellulose, promoting the hydrolytic cleavage of glycosidic bonds and the release of individual crystallites [2, 5].

#### **7.A.3.4 Scanning electron microscopy**

Scanning electron microscopic analysis of treated and untreated sisal fibers in various forms were carried out to assess their surface morphology. Figure 7a.4 gives the SEM photographs of raw sisal fiber, alkali treated fiber, bleached fiber and cellulose nano fiber.



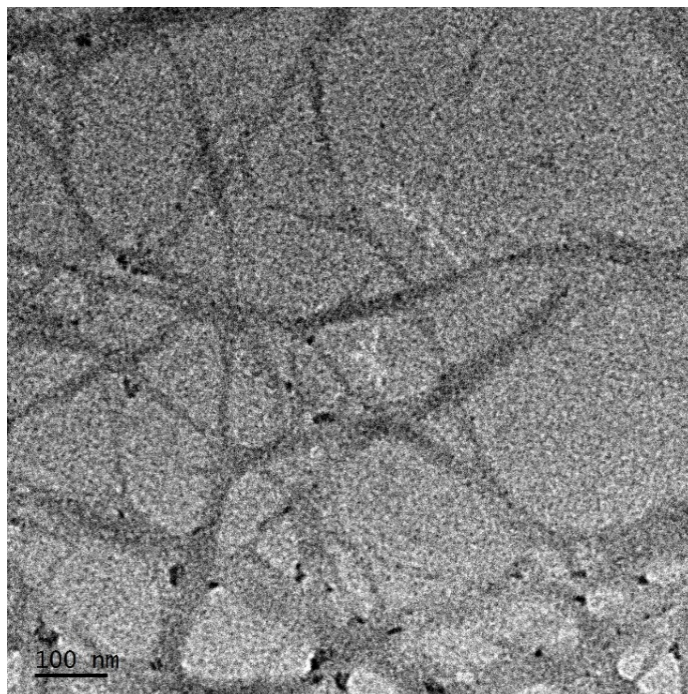
**Figure 7a.4 SEM photographs of (a) Raw fiber (b) Alkali treated fiber (c) Bleached fiber and (d) Cellulose nano fiber**

Figure 7a.4 (a) depicts the SEM photograph of raw sisal fiber. The raw sisal fiber bundles are composed of individual fibers linked together by massive cementing materials like lignin, hemicellulose, wax and oils. Figure 7a.4 (b) illustrates the SEM photograph of alkali treated fiber. Lignin has an alkali soluble character and hemicellulose is a water soluble polysaccharide. The alkali treatment removes a certain amount of cementing material and defibrillates the external cellulose microfibrils. Figure 7a.4(c) shows the SEM image of bleached fiber. Bleaching of alkali treated fiber removes the remaining cementing materials. The percentage of cementing materials decreases from raw fiber to bleached fiber. Figure 7a.4 (d) gives the SEM photograph of cellulose nano fiber. The SEM images reveal that fibers are separated into individual fibrils after the dissolution of the cementing materials during the process.

#### **7. A.3.5 Transmission electron microscopy**

Figure 7a.5 shows the TEM image of a dilute suspension of cellulose nano fiber. In TEM, aggregates of wire like cellulose nano fibers with nanoscale dimensions can be observed. It is clear from the image that 90% of the cellulose nano fibers generated is distributed in the range of 40 to 10 nm with more than 60% of the fibers with a diameter in the range of 14-20 nm and lengths of several thousand nanometers. Similar results were observed by Cintil *et.al* in their observations [23].





**Figure 7a.5 TEM of Cellulose nano fiber**

#### **7. A.3.6 Thermogravimetric analysis**

Sisal fiber specimens were thermogravimetrically analyzed to compare the degradation characteristics of chemically treated fibers with untreated fiber. Hemicellulose, cellulose and lignin usually decompose at different temperatures because of the differences in their chemical structures. The TG and DTG curves for treated and untreated sisal fibers are given in Figures 7a.6 & 7a.7 respectively. The raw fiber shows four peaks in its degradation pattern (Figure 7a.7). The initial weight loss in the region 100-200°C is mainly due to moisture evaporation. The temperature region ranging from 250–310°C is mainly attributed to thermal depolymerization of hemicellulose and the cleavage of glycosidic linkages in cellulose. The broad

peak in the region from 250 to 510°C is contributed by lignin components and the degradation of cellulose takes place between 275 and 400°C [14, 24]. Nunez *et al.* reported that the degradation of cellulose took place at high temperature along with pyrolytic degradation of lignin [25]. Kim *et al.* observed that the hemicellulose degraded between 180 to 350°C and lignin between 250 to 500°C while degradation of cellulose took place between 275 to 350°C [26].

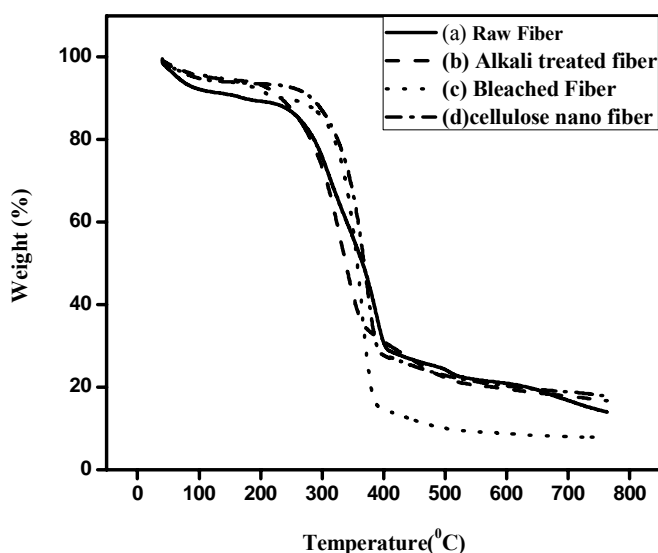


**Figure 7a.6** TG curve of (a) Raw fiber (b) Alkali treated fiber (c) Bleached fiber and (d) Cellulose nano fiber

The DTG curve of alkali treated fibers shows two peaks (Figure 7a.7). The first peak at 332°C is due to the thermal decomposition of  $\alpha$ -cellulose and the second peak at 466°C is due to the thermal degradation of lignin [27]. Similar curves were obtained for bleached fibers, one at 364°C which is due to the thermal decomposition of  $\alpha$ -cellulose and a small peak at 486°C, which corresponds to the degradation of lignin. In the DTG curve of cellulose

nano fiber a major decomposition peak is observed at 371 °C due to  $\alpha$ -cellulose decomposition. Cellulose nano fiber shows higher degradation temperature than raw fiber.

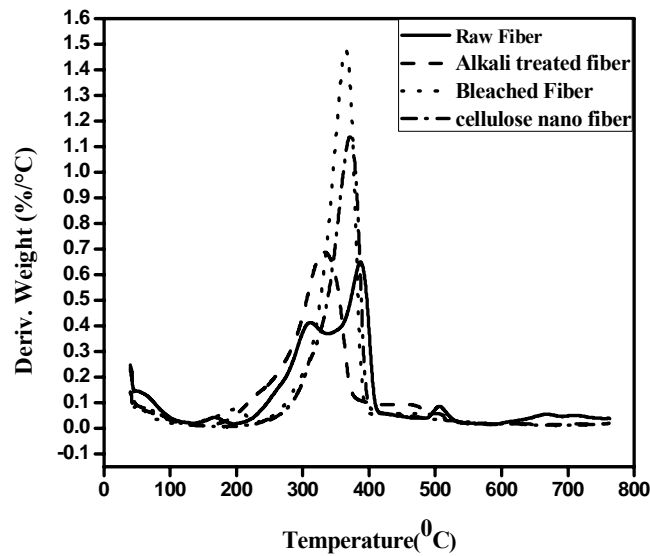


**Figure 7a.7 DTG curve of raw fiber, alkali treated fiber, bleached fiber and cellulose nano fiber**

In raw fiber the cellulose is organized into fibrils and is surrounded by a matrix of lignin, hemicellulose and pectins. Hemicellulose is incorporated into the structure of the cellulose and is located within and between the cellulose fibrils. The presence of these impurities may initiate more active sites and accelerate the beginning of thermal degradation as indicated by the lower degradation temperature in raw fibers [28, 29].

### **7. A.4 Conclusions**

Chemical analysis of the fibers reveals substantial removal of hemicellulose and lignin from the sisal fibers. The  $\alpha$ -cellulose content of the

fibers is increased from 74% to 95% while hemicellulose and lignin content is significantly decreased to 0.5% and 1.6%, respectively. The FTIR studies show the evidence for the dissolution and chemical modification of lignin and hemicellulose during various treatments. SEM reveals that there is a reduction in the fiber diameter during the steam explosion in acidic medium. It confirms the dissolution of the non-cellulosic components present in the fiber cell wall by the acid correlated steam treatment process, which enhances the extraction of crystalline cellulose components from the fiber. TEM image evidence the formation of nano fibers and the average diameter is found to be between 10-40 nm. DTG results show that cellulose nano fibers exhibit enhanced thermal stability. The higher thermal stability of the prepared cellulose nano fibers has been related to the higher crystallinity of the cellulose obtained after the removal of hemicellulose and lignin components from the fiber.

## References

- [1]. Adriana N. Frone, Denis M. Panaitescu, Dan Donescu, U.P.B. Scientific Bulletin, Series B, 2011, 73(2).
- [2]. E. Abraham, B. Deepa, L.A. Pothan, M. Jacobc, S. Thomas, U. Cvelbar, R. Anandjiwala, Carbohydrate Polymers, 2011, 86, 1468– 1475.
- [3]. Hanieh Kargarzadeh , Ishak Ahmad , Ibrahim Abdullah, Alain Dufresne , Siti Yasmine Zainudin , Rasha M. Sheltami, Cellulose, 2012, 19,855–866.
- [4]. M.F. Rosa, E.S. Medeiros, J.A. Malmonge, K.S. Gregorski b, D.F. Wood, L.H.C. Mattoso, G. Glenn, W.J. Orts, S.H. Imam, Carbohydrate Polymers ,2010, 81, 83–92.
- [5]. Farah Fahma , Shinichiro Iwamoto ,Naruhito Hori , Tadahisa Iwata , Akio Takemura ,Cellulose, 2010, 17, 977–985 .

- [6]. D Dai, M Fa, P Collins, *Industrial crops and products*, 2013, 44, 192–199.
- [7]. Kuruvilla Joseph, Romildo Dias Tolêdo Filho, Beena James, Sabu Thomas, Laura Hecker de Carvalho, *R. Bras. Eng. Agríc. Ambiental, Campina Grande*, 1999, 3(3), 367-379.
- [8]. Juan I. Mora'n Æ Vera A. Alvarez, Viviana P. Cyras, Analia Vazquez; *Cellulose*, 2008, 15, 149–159.
- [9]. Hudson Alves Silverio , Wilson Pires Flauzino Neto, Noelio Oliveira Dantas, Daniel Pasquini; *Industrial Crops and Products*,2013, 44 ,427– 436.
- [10]. Daniel Pasquini, Eliângela de Moraes Teixeira, Antônio Aprígio da Silva Curvelo, Mohamed Naceur Belgacemc, Alain Dufresne; *Industrial Crops and Products* ,2010, 32 , 486–490.
- [11]. Wenshuai Chen, Haipeng Yu, Yixing Liu, Yunfei Hai, Mingxin Zhang, Peng Chen, *Cellulose* ,2011, 18(2), 433-442.
- [12]. S. Panthapulakkal and M. Sain, *International Journal of Polymer Science*, 2012, Article ID 381342, 6.
- [13]. M. Paakko,. Ankerfors, H. Kosonen, A. Nykanen,S. Ahola, M. O sterberg, J. Ruokolainen, J. Laine, P. T. Larsson, O. Ikkala, T. Lindstrom, *Biomacromolecules*, 2007, 8, 1934-1941.
- [14]. B. Deepa, Eldho Abraham, Bibin Mathew Cherian, Alexander Bismarck, Jonny J. Blaker, Laly A. Pothan, Alcides Lopes Leao, Sivoney Ferreira de Souza , M. Kottaisamy, *Bioresource Technology*, 2011, 102 , 1988–1997.
- [15]. Bibin Mathew Cherian, Laly A. Pothan, Tham Nguyen-Chung, Gunter Mennig, M. Kottaisamy, Sabu Thomas , *Journal of Agriculture Food & Chemistry*, 2008, 56, 5617–5627.
- [16]. Jiebing Li, Gunnar Henriksson, Göran Gellerstedt; *Bioresource Technology*, 2007, 98, 3061–3068.

- [17]. B Xiao, X F Sun, C S Run, *Polymer Degradation & Stability*, 2001, 74, 307–319.
- [18]. Nereida Cordeiro, Carlos Pascoal Neto, Joao Rocha, Mohamed N. Belgacem , Alessandro Gandini, *Holzforschung*, 2002, 56, 135-142.
- [19]. Wilson Pires Flauzino Neto, Hudson Alves Silverio, Noelio Oliveira Dantas, Daniel Pasquini, *Industrial Crops and Products*, 2013, 42, 480– 488.
- [20]. Z.C. Geng, R.C. Sun, X.F. Sun, Q. Lu; *Polymer Degradation and Stability*, 2003, 80, 315–325.
- [21]. X. F. Sun,a,c F. Xu, R. C. Sun, P. Fowler , M. S. Baird; *Carbohydrate Research*,2005, 340 , 97–106.
- [22]. Y. M. Zhou, S. Y. Fu, L. M. Zheng, H. Y. Zhan, *eXPRESS Polymer Letters*, 2012, 6(10), 794–804.
- [23]. Cintil Jose Chirayil, Jithin Joy, Lovely Mathew, Miran Mozetic,Joachim Koetz, Sabu Thomas; *Industrial Crops and Products*, 2014,59 , 27–34.
- [24]. R Chandrahas, N P Rajamane, Jeyalakshmi; *International Journal of Emerging Technology and Advanced Engineering ISSN 2250-2459*, 2014, 4(4).
- [25]. A.J. Nunez, J.M. Kenny, M.M. Reboredo, M.I. Aranguren, N.E. Marcovich, *Polymer Engineering and Science*, 2002, 42, 733.
- [26]. Hee-Soo Kim, Sumin Kim, Hyun-Joong Kim, Han-Seung Yang ; *Thermochimica Acta*, 2006, 451 , 181–188.
- [27]. J Lu, TWang, L T Drzal, *Composites Part A: Applied Science and Manufacturing*, 2008, 39, 738–746.
- [28]. T Nguyen, E Zavarin, E M Barrall, *Journal of Macromolecular Science: Part C: Polymer Reviews*. 1981, 20, 1–65.
- [29]. Duchesne,E L Hult, U Molin, G Daniell, T Iversen, H Lennholm, , *Cellulose*,2001, 8, 103–111.

## **Part- B**

### **Polypropylene/Polystyrene/cellulose nano fiber composites**

#### **Abstract**

*Nanocomposites of polypropylene /polystyrene blends reinforced with cellulose nano fiber (CNF) were prepared by melt mixing in a Thermo Haake Rheocord mixer. The effect of CNF on the properties of nanocomposites has been evaluated. Thermal, mechanical, morphological and sorption characteristics of nanocomposites were studied. TEM images reveal that the CNF is found at the interface between the blend components. TGA studies show that there is an increase in thermal stability with increasing CNF content. Water transmission data shows that the addition of 0.5 wt% CNF decreased the transmission rate in the composite. Mechanical properties improve with the incorporation of cellulose nano fiber.*

#### **7. B.1 Introduction**

Cellulose based nanocomposites have been receiving considerable attention because of their low density, nonabrasive nature, nontoxicity, low cost and interesting specific properties [1,2]. Cellulose, which is a natural polysaccharide, is the most abundant natural biopolymer in the world, which is renewable and biodegradable. Cellulose fibrils in micro and nano scale dimensions have high reinforcing efficiency in polymeric matrices due to their good mechanical properties [3]. The potential applicability of nano cellulose is in packaging products, construction, automotive, furniture, electronics, pharmacy, cosmetics and as membranes for combustible cells. High strength and stiffness as well as small dimensions of nano cellulose may impart useful properties to composite materials which could be used in a wide range of applications.

Cellulose nano fibers are fibrillar units containing both amorphous and crystalline regions and have the ability to create entangled networks. It has cross-sectional dimension in nanometer scale (1-100nm). Despite the amorphous portion, the nano fibers have a tensile modulus of 138 GPa and tensile strength of about 10 GPa [4, 5]. Navin Chand *et.al* reported that the selection of cellulose fillers in various applications depends upon their composition and physical properties. They also reported that cellulose fibers obtained from wheat, rice straw etc. are used for pulp and paper making while coir, pineapple and banana leaves are used in textiles and in polymer based composites[6]. In this work sisal is used for the preparation of cellulose nano fibers. Navin Chand *et al.* prepared the nano fibers by using acid hydrolysis and studied the reinforcing effect of nano fibers in different polymers such as LDPE, LLDPE and PP. Gilberto Siqueira *et al.* studied the effect of nanowhiskers and microfibrillated cellulose (MFC) both extracted from sisal on polycaprolactone (PCL) and they found that the modulus was higher for MFC-reinforced composites, whereas the elongation at break was lower for a given loading level [7].

Numerous researchers have investigated PP/cellulose nano fiber composites [8, 9] and PS/cellulose nano fiber composite systems [10, 11] individually. In this part of the work it is proposed to study the reinforcing effect of cellulose nano fibers on the properties of Polypropylene/ Polystyrene blends.



## **7. B.2 Methodology**

### **7. B.2.1 Materials**

The details of the polymers and nanoclay types used for the study are discussed in Chapter 2 (sections 2.1.1 & 2.1.2). Sisal cellulose nano fibers were extracted from the leaves of sisal plant using steam explosion technique.

### **7. B.2.2 Nanocomposite preparation**

PP/PS (80/20) and the cellulose nano fibers in varying amounts (0.25 -5wt.%) were prepared by melt mixing using an internal mixer (Haake Rheomix 600) at 180°C with a rotor speed of 50 rpm. Mixing time was 8 min for each sample. After mixing, the melt was pressed in a hydraulic press, cut into pieces and injection molded in a DSM Micro 10cc Injection Molding Machine, with a barrel temperature of 190°C. Tensile properties, flexural properties, impact strength, hardness, dynamic mechanical properties, thermal properties and morphology of the composites were analyzed according to various standards as described in Chapter 2 (section 2.2.3). Water Vapor Transmission Rate ( $\text{gm/mm/mm}^2/24\text{hr}$ ) is found out using the procedure given below.

#### *Procedure*

The water vapor transmission rates (WVTR) of each material were measured by a modified technique of wet cup method, according to ASTM D 1653. 50 mm diameter and 3 mm thick samples were taken as the testing specimens. The thickness of the sample was measured accurately by digital micrometer. Five measurements were carried out and the mean value of the sample thickness was taken to calculate the water vapor permeability. The

sample was fixed on the top of the cup containing distilled water using a cap and with the use of grease to ensure leak proof condition. The cups were periodically removed and weighed after 24 hrs. The mass of water loss from the cups were monitored as a function of time. Water vapor transmission rate (gm/mm/mm<sup>2</sup>/24hr) is the steady water vapor flow in unit time through unit area of body according to ASTM D 1653. The rate of water vapor transmission is calculated by the following equation.

$$\text{WVTR} = (G/t) D/A = \text{grams per mm per mm}^2 \text{ per 24 h} \dots\dots\dots(7b.1)$$

Where;

G = Weight change in grams

D = Thickness of the film in mm

t = Time during which G occurred in hrs

A = Test area in mm<sup>2</sup>

## 7. B.3 Results and Discussion

### 7. B.3.1 Mechanical properties

#### (a) Tensile properties

The tensile strength and tensile modulus as a function of increasing CNF loading is given in Figure 7b.1. The figure indicates that the strength and modulus of the PP/PS blend increases with the incorporation of nano fibers. The tensile strength of the composites increases up to 32% and tensile modulus increases up to 168 % at 0.5 wt % nano fibers. The increase in tensile properties may be due to their large surface area on account of which they can interact more with polymer matrix and decrease the chain mobility [9].

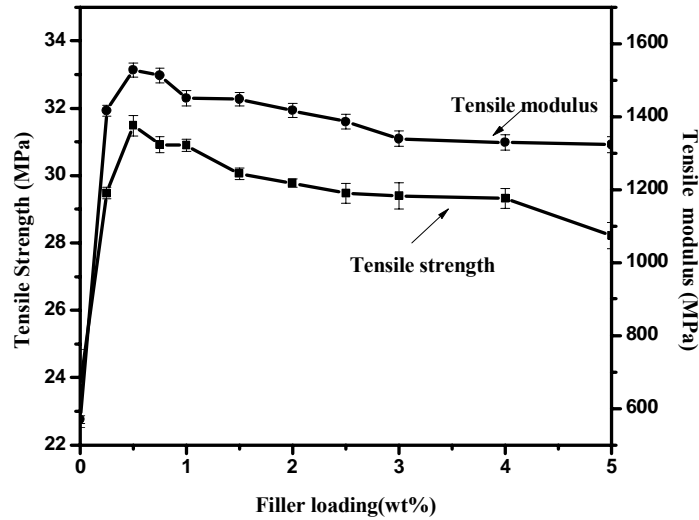


**Figure 7b.1** Variation of tensile properties with filler loading

Cintil *et.al* reported similar trend in their study on the reinforcing efficiency of isora nano fibrils in unsaturated polyester matrix. They found that the addition of nano fibrils improved the strength and stiffness along with a significant improvement in toughness [12]. The decrease in tensile properties beyond the optimum filler loading is due to the inadequate wetting of the fiber with the matrix. The poor adhesion between matrix and fiber leads to voids at the fiber matrix interface and the stress transfer to the fibers becomes inefficient leading to lower tensile properties [13].

**(b) Flexural properties**

Effect of CNF on flexural properties of nanocomposites is illustrated in Figure 7b.2. The increase in flexural strength and modulus indicates that the nanocomposites have become more rigid and less flexible. The flexural strength of the composites increases up to 31% and flexural modulus increases up to 262 % at 0.5 wt % nano fibers.

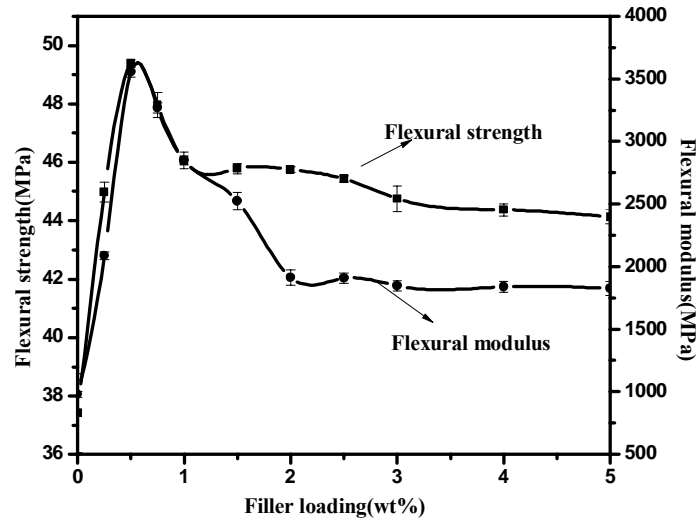
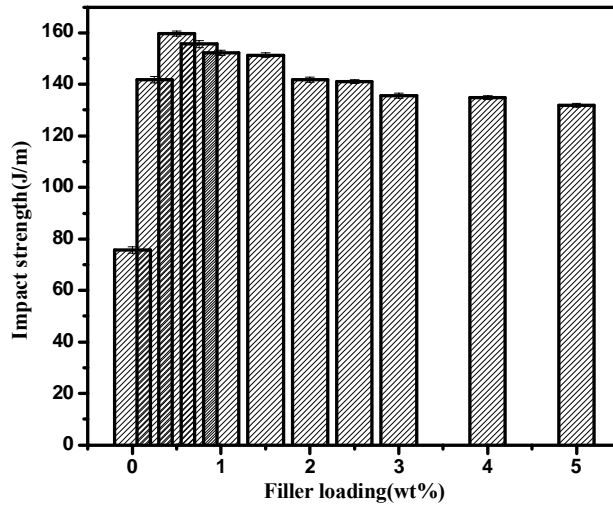


Figure 7b.2 Variation of flexural properties with filler loading

### (c) Impact properties

The unnotched impact energy is an indication of both crack initiation and propagation. The crack initiation energy is a function of matrix properties, filler morphology and adhesion between the filler and the matrix and it tends to dominate the fracture process [14]. The effect of CNF on the impact strength with increasing loadings is illustrated in Figure 7b.3. The impact strength increases with cellulose nano fiber loading and then decreases after reaching a maximum. From the above results it is obvious that the force required for the crack initiation of the nanocomposites is higher than that for the pure polymer matrix. Cellulose nano fibers resist the crack propagation and it act as a load transfer medium.

There is a slight decrease in impact strength with increasing filler loading. At higher filler loadings, the fillers tend to agglomerate which causes easy propagation of cracks in the composite [15].



**Figure 7b.3 Variation of impact strength with filler loading**

**(d) Hardness**

Hardness of PP/PS/cellulose nano fiber composites with varying loading is given in the Figure 7b.4.

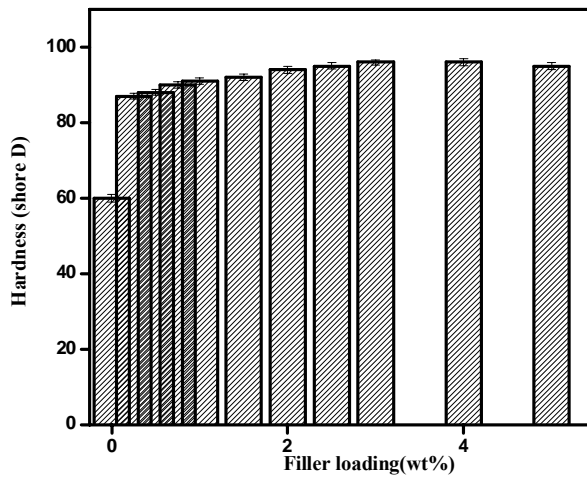


**Figure 7b.4 Variation of hardness with filler loading**

The hardness increases up to 4 wt %, reaches a maximum and thereafter decreases. The increase in hardness may be due to the increase in stiffness of composites after the addition of cellulose nano fiber and the decrease may be due to the agglomeration of cellulose nano fiber.

### 7. B.3.2 Melt Flow Index

Figure 7b.5 depicts the variation of MFI with CNF loading. A slight decrease in MFI is observed with increasing CNF loading. This result indicates that the melt viscosity of the polymer blend increases with increasing CNF loading.

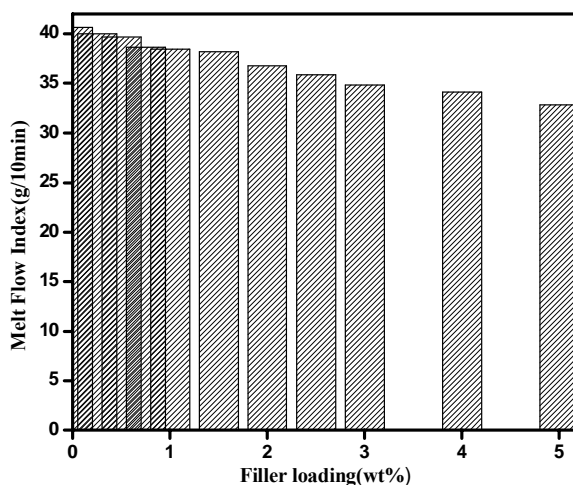
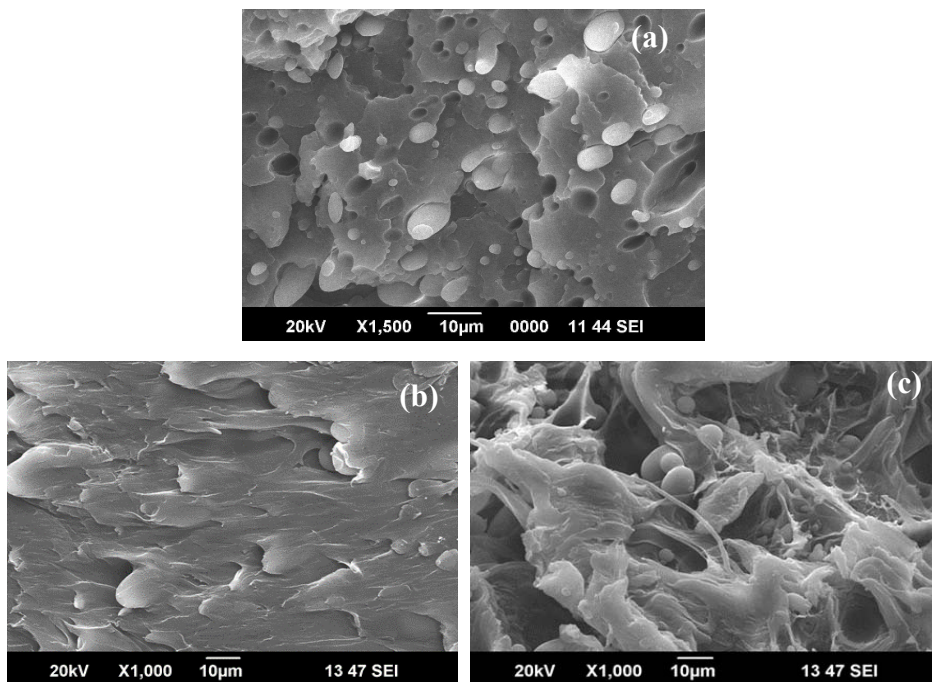


Figure 7b.5 Variation of MFI with filler loading

### 7. B.3.3 Scanning electron microscopy

Figures 7b.6 (a), 7b.6 (b) & 7b.6 (c) show the morphology of the fractured cross sections of tensile samples of PP/PS blend and CNF reinforced PP/PS blend having 0.5 and 5wt% fiber concentration. Morphology of PP/PS blend (Figure 7b.6 (a)) shows spherical domains of

PS phase are surrounded by the continuous PP phase. PS phase and the PP matrix show weak interfacial adhesion. After the addition of 0.5 wt % of CNF [Figure 7b.6(b)] adhesion between the two components is improved and shows a more homogeneous structure which reveals better stress transfer between the components.

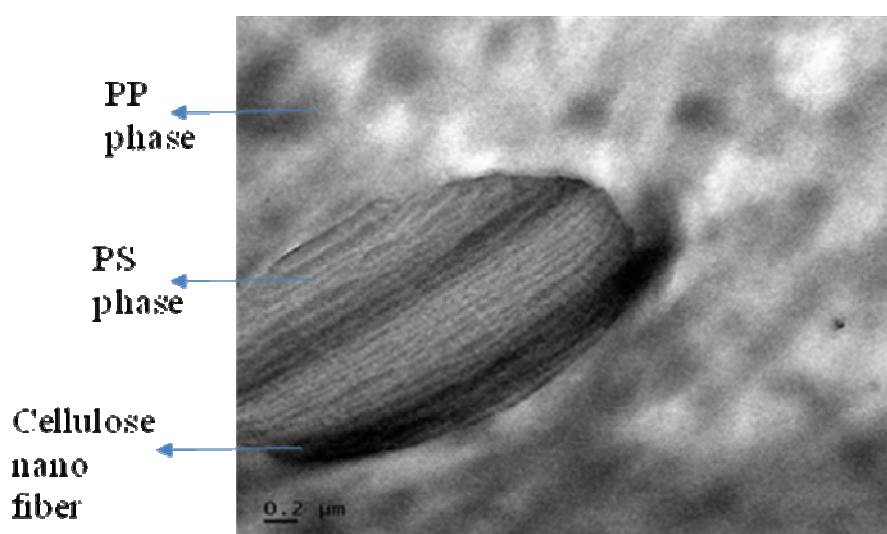


**Figure 7b.6 SEM images of (a) PP/PS blend, (b) PP/PS/0.5wt% cellulose nano fiber and (c) PP/PS/5wt% cellulose nano fiber**

Figure 7b.6(c) shows the SEM photograph of 5 wt% CNF filled PP/PS blend. SEM analysis shows a weak interface between the dispersed phase (PS) and the continuous phase (PP) which results in reduction of properties due to agglomeration at higher loadings. This result gives good explanation for the improvement in mechanical properties (section 7.B.3.1).

### 7. B.3.4 Transmission electron microscopy

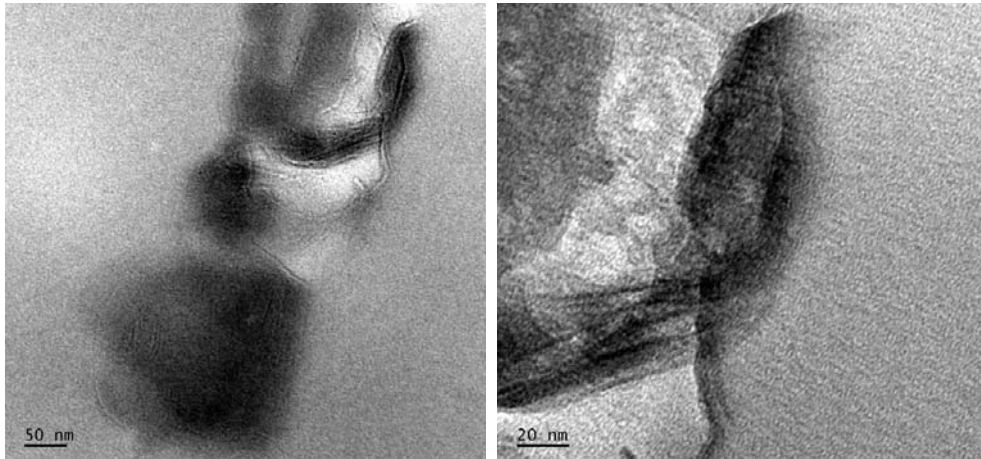
The dispersion and location of cellulose nano fiber in the polymer blends have a significant influence on the morphological development of the blends as well as effect of CNF as a modifier. Transmission electron microscopy is an effective method to find out the location of cellulose nano fiber in polymer.



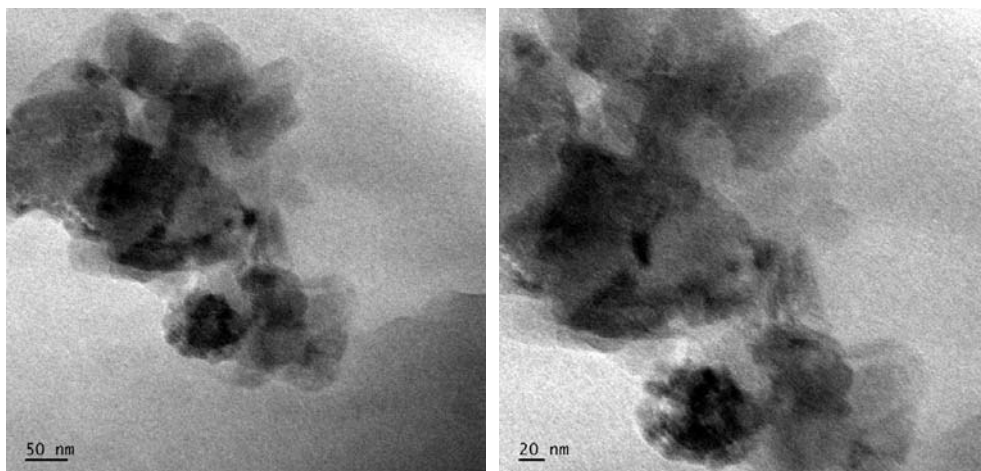
**Figure 7b.7 Low magnification transmission electron microscopic image of PP/PS/0.5wt% cellulose nano fiber**

Figure 7b.7 depicts a bright field TEM image of 0.5 wt % CNF -filled PP/PS blend that gives a general view of the dispersed PS domains (ellipsoid) in the PP matrix. Besides, the CNF (dark lines) is easily visualized in the TEM photographs and it reveals that the cellulose nano fiber is located at the interface between the blend components and thereby increases the effective stress transfer between the CNF and the polymer matrices.





**Figure 7b.8** Transmission electron microscopic bright field images of PP/PS/0.5wt% cellulose nano fiber at different magnifications (a) at 50 nm (b) at 20 nm



**Figure 7b.9** Transmission electron microscopic bright field images of PP/PS/5wt% cellulose nano fiber at different magnifications (a) at 50 nm (b) at 20nm

The transmission electron photographs in Figure 7b.8 exhibit the dispersion of 0.5wt% cellulose nano fibers in PP/PS blend at two different magnifications ((a) 50nm and (b) 20nm). At 0.5 wt% cellulose nano fiber, a better dispersion is observed without any agglomeration. When there is a

better fiber distribution, crack propagation will be prevented by the neighboring fibrils [12, 16].

Figure 7b.9 gives the dispersion state of 5wt% cellulose nano fiber in PP/PS blend at two different magnifications ((a) 50nm and (b) 20nm). At higher fiber concentrations there will be agglomeration of nano fiber. This generates matrix rich regions thereby causing easier failure of the bonding at the interfacial region and thus leading to poor mechanical properties.

### 7. B.3.5 Thermogravimetric analysis

To investigate the thermal characteristics of cellulose nano fiber on the PP/PS blend TGA was performed; Table 7b.1 presents the results from the DTG curves of PP/PS/CNF composites. Figure 7b.10 shows the TG curves of PP/PS/CNF composites [0.25, 0.5, 1.5, 3, &5 wt%].

Pure blend shows a maximum degradation temperature ( $T_{max}$ ) of 434.4 °C and it increases with increasing cellulose nano fiber. It reveals that thermal stability increases with CNF which indicates the suitability of these fibers for processing with thermoplastics, even with high melting polymers. S. Panthapulakkal and M.Sain compared the TGA curves of the wood fiber sheets and nano fiber sheets in their study. They reported that the enhanced stability was due to the absence of lignin and hemicellulose [17]. Higher the values of oxidation index (OI), higher will be the thermal stability. It is observed that the OI values increases with increase in cellulose nano fiber. This study indicates that the PP/PS/cellulose nano fiber composites are more thermally stable than PP/PS blend.

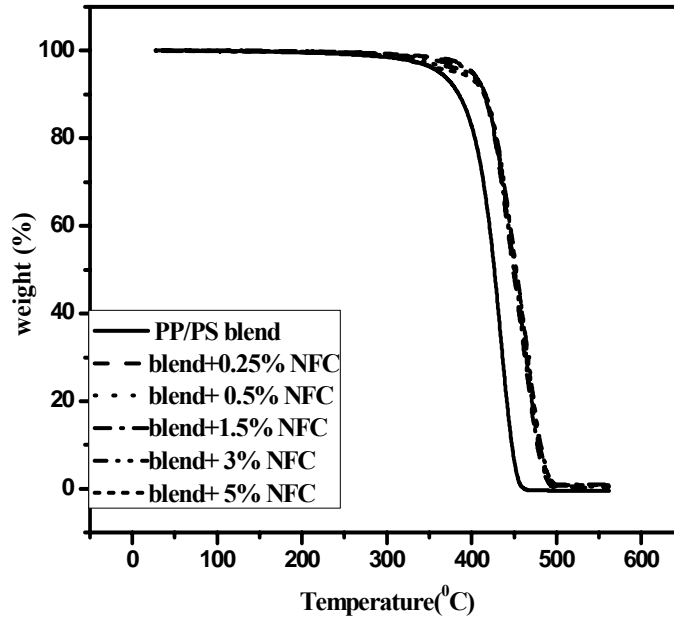


Figure 7b.10 TG curves of PP/PS blend, PP/PS/cellulose nanofiber composites

Table 7b.1 Results obtained from DTG curves of PP/PS blend, PP/PS/CNF composites

Samples	50% mass loss (°C)	T <sub>onset</sub> (°C)	T <sub>max</sub> (°C)	Residue at 600 °C (%)	OI
PP/PS blend	426.6	370.5	434.4	0.456	0.032
Blend +0.25wt%CNF	448.6	387.3	462.1	0.498	0.033
Blend +0.5wt% CNF	449.6	393.8	464.0	0.576	0.040
Blend +1.5 wt % CNF	450.4	393.9	464.3	0.584	0.041
Blend +3% wt CNF	452.5	394.1	465.8	0.861	0.060
Blend +5wt% CNF	452.8	395.7	468.4	0.999	0.070

### 7. B.3.5 .1 Kinetic analysis of thermal decomposition

Kinetic parameters were evaluated from the TGA curves using the plots of Horowitz-Metzger method, Broido's method and Coats Redfern methods.

The CR, BR and HM plots for the thermal degradation of PP/PS/CNF composites with different weight percentage of cellulose nano fiber (0.25,0.5,1.5,3,5 wt %) from the onset degradation temperature to the maximum degradation temperature are shown in the Figures 7b.11 (a), 7b.11 (b) & 7b.11 (c) respectively. The activation energy for each method is given in Table 7b.2. The activation energy of the CNF reinforced composites is higher than that of pure blend. The improvement in thermal stability and activation energy in the CNF reinforced composites are due to the presence of crystalline cellulose nanofiber [18].

**Table 7b.2** Activation energy (J/mol) calculated by Horowitz-Metzger, Broido's and Coats-Redfern methods of PP/PS/CNF composites

Samples	Coats –Redfern	Broido's	Horowitz- Metzger
PP/PS Pure blend	174	181	175
Blend+0.25wt%CNF	223	211	186
Blend +0.5wt%CNF	227	213	193
Blend +1.5wt%CNF	229	218	208
Blend +3 wt% CNF	230	220	209
Blend +5wt%CNF	232	222	212

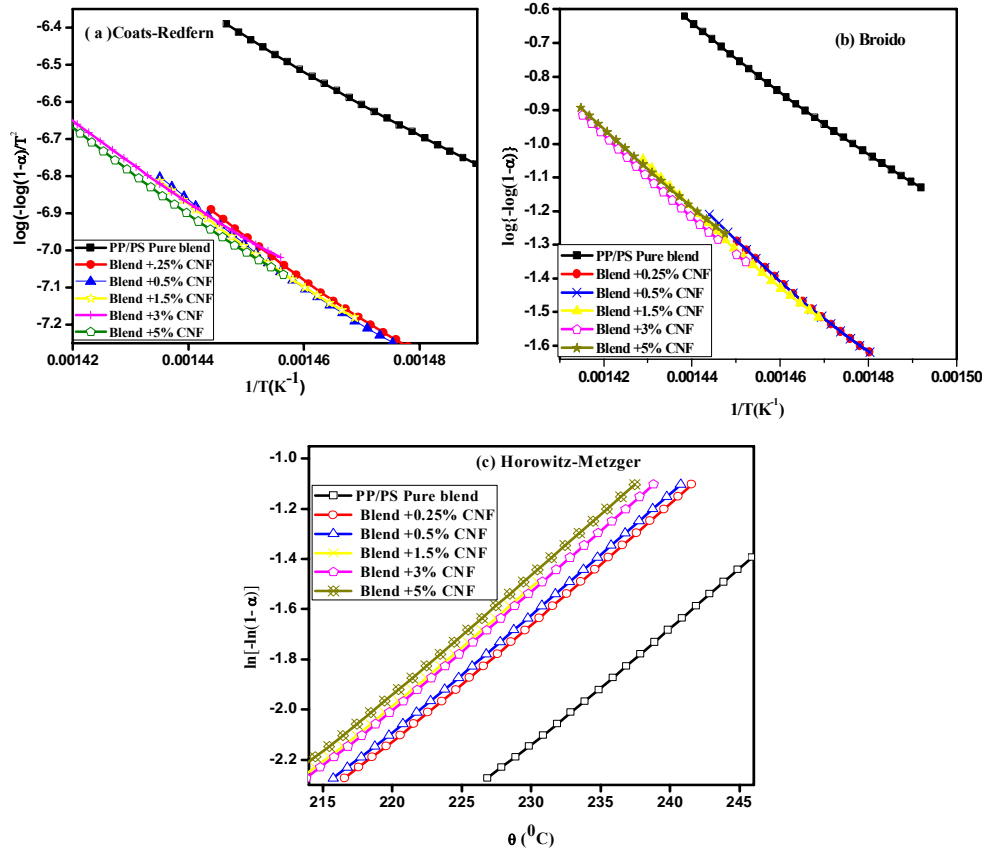


**Figure 7b.11** Kinetic plots for the determination of activation energy of PP/PS blend and PP/PS/CNF composites (0.25, 0.5, 1.5, 3 & 5 wt %) using (a) Coats-Redfern equation (b) Broido's method and (c) Horowitz-Metzger equation

### 7. B.3.6 Dynamic mechanical analysis

In order to investigate the reinforcing effect of cellulose nano fiber in PP/PS blend, dynamic mechanical analysis has been carried out at a fixed frequency of 1Hz in the temperature range of 40 to 125°C. The temperature dependence of the storage modulus of PP/PS blend and PP/PS cellulose nano fiber composites with varying amounts of CNF (0.25, 0.5, 1.5, 3 and 5 wt%) is given in the Figure 7b.12. Storage modulus decreases with addition

of 0.25wt% CNF and this is due to insufficient fibers unable to bear the stress transferred from the polymer matrix [19].

Nanocomposite with 0.5wt% cellulose nano fiber shows higher storage modulus as evident from the Figure 7b.12. The storage modulus of pure blend increases by 32% at 80°C with the incorporation of 0.5wt % CNF. This behavior is due to the reinforcing effect imparted by CNF that allows a better stress transfer at the interface. Table 7b.3 depicts the storage moduli and glass transition temperatures ( $T_g$ ) of the PP/PS blend and PP/PS/CNF composites.

**Table 7b.3 Results obtained from DMA curves of PP/PS blend, PP/PS/CNF composites**

Samples	Storage modulus				$T_g$ (°C) from $\tan \delta$ value
	45°C	80°C	100°C	120°C	
<b>PP/PS blend</b>	1007	525.3	374.1	159	114.95
<b>Blend+0.25%CNF</b>	677.2	378.8	278.9	116	114.60
<b>Blend+0.5%CNF</b>	1236	696	504.6	225.7	115.11
<b>Blend+1.5%CNF</b>	1126	631.2	456.1	191.4	114.25
<b>Blend+3%CNF</b>	971.4	554.4	400.3	183.2	113.88
<b>Blend+5%CNF</b>	904.4	502.4	357.9	155.1	112.85

There is a decrease in storage modulus at higher filler loading (3 & 5wt %). This is due to the agglomeration of cellulose nano fiber within the matrix.

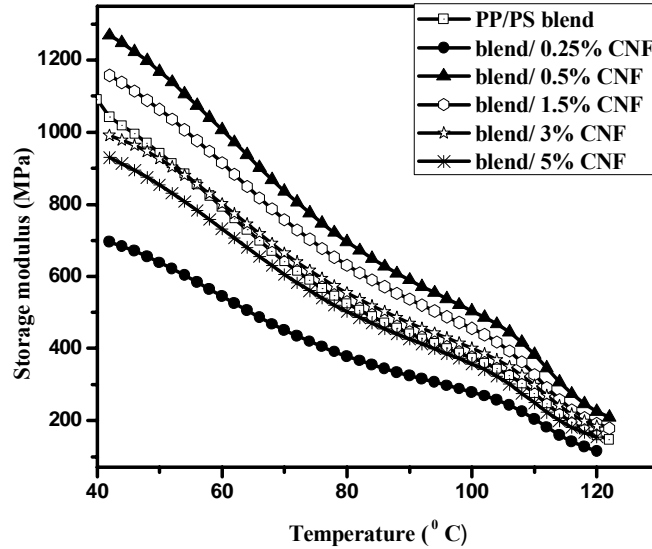


Figure 7b.12 Storage modulus curves of PP/PS blend, PP/PS/cellulose nano fiber composites

In DMA,  $\tan \delta$  ( $\tan \delta = E''/E'$ ) represents the damping within the material and it can be associated with macroscopic physical transitions.  $\tan \delta$  curves for pure PP/PS blend, PP/PS/CNF composites are shown in Figure 7b.13. From Table 7b.3, it is evident that  $T_g$  value is higher for 0.5 wt % cellulose nano fiber. The increase in  $T_g$  is due to the immobilization of polymer molecules caused by the better dispersion of cellulose nano fiber. As the dispersion increases the mobility of macromolecular chain reduces and the  $T_g$  shifts to higher temperature [20]. With further increase of cellulose nano fiber content,  $\tan \delta$  curve is shifted to lower temperature. Similar results were obtained for Issam Qamhia *et al.* in their studies [21]. At higher loading the agglomeration of cellulose nano fiber leads to decrease in interaction and results in increase in mobility of polymer chains and decrease in  $T_g$  values.

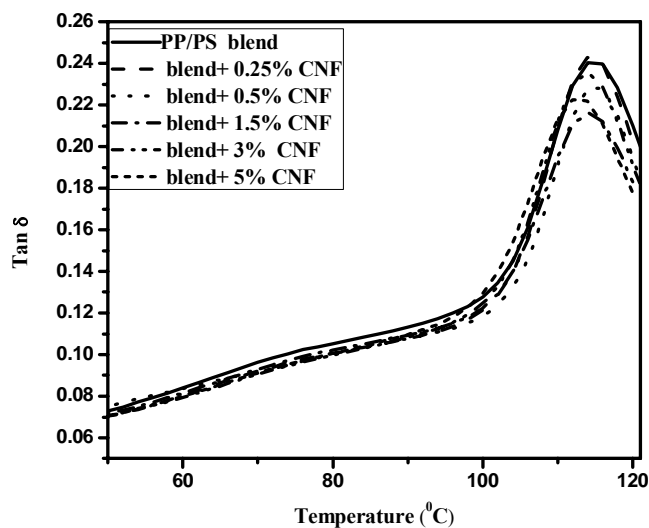


Figure 7b.13 Tan  $\delta$  curves of PP/PS blend, PP/PS/cellulose nano fiber composites

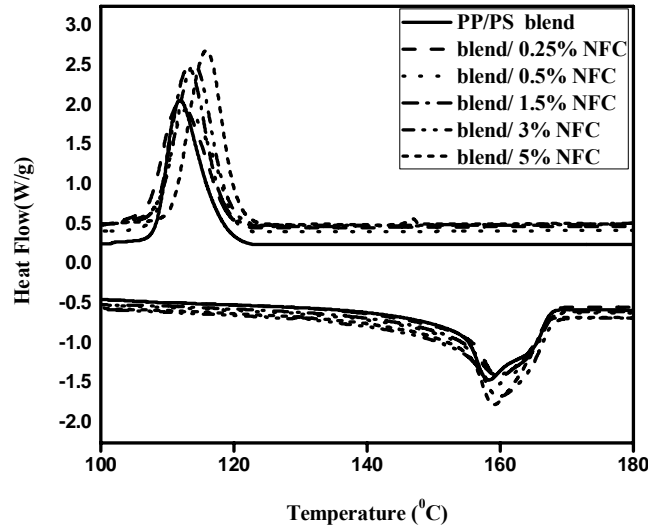
### 7. B.3.7 Differential scanning calorimetry (DSC)

Figure 7b.14 depicts the DSC melting and cooling curves for PP/PS blend and blends containing 0.25, 0.5, 1.5, 3 & 5 wt. % of CNF. The crystallization temperature, the apparent melting temperature and the corresponding enthalpies are shown in the Table 7b.4.

Table 7b.4 DSC parameters of PP/PS blend, PP/PS/CNF composites

Samples	$T_c$ (°C)	$\Delta H_c$ (J/g)	$T_m$ (°C)	$\Delta H_m$ (J/g)
PP/PS blend	111.9	61.1	158.4	32.4
Blend+0.25%CNF	111.9	63.9	154.9	44.1
Blend+0.5%CNF	112.9	66.9	159.3	46.9
Blend+1.5%CNF	113.1	69.3	159.7	47.1
Blend+3%CNF	114.0	62.1	159.1	47.4
Blend+5%CNF	115.9	76.7	159.9	57.4





**Figure 7b.14 DSC melting and crystallization curves of PP/PS blend and PP/PS/CNF composites**

There is no significant change observed in melting temperature ( $T_m$ ) & Heat of fusion ( $\Delta H_m$ ). The  $T_c$  and  $\Delta H_c$  values for cellulose nano fibers are shifted towards the higher temperature range with increasing cellulose nano fiber content. This may be due to the role of cellulose nano fiber as nucleating agent. Similar results were observed by other authors [22, 23].

### **7. B.3.8 Water vapor transmission rate (WVTR)**

Figure 7b.15 illustrates the variation of water vapor transmission rate with time for PP/PS/cellulose nano fiber composites. It is found that the addition of cellulose nano fibers restricts the water transmission in composites. The reduction in water vapor transmission rate is due to the presence of dispersed phase of cellulose nano fiber. The presence of dispersed phase of cellulose nano fiber increases the interfacial interaction and prevents the easy penetration of water vapor. The water sorption is found in the order  $5 > 3 > 1.5 > neat > 0.25 > 0.5$ . Significant decrease in

WVTR value is recorded as the cellulose nano fiber content increases up to 0.5 wt%. Further increase in CNF content enhances the WVTR value [24].

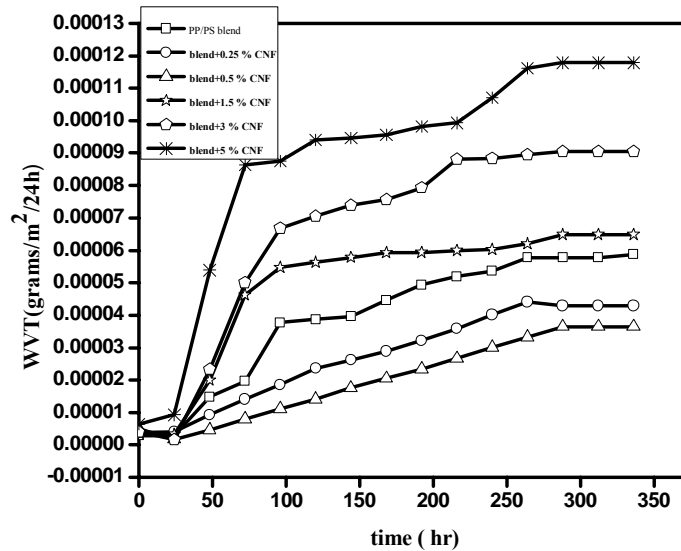


Figure 7b.15 Effect of CNF content on the WTVR of PP/PS/CNF composites

At higher concentrations the poor adhesion between matrix and fiber leads to voids at the fiber matrix interface and there by enables a path for the water molecules to pass through and increases the water vapor transmission.

**Transport Mechanism**

The transport properties of polymeric membranes can be followed by the empirical equation [25-27]:

$$\log\left(\frac{M_t}{M_\infty}\right) = \log k + n \log t \dots\dots\dots(7b.2)$$

where  $M_t$ ,  $M_\infty$ ,  $k$ , and  $n$  are the water absorption at time  $t$ , the water absorption at the saturation point, and constants respectively. The value of  $n$

is different for the different cases as follows: In Fickian diffusion  $n = 0.5$ , relaxation  $n > 0.5$  and anomalous transport  $0.5 < n < 1$ . The coefficients ( $n$  and  $k$ ) are calculated from slope and intercept of the log plot of  $M_t/M_\infty$  versus time which can be drawn from experimental data.

**Table 7b.5 Diffusion characteristics of cellulose nano fiber composite**

Samples	n	k(h <sup>-2</sup> )
PP/PS blend	0.496	24.70
Blend+0.25%CNF	0.497	20.04
Blend+0.5%CNF	0.529	23.44
Blend+1.5%CNF	0.556	25.32
Blend+3%CNF	0.567	25.51
Blend+5%CNF	0.578	25.81

Table 7b.5 presents the  $n$  and  $k$  values of PP/PS/cellulose nano fiber composites. The  $n$  values are similar for all nanocomposites and is close to 0.5. Therefore, it can be concluded that the moisture absorption of all nanocomposites approach the Fickian diffusion case. The  $k$  values give the structural characteristics of the polymer and it also gives an idea about the nature of interaction between the polymer and the solvent. Higher the  $k$  value higher is the interaction between the polymer and the solvent. The  $k$  values of 0.25% and 0.5 wt % CNF filled samples are lower than pure blend while it is higher at higher loadings [28].

***Sorption behavior***

The percentage of water absorption in the nanocomposites is calculated by weight difference between dry samples and the samples immersed in water using the following equation [29]:

$$\Delta M_t (\%) = M_t - M_0 / M_0 \times 100 \quad \dots\dots\dots(7b.3)$$

where  $\Delta M(t)$  is moisture uptake,  $M_0$  and  $M_t$  are the mass of the specimen before and after immersion, respectively.

Diffusion is a kinetic parameter related to the penetrant size and to the polymer segmental mobility.

The diffusion coefficient is calculated for one-dimensional Fickian theory for unsteady diffusion process. The percentage of moisture gain at any time  $t$ , ( $M_t$ ) can be obtained from the solution of the one-dimensional Fickian model with constant boundary conditions [30] as

$$\frac{M_t}{M_\infty} = 1 - \left( \frac{8}{\pi^2} \right) \sum_{n=0}^{\infty} \sum \frac{1}{(2n+1)^2} \exp(-D(2n+1)^2 \pi^2 t / h^2) \quad \dots\dots\dots(7b.4)$$

where  $t$  is the time,  $h$  is the initial thickness of the sample,  $D$  is the diffusion coefficient and  $n$  is an integer. From this equation it can be found that a plot of  $M_t$  versus  $t^{1/2}$  is linear at short time and  $D$  can be calculated from the initial slope. The equation for short time limiting is [31]

$$\frac{M_t}{M_\infty} = \left( \frac{4}{h} \right) (D / \pi) \frac{1}{2} t^{1/2} \quad \dots\dots\dots(7b.5)$$

By rearranging the equation, the diffusion coefficient ( $D$ ) can be calculated [32].

$$D = \pi (h\theta / 4_\infty)^2 \quad \dots\dots\dots(7b.6)$$

where  $\theta$  is the slope of the initial portion of the  $M_t$  Vs  $t^{1/2}$  plot and  $M_\infty$  is the equilibrium mole percentage uptake. The liquid sorption tends towards an

equilibrium value, which depends upon the nature of the material. The permeability (P) is given by the equation [27].

$$P = DS \dots\dots\dots(7b.7)$$

where, D and S are the diffusion and sorption coefficient respectively. Sorption coefficient is related to the equilibrium sorption of the penetrant and can be calculated as

$$S = M_s/M_p \dots\dots\dots(7b.8)$$

where  $M_s$ , is the mass of the solvent at equilibrium and  $M_p$  is the mass of polymer sample.

The permeation of small molecules through polymer occurs through solution diffusion kinetics i.e. the penetrant molecules are first absorbed by the polymer followed by diffusion through the polymer [33]. Therefore the permeation through any matrix is a combination of diffusivity as well as sorption of the penetrant in the polymer [33,34].

**Table 7b.6 Variation of diffusion coefficient (D), sorption coefficient (S), permeation coefficient (P) of PP/PS/CNF composites**

Samples	D×10 <sup>-10</sup> (cm <sup>2</sup> /s)	S	P×10 <sup>-10</sup> (cm <sup>2</sup> /s)
PP/PS blend	1.39	0.689	0.958
Blend+0.25%CNF	1.38	0.684	0.944
Blend+0.5%CNF	1.24	0.611	0.758
Blend+1.5%CNF	1.56	0.692	1.080
Blend+3%CNF	1.78	0.712	1.267
Blend+5%CNF	2.00	0.887	1.774

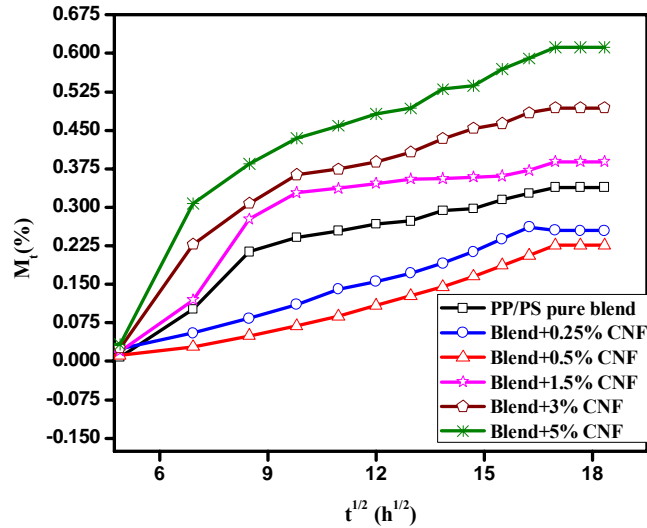


Figure 7b.16  $M_t$  Vs  $t^{1/2}$  (h<sup>1/2</sup>) plot of PP/PS /CNF composites

Figure 7b.16 shows the percentage of weight gain as a function of square root of time for PP/PS blend and composites with various CNF loadings. The water transmission process for all specimens are linear in the beginning, then slows and approaches saturation after prolonged time, following a Fickian diffusion process. The diffusivity (D), sorption coefficient (S) and permeability (P) values calculated using Eqs 7b.6, 7b.7 & 7b.8 are summarized in Table 7b.6. The diffusion of penetrant depends upon the concentration of available space which is large enough to accommodate the penetrant molecule. A penetrant molecule exists in a hole of sufficient size can jump into a neighboring hole once it acquires sufficient energy. This diffusion mechanism is not possible when CNF is dispersed in polymer matrix and CNF acts as a barrier to the diffusion of the water molecules. The diffusion coefficient is lesser for 0.5wt% CNF reinforced composites. The increased permeability for PP/PS blend is due to the poor interfacial interaction between the blends. 0.5wt% CNF reinforced PP/PS blend exhibit reduced permeability than other

systems and is in good agreement with the improved mechanical properties. The reduced permeability is due to the better dispersion of CNF in PP/PS blend. At higher CNF content, the aggregation of particles results in the formation of voids. The increase in permeation at higher loadings may be due to the presence of these micro voids at the interfacial region [35,36]. The excellent resistance to water permeation of the PP/PS/0.5 wt% CNF composites is due to the decrease in diffusion coefficient.

#### **7. B.4 Conclusions**

The addition of cellulose nano fibers improves the strength and modulus of PP/PS blend along with improvement in toughness. The tensile modulus of the composite when compared to neat PP/PS blend, increases by 168% with the addition of 0.5 wt% CNF, while impact strength increases by 111%. TEM images reveal that the CNF remains at the interface between the blend components and thereby increases the effective stress transfer between the CNF and the polymer matrices. Storage modulus is found to be higher for 0.5wt% CNF and the increased modulus, is attributed to better dispersion of CNF in polymer matrix that restricts the segmental mobility of polymer chains in the vicinity of the CNF. TGA studies show that thermal stability improves with increase in CNF and it shows their suitability of processing with thermoplastics. Water transmission data show that the addition of 0.5 wt% CNF decreases the transmission rate of the composite and at higher loading the water transmission increases, due to the agglomeration of CNF in the polymer matrix

## References

- [1]. Susheel Kalia, Alain Dufresne, Bibin Mathew Cherian, B. S. Kaith, Luc Av'eros, James Njuguna, Elias Nassiopoulos, International Journal of Polymer Science, 2011, Article ID 837875, 35.
- [2]. E. Abraham, B. Deepa, L.A. Pothan, M. Jacob, S. Thomas, U. Cvelbar, R. Anandjiwala; Carbohydrate Polymers, 2011, 86, 1468–1475.
- [3]. Mariana Pereda, Guillermina Amica, Iona Racz, Norma E. Marcovich; Journal of food Engineering, 2011,103, 76-83.
- [4]. Cellulose Microfibril/Nanofibril and its nanocomposites, Siqun Wang, Qingzheng Cheng, Tim G. Rials and Seung-Hwan Lee, Proceedings of the 8th Pacific Rim Bio-Based Composites Symposium.
- [5]. Takashi Nishino, Klyofuml Takano, Katsuhiko Nakamae, Journal of Polymer Science: Part B: Polymer Physics, 1995, 33, 1647-1651.
- [6]. Navin Chand, Suresh Chandra Prajapati, R.K Singh, Journal of Scientific Research and Reviews, 2012, 1(3), 026 – 032.
- [7]. Gilberto Siqueira, Julien Bras, Alain Dufresne; Biomacromolecules 2009, 10, 425–432.
- [8]. Seung-Hwan Lee, Siqun Wang, George M. Pharr, Haitao Xu, Composites: Part A, 2007, 38, 1517–1524.
- [9]. Elif Bahar, Nuray Ucar, Aysen Onen, Youjiang Wang, Mustafa Oksuz, Onur Ayaz, Mehmet Ucar, Ali Demir, Journal of Applied Polymer Science, 125, 4, 2012, 2882-2889
- [10]. Ucar, Ali Demir, Journal of Applied Polymer Science, 2012, 125(4), 2882–2889.
- [11]. Jooyoun Kim, Gerardo Montero, Youssef Habibi, Juan P. Hinestroza, Jan Genzer, Dimitris S. Argyropoulos, Orlando J. Rojas, Polymer Engineering & Science, 2009, 49(10), 2054–2061.



- [12]. Cintil Jose Chirayil, Jithin Joy, Lovely Mathew, Joachim Koetz, Sabu Thomas, *Industrial Crops and Products*, 2014, 56, 246–254.
- [13]. Ning Lin , Alain Dufresne, *Macromolecules*, 2013, 46 (14), 5570–5583.
- [14]. Dmitri Shumigin , Elvira Tarasova, Andres Krumme, Pille Meier; ISSN 1392–1320 *Materials Science (Medžiagotyra)*, 2011, 17(1).
- [15]. Yuanfeng Pana, Michael Z. Wang, Huining Xiao; *Composites Science and Technology*, 2013, 77, 81–86.
- [16]. Han-Seung Yang, Douglas J. Gardner, Jacques W. Nader; *Composites: Part A* , 2011, 42, 2028–2035.
- [17]. L.A Pothan, Z Oommen, S Thomas, *Composite. Science & Technology* 2003,63(2), 283–293.
- [18]. Preparation and Characterization of Cellulose Nanofibril Films from Wood Fibre and their Thermoplastic Polycarbonate Composites, S. Panthapulakkal and M. Sain; *International Journal of Polymer Science*, 2012, Article ID 381342, 6.
- [19]. Sun-Young Lee, D. Jagan Mohan, In-Aeh Kang, Geum-Hyun Doh, Soo Lee, Seong Ok Han, *Fibers and Polymers*, 2009, 10(1), 77-82.
- [20]. Sukanya Satapathy, Golok Bihari Nando, Ahin Nag, *International Journal of Plastic Technology*, 13(2),95–111.
- [21]. Mehdi Jonoobi, Aji P. Mathew, Mahnaz M. Abdi Majid Davoodi Makinejad, Kristiina Oksman, *Journal of Polymers & the Environment*, 2012, 20 (4), 991.
- [22]. Issam I.Qamhai, Ronald C Sabo, Rani F Elhajjar, *Bioresources* ,2014, 9(1), 381-392.
- [23]. Adriana N. Frone, Sophie Berlioz, Jean-Fran, ois Chailan, Denis M. Panaitescu, *Carbohydrate Polymers* , 91 (2013), 377–384.
- [24]. K. T. B . Padal, K. Ramji, V. V. S. Prasad, *International Journal of Engineering Research*, 3(5), 333-335.

- [25]. N.R. Savadekar, V.S. Karande, N. Vigneshwaran, A.K. Bharimalla, S.T. Mhaske, *International Journal of Biological Macromolecules* ,2012, 51 , 1008– 1013.
- [26]. Ismaeil Ghasemi , Behzad Kord; *Iranian Polymer Journal*, 2009, 18 (9) .
- [27]. J. S. Chiou , D. R. Paul; *Polymer Engineering and Science*, 1986, 26(77).
- [28]. Ajalesh Balachandran Nair, Philip Kurian, Rani Joseph, *Materials and Design*, (2012), 40 80–89.
- [29]. Ranimol Stephen, Siby Varghese, Kuruvilla Joseph, Zachariah Oommen, Sabu Thomas, *Journal of membrane science* ,2006, 282, 162-170.
- [30]. N. Abacha, M. Kubouchi, T. Sakai , *eXPRESS Polymer Letters*,2009, 3(4) , 245–255.
- [31]. H.N. Dhakal , Z.Y. Zhang, M.O.W. Richardson; *Composites Science and Technology* ,2007,67(7-8), 1674–1683.
- [32]. Moisture Absorption Behavior and its Effect on Flexure Properties of Polyurethane Foams M. C. Saha, S. Mohan, D. Hickman, and A. Balakrishnan; *Proceedings of the XIth International Congress and Exposition June 2-5, 2008 Orlando, Florida USA*©2008 Society for Experimental Mechanics Inc.
- [33]. Aithal US, Aminabhavi TM, Cassidy PE, *Journal of memberane science*, 1990, 50, 225–47.
- [34]. K.A Dubey, Y.K.Bhardwaj, C.V.Chaudhari, Virendra Kumar, N.K.Goel, S.Sabharwal; *Nuclear instruments and methods in physics research B*, 2009, 267, 795-801.
- [35]. Shyla George, Prajitha kumara, G unnikrishnan, *Journal of elastomers and plastics*, 2009, 41.
- [36]. Ranimol Stephan, C.Ranganataiah, Siby Varghese; Kuruvila Joseph, Sabu Thomas, *Polymer*, 2006, 47, 858-870.

.....❧.....

# Summary and Conclusions

A brief summary of the work described in this thesis is reported in this chapter. The scope of future work is also presented.

Blending of polymers offers a good possibility to modify thermoplastic materials so as to develop a new material with a wide range of properties. Polypropylene (semi crystalline) / Polystyrene (amorphous) blend are used in this study as the control blend. Blending an amorphous polymer and a semi crystalline polymer will offer a balance of impact strength/ stiffness. Polypropylene (PP) and Polystyrene (PS) used in this study are immiscible and hence these blends are multiphase systems. Good interfacial interaction is necessary for the effective stress transfer between the polymer matrices; therefore modifiers are required. So nanoclays and cellulose nano fiber are used as modifiers in this study. A systematic study is proposed to be undertaken to understand the mechanical, thermal and morphological properties of modified nanocomposites. The degree of dispersion of nanoclay particles in polymer matrix and the morphology of nanocomposites were evaluated from X-ray diffraction (XRD), Dynamic mechanical analysis (DMA), Differential scanning calorimetry (DSC), Thermogravimetric analysis (TGA), Transmission electron microscopy (TEM) and Scanning electron microscopy (SEM).

The present study on the effect of five different kaolin nanoclays, Nanocaliber 100(unmodified kaolin nanoclay) and modified kaolin nanoclays [Nanocaliber 100 V (Vinyl silane modified clay), Nanocaliber 100Z (Dialkyl silane modified clay, Nanocaliber 100A (Amino silane modified clay), Nanocaliber 100M (Mercapto modified clay)] on the properties of Polypropylene/Polystyrene (PP/PS: 80/20) blend show that modified clays can improve tensile modulus and strength of polymer blends compared to unmodified clay. Vinyl silane and dialkyl silane modified nanocomposites give maximum improvement in mechanical properties, suggesting that vinyl silane and dialkyl silane provide better interfacial interaction. Comparison between the experimental data and the results provided by various theoretical models fit elastic moduli (Halpin-Tsai model, Takayanagi model, Hui-Shia, Voigt upper bound model and Reuss lower-bound) for PP/PS/ modified kaolin clay nanocomposites with N100Z and N100V respectively has been presented. The experimental results show close proximity to the Hui Shia model which indicates a perfect interfacial bonding between nanoclay and the polymer matrix as per the assumptions of the model. Thermogravimetric studies proved that the thermal stability of the polymer blends can be improved by the incorporation of nanoclays. The dynamic mechanical analysis shows higher storage moduli over a temperature range of 40–125°C for nanocomposites and the extent of increase in the storage modulus is dependent on the type of nanoclay. Transmission electron microscopic observations show that vinyl silane modified nanoclay layers are intercalated on the polymer matrix and are located at the interface between the two polymers and dialkyl silane modified nanoclay layers are partially exfoliated on the polymer matrix and

were located at the interface and also on the PP phase. The XRD does not show any shift in the diffraction peak for the PP/PS/Nanocaliber100A, PP/PS/Nanocaliber100M and PP/PSNanocaliber100 nanocomposites. For the PP/PS/Nanocaliber100V nanocomposite, the characteristics peak of Nanocaliber100V is shifted to  $2\theta = 12.08^\circ$ , corresponding to a d-spacing of 7.32 nm, which indicates that some PP/PS molecular chains are intercalated between the clay galleries, forming an intercalated structure. A broadening of peak and reduction of intensity is observed in the case of PP/PS/Nanocaliber 100Z modified clay nanocomposite. This shows an improved dispersion of nanoclay layers in the polymer matrix. The study also shows that the modified kaolin nanoclays can impart better thermal stability than PP/PS pure blend.

The effect of modified kaolin nanoclays (N100V & N100Z) on the properties of PP/PS/E-glass fiber (PP/PS/EGF) composites and PP/PS/alkali resistant glass fiber (PP/PS/ARGF) composites were also investigated. The combined use of micro/nano fillers improved the properties of polymer blends. The improvement depends on the type of fillers, concentration and interaction between the polymer matrix, fiber and the nano filler. This study also shows that nanoclay can be used to modify fiber-reinforced composite materials to enhance their resistance to thermal degradation processes and improve their mechanical properties. XRD and SEM show better dispersion of clay particles in both alkali resistant and E-glass fiber reinforced composites. A comparison between experimental results (tensile modulus) and various models [Parallel and Series model, Hirsch, Halpin-Tsai model, Modified Halpin –Tsai, Halpi – Pagano and Hui-Shia model] of both glass fiber composites has been presented. The experimental results show close

proximity to the Hui Shia model which indicates a perfect interfacial bonding between glass fiber and the polymer matrix as per the assumptions of the model. A comparison between experimental results (tensile modulus) and various models [Parallel and series model, Guth model, Paul model, Counto model, Hirsch model, Halpin – Tsai] of hybrid composites has been presented. The better prediction of these models (Paul and Counto model) at lower percentage may be due to the presence of nanoclay at the interface which results in better adhesion between the polymer matrix and glass fiber increases and better stress transfer at the interface.

Kaolin nanoclay has relatively low cationic exchange capacity. Kaolin clay is a 1:1 dioctahedral aluminosilicate with two distinct basal layers. Because of the hydrophilic character of kaolin and hydrophobic properties of polymer the modification of kaolin is necessary. Kaolin clay can interact with organic molecules by intercalation. The kind of guest species intercalated between the layers of kaolin is limited due to the hydrogen bonding between the octahedral side and tetrahedral side. Intercalation of kaolin with guest species can be done by displacement reactions. The separation of kaolin layers results in particle size reduction and an increase of the specific surface area. A good kaolin nanoclay modification results in better intercalation between filler and polymer matrix. The modification of unmodified kaolin clay using vinyltriethoxysilane (VTES) by guest displacement method and its effect on the properties of Polypropylene/Polystyrene (80/20) blend was investigated. Modification of kaolin nanoclay includes two steps. In first step kaolin nanoclay was treated with Dimethylsulphoxide (DMSO) as precursor and the second step is the displacement of DMSO by vinyltriethoxysilane. The X-ray diffractograms

reveals the intercalation of DMSO, and subsequently the displacement of DMSO by VTES. The thermogravimetric curves of the kaolin clay functionalized with VTES indicate that the material is thermally stable up to 515°C. Infrared analysis results supported the occurrence of a partial delamination of kaolin nanoclay with DMSO and the further evidence of the substitution of DMSO molecules by vinyltriethoxysilane in the interlamellar space of the clay mineral. The studies on the effect of vinyltriethoxysilane modified kaolin clay on the properties of Polypropylene/ Polystyrene blend reveal that mechanical properties can be subsequently improved at the addition of 3 wt% modified kaolin nanoclay due to the improved interfacial interaction. XRD and SEM reveal better intercalation of clay particles in the polymer matrices. The improvement in thermal stability of nanocomposites was confirmed by increasing the activation energy ( $E_a$ ).

The effect of two types of compatibilizers (itaconic acid and dimethyl itaconate) on the properties of Polypropylene/ Polystyrene clay nanocomposite was also investigated. In this study the compatibilizers were added directly into the clay nanocomposites. Itaconic acid (IA) and its derivative dimethyl itaconate (DMI) were used as compatibilizers in this study. It was selected for the study because it is less hazardous compared to other kinds of anhydrides, such as maleic anhydride. Due to its double functionality, IA and its derivatives (DMI) offer interesting possibilities as polar functional monomers for the modification of nonpolar polymers. Better dispersion is achieved by using compatibilizers, which can enhance the intercalation of the polymer chains within the nanoclay gallery. The hydroxyl group of clay can react with the compatibilizer to disperse the nanoclay well within polymer matrix through in-situ compatibilization. The existence of grafted compatibilizers in PP/PS was

confirmed by FTIR spectroscopy. Mechanical properties found to improve in the presence of both the compatibilizers. XRD and TEM results confirm the improvement in nanoclay dispersion in polymer matrix after the addition of compatibilizers (IA and DMI). Storage modulus is also found to improve in the presence of compatibilizers. SEM results show a homogeneous morphology in compatibilized clay nanocomposites. TGA studies show improvement in thermal stability in compatibilized clay nanocomposites.

The last part of the work is the isolation of cellulose nano fiber (CNF) from sisal leaves and its effect on PP/PS (80/20) blend. XRD studies reveal an increase in the percentage crystallinity of sisal fiber. SEM shows that there is a reduction in the fiber diameter during the steam explosion in acidic medium. This is obviously due to the dissolution of the non-cellulosic components present in the fiber cell wall by the acid correlated steam treatment process, which enhances the extraction of crystalline cellulose components from the fiber. TEM image supports the evidence for the formation of nano fibers and the average diameter is found to be between 10- 40 nm. FTIR spectra confirm the evidence for the removal of lignin and hemicellulose. Chemical analysis supports the removal of lignin and hemicellulose and the extraction of cellulose nano fiber. The studies show that the addition of cellulose nano fibers (CNF) improves the strength and modulus of the blend along with improvement in toughness. The tensile modulus of the composite when compared to neat PP/PS blend is found to improve by 168% with the addition of 0.5 wt% CNF, while impact strength increases by 111%. TEM images reveal that the CNF is found at the interface between the blend components and thereby improving the effective stress transfer between the CNF and the polymer matrices. Storage modulus is found to be higher for 0.5wt% CNF and the increased modulus, is



attributed to better dispersion of CNF in polymer matrix that restrict the segmental mobility of the polymer chains in the vicinity of the CNF. TGA studies show that there is an increase in thermal stability with increasing CNF and it makes processing safe. The addition of 0.5 wt% CNF decreases the water transmission rate of the composite.

#### **Future scope of the work**

- 1) **Chemical modification of cellulose nano fibers:** Cellulose nano fibers have certain disadvantages like poor solubility in common solvents, poor crease resistance, poor dimensional stability, lack of antimicrobial properties etc. Because of the hydrophilic nature of the cellulose nano fibers it forms agglomerates and it is incompatible with hydrophobic polymers. To overcome such drawbacks, the controlled physical or chemical modification of the cellulose nano fiber is necessary.
- 2) **Studies on the effect of compatibilizers:** In immiscible PP/PS blends, the clay dispersion and location are influenced by the polarity of PP and PS. The nanoclay location can be controlled by the alternation of the polarity of PP and PS by chemical modification. So polarity of PP and PS can be changed by physically functionalized PP and PS.
- 3) **Studies on the effect of different compatibilizers:** In the present study itaconic acid and its derivative dimethyl itaconate are used as compatibilizers. The effect of other compatibilizers can also be investigated.
- 4) **Fabrication of useful products:** The nanocomposites can be used in many applications like automobile, packaging etc.



## *Abbreviations and Symbols*

ASTM	American Society for Testing and Materials
AR Glass fiber	Alkali Resistant Glass fiber
BET	Brunauer, Emmett and Teller
BR	Broido's
$\beta$	Heating rate
CR	Coats Redfern
CNF	Cellulose nano fiber
D	Diffusion coefficient
DCP	Dicumyl peroxide
DMA	Dynamic mechanical analysis
DMI	Dimethyl itaconate
DMSO	Dimethylsulfoxide
DSC	Differential Scanning Calorimetry
DTG	Derivative thermogravimetry
$E_a$	Activation energy
$E'$	Storage modulus
$E''$	Loss modulus
$E_c$	Modulus of composite
$f$	Frequency
FTIR	Fourier transform infrared spectroscopy
$\Phi_f$	Filler volume fraction
$\phi_{\max}$	Maximum volume fraction
HM	Horowitz-Metzger
H-T model	Halpin-Tsai model
HS model	Hui Shia model
IA	Itaconic acid
N100	Nanocaliber 100
N100V	Nanocaliber 100V
N100Z	Nanocaliber 100Z

N100M	Nanocaliber 100M
N100A	Nanocaliber 100A
nm	Nanometer
μm	Micrometer
MFI	Melt Flow Index
P	Permeability
PP	Polypropylene
PS	Polystyrene
[PP/PS]-g-IA	Itaconic acid grafted Polypropylene/Polystyrene blend
S	Sorption coefficient
SEM	Scanning electron microscopy
Tan δ	Loss factor
TEM	Transmission electron microscopy
VTES	Vinyltriethoxysilane
WVTR	Water vapor transmission rate
XRD	X-ray Diffraction

## *List of Publications*

### **Publications in international/national journals**

- 1) Effect of Modified Kaolin Clays on the Mechanical Properties of Polypropylene/Polystyrene Blends, **Asha K. Krishnan**, Tresa Sunitha George, R. Anjana, Newly Joseph, K. E. George, Journal of Applied Polymer Science; Vol. 127, Issue 2, p 1409–1415, 2013.
- 2) Polymer blend nanocomposites: Effect of mercapto silane modified kaolin clay on the thermal properties of Polypropylene/Polystyrene blend, **Asha Krishnan. K** and K. E. George, Polymers for Advanced Technologies, Vol. 25, Issue 9, p 955–962, 2014.
- 3) Effect of alkali-resistant glass fiber on Polypropylene/Polystyrene blends: modeling and characterization, **Asha Krishnan K**, Anjana R, K.E. George, Polymer Composites, DOI: 10.1002/pc.23193.
- 4) Mechanical and morphological properties of Organomodified kaolin/ Polypropylene/ Polystyrene nanocomposites, **Asha Krishnan K**, Tresa Sunitha George; K.E. George, Pauline Journal of research and studies, Vol.1.No.1, 2013.
- 5) Hybrid composites from blends of Polypropylene and Polystyrene reinforced with nanoclay and E-glass fiber, **Asha Krishnan. K**, Ajalesh B Nair, K.E.George (Communicated).
- 6) Effect of Itaconic acid grafting on Nanokaolin clay reinforced Polypropylene/ Polystyrene blend **Asha Krishnan. K**, K.E.George (Communicated).
- 7) Effect of Dimethyl itaconate grafting on Nanokaolin clay reinforced Polypropylene/Polystyrene blend, **Asha Krishnan. K**, K.E. George (Communicated).

- 8) Isolation and characterization of Cellulose nanofibers from sisal and its effect on Polypropylene/Polystyrene blend, **Asha Krishnan. K**, Cintil Jose, Rohith K. R, K.E.George (Communicated).
- 9) Preparation and Characterization of cellulose nano fibers reinforced Polypropylene/ Polystyrene nanocomposites, **Asha Krishnan. K**, K.E.George (Communicated).

### **Presentations in Conferences**

- 1) Effect of different Organomodified Clays on the Compatibility on Polypropylene/ Polystyrene Nanocomposites, **Asha Krishnan K**, Tresa Sunitha George, Newly Joseph, Dr.K.E. George, PSE – 2010, “Polymer Science and Engineering: Emerging Dimensions”, University Institute of Chemical Engineering and Technology, Punjab University, Chandigarh, November 26-27, 2010.
- 2) Modification of Polypropylene/Polystyrene blends using Nanoclay, **Asha Krishnan. K**, Tresa sunitha George, Newly Joseph, Dr.K.E.George, International conference on materials for future-ICMF-2010, GEC, Thrissur.
- 3) Effect of vinyltriethoxy silane modified kaolin clay on the mechanical properties of Polypropylene/ Polystyrene blend, **Asha Krishnan K**, Tresa Sunitha George, K.E George, International Conference on Advances in Material Science ICAMS 2013, Sree Sankara College, Kalady, Kerala, India.
- 4) Polymer nanocomposites based on blends: Effect of vinyl silane modified clay on Polypropylene/ Polystyrene Nanocomposites, **Asha Krishnan. K**, Tresa Sunitha George, K.E George, National Seminar on Recent Advances in Polymer Science and Technology, June 23, 2012; Society for Polymer Science India, Thiruvananthapuram Chapter and Department of Chemistry, Mar Ivanios College, Thiruvananthapuram.

- 5) Modification of Polypropylene/Polystyrene blends using Vinyl silane modified kaolin clay, **Asha Krishnan K**, K.E. George, National seminar on Emerging Nanoscience and its future in Biology, August 2012, Department of Zoology and Aquaculture, St. Aloysius college, Edathuva, Kottayam.
- 6) Effect of dialkyl modified kaolin on the mechanical properties of Polypropylene/Polystyrene blends, **Asha Krishnan. K**, Tresa sunitha George, Dr.K.E.George, National Conference on Advances in Materials Science: Macro to Nano Scales, Department of chemistry, Union Christian College; March 2012.
- 7) Effect of modified kaolin on the mechanical properties of Polypropylene/Polystyrene Nanocomposites, **Asha Krishnan. K**, Tresa sunitha George, Newly Joseph, Dr.K.E.George; Emerging Trends in Nanotechnology, Department of Chemistry, Bishop Kurialacherry College for women; September 2011.
- 8) Effect of Dialkyl silane modified kaolin clay on the mechanical properties of Polypropylene/Polystyrene Nanocomposites, **Asha Krishnan. K**, Tresa sunitha George, Newly Joseph, Dr.K.E.George, International Research Conference on Advanced Techniques in Chemistry, Department of chemistry, St. Albert's college; Ernakulum; January 2014.



## Curriculum Vitae

### Asha Krishnan K

Kanol kudy (H)  
Iringole P.O  
Perumbavoor,  
Ernakulam (Dist.),  
Kerala, India.



Tel:0484-2529100  
Ph: +91-9539024092  
Email: ashakris8@gmail.com

### Personal Details

Nationality : Indian  
Sex and Marital Status : Female, Single  
Language Proficiency : English, Hindi, Malayalam, Tamil (Talk)  
Present Address : Research Scholar  
Department of Polymer Science and Rubber  
Technology, Cochin University of Science  
and Technology(CUSAT)  
Cochin, Pin: 682022  
Kerala, India  
Ph: +91-4842575723

### Educational Qualifications

- M. Tech in Polymer Science and Rubber Technology,  
Cochin University of Science and Technology, Kerala, India
- M. Sc Chemistry (Polymer), Mahatma Gandhi  
University, Kerala, India.

### Research Experience

*Five years in Polymer Science and Rubber technology,*  
One year at Corporate R&D centre of HLL Life care Limited, Trivandrum,  
Kerala, India and One month training in Rubber board Training center  
Kottayam (as a part of M.Tech)  
6 months at National Chemical Laboratory, Pune, India (as a part of M sc.)

### Teaching experience

1 year (Engineering Chemistry)

### Awards

**Gate Qualified in Engineering Sciences (XE) (2013)**



### **List of other Research Publications**

- 1) Effect of Maleic Anhydride Grafting on Nanokaolin clay Reinforced Polystyrene/High Density Polyethylene Blends, Tresa Sunitha George, **Asha Krishnan**, Newly Joseph, R. Anjana, K.E. George, Polymer Composites, 33(9), 1465–1472, 2012.
- 2) Optimisation of Processing Conditions of PP/HDPE/nano kaolinite clay composites by Response Surface Methodology, Anjana Ramachandaran, **Asha Krishnan**, Tresa Sunitha George, George K E, International Journal of Plastics Technology, December 2012, 16(2), 136-149,2012
- 3) Design of experiments for thermo-mechanical behavior of polypropylene/high density polyethylene/ nanokaolinite clay composites, R Anjana, **Asha K Krishnan**, Tresa Sunitha George, K.E. George, Polym. Bull. , 2014, 71:315–335.
- 4) Polypropylene/High Density Polyethylene/Glass Fibre/Nanokaolinite Clay Composites- A Novel Material For Light Weight ManufacturingnSystems; Anjana R, **Asha Krishnan**, Tresa Sunitha George, K E George, Advanced Materials Research , 816-817 , 2013 ,96-100.
- 5) Studies on Nano Kaolin Clay Reinforced PS-HDPE Nanocomposites ;Tresa Sunitha George, **Asha Krishnan K**, Anjana R, K E George; Indian Journal of Advances in Chemical Science 1 (4) , 2013, 201-206.
- 6) Reinforcing Effect of Organo Modified Kaolin Clay On Polypropylene-Short Glass Fibre Composites, Newly Joseph, Sinto Jacob, Tresa Sunitha George, **Asha Krishnan** and George KE, ISSN: 0973-7464 Vol. XVI: No.1 & 2 SB Academic Review 2009, 152-163.
- 7) Mechanical and morphological properties of short nylon fiber reinforced PS/HDPE composites; Tresa Sunitha George, **Asha Krishnan K**, Anjana R, Newly Joseph, K.E.George; Pauline Journal of Research and Studies; Vol.1, No1. (2013).

### **Other Presentations in International/National Conferences**

- 1) Nano Kaolin Clay as a Modifier for Glass Fiber Reinforced Thermoplastics , Tresa Sunitha George, **Asha Krishnan K** and George.K.E, National Seminar on Recent Advances in Polymer Science and Technology ;June 23, 2012, Society for Polymer Science India, Thiruvananthapuram Chapter and Department of Chemistry, Mar Ivanios College, Thiruvananthapuram.
- 2) Modification of Polystyrene and High Density Polyethylene Blends using Nano Kaolinite Clay; Tresa Sunitha George, **Asha Krishnan K**, Newly Joseph, K E George, International conference in Advancements in Polymeric

Materials, Central Institute Of Plastics Engineering And Technology, Chennai, 2011.

- 3) Synergetic effect of Organomodified Kaolin clay and short Glass fiber on HDPE-composites. Newly Joseph, **Asha Krishnan**, Tresa Sunitha George, George K. E. ;International conference in Advancements in Polymeric Materials, Central Institute Of Plastics Engineering And Technology, Chennai, 2011.
- 4) Performance improvement of Nanoclay filled PS/ HDPE nanocomposites through various Organomodified clays during Melt intercalation; Tresa Sunitha George, **Asha Krishnan.K**, Newly Joseph, K.E George, PSE – 2010, “Polymer Science and Engineering: Emerging Dimensions”, University Institute of Chemical Engineering and Technology, Panjab University, Chandigarh, November 26-27, 2010.
- 5) Nano Kaolin Clay as a Modifier for Glass Fiber Reinforced Thermoplastics ; Tresa Sunitha George, **Asha Krishnan K** and George K. E, International Conference On Advances In Material Science ICAMS 2013, Sree Sankara College ,Kalady, Kerala , India.
- 6) Influence of modified nanoclay on the mechanical properties of HDPE-Coir fibre composites with and without weld line, Newly Joseph, Bipin Pal, **Asha Krishnan K**, Tresa Sunitha George, George K. E, International Conference On Advances In Material Science ICAMS 2013, Sree Sankara College Kalady, Kerala , India.
- 7) Performance improvement of Nanoclay filled PS/ HDPE nanocomposites through various organomodified clays during Melt intercalation, Tresa Sunitha George, **Asha Krishnan.K**, Newly Joseph, K.E George; PSE – 2010, “Polymer Science and Engineering: Emerging Dimensions”, University Institute of Chemical Engineering and Technology, Panjab University, Chandigarh, November 26-27, 2010.
- 8) Thermomechanical behaviour of PS/HDPE blends containing nanokaolinite clay; Tresa Sunitha George, **Asha Krishnan K**, Newly Joseph, K E George, International conference on materials for future-ICMF-2010 ,GEC, Thrissur.
- 9) Modification of polystyrene and high density polyethylene blends using nano kaolinite clay, Tresa Sunitha George, **Asha Krishnan K**, Newly Joseph, K E George; International conference on Advances in polymeric materials –APM 2011,cipet,guindy,Chennai.
- 10) Effect of processing parameters on the mechanical performance of PS/HDPE /clay nanocomposites; Tresa sunitha George, **Asha Krishnan K**, Newly Joseph, and George K.E, National Conference on Nanotechnology-2011, St. Theresa’s College, Ernakulum.

- 11) Synergetic effect of Organomodified Kaolin clay and short Glass fiber on the weld line strength of Polyethylene composites, Newly Joseph, **Asha Krishnan K** ,Tresa ,Sunitha George, K E George, International conference on materials for future-ICMF-2010 ,GEC, Thrissur.
- 12) Synergetic effect of Organomodified Kaolin clay and short Glass fiber in Polypropylene composites, Newly Joseph, Tresa Sunitha George, **Asha Krishnan K** , K E George, International conference on Latest in Polymers, LAP 2011, Perumbavoor, Kerala.
- 13) Influence of modified nanoclay on the mechanical properties of HDPE-Coir fibre composites, Newly Joseph, Tresa Sunitha George, **Asha Krishnan K** , K E George, National Conference on Nanotechnology - 2011, St. Theresa's College, Ernakulam.

.....❧.....